

DETECTION OF PHARMACEUTICALS AND ANIONS IN WATER USING CARBON-BASED ELECTRODES

Teză destinată obținerii
titlului științific de doctor inginer
la
Universitatea Politehnica Timișoara
în domeniul INGINERIE CHIMICĂ
de către

fiz. Dorica-Magdalena Ardelean

Conducător științific:
Referenți științifici:

prof.univ.dr.ing. Rodica Pode
prof.univ.dr. Joop Schoonman
prof.univ.dr. Ciprian Radovan
prof.univ.dr.ing. Florica Manea

Ziua susținerii tezei: 3.04.2015

Seriile Teze de doctorat ale UPT sunt:

- | | |
|---|--|
| 1. Automatică | 9. Inginerie Mecanică |
| 2. Chimie | 10. Știința Calculatoarelor |
| 3. Energetică | 11. Știința și Ingineria Materialelor |
| 4. Ingineria Chimică | 12. Ingineria sistemelor |
| 5. Inginerie Civilă | 13. Inginerie energetică |
| 6. Inginerie Electrică | 14. Calculatoare și tehnologia informației |
| 7. Inginerie Electronică și Telecomunicații | 15. Ingineria materialelor |
| 8. Inginerie Industrială | 16. Inginerie și Management |

Universitatea Politehnica Timișoara a inițiat seriile de mai sus în scopul diseminării expertizei, cunoștințelor și rezultatelor cercetărilor întreprinse în cadrul Școlii doctorale a universității. Seriile conțin, potrivit H.B.Ex.S Nr. 14 / 14.07.2006, tezele de doctorat susținute în universitate începând cu 1 octombrie 2006.

Copyright © Editura Politehnica – Timișoara, 2015

Această publicație este supusă prevederilor legii dreptului de autor. Multiplicarea acestei publicații, în mod integral sau în parte, traducerea, tipărirea, reutilizarea ilustrațiilor, expunerea, radiodifuzarea, reproducerea pe microfilme sau în orice altă formă este permisă numai cu respectarea prevederilor Legii române a dreptului de autor în vigoare și permisiunea pentru utilizare obținută în scris din partea Universității Politehnica Timișoara. Toate încălcările acestor drepturi vor fi penalizate potrivit Legii române a drepturilor de autor.

România, 300159 Timișoara, Bd. Republicii 9,
Tel./fax 0256 403823
e-mail: editura@edipol.upt.ro

Acknowledgement

This thesis was elaborated during my activity as a PhD student of **Politehnica** University of Timișoara, Faculty of Industrial Chemistry and Environmental Engineering.

This work was partially supported by the Romanian National Research Program PNII-60/2012 and by the Romanian-Swiss Joint Research Program IZERZO -142210/1 and by the strategic grant POSDRU/159/1.5/S/137070 (2014) of the Ministry of National Education Protection, Romania, co-financed by the European Social Fund–Investing in People, within the Sectorial Operational Programme Human Resources Development 2007-2013.

In this context, I would like to express all my gratitude to my PhD supervisor **Prof. PhD. Eng. Rodica PODE** for all her support, encouragement and advices.

All my profound gratitude is heading to **Prof. PhD. Eng. Florica MANEA** for all the support, precious advices and guidance during these years. Thank you for believing in me and accepting me as a member of your research group. I hope this collaboration was as fruitful as it was for me.

Very special thanks are headed to my supervising committee **Prof. PhD. Eng. Francisc PETER**, **Prof. PhD. Joop SCHOONMAN** and **Prof. PhD. Ciprian RADOVAN** for finding time to read and evaluate this manuscript and also for their valuable suggestions.

This work would not be possible without my former preparation as a student of **West University of Timișoara, Faculty of Physics**. For this reason I would like to acknowledge all my former professors of this faculty, and especially **Prof. PhD. Agneta BALINT** for her constant support and encouragements.

Le mulțumesc din sulfet prietenilor dragi și oamenilor minunați care mi-au fost alături, uneori mai mult, alteori mai puțin, și au pus o pietricică la formarea mea ca și **om**. Vă mulțumesc pentru toate gândurile bune, sfaturile, criticile și suportul moral.

Nu în ultimul rând le mulțumesc părinților mei pentru educația oferită și pentru toate eforturile pe care le-au făcut pentru mine și fratele meu. De asemenea, îi mulțumesc fratelui meu pentru toate criticile, încurajările și ajutorul acordat. Chiar dacă uneori gândim diferit, sunt mândră de tine, Bro!

Timișoara, April 2015

Magdalena Ardelean

Ardelean, Dorica-Magdalena

Detection of pharmaceuticals and anions in water using carbon-based electrodes

Teze de doctorat ale UPT, Seria 4, Nr. 83, Editura Politehnica, 2015, 152 pagini, 93 figuri, 52 tabele.

ISSN: 1842-8223

ISBN: 978-606-554-935-7

Cuvinte cheie: carbon nanofiber, carbon nanotube, electrochemical techniques, fluoxetine, naproxen, tetracycline, sulfide, nitrite

Rezumat,

Important resource for supporting life in all ecosystems, water is daily affected by the anthropogenic pressures which will impose serious repercussions over its quality. For this reason, at global level several regulations were adopted in order to reduce the pollution, but also to improve the quality of water.

With all this, in the last years, the occurrence in water of a new class of emerging pollutants - pharmaceuticals was revealed by several studies. Their detection mainly through chromatographic methods is quite laborious and time-consuming. In this context, an alternative to classical methods is developed by employing the applications of electroanalysis.

The aim of this study consisted of the development of fast and low-cost individual/simultaneous procedure for pharmaceuticals detection in aqueous solutions using electrochemical techniques and carbon-based electrode materials. In addition, similar procedures for the detection of specific anions in water by using the same carbon-based electrode materials were developed.

Several types of composite electrodes based on carbon nanofiber and carbon nanotube were prepared. The morphostructural, electrical and electrochemical characterization of these electrodes showed a great potential for electroanalytical applications. The electrochemical behaviour of each target analyte on the composite electrodes was studied by cyclic voltammetry in the presence of various concentration ranges. Based on the best sensitivity and lowest potential detection value, it was selected the electrode materials for voltammetric/amperometric detection schemes. The individual/simultaneous detection protocols for target pharmaceutical compounds, *i.e.*, fluoxetine, naproxen, tetracycline, and for sulfide and nitrite anions were developed in relation with the electrode material and the electrochemical technique. The obtained results are very promising and constitute the first step for developing *in-situ* or *in-field* detection applications.

CONTENT

| | |
|---|----|
| Abbreviation | 7 |
| List of figures | 9 |
| List of tables | 19 |
| Extended abstract | 21 |
| Chapter 1. Introduction | 27 |
| 1.1. References | 28 |
| Chapter 2. Pharmaceuticals and anions for water quality | 29 |
| 2.1. Pharmaceuticals and water quality | 29 |
| 2.2. Anions and water quality | 32 |
| 2.2.1. Nitrite and nitrate anions for water quality | 33 |
| 2.2.2. Sulfide anions for water quality | 34 |
| 2.3. References | 36 |
| Chapter 3. Carbon-based electrodes | 38 |
| 3.1. Carbon electrodes | 38 |
| 3.1.1. Boron-doped diamond electrodes | 38 |
| 3.1.2. Carbon nanotubes | 39 |
| 3.1.3. Carbon nanofibers | 41 |
| 3.2. Chemically-modified electrodes | 43 |
| 3.2.1. Zeolite-modified electrodes | 43 |
| 3.2.2. Electrochemically decorated electrodes | 44 |
| 3.3. References | 44 |
| Chapter 4. Electrochemical techniques used in analytical applications | 49 |
| 4.1. Cyclic voltammetry | 49 |
| 4.2. Differential-pulsed voltammetry..... | 54 |
| 4.3. Square wave voltammetry | 57 |
| 4.4. Chronoamperometry | 59 |
| 4.5. References | 60 |
| Chapter 5. Motivation, scope and thesis objectives | 64 |
| Chapter 6. Preparation of carbon-based composite electrodes | 66 |
| 6.1. Materials | 66 |
| 6.2. Preparation methodology of carbon-based composite electrodes | 67 |
| 6.2.1. Preparation of CNF/CNT composite electrodes | 67 |
| 6.2.2. Preparation of AgZ-CNF/AgZ-CNT composite electrodes | 67 |
| 6.2.3. Preparation of Ag-CNF composite electrode | 68 |
| 6.3. Techniques and methods for electrode characterization | 68 |
| 6.3.1. Morphology characterization | 68 |
| 6.3.2. Electrical characterization | 68 |
| 6.3.3. Electrochemical characterization | 69 |
| 6.4. References | 69 |
| Chapter 7. Characterization of carbon-based composite electrodes | 71 |
| 7.1. Morphology of carbon-based composite electrodes..... | 71 |
| 7.2. Electrical conductivity of carbon-based composite electrodes | 73 |
| 7.3. Electrochemical characterization of carbon-based composite electrodes.. | 74 |
| 7.4. References | 78 |
| Chapter 8. Electrochemical detection of pharmaceuticals in water | 79 |
| 8.1. Electrochemical detection of fluoxetine in water | 79 |
| 8.1.1. Introduction | 79 |
| 8.1.2. Electrochemical characterization of carbon-based materials in the presence of fluoxetine | 80 |

| | |
|--|-----|
| 8.1.2.1. Electrochemical detection of fluoxetine on BDD electrode | 82 |
| 8.1.2.2. Electrochemical detection of fluoxetine on CNF electrode | 88 |
| 8.1.2.3. Electrochemical detection of fluoxetine on AgZ-CNF electrode | 91 |
| 8.1.2.4. Electrochemical detection of fluoxetine on Ag-CNF electrode | 95 |
| 8.1.3. Conclusions | 97 |
| 8.2. Electrochemical detection of naproxen in water | 98 |
| 8.2.1. Introduction | 98 |
| 8.2.2. Electrochemical detection of naproxen | 99 |
| 8.2.3. Conclusions | 102 |
| 8.3. Electrochemical detection of tetracycline in water | 103 |
| 8.3.1. Introduction | 103 |
| 8.3.2. Electrochemical detection of tetracycline | 104 |
| 8.3.3. Conclusions | 106 |
| 8.4. Simultaneous electrochemical detection of pharmaceuticals in water.... | 107 |
| 8.4.1. Simultaneous electrochemical detection of naproxen and fluoxetine | 107 |
| 8.4.2. Simultaneous electrochemical detection of tetracycline and fluoxetine | 109 |
| 8.4.3. Conclusions | 112 |
| 8.5. References | 113 |
| Chapter 9. Electrochemical detection of anions in water | 117 |
| 9.1. Electrochemical detection of sulfide anion in water | 117 |
| 9.1.1. Introduction | 117 |
| 9.1.2. Carbon-based materials tested for sulfide detection | 118 |
| 9.1.3. Application on surface water sample | 130 |
| 9.1.4. Conclusions | 132 |
| 9.2. Simultaneous electrochemical detection of sulfide and nitrite anions in water | 132 |
| 9.2.1. Introduction | 132 |
| 9.2.2. Simultaneous electrochemical detection of sulfide and nitrite on boron-doped diamond electrode using voltammetric/amperometric techniques | 133 |
| 9.3. Conclusions | 142 |
| 9.4. References..... | 143 |
| Chapter 10. General conclusions..... | 145 |
| List of publications | 149 |

ABBREVIATIONS

| | |
|-----------------------|--|
| a | Pulse amplitude |
| Ag-CNF | Silver electrodeposited carbon nanofiber electrode |
| AgZ | Silver-modified zeolite |
| AgZ-CNF | Silver-modified zeolite carbon nanofiber electrode |
| AgZ-CNT | Silver-modified zeolite carbon nanotube electrode |
| AVS | Anodic stripping voltammetry |
| BDD | Boron-doped diamond electrode |
| BIA | Batch injection analysis |
| CA | Chronoamperometry |
| CE | Counter electrode |
| CME | Chemically modified electrodes |
| CNF | Carbon nanofiber |
| CNT | Carbon nanotube |
| CPE | Carbon paste electrode |
| CV | Cyclic voltammetry |
| CVD | Chemical vapour deposition |
| DPV | Differential-pulsed voltammetry |
| DyNW | Dysprosium nanowires |
| EDX | Energy dispersive X-ray spectroscopy |
| EE2 | Ethinyl estradiol |
| EIC | Expected introductory concentration |
| EPPG | Edge plane-pyrolytic graphite electrode |
| E_{ox} | Oxidation potential |
| ΔE_s | Step potential |
| f | Frequency |
| FXT | Fluoxetine |
| FPP | Four-point probe |
| GCE | Glassy carbon electrode |
| LOD | Limit of detection |
| LOQ | Limit of quantification |
| LSV | Linear sweep voltammetry |
| MWCNT | Multi-walled carbon nanotubes |
| NPs | Nanoparticles |
| NPX | Naproxen |
| NSAIDs | Non-steroidal anti-inflammatory drugs |
| PAD | Pulsed amperometric detection |
| PBS | Phosphate buffer saline |
| RE | Reference electrode |
| RSD | Relative standard deviation |
| SCE | Saturated calomel reference electrode |
| SEM | Scanning electronic microscopy |
| STP | Sewage treatment plant |
| SWCNT | Single-walled carbon nanotubes |
| SWV | Square wave voltammetry |

8 Abbreviations

| | |
|-------------|----------------------------|
| TC | Tetracycline |
| THF | Tetrahydrofuran |
| TRM | Two-roll mill procedure |
| v | Scan rate |
| WE | Working electrode |
| WWTP | Wastewater treatment plant |

LIST OF FIGURES

- Figure 1.1.** Water distribution diagram on Earth
- Figure 2.1.** The global pharmaceuticals market evolution between 2003-2011
- Figure 2.2.** Representation of sources and fate of pharmaceuticals in the environment (adapted after Santos [12])
- Figure 2.3.** Nitrate vulnerable areas in the Danube river basin
- Figure 3.1.** Structure of **a.** fullerene; **b.** SWCNT and **c.** MWCNT
- Figure 3.2.** Structures of carbon nanofibers
- Figure 4.1.** Experimental set-up used to record cyclic voltammograms
- Figure 4.2.** Potential-time excitation signal in a cyclic voltammetry experiment
- Figure 4.3.** Typical cyclic voltammogram of a reversible redox couple during a single potential scan
- Figure 4.4.** Scan rate vs. irreversibility dependence
- Figure 4.5.** **a.** Pulse excitation signal and **b.** corresponding differential-pulsed voltammogram
- Figure 4.6.** **a.** Pulse excitation signal and **b.** corresponding square wave voltammogram
- Figure 4.7.** Potential –time waveform (left) and current-time response (right) in **a.** single step, **b.** double step of chronoamperometry
- Figure 6.1.** Schematically protocol of CNF/CNT composite electrode preparation
- Figure 6.2.** Schematically protocol of AgZ-CNF composite electrode preparation
- Figure 6.3.** **a)** Image of a potentiostat / galvanostat type PGSTAT 302 (EcoChemie); **b)** three –electrode cell.
- Figure 7.1.** SEM image of: **a.** CNF, **b.** AgZ-CNF composite electrode
- Figure 7.2.** SEM image of Ag-CNF composite electrode
- Figure 7.3.** EDX spectrum of Ag-CNF composite electrode
- Figure 7.4.** SEM image of: **a.** CNT and **b.** AgZ-CNT composite electrode.
- Figure 7.5.** Cyclic voltammograms recorded on carbon-based composite electrode in 1M KNO₃ supporting electrolyte and in the presence of 4mM K₃Fe(CN)₆ at different potential scan rates 1- 0.025, 2- 0.05, 3- 0.1, 4- 0.2, 5- 0.3 Vs⁻¹ in the potential range from -1 to +1.5 V/SCE at: **a.** CNF electrode; **b.** AgZ-CNF electrode; **c.** CNT electrode; **d.** AgZ-CNT electrode.
- Figure 7.6.** Plots of the anodic and cathodic peaks vs. the logarithm of the scan rate: 0.025, 0.05, 0.1, 0.2, 0.3, Vs⁻¹, of CV recorded on **a.** CNF electrode; **b.** AgZ-CNF electrode; **c.** CNT electrode; **d.** AgZ-CNT electrode.
- Figure 7.7.** Calibration plots of the anodic and cathodic peak currents vs. the square root of the scan rate: 0.025, 0.05, 0.1, 0.2, 0.3, Vs⁻¹ of CV recorded on: **a.** CNF electrode; **b.** AgZ-CNF electrode; **c.** CNT electrode; **d.** AgZ-CNT electrode.
- Figure 8.1.** Cyclic voltammograms recorded using 0.1 M Na₂SO₄ supporting

- electrolyte (curve 1) on **a.** BDD electrode in the presence of 0.5 μM FXT (curves 2), **b.** CNF, **c.** AgZ-CNF, **d.** CNT electrode in the presence of 1 μM FXT (curves 2) at a potential scan rate of 0.05 Vs^{-1} .
- Figure 8.2.** **a.** Cyclic voltammograms recorded at BDD electrode in 0.1 M Na_2SO_4 supporting electrolyte (curve 1) in the presence of 0.05-0.5 μM FXT (curves 2-11), at a potential scan rate of 0.05 Vs^{-1} in a potential range from 0 to +1.5 V/SCE; **b.** The calibration plot of the currents recorded at $E=+1.35$ V/SCE vs. FXT concentration.
- Figure 8.3.** **a.** Cyclic voltammograms recorded on BDD electrode in 0.1 M Na_2SO_4 (curve 1) supporting electrolyte in the presence of 0.5 μM FXT at different scan rates 0.01 - 0.2 Vs^{-1} (curves 2-9); **b.** The calibration of the anodic peak current vs. the square root of the scan rate; **c.** Calibration plot of the peak potential E vs. $\log(v)$.
- Figure 8.4.** Molecular structure of radical R.
- Figure 8.5.** Differential-pulsed voltammograms recorded on BDD electrode in 0.1 M Na_2SO_4 supporting electrolyte (curve 1) in the presence of 0.2 μM FXT in a potential range from +0.5 to +1.5V/SCE at modulation amplitude of 0.2V, potential scan rate of 0.05 Vs^{-1} and step potential of 0.01V (curve 2), 0.025V (curve 3), 0.05V (curve 4).
- Figure 8.6.** **a.** Differential-pulsed voltammograms recorded on BDD electrode under optimized conditions: modulation amplitude of 0.2V, step potential of 0.05V and potential scan rate of 0.025 Vs^{-1} in a potential range from +0.5 to +1.5V vs. SCE in 0.1 M Na_2SO_4 supporting electrolyte (curve 1) in the presence of different FXT concentrations: 0.05- 0.5 μM (curves 2-11); **b.** The calibration plot of the currents recorded at $E=+1.25$ V/SCE vs. FXT concentration.
- Figure 8.7.** **a.** Square wave voltammograms recorded on BDD electrode under 0.2 V modulation amplitude, 0.05 Vstep potential, 50 Hz frequency in a potential range from 0 to +1.5V/SCE in 0.1 M Na_2SO_4 supporting electrolyte (curve 1) in the presence of 0.05-0.5 μM FXT (curves 2-11); **b.** The calibration plot of the currents recorded at $E=+1.247$ V/SCE vs. FXT concentration.
- Figure 8.8.** **a.** Square wave voltammograms recorded on BDD electrode under optimized conditions: 0.2 V modulation amplitude, 0.05 V step potential, 100 Hz frequency in a potential range from 0 to +1.5 V/SCE in 0.1 M Na_2SO_4 supporting electrolyte (curve 1) in the presence of 0.05-0.5 μM FXT (curves 2-11); **b.** The calibration plot of the currents recorded at $E=+1.25$ V/SCE vs. FXT concentration.
- Figure 8.9.** **a.** Chronoamperogram recorded at $E=+1.4$ V/SCE on BDD electrode in 0.1 M Na_2SO_4 supporting electrolyte and in the presence of 0.05-0.4 μM FXT; **b.** The calibration plot of the currents vs. FXT concentration.
- Figure 8.10.** **a.** Cyclic voltammograms recorded at CNF electrode in 0.1 M Na_2SO_4 supporting electrolyte (curve 1) and in the presence of 1-6 μM FXT (curves 2-7), at a potential scan rate of 0.05 Vs^{-1} in a potential range from 0 to +1.5 V/SCE; **b.** The calibration plot of the currents recorded at $E=+0.98$ V/SCE vs. FXT concentration.

- Figure 8.11.** **a.** Differential-pulsed voltammograms recorded on CNF electrode under modulation amplitude of 0.2V, step potential of 0.05V and potential scan rate of 0.025 Vs^{-1} in a potential range from 0 to +1.25 V/SCE in 0.1 M Na_2SO_4 supporting electrolyte (curve 1) and in the presence of 0-6 μM FXT (curves 2-7); **b.** The calibration plot of the currents recorded at $E=+0.723 \text{ V/SCE}$ vs. FXT concentration.
- Figure 8.12.** **a.** Differential-pulsed voltammograms recorded on CNF electrode under optimized conditions: modulation amplitude of 0.05V, step potential of 0.01V and potential scan rate of 0.001 Vs^{-1} in a potential from +0.25 to +1.25 V/SCE in 0.1 M Na_2SO_4 supporting electrolyte (curve 1) in the presence of 0-6 μM FXT (curves 2-7); **b.** The calibration plot of the currents recorded at $E=+0.721 \text{ V/SCE}$ vs. FXT concentration.
- Figure 8.13.** **a.** Cyclic voltammograms recorded at Ag electrode in 0.1 M Na_2SO_4 supporting electrolyte (curve 1) in the presence of 1-6 μM FXT (curves 2-7) at a potential scan rate of 0.05 Vs^{-1} in a potential range from -0.35 to +0.35 V/SCE; **b.** The calibration plot of the currents recorded at $E=+0.312 \text{ V/SCE}$ vs. FXT concentration.
- Figure 8.14.** **a.** Cyclic voltammograms recorded at AgZ-CNF electrode in 0.1 M Na_2SO_4 supporting electrolyte (curve 1) in the presence of 1-5 μM FXT (curves 2-6) at potential scan rate of 0.05 Vs^{-1} in a potential range from 0 to +1.5 V/SCE; **b.** Calibration plots of the currents vs. FXT concentration.
- Figure 8.15.** Cyclic voltammograms recorded at AgZ-CNF electrode in 0.1 M Na_2SO_4 supporting electrolyte (curve 1) in the presence of 1-5 μM FXT (curves 2-6) at potential scan rate of 0.05 Vs^{-1} in a potential range from -0.35 to +0.35 V/SCE; **b.** Calibration plot of the currents recorded at $E=+0.331 \text{ V/SCE}$ vs. FXT concentration.
- Figure 8.16.** **a.** Cyclic voltammograms recorded at AgZ-CNF electrode in 0.1 M Na_2SO_4 supporting electrolyte (curve 1) in the presence of 0.5-3.5 μM FXT (curves 2-8) at potential scan rate of 0.05 Vs^{-1} in the potential range from -0.35 to +0.35 V/SCE; **b.** Calibration plot of the currents recorded at $E=+0.335 \text{ V/SCE}$ vs. FXT concentration.
- Figure 8.17.** **a.** Chronoamperograms recorded at AgZ-CNF electrode in 0.1 M Na_2SO_4 supporting electrolyte (curve 1) at the potential values of $E_1=+0.35\text{V/SCE}$ and $E_2=+1.1 \text{ V/SCE}$ in the presence of 1-6 μM FXT (curves 2-7); Inset: Detail of chronoamperograms recorded at potential value of $E_1=+0.35 \text{ V/SCE}$; **b.** Calibration plots of the currents recorded at $E_1=+0.35 \text{ V/SCE}$ and $E_2=+1.1 \text{ V/SCE}$ vs. FXT concentration.
- Figure 8.18.** **a.** Chronoamperograms recorded at AgZ-CNF electrode in 0.1 M Na_2SO_4 supporting electrolyte at the potential values of +0.35 V/SCE in the presence of 1-6 μM FXT; **b.** Calibration plot of the currents vs. FXT concentrations recorded at $E=+0.35\text{V/SCE}$.
- Figure 8.19.** **a.** Chronoamperograms recorded at AgZ-CNF electrode in 0.1 M Na_2SO_4 supporting electrolyte at the potential values of +1.1 V/SCE in the presence of 1-6 μM FXT; **b.** Calibration plot of the currents vs. FXT concentration recorded at $E=+1.1 \text{ V/SCE}$.
- Figure 8.20.** **a.** Cyclic voltammograms recorded at Ag-CNF electrode in 0.1 M

- Figure 8.21.** **a.** Cyclic voltammograms recorded at Ag-CNF electrode in 0.1 M Na₂SO₄ supporting electrolyte (curve 1) in the presence of 1-6 μM FXT (curves 2-7) at potential scan rate of 0.05 Vs⁻¹ in a potential range from 0 to +1.5 V/SCE; **b.** The calibration plot of the currents recorded at E=+1.167 V/SCE vs. FXT concentration.
- Figure 8.22.** **a.** Chronoamperograms recorded on Ag-CNF electrode at the potential values of E₁=+0.35V/SCE and E₂=+1.1 V/SCE in 0.1 M Na₂SO₄ supporting electrolyte (curve 1) in the presence of 1-6 μM FXT (curves 2-7); Inset: Detail of chronoamperograms recorded at +0.35 V/SCE potential value; **b.** Calibration plots of the currents vs. FXT concentrations.
- Figure 8.23.** **a.** Cyclic voltammograms recorded on BDD electrode in 0.1 M Na₂SO₄ supporting electrolyte (curve 1) in the presence of 50 μL 0.1M NaOH (curve 2) and 0.1-1 μM NPX (curves 3-12), at a potential scan rate of 0.05 Vs⁻¹ in a potential range from 0 to +1.5 V/SCE; **b.** Calibration plot of the currents recorded at E=+1.425 V/SCE vs. NPX concentration.
- Figure 8.24.** **a.** Cyclic voltammograms recorded on CNF electrode in 0.1 M Na₂SO₄ supporting electrolyte (curve 1) in the presence of 50 μL 0.1M NaOH (curve 2) and 1-10 μM NPX (curves 3-12), at a potential scan rate of 0.05 Vs⁻¹ in a potential range from 0 to +1.5 V/SCE; **b.** Calibration plot of the currents recorded at E=+1.21 V/SCE vs. NPX concentration.
- Figure 8.25.** **a.** Differential-pulsed voltammograms recorded on CNF electrode under modulation amplitude of 0.2V, step potential of 0.05V and potential scan rate of 0.025 Vs⁻¹ in a potential range from +0.35 to +1.35 V/ SCE in 0.1 M Na₂SO₄ supporting electrolyte (curve 1) in the presence of 50 μL 0.1M NaOH (curve 2) and 1-6 μM NPX (curves 3-8); **b.** Calibration plot of the currents recorded at E=+0.95 V/SCE vs. NPX concentration.
- Figure 8.26.** **a.** Square wave voltammograms recorded on CNF electrode under modulation amplitude of 0.05V, step potential of 0.005V and a frequency of 10 Hz in a potential range from 0 to +1.45 V/SCE in 0.1 M Na₂SO₄ supporting electrolyte (curve 1) in the presence of 50 μL 0.1M NaOH (curve 2) and 1-6 μM NPX (curves 3-8); **b.** Calibration plot of the currents recorded at E=+1.1V/SCE vs. NPX concentration.
- Figure 8.27.** **a.** Cyclic voltammograms recorded on CNF electrode in 0.1 M Na₂SO₄ supporting electrolyte (curve 1) in the presence of 50 μL 0.1M NaOH (curve 2) and 1-10 μM TC (curves 3-12), at a potential scan rate of 0.05 Vs⁻¹ in a potential range from 0 to +1.5 V/SCE; **b.** Calibration plots of the currents recorded at E₁=+0.714 V/SCE and E₂=+1.0745 V/SCE vs. TC concentrations.
- Figure 8.28.** **a.** Differential-pulsed voltammograms recorded on CNF electrode under modulation amplitude of 0.2V, step potential of 0.05V and potential scan rate of 0.025 Vs⁻¹ in a potential range from 0 to +1.25 V/SCE in 0.1 M Na₂SO₄ supporting electrolyte (curve 1) in

- the presence of 50 μL 0.1M NaOH (curve 2) and 1-10 μM TC (curves 3-12); **b.** Calibration plots of the current recorded at $E_1=+0.48$ V/SCE and $E_2=+0.925$ V/SCE vs. TC concentrations.
- Figure 8.29.** **a.** Square wave voltammograms recorded on CNF electrode under optimized conditions: modulation amplitude of 0.2V, step potential of 0.05V and a frequency of 100 Hz in a potential range from +0.35 to +1.35 V/SCE in 0.1 M Na_2SO_4 supporting electrolyte (curve 1) in the presence of 50 μL 0.1M NaOH (curve 2) and 1-10 μM TC (curves 3-12); **b.** Calibration plots of the currents recorded at $E_1=+0.645$ V/SCE and $E_2=+1.02$ V/SCE vs. TC concentrations.
- Figure 8.30.** **a.** Chronoamperograms recorded on CNF electrode at the potential values of $E_1=+0.75$ V/SCE and $E_2=+1.2$ V/SCE in 0.1 M Na_2SO_4 supporting electrolyte (curve 1) in the presence of 50 μL 0.1M NaOH (curve 2) and 1-10 μM TC (curves 3-12); Inset: Detail of chronoamperograms recorded at +0.75 V/SCE potential value; **b.** Calibration plots of the currents vs. TC concentrations.
- Figure 8.31.** **a.** Cyclic voltammograms recorded on CNF electrode in 0.1 M Na_2SO_4 supporting electrolyte (curve 1) in the presence of 50 μL 0.1M NaOH (curve 2) and 3-15 μM NPX (curves 3-7), and 3-15 μM FXT (curves 8-12) at a potential scan rate of 0.05 Vs^{-1} in a potential range from 0 to +1.5 V/SCE; **b.** Calibration plots of the currents recorded at $E_{\text{NPX}}=+1.36$ V/SCE and $E_{\text{FXT}}=+0.785$ V/SCE vs. NPX and FXT concentrations.
- Figure 8.32.** **a.** Differential pulsed voltammograms recorded on CNF electrode under conditions of 0.2V modulation amplitude, 0.1V step potential and 0.05 Vs^{-1} potential scan rate for a potential range from 0 to +1.4 V/SCE in 0.1 M Na_2SO_4 supporting electrolyte (curve 1) in the presence of 50 μL 0.1M NaOH (curve 2) and 3 - 15 μM TC (curves 3-7), and 3 - 15 μM FXT (curves 8-12); **b.** Calibration plots of the currents $E_{\text{NPX}}=+1.202$ V/SCE and $E_{\text{FXT}}=+0.607$ V/SCE vs. NPX and FXT concentrations.
- Figure 8.33.** **a.** Cyclic voltammograms recorded on CNF electrode in 0.1 M Na_2SO_4 supporting electrolyte (curve 1) in the presence of 50 μL 0.1M NaOH (curve 2) and 0.5-2.5 μM TC (curves 3-7), and 2-10 μM FXT (curves 8-14) at a potential scan rate of 0.05 Vs^{-1} in a potential range from 0 to +1.35 V/SCE; **b.** Calibration plots of the currents recorded at $E_1=+0.815$ V/SCE and $E_2=+1.14$ V/SCE vs. TC concentrations; **c.** Calibration plot of the currents recorded at $E=+0.815$ V/SCE vs. FXT concentrations.
- Figure 8.34.** **a.** Differential-pulsed voltammograms recorded on CNF electrode under optimized conditions: modulation amplitude of 0.2V, step potential of 0.05V and potential scan rate of 0.025 Vs^{-1} in a potential range from 0 to +1.35 V/SCE in 0.1 M Na_2SO_4 supporting electrolyte (curve 1) in the presence of 50 μL 0.1M NaOH (curve 2) and 0.5-2.5 μM TC (curves 3-7), and 2-10 μM FXT (curves 8-12); **b.** Calibration plots of the currents at $E_1=+0.665$ V/SCE and $E_2=+0.956$ V/SCE vs. TC concentrations; **c.** Calibration plot of the currents vs. FXT concentration recorded at $E_{\text{FXT}}=+0.665$ V/SCE.
- Figure 8.35.** **a.** Square wave voltammograms recorded on CNF electrode under

- optimized conditions: modulation amplitude of 0.2V, step potential of 0.05V and a frequency of 100 Hz in a potential range from 0 to +1.35V/SCE in 0.1 M Na₂SO₄ supporting electrolyte (curve 1) in the presence of 50 μL 0.1M NaOH (curve 2) and 0.5-2.5 μM TC (curves 3-7), and 2-10 μM FXT (curves 8-12); **b.** Calibration plots of the currents recorded at E₁= +0.675V/SCE and E₂=+1.116 V/SCE vs. TC concentrations; **c.** Calibration plot of the currents recorded at E=+0.74V/SCE vs. FXT concentration.
- Figure 9.1.** Cyclic voltammograms recorded on: **a.** BDD, **b.** CNF, **c.** CNT, **d.** AgZ-CNT electrode in 0.1 M Na₂SO₄ supporting electrolyte (curve 1) in the presence of 0.5 mM (curves 2) sulfide, at a potential scan rate of 0.05 Vs⁻¹ in a potential range from 0 to +1 V/SCE for BDD electrode and from -0.5 to +1.1V/SCE for composite electrodes.
- Figure 9.2.** **a.** Cyclic voltammograms recorded on BDD electrode in 0.1 M Na₂SO₄ supporting electrolyte (curve 1) in the presence of 0.1-0.7; 1 mM (curves 2-9) sulfide, at a potential scan rate of 0.05 Vs⁻¹ in a potential range from 0 to +1 V/SCE; **b.** The calibration plot of the currents recorded at E=+0.92 V/SCE vs. sulfide concentration.
- Figure 9.3.** **a.** Cyclic voltammograms recorded on CNF electrode in 0.1 M Na₂SO₄ supporting electrolyte (curve 1) in the presence of 0.1-1 mM sulfide (curves 2-11) at a potential scan rate of 0.05 Vs⁻¹ in a potential range from -0.5 to +1.1 V/SCE; **b.** The calibration plot of the currents recorded at E=+0.715 V/SCE vs. sulfide concentration.
- Figure 9.4.** Cyclic voltammograms recorded at **a.** BDD and **b.** CNF electrode in 0.1 M Na₂SO₄ supporting electrolyte (curve 1) and simulated seawater (curve 2) at a potential scan rate of 0.05 Vs⁻¹.
- Figure 9.5.** **a.** Cyclic voltammograms recorded on BDD electrode in simulated seawater (curve 1) supporting electrolyte in the presence of 0.1-1 mM sulfide (curves 2-11), at a potential scan rate of 0.05 Vs⁻¹ in a potential range from 0 to +1 V/SCE; **b.** The calibration plot of the currents recorded at E=+0.915 V/SCE vs. sulfide concentration.
- Figure 9.6.** **a.** Cyclic voltammograms recorded on CNF electrode in simulated seawater (curve 1) supporting electrolyte in the presence of 0.1-1 mM sulfide (curves 2-11) at a potential scan rate of 0.05 Vs⁻¹ in a potential range from -0.5 to +1.1 V/SCE; **b.** The calibration plot of the currents recorded at E=+0.8 V/SCE vs. sulfide concentrations.
- Figure 9.7.** The distribution diagram of sulfide species. *Source: Duranceau et al. (2010)
- Figure 9.8.** Cyclic voltammograms recorded on BDD electrode in simulated seawater (curve 1) supporting electrolyte in the presence of 0.05 mM sulfide (curve 2) at a potential scan rate of 0.05 Vs⁻¹ in a potential range from -0.5 to +1.1 V/SCE at a pH value of **a.** 4; **b.** 7; **c.** 11.
- Figure 9.9.** Cyclic voltammograms recorded on BDD electrode in simulated seawater (curve 1) supporting electrolyte in the presence of 0.5 mM sulfide in a potential range from 0 to +1 V/SCE, at different

- scan rates: 0.01, 0.02, 0.03, 0.04, 0.05, 0.075, 0.1, 0.2 Vs^{-1} (curves 2-8); **b.** The calibration plots of the anodic peak current vs. square root of the scan rate; **c.** The calibration plots of the peak potential E vs. $\log(v)$.
- Figure 9.10.** **a.** Cyclic voltammograms recorded on CNF electrode in simulated seawater supporting electrolyte (curve 1) in the presence of 0.5 mM sulfide in a potential range from 0 to +1.1 V/SCE, at different scan rates: 0.01, 0.02, 0.03, 0.04, 0.05, 0.075, 0.1, 0.2 Vs^{-1} (curves 1-8); **b.** The calibration plots of the anodic peak current vs. square root of the scan rate; **c.** The calibration plots of the peak potential E vs. $\log(v)$.
- Figure 9.11.** **a.** Differential-pulsed voltammograms recorded on CNF electrode in simulated seawater supporting electrolyte (curve 1) under optimized conditions: $a=0.2\text{V}$; $\Delta E_s=0.05\text{V}$; $v=0.05\text{Vs}^{-1}$, in a potential range from -0.2 to +1 V/SCE in the presence of 0.1-0.7 mM sulfide (curves 2-8); **b.** The calibration plot of the currents recorded at $E=+0.22$ V/SCE vs. sulfide concentration.
- Figure 9.12.** **a.** Differential-pulsed voltammograms recorded on CNF electrode in simulated seawater supporting electrolyte (curve 1) under: $a=0.05\text{V}$; $\Delta E_s=0.01\text{V}$; $v=0.05\text{Vs}^{-1}$, in a potential range from -0.2 to +1 V/SCE in the presence of 0.1-1 mM sulfide (curves 2-11); **b.** The calibration plot of the currents recorded at $E=+0.696$ V/SCE vs. sulfide concentration.
- Figure 9.13.** **a.** Differential-pulsed voltammograms recorded on CNF electrode in simulated seawater supporting electrolyte (curve 1) under: $a=0.1\text{V}$; $\Delta E_s=0.02\text{V}$; $v=0.05\text{Vs}^{-1}$, in a potential range from -0.2 to +1 V/SCE in the presence of 0.1-1 mM sulfide (curves 2-11); **b.** The calibration plot of the currents recorded at $E=+0.66$ V/SCE vs. sulfide concentration.
- Figure 9.14.** **a.** Differential-pulsed voltammograms recorded on CNF electrode in simulated seawater supporting electrolyte (curve 1) under: $a=0.2\text{V}$; $\Delta E_s=0.01\text{V}$; $v=0.05\text{Vs}^{-1}$, in a potential range from -0.2 to +1 V/SCE in the presence of 0.1-1 mM sulfide (curves 2-11); **b.** The calibration plot of the currents recorded at $E=+0.193$ V/SCE vs. sulfide concentration.
- Figure 9.15.** **a.** Differential-pulsed voltammograms recorded on CNF electrode in simulated seawater supporting electrolyte (curve 1) under: $a=0.2\text{V}$; $\Delta E_s=0.1\text{V}$; $v=0.1\text{Vs}^{-1}$, in a potential range from -0.1 to +0.9 V/SCE in the presence of 0.1-0.8 mM sulfide (curves 2-9); **b.** The calibration plot of the currents recorded at $E=+0.305$ V/SCE vs. sulfide concentration.
- Figure 9.16.** **a.** Square wave voltammograms recorded on CNF electrode in simulated seawater supporting electrolyte (curve 1) under: $a=0.2\text{V}$; $\Delta E_s=0.05\text{V}$; $f=10$ Hz in a potential range from +0.2 to +1 V/SCE in the presence of 0.1-1 mM sulfide (curves 2-11); **b.** The calibration plot of the currents recorded at $E=+0.8$ V/SCE vs. sulfide concentration.
- Figure 9.17.** **a.** Square wave voltammograms recorded on CNF electrode in simulated seawater supporting electrolyte (curve 1) under: $a=0.2\text{V}$; $\Delta E_s=0.05\text{V}$; $f=25$ Hz in the potential range from +0.2 to +1 V/SCE in the presence of 0.1-1 mM sulfide (curves 2-11); **b.**

- The calibration plot of the currents recorded at $E=+0.83$ V/SCE vs. sulfide concentration.
- Figure 9.18.** **a.** Square wave voltammograms recorded on CNF electrode in simulated seawater supporting electrolyte (curve 1) under optimized conditions: $a=0.2$ V; $\Delta E_s=0.05$ V; $f=50$ Hz in a potential range from $+0.2$ to $+1$ V/SCE in the presence of 0.1 - 1 mM sulfide (curves 2-11); **b.** The calibration plots of the currents recorded at $E=+0.85$ V/SCE vs. sulfide concentration.
- Figure 9.19.** **a.** Chronoamperogram recorded on CNF electrode in simulated seawater supporting electrolyte at $E=+0.9$ V/SCE in the presence of 0.1 - 1 mM sulfide concentrations. **b.** The calibration plot of the currents vs. sulfide concentration.
- Figure 9.20.** **a.** Cyclic voltammograms recorded on CNF electrode in a real water sample (curve 1) in the presence of 0.1 - 1 mM sulfide (curves 2-11), at a potential scan rate of 0.05 Vs⁻¹ in a potential range from -0.5 to $+1.1$ V/SCE; **b.** The calibration plot of the currents recorded at $E=+0.85$ V/SCE vs. sulfide concentration.
- Figure 9.21.** **a.** Square-wave voltammograms recorded on CNF electrode in a real water sample (curve 1) under optimized conditions: $a=0.2$ V; $\Delta E_s=0.05$ V; $f=50$ Hz in a potential range from 0 to $+2$ V/SCE in the presence of 0.1 - 1 mM sulfide (curves 2-11); **b.** The calibration plot of the currents recorded at $E=+1.435$ V/SCE vs. sulfide concentration.
- Figure 9.22.** **a.** Chronoamperogram recorded on CNF electrode in a real water sample at $E=+0.9$ V/SCE in the presence of 0.1 - 1 mM sulfide concentrations. **b.** The calibration plot of the currents vs. sulfide concentration.
- Figure 9.23.** **a.** Cyclic voltammograms recorded at BDD electrode in 0.1 M Na₂SO₄ supporting electrolyte (curve 1) in the presence of 0.2 - 1 mM nitrite (curves 2-6), at a potential scan rate of 0.05 Vs⁻¹ in a potential range from $+0.5$ to $+1.5$ V/SCE; **b.** Calibration plot of the current recorded at $E=+1.35$ V/SCE vs. nitrite concentration.
- Figure 9.24.** **a.** Cyclic voltammograms recorded at BDD electrode in 0.1 M Na₂SO₄ supporting electrolyte (curve 1) in the presence of 0.02 - 0.1 mM sulfide (curves 2-5; Inset of figure), and 0.02 - 0.1 mM nitrite (curves 6-10) at a potential scan rate of 0.05 Vs⁻¹ in a potential range from $+0.5$ to $+1.5$ V/SCE; **b.** Calibration plots of the currents recorded at $E=+0.89$ V/SCE for sulfide and $E=+1.4$ V/SCE for nitrite vs. anion concentrations.
- Figure 9.25.** **a.** Cyclic voltammograms recorded at BDD electrode in 0.1 M Na₂SO₄ supporting electrolyte (curve 1) in the presence of 0.02 - 0.1 mM sulfide (curves 2-11) at a potential scan rate of 0.05 Vs⁻¹ in a potential range from $+0.5$ to $+1.5$ V/SCE; **b.** Calibration plots of the currents recorded at $E=+1$ V/SCE for sulfide and $E=+1.405$ V/SCE for nitrite vs. anion concentrations.
- Figure 9.26.** **a.** Differential-pulsed voltammograms recorded at BDD electrode in 0.1 M Na₂SO₄ supporting electrolyte (curve 1) in the presence of 0.02 - 0.1 mM of sulfide (curves 2-6) and a mixture of 0.1 mM sulfide and 0.02 - 0.1 mM nitrite (curves 7-11), under 0.1 V modulation amplitude, 0.025 V step potential, and 0.025 Vs⁻¹ scan rate in a potential range from $+0.25$ to $+1.5$ V/SCE; **b.**

- Calibration plots of the currents recorded at $E=+0.8$ V/SCE for sulfide and $E=+1.3$ V/SCE for nitrite vs. anion concentrations.
- Figure 9.27.** **a.** Differential-pulsed voltammograms recorded at BDD electrode in 0.1 M Na_2SO_4 supporting electrolyte (curve 1) in a mixture of 0.02-0.2 mM sulfide and 0.02-0.2 mM nitrite (curves 2-11), under 0.2V modulation amplitude, 0.01V step potential, and 0.1Vs^{-1} scan rate in a potential range from +0.25 to +1.5 V/SCE; **b.** Calibration plots of the currents recorded on $E=+0.775$ V/SCE for sulfide and $E=+1.275$ V/SCE for nitrite vs. anion concentrations.
- Figure 9.28.** **a.** Square wave voltammograms recorded on a BDD electrode under 0.001 V step potential and 0.01 V modulation amplitude, 50 Hz frequency, scan rate 0.05Vs^{-1} , in a potential range from +0.25 to +1.5 V/SCE in 0.1 M Na_2SO_4 supporting electrolyte (curve 1) and in the presence of 0.02– 0.14 mM sulfide and 0.02-0.14 mM nitrite concentrations (curve 2-8); **b.** Calibration plots of the currents recorded on $E=+0.905$ V/SCE for sulfide and $E=+1.35$ V/SCE for nitrite vs. anion concentrations.
- Figure 9.29.** **a.** Square wave voltammograms recorded on a BDD electrode under 0.001 V step potential and 0.01 V modulation amplitude, 100 Hz frequency, scan rate 0.1Vs^{-1} , in a potential range from +0.25 to +1.5 V/SCE in 0.1 M Na_2SO_4 supporting electrolyte (curve 1) and in the presence of 0.02– 0.2 mM sulfide and 0.02-0.2 mM nitrite concentrations (curve 2 - 11); **b.** Calibration plots of the currents recorded on $E=+0.918$ V/SCE for sulfide and $E=+1.385$ V/SCE for nitrite vs. anion concentrations.
- Figure 9.30.** Square wave voltammograms recorded at BDD electrode in 0.1 M Na_2SO_4 supporting electrolyte (curve 1) in the presence of 0.02-0.1 mM of sulfide (curves 2-6) and a mixture of 0.1mM sulfide and 0.02-0.1mM nitrite (curves 7-11), under 0.1V modulation amplitude, 0.01V step potential, and 10 Hz frequency in a potential range from +0.25 to +1.5 V/SCE; **b.** Calibration plots of the currents recorded on $E=+0.825$ V/SCE for sulfide and $E=+1.34$ V/SCE for nitrite vs. anion concentrations.
- Figure 9.31.** **a.** Square wave voltammograms recorded at BDD electrode in 0.1 M Na_2SO_4 supporting electrolyte (curve 1) in a mixture of 0.02-0.2 mM sulfide and nitrite (curves 2-11), under 0.1V modulation amplitude, 0.01V step potential, and 10Hz frequency in a potential range from +0.25 to +1.5 V/SCE; **b.** Calibration plots of the currents recorded on $E=+0.58$ V/SCE for sulfide and $E=+1.35$ V/SCE for nitrite vs. anion concentrations.
- Figure 9.32.** **a.** Square wave voltammograms recorded at BDD electrode in 0.1 M Na_2SO_4 supporting electrolyte (curve 1) in a mixture of 0.02-0.2 mM sulfide and of 0.02-0.2 mM nitrite (curves 2-11), under 0.2V modulation amplitude, 0.01V step potential and 10 Hz frequency in a potential range from +0.25 to +1.5 V/SCE; **b.** Calibration plots of the currents recorded on $E=+0.8$ V/SCE for sulfide and $E=+1.3$ V/SCE for nitrite vs. anion concentrations.
- Figure 9.33.** **a.** Square wave voltammograms recorded on a BDD electrode under 0.02 V step potential and 0.2 V modulation amplitude, 10 Hz frequency, scan rate 0.2Vs^{-1} , in a potential range from + 0.25

- to +1.5 V/SCE in 0.1 M Na₂SO₄ supporting electrolyte (curve 1) and in the presence of 0.02– 0.2 mM sulfide and 0.02– 0.2 mM nitrite concentrations (curve 2 - 6); **b.** Calibration plots of the currents recorded on E=+0.805 V/SCE for sulfide and E=+1.3 V/SCE for nitrite vs. anion concentrations.
- Figure 9.34.** **a.** Square wave voltammograms recorded on a BDD electrode under 0.02 V step potential and 0.5 V modulation amplitude, 10 Hz frequency, scan rate 0.2Vs⁻¹, in a potential range from +0.25 to +1.5 V vs. SCE in 0.1 M Na₂SO₄ supporting electrolyte (curve 1) and in the presence of 0.02– 0.2 mM sulfide and 0.02– 0.2 mM nitrite concentrations (curve 2 - 6), **b.** Calibration plots of the currents recorded on E=+0.515 V/SCE for sulfide and E=+1.035 V/SCE for nitrite vs. anion concentrations.
- Figure 9.35.** **a.** Chronoamperograms recorded at BDD electrode in 0.1 M Na₂SO₄ supporting electrolyte (curve 1) in a mixture of 0.02-0.1mM sulfide and 0.02-0.1mM nitrite (curves 2-6; see inset) and in the presence of 0.02-0.1mM nitrite (curves 7-11), under potentials E₁=+0.85V/SCE for sulfide and E₂=+1.25V/SCE for nitrite; **b.** Calibration plots of the currents recorded at E=+0.85 V/SCE for sulfide, respectively E=+1.25 V/SCE for nitrite vs. anion concentrations.

LIST OF TABLES

| | |
|--------------------|---|
| Table 2.1. | Occurrence of some pharmaceutical compounds in waters |
| Table 2.2. | Applied methods in pharmaceuticals detection |
| Table 2.3. | Characteristics of nitrate and nitrite |
| Table 2.4. | Nitrite and nitrate threshold values proposed by WHO and transposed under Romanian legislation |
| Table 2.5. | Human health effects of hydrogen sulfide exposure |
| Table 2.6. | Measured levels of hydrogen sulfide in the environment |
| Table 2.7. | Threshold values of sulfide under Romanian legislation |
| Table 3.1. | Basic properties of undoped diamond |
| Table 3.2. | Characteristics of SWCNTs and MWCNTs |
| Table 3.3. | Chemical and physical properties of CNF |
| Table 4.1. | Reversibility conditions used applied in cyclic voltammetry |
| Table 4.2. | Optimization criteria and the results obtained under optimization procedures |
| Table 4.3. | Dependence frequency vs. peak current in relation with the type of reaction |
| Table 4.4. | Research studies that applied the optimization methodology |
| Table 6.1. | Carbon based composite electrodes prepared in the laboratory |
| Table 7.1. | Electrical conductivity of composite electrodes |
| Table 7.2. | Assessment criteria of the reversible system |
| Table 7.3. | The electrochemical parameters of the redox system (ferri/ferrocyanide) determined from the anodic and cathodic branches of CVs on carbon nanofibers based composite electrodes |
| Table 7.4. | The electrochemical parameters of the redox system (ferri/ferrocyanide) determined from the anodic and cathodic branches of CVs on carbon nanotubes based composite electrodes |
| Table 7.5. | The reversibility parameters of the ferri/ferrocyanide redox system on tested carbon-based electrodes |
| Table 7.6. | The apparent diffusion coefficient and the electroactive surface area of the carbon nanostructured based composite electrodes |
| Table 8.1. | Information on fluoxetine, and fluoxetine hydrochloride |
| Table 8.2. | Useful signals of FXT on tested electrodes |
| Table 8.3. | The useful signal recorded for 0.2 μM FXT detection at various operating DPV parameters |
| Table 8.4. | The electroanalytical parameters of FXT detection at BDD electrode using SWV at different frequencies |
| Table 8.5. | The analytical parameters obtained at a BDD electrode using electrochemical techniques |
| Table 8.6. | The electroanalytical parameters obtained on CNF electrode |
| Table 8.7. | Electroanalytical parameters obtained at AgZ-CNF electrode for fluoxetine detection |
| Table 8.8. | The electroanalytical parameters obtained for Ag-CNF electrode |
| Table 8.9. | The electroanalytical parameters obtained for fluoxetine detection on tested electrodes |
| Table 8.10. | Information on naproxen, respectively naproxen sodium |

- Table 8.11.** Electrochemical studies performed in naproxen detection
- Table 8.12.** Useful signal of naproxen oxidation on tested electrodes
- Table 8.13.** Electroanalytical parameters obtained on studied electrodes for naproxen detection
- Table 8.14.** Information on tetracycline and tetracycline hydrochloride
- Table 8.15.** Electroanalytical parameters obtained on studied electrodes for tetracycline detection
- Table 8.16.** Electroanalytical parameters obtained for individual and simultaneous detection of fluoxetine and naproxen on CNF electrode
- Table 8.17.** Electroanalytical parameters obtained for simultaneous detection of fluoxetine and naproxen on CNF electrode
- Table 8.18.** Electroanalytical parameters obtained for individual and simultaneous detection of fluoxetine and tetracycline on CNF electrode
- Table 8.19.** Electroanalytical parameters obtained for simultaneous detection of fluoxetine and tetracycline on CNF electrode
- Table 9.1.** Analytical parameters obtained on various carbon substrates on sulfide detection
- Table 9.2.** Useful signal of composite and commercial tested electrodes
- Table 9.3.** Useful signals obtained for different pH values on BDD electrode
- Table 9.4.** The dependence of the sensitivity on the operating DPV parameters: modulation amplitude (**a**), step potential (ΔE_s) and scan rate (**v**)
- Table 9.5.** The dependence of sensitivity and correlation coefficient on square-wave voltammetry frequency applied under the optimized operating conditions: modulation amplitude of 0.2 V and step potential of 0.05 V
- Table 9.6.** Electroanalytical parameters obtained for the detection of sulfide in sodium sulphate and simulated seawater on studied electrode by applying electrochemical techniques
- Table 9.7.** Electroanalytical parameters obtained for the detection of sulfide in a real sample (Bega river) at CNF electrode by applying electrochemical techniques
- Table 9.8.** Electroanalytical parameters obtained on BDD electrode in simultaneous detection of sulfide and nitrite
- Table 9.9.** Electroanalytical parameters obtained under DPV operating conditions on BDD electrode
- Table 9.10.** Optimization of operating parameters of SWV and electroanalytical obtained on BDD electrode for simultaneous detection of sulfide and nitrite
- Table 9.11.** Electroanalytical parameters obtained for the simultaneous detection of nitrite and sulfide anions on BDD electrode
- Table 9.12.** The legal threshold values of both anions according to Romanian legislation

ABSTRACT EXTINS

Sursă importantă în menținerea echilibrului ecosistemelor, apa este supusă mereu numeroaselor presiuni antropice și naturale ce vor avea repercursiuni asupra calității acesteia, și prin urmare asupra bunei funcționări a ecosistemelor.

Numeroasele discuții din ultimii ani privind modificarea parametrilor de calitate datorită volumelor și toxicității poluanților, precum și existența anumitor deficiențe privind degradarea incompletă a anumitor poluanți în cadrul proceselor de epurare dovedesc o nevoie cât mai acută de a dezvolta noi metodologii eco-friendly atât pentru îmbunătățirea acestora, cât și pentru monitorizarea parametrilor și indicilor de calitate. În acest sens, luând în considerare propunerile oferite de către Organizația Mondială a Sănătății au fost adoptate numeroase măsuri legislative cu rolul de a impune o reducere a poluanților, respectiv a întregului proces de poluare, asigurând astfel o îmbunătățire a parametrilor de calitate. Cu toate acestea, poluarea este un proces continuu, iar datorită utilizării unui spectru extins de substanțe s-a conturat o nouă clasă de poluanți-compuși farmaceutici cu efecte diverse asupra mediului acvatic.

Deteția acestor compuși este destul de laborioasă și consumatoare de timp, bazându-se pe metode cromatografice, în principiu cromatografia gazoasă sau cromatografia lichidă, cuplate cu metode spectrometrice, de obicei spectrometria de masă. Din acest motiv, dezvoltarea unor metode de detecție mai ieftine și cu un timp de analiză redus, dar care să ofere o bună sensibilitate și selectivitate sunt binevenite, electroanaliza oferind astfel o alternativă.

În acest context, obiectivul major al acestui studiu îl constituie dezvoltarea unor proceduri de detecție individuale sau simultane, rapide, precise și ieftine, care să ofere o bună sensibilitate și selectivitate a unor compuși farmaceutici în apă utilizând tehnici electrochimice și materiale de electrod pe bază de carbon. În plus, au fost luați în considerare și doi anioni: sulfură și respectiv, nitrit pentru care au fost dezvoltate proceduri de detecție similare.

Obiectivele specifice conexe obiectivului general sunt următoarele:

- Dezvoltarea unor electrozi compoziți pe bază de carbon nanostructurat dedicați electroanalizei;
- Dezvoltarea unor electrozi modificați chimic (EMC) pe bază de carbon nanostructurat care să încorporeze argintul în compoziția electrodului pentru îmbunătățirea performanțelor electroanalitice;
- Caracterizarea morfologică, electrică și electrochimică a electrozilor compoziți pe bază de carbon nanostructurat în relație directă cu aplicațiile de electroanaliză;
- Elaborarea unor protocoale/scheme pentru analiza individuală/simultană a compușilor farmaceutici în matrici apoase pe baza tehnicilor electrochimice voltametrice/amperometrice. Pentru acest obiectiv sunt considerate două abordări, una se referă la detecția compușilor farmaceutici ca și poluanți emergent, iar cealaltă la dozarea acestora în formule farmaceutice pentru uz clinic;

- Elaborarea unor protocoale/scheme pentru analiza individuală/simultană a unor anioni specifici în apă, considerați ca și indicatori de calitate ai apei.

Astfel, au fost obținuți o serie de electrozi pe bază de nanotuburi de carbon, respectiv nanofibră de carbon înglobați în matricea polimerică epoxi: nanotuburi de carbon-epoxi (CNT), nanofibră de carbon-epoxi (CNF), nanofibră de carbon - zeolit natural dopat cu argint-epoxi (AgZ-CNF), nanofibre de carbon-epoxi decorat electrochimic cu argint (Ag-CNF) utilizând procedura cu două mori rulante. Sinteza materialelor de electrod compozit s-a bazat pe un protocol stabilit anterior, pentru care a fost determinat un conținut optim de material carbonic de 20%. Utilizarea argintului în compoziția electrodului a fost abordată în scopul îmbunătățirii performanțelor electroanalitice.

În urma caracterizărilor morfostructurale, și respectiv, electrochimice a acestor electrozi s-a observat că prin utilizarea procedurii cu două mori rulante, respectiv a tetrahidrofuranului ca și agent de dispersie o bună distribuție a filerelor de carbon (nanotuburi de carbon, nanofibră de carbon) în matricea epoxi a fost obținută, imaginile SEM confirmând acest aspect. De asemenea, prezența argintului immedie pe substratul de nanofibră de carbon a fost confirmat prin spectrul EDX, imaginile SEM arătând o distribuție aleatorie a particulelor electrodepuse. Aceste particule prezintă o afinitate mai ridicată pentru zonele cu imperfecțiuni ale suprafeței electrodului, observându-se o aglomerare mai mare în aceste zone.

Conductivitatea electrică a electrozilor obținuți a fost determinată folosind metoda « prin patru puncte » utilizând curent continuu. Astfel, s-a observat că tipul, încărcarea și distribuția filerului conductiv de carbon în matricea epoxidică influențează conductivitatea electrică. De asemenea, conținutul de argint și distribuția în compoziția materialului de electrod au contribuit la îmbunătățirea proprietăților electrice ale materialului compozit.

În urma investigării comportării electrochimice a sistemului redox standard de feri/ferocianură au fost determinate ariile suprafețelor electroactive ale acestor electrozi observându-se că aria suprafeței electroactive este mai mare sau cel puțin egală cu aria geometrică, cea mai bună arie a suprafeței electroactive fiind obținută pentru electrodul compozit de nanotuburi de carbon-epoxi.

Rezultatele obținute în urma caracterizărilor morfostructurale, electrice și electrochimice confirmă potențialul pentru aplicații electroanalitice a acestor electrozi de tip compozit, în continuare studiindu-se detecția amperometrică/voltametrică a analiților țintă atât din clasa compușilor farmaceutici, cât și din clasa anionilor.

Selecția analiților țintă din clasa compușilor farmaceutici a luat în considerare recurența acestora în apele de suprafață, respectiv influența și efluentul stațiilor de epurare. Astfel, au fost selectați trei compuși aparținând unor clase terapeutice diferite: fluoxetină din clasa antidepressivelor, naproxen din clasa antiinflamatoarelor și tetraciclină din clasa antibioticelor, fiind elaborate atât scheme individuale, cât și simultane de detecție.

♦ **Detecție individuală a compușilor farmaceutici**

Comportamentul electrochimic al *fluoxetinei* (FXT) a fost studiat prin voltametrie ciclică pr mai multe tipuri de materiale de electrod compozite de CNT și CNF, comparativ cu electrodul comercial de diamant dopat cu bor (BDD), cele mai promițătoare rezultate privind sensibilitatea și potențialul de detecție fiind obținute pentru electrozii de CNF și BDD. Pentru electrodul comercial de diamant dopat cu bor (BDD) au fost explorate și optimizate tehnicile voltametrice cu puls diferențial, respectiv undă rectangulară, care au permis atingerea celor mai bune rezultate în relație cu sensibilitatea ($244.106 \mu\text{A}\mu\text{M}^{-1}$ în condiții optime de voltametrie cu undă

rectangulară), respectiv cea mai mică limită de detecție ($0.037 \mu\text{gL}^{-1}$ în condiții optime de voltametrie cu puls diferențial). Totuși, potențialul de detecție mai mare de $+1 \text{ V/SCE}$ poate conduce la producerea unor interferențe în cazul unor aplicații practice, din acest motiv fiind necesară utilizarea unor materiale alternative. În acest scop, utilizarea electrozilor compoziți a permis deplasarea spre valori mai puțin pozitive a potențialului de detecție evitându-se astfel posibilele interferențe ($+1.35\text{V/SCE}$ pentru BDD în comparație cu $+0.98 \text{ V/SCE}$ pentru CNF). În plus, s-a urmărit îmbunătățirea rezultatelor obținute pe CNF prin modificarea acestui tip de electrod cu zeolit natural dopat cu argint (AgZ-CNF) și prin decorarea electrochimică cu argint (Ag-CNF). Aceste modificări au permis deplasarea spre valori și mai puțin pozitive: $+0.324 \text{ V/SCE}$ pentru electrodul Ag-CNF, respectiv $+0.335 \text{ V/SCE}$ pentru electrodul AgZ-CNF. De asemenea, un efect sinergic în relație cu sensibilitatea obținută pentru electrodul comercial de Ag, respectiv sensibilitatea obținută pentru electrodul CNF a fost etalat de către electrodul obținut prin electrodepunere. În plus, utilizarea zeolitului natural dopat cu argint în structura compozitului a permis detecția acestui compus farmaceutic la nivel de urme. În Tabelul 1 sunt prezentate rezultatele obținute pentru electrozi discutați în detecția fluoxetinei.

Tabelul 1. Parametrii electroanalitici obținuți pentru electrozi testați în vederea detecției fluoxetinei

| Elect. | Tehn. | E_{ox} (V/SCE) | Sens. ($\mu\text{A}\mu\text{M}^{-1}$) | R^2 | RSD (%) | LOD (μM) | LOQ (μM) |
|----------------|--------|---------------------|--|-------|------------|--------------------------|--------------------------|
| BDD | CV | 1.350 | 15.870 | 0.990 | 6.54 | $3.17 \cdot 10^{-3}$ | $10.57 \cdot 10^{-3}$ |
| | DPV | 1.250 | 81.210 | 0.998 | 0.25 | $0.11 \cdot 10^{-3}$ | $0.39 \cdot 10^{-3}$ |
| | SWV | 1.250 | 244.110 | 0.996 | 0.34 | $1.71 \cdot 10^{-3}$ | $5.75 \cdot 10^{-3}$ |
| | CA | 1.400 | 1.446 | 0.993 | 5.10 | 0.015 | 0.050 |
| CNF | CV | 0.980 | 3.686 | 0.983 | 3.52 | 0.133 | 0.446 |
| | DPV | 0.723 | 10.622 | 0.967 | 3.62 | 0.385 | 1.285 |
| AgZ-CNF | CV_ads | 0.335 | 2.007 | 0.921 | 3.05 | 0.019 | 0.064 |
| Ag-CNF | CV | 0.324 | 5.816 | 0.993 | 0.73 | 0.081 | 0.270 |
| | | 1.167 | 6.252 | 0.982 | 4.82 | 0.189 | 0.631 |

În concluzie, utilizarea unui substrat de nanofibră de carbon și a nanoparticulelor de Ag poate fi aplicată cu succes în elaborarea unor senzori mai performanți capabili să detecteze fluoxetina în soluții apoase, dar și ca metodă de validare pentru controlul de calitate.

În cazul *naproxenului* (NPX), comportamentul său electrochimic a fost studiat utilizând electrodul de tip compozit-CNF și comparativ electrodul comercial BDD. Plecând de la același criteriu-potențialul de detecție, electrodul compozit a fost utilizat pentru studii mai amănunțite. Prin utilizarea tehnicilor pulsate și anume voltametrie cu puls diferențial, respectiv voltametrie cu undă rectangulară, s-au obținut îmbunătățiri privind atât potențialul de detecție care s-a deplasat spre valori mai puțin pozitive cât și sensibilitatea, după cum se observă din Tabelul 2.

Tabelul 2. Parametrii electroanalitici obținuți pentru electrozi testați în vederea detecției naproxenului

| Electrod | Tehn. | E_{ox} (V/SCE) | Sens. ($\mu\text{A}\mu\text{M}^{-1}$) | R^2 | RSD (%) | LOD (μM) | LOQ (μM) |
|------------|-------|---------------------|--|-------|------------|--------------------------|--------------------------|
| BDD | CV | 1.425 | 5.364 | 0.98 | 4.42 | 0.027 | 0.090 |
| CNF | CV | 1.210 | 4.028 | 0.988 | 5.20 | 0.133 | 0.444 |
| | DPV | 0.950 | 9.959 | 0.971 | 4.24 | 0.146 | 0.450 |
| | SWV | 1.100 | 4.366 | 0.997 | 19.01 | 0.124 | 0.415 |

Comportamentul electrochimic al *tetraciclinei* (TC) a fost studiat doar la electrodul compozit de nanofibră de carbon, observându-se că oxidarea acestui compus are loc în două etape. Îmbunătățiri privind potențialul de detecție care s-a deplasat spre valori mai puțin pozitive cât și sensibilitatea au fost obținute în condiții optime de voltametrie puls diferențială așa cum reiese din Tabelul 3.

Tabelul 3. Parametrii electroanalitici obținuți pentru electrodul CNF testat în vederea detecției tetraciclinei

| Tehn. | E (V/SCE) | Sens. ($\mu\text{A}\mu\text{M}^{-1}$) | R ² | RSD (%) | LOD (μM) | LOQ (μM) |
|-------|-----------|---|----------------|---------|-----------------------|-----------------------|
| CV | 0.714 | 0.926 | 0.978 | 7.74 | 0.248 | 0.828 |
| | 1.0745 | 3.975 | 0.998 | 3.07 | 0.055 | 0.184 |
| DPV | 0.480 | 1.376 | 0.996 | nd* | nd | nd |
| | 0.925 | 5.215 | 0.976 | 3.88 | 0.165 | 0.551 |
| SWV | 0.645 | 1.753 | 0.963 | nd | nd | nd |
| | 1.020 | 4.254 | 0.967 | 8.50 | 0.441 | 1.470 |
| CA | 0.750 | 0.125 | 0.985 | 9.50 | 0.527 | 1.759 |
| | 1.200 | 1.239 | 0.997 | 9.75 | 0.088 | 0.293 |

*nd – nedeterminat

Aceste rezultate promițătoare obținute pentru detecția individuală au fost fructificate în elaborarea unor protocoale de detecție simultană a acestora.

♦ Detecție simultană a compușilor farmaceutici

Având în vedere rezultatele obținute pentru detecția individuală a fiecărui compus farmaceutic și considerând fluoxetina ca și compus referință au fost elaborate protocoale de detecție pentru naproxen și fluoxetină, respectiv, tetraciclină și fluoxetină utilizând electrodul compozit pe bază de nanofibră de carbon. În ambele cazuri s-a observat o bună separare a picurilor de oxidare rezultate, datorită potențialului de detecție specific fiecărui compus farmaceutic studiat. Utilizarea tehnicilor pulsate a dus la îmbunătățirea performanțelor electrochimice privind potențialul de detecție, respectiv sensibilitatea, așa cum se observă din Tabelul 4.

Tabelul 4. Parametrii electroanalitici obținuți pentru electrodul CNF testat în vederea detecției simultane a compușilor farmaceutici

| Schemă detecție | Tehn. | Analit | E (V/SCE) | Sens. ($\mu\text{A}\mu\text{M}^{-1}$) | Conc. range (μM) |
|-----------------|-------|--------|-----------|---|-------------------------------|
| NPX vs. FXT | CV | FXT | 0.785 | 1.439 | 0→15 |
| | | NPX | 1.360 | 4.732 | 0→15 |
| | DPV | FXT | 0.604 | 1.966 | 0→15 |
| | | NPX | 1.202 | 7.260 | 0→15 |
| TC vs. FXT | CV | FXT | 0.815 | 0.323 | 0→10 |
| | | TC | 0.815 | 0.960 | 0→2.5 |
| | | | 1.140 | 3.695 | |
| | DPV | FXT | 0.665 | 1.847 | 0→10 |
| | | TC | 0.665 | 4.732 | 0→2.5 |
| | | | 0.956 | 17.302 | |
| | SWV | FXT | 0.740 | 0.772 | 0→10 |
| | | TC | 0.675 | 2.606 | 0→2.5 |
| | | | 1.116 | 14.413 | |

♦ Detecție individuală/simultană a anionilor de nitrit și sulfură

O altă direcție de cercetare a fost îndreptată asupra detecției a doi anioni: sulfură și nitrit care pot fi utilizați ca și indicatori de calitate ai apei. Studiile de detecție au fost realizate folosind comparativ electrodul comercial BDD și electrodul compozit CNF. În prima etapă s-a observat superioritatea electrodului compozit față de cel comercial privind atât potențialul de detecție, cât și sensibilitatea. Apoi, în etapa a doua, s-a studiat detecția sulfurii vizând ca și aplicație apa de mare, pentru studii amănunțite fiind selectat electrodul compozit. Cele mai bune performanțe au fost obținute în condiții de voltametrie cu undă rectangulară. În plus, a fost pus în evidență comportamentul de microporț al materialului compozit prin aplicare acestuia pe probe de apă de suprafață reală, această absorbare dovedindu-se a fi un bun început pentru dezvoltarea aplicațiilor de detecție de tip *in-field*.

Cele mai bune performanțe în cazul detecției anionului de sulfură atât în apă de mare simulată cât și în apă de suprafață au fost obținute în condiții de voltametrie cu undă rectangulară, după cum se observa din Tabelul 5.

Tabelul 5. Parametrii electroanalitici obținuți pentru electrodul CNF testat în vederea detecției anionului de sulfură

| Tehn. | Electrolit suport | E_{ox} (V/SCE) | Sens. (μAmM^{-1}) | R^2 | RSD (%) | LOD (mgL^{-1}) | LQ (mgL^{-1}) |
|-------|----------------------|------------------|--------------------------------|-------|---------|---------------------------|--------------------------|
| CV | apă de mare simulată | 0.800 | 59.983 | 0.997 | 2.32 | 0.141 | 0.470 |
| DPV | | 0.220 | 86.350 | 0.984 | 0.22 | 0.048 | 0.161 |
| SWV | | 0.855 | 347.899 | 0.958 | 3.40 | 0.941 | 3.139 |
| CA | | 0.900 | 17.027 | 0.986 | 12.91 | 0.401 | 1.337 |
| CV | apă de suprafață | 0.850 | 37.619 | 0.985 | 6.95 | 0.288 | 0.963 |
| SWV | | 1.435 | 108.44 | 0.998 | 0.24 | 0.117 | 0.390 |
| CA | | 0.900 | 15.882 | 0.996 | 4.94 | 0.056 | 0.187 |

În plus, utilizând electrodul de BDD au fost elaborate protocoale pentru detecția simultană a sulfurii și a nitritului, compus anorganic foarte toxic. În cazul tuturor tehnicilor aplicate: voltametrie ciclică, voltametrie cu puls diferențial, voltametrie cu undă rectangulară o bună separare a picurilor de oxidare aferente anionilor a fost observată, ceea ce sugerează o posibilă utilizare a acestui tip de material în aplicații practice de detecție simultană. Cele mai bune rezultatele obținute în detecția simultană a acestor anioni sunt prezentate în Tabelul 6.

Tabelul 6. Parametrii electroanalitici obținuți pentru electrodul BDD testat în vederea detecției simultane a anionilor de sulfură și nitrit

| Tehn. | An. | E_{ox} (V/SCE) | Sens. (μAmM^{-1}) | R^2 | RSD (%) | LOD (mgL^{-1}) | LOQ (mgL^{-1}) |
|-------|-----------------|------------------|--------------------------------|-------|---------|---------------------------|---------------------------|
| CV | S^{2-} | 0.890 | 56.630 | 0.983 | 8.50 | 0.187 | 0.624 |
| | NO_2^- | 1.400 | 77.594 | 0.996 | 3.10 | 0.298 | 0.994 |
| DPV | S^{2-} | 0.775 | 68.906 | 0.994 | 0.33 | 0.003 | 0.010 |
| | NO_2^- | 1.275 | 98.411 | 0.994 | 1.89 | 0.155 | 0.519 |
| SWV | S^{2-} | 0.800 | 95.573 | 0.998 | 0.44 | 0.006 | 0.020 |
| | NO_2^- | 1.300 | 177.629 | 0.993 | 1.30 | 0.087 | 0.291 |
| CA | S^{2-} | 0.850 | 7.680 | 0.992 | 5.97 | 0.315 | 0.105 |
| | NO_2^- | 1.200 | 25.237 | 0.992 | 3.97 | 0.032 | 0.109 |

Rezultatele obținute în condiții de voltametrie cu undă rectangulară sunt comparabile cu cele stabilite de legislația românească privind valorile limită pentru apa potabilă cât și pentru apa uzată deversată într-un receptor natural.

În concluzie, selecția tipului de electrod, a tehnicii electrochimice și a condițiilor de operare se impune a fi făcută având în vedere cerințele specifice impuse de aplicațiile practice. Astfel, este necesară elaborarea unor protocoale de detecție specifice fiecărui tip de aplicație și scop binedefinit.

Totuși, ținând cont de de complexitatea acestui studiu, elaborarea, caracterizarea și utilizarea materialului de electrod ca senzor, sunt necesare viitoare studii în vederea stabilirii tuturor tipurilor de interferențe și a duratei de viață a senzorilor selectați pentru aplicații practice.

1. INTRODUCTION

Water is an important resource for supporting life in all ecosystems. Generically called „The Blue Planet“, on Earth the water resources represent about 71% of its surface, representing a total volume of $1.37 \cdot 10^9 \text{ km}^3$. Only about 2.5% represents the freshwater resources, the rest of 97.5% representing the saline waters resources (oceans, seas). In Figure 1.1 the diagram of water distribution on Earth is represented [1].

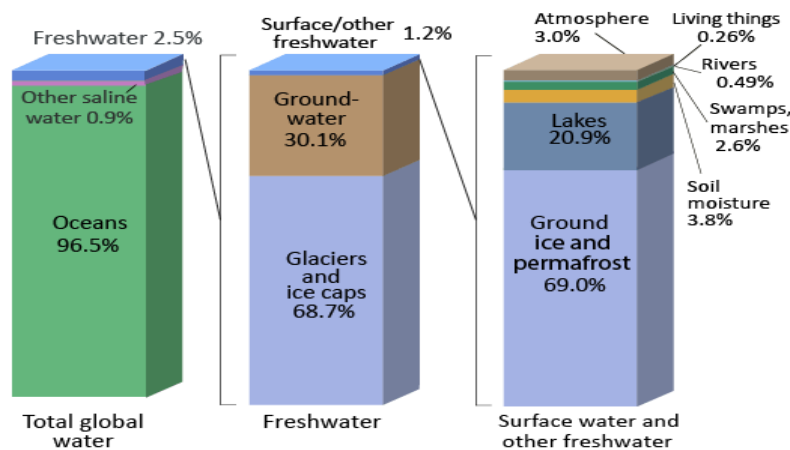


Figure 1.1. Water distribution diagram on Earth

From the total amount of water available on Earth only 0.7% representing $0.959 \cdot 10^7 \text{ km}^3$ is used for consumption or domestic activities [2]. These water resources randomly distributed should serve all the needs of a growing population of over 7 billions people. However, according to the World Health Organization (WHO) around 2.3 billions of people are affected by the low acces to safe drinking water sources, even if between 1990-2002 the availability of drinking water sources in developing regions has increased from 17% to 87%, the more affected regions still being Southern Asia and Saharian Africa [3]. Although at global level many efforts to improve this situation are being undertaken, a water crisis is almost imminent.

WHO, United Nations Children's Fund (UNICEF), and other global organizations are militating constantly in favor of improving the water quality in developed, developing, and least developed countries all over the globe. Regulations related to water, e.g., supply, quality, are imposed in order to reduce the effects caused by intensive industrial and agricultural activities by following the DPSIR (driving forces–pressures–states–impact–responses) framework. By the intensification of industrial activities, severe changes may occur on local, regional, and global level. Nowadays, a lot of attention has been received by the climate changes. These climate changes associated with the population growth, economic

growth, technological development and other socio-economic factors [4-6] will increase the vulnerability of freshwater resources, having as a consequence the multiplication of pathogens, human health problems, adverse effects on aquatic medium, etc.

One common cause that increase the vulnerability of freshwater resources is the pollution of water with various chemical compounds. Due to their harmful effects, specific regulations have been adopted in order to reduce their emissions in the environment.

In the European Union a crucial step in monitoring and improving the water quality was represented by the introduction of the Water Framework Directive (2000/60/EC). Due to the complexity of this topic, by directive 2006/105/EC were established 33 priority substances, *e.g.*, benzene, mercury and its compound, nickel, simazine, trifluralin etc. In addition, beside these priority substances, there were established other substances that could harm the water quality [7]. Among these priority substances, 20 of them are considered hazardous due to their adverse effects on the environment. Once released into rivers, these substances as originated from industrial residues as heavy metals, agriculture and mining related substances, can be transported downstream and be introduced into coastal waters. Although in the stream several treatment processes to reduce the transport of hazardous substances into marine waters like the sedimentation on the river bed and the removal efficiency of wastewater treatment plants occur, these influence the discharge into coastal waters [8].

To date, a new class of compounds generically referred as emerging pollutants, *e.g.*, pharmaceuticals, pesticides etc., are receiving a lot of attention from the scientific community. For that reason, this type of compounds will be discussed further in this thesis.

1.1. References

- [1] I.A. Shilkomanov, Water in crisis, Chapter 2, Oxford University Press, New York, 1993.
- [2] M. Gheju, Chimia apelor naturale, Editura de Vest, Timișoara, 2013.
- [3] WHO and UNICEF, Progress in drinking water and sanitation. 2014 update, WHO Press, Geneva, 2014
- [4] N.W. Arnell, Climate change and global water resource, Glob. Environ. Change, (1999) 9, S31-S49.
- [5] C. Vörösmarty, P. Green, J. Salisbury, R.B. Lammers, Global water resources: vulnerability from climate change and population growth, Science, (2000) 289, 284-288.
- [6] J. Alcamo, M. Floeke, M. Marker, Future long-term changes in global water resources driven by socio-economic and climatic changes, Hydrolog. Sci. J., (2007) 52(2), 247-275.
- [7] European Environmental Agency website, <http://www.eea.europa.eu/themes>
- [8] EEA technical report, Hazardous substances in Europe's fresh and marine waters, An overview, EEA, Copenhagen, 8/2011.

2. PHARMACEUTICALS AND ANIONS FOR WATER QUALITY

2.1. Pharmaceuticals and water quality

The first studies that revealed the presence of pharmaceutical compounds in water have been conducted in 1970 in the USA and continued in 1985 in the UK. The mid nineties revealed the “boom” of this new research topic – pharmaceuticals as emerging pollutants in water. Since then, a huge number of scientific papers appeared discussing the occurrence, sources, fate and effects of these compounds in surface waters, groundwater, and sewage treatment plant (STP) influent and effluent being identified more than 100 pharmaceutical compounds [1-12].

One of the most important sources of pharmaceutical compounds is represented by the pharmaceutical industry itself. The major changes on the global pharmaceutical market are reflecting the development of this industry, an increasing trend being noticed (Figure 2.1). According to the IMS Institute for Healthcare Informatics it is expected that until 2016 the global market will reach nearly 1200 billion dollars [13], growth assigned to market expansion in the leading emerging countries. The growth of the market will be seen in the prescriptions and sales and will affect indirectly the equilibrium of the environment.

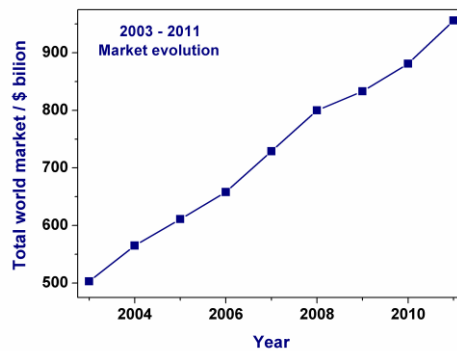


Figure 2.1. The global pharmaceuticals market evolution between 2003-2011.

The main *sources* of environmental contamination with pharmaceutical compounds are the metabolism post-consumption, the disposal of unused drugs, the manufacturing residues, the hospitals and landfill disposal. A brief overview (representation) of the sources and the fate of pharmaceuticals in the environment is presented in Figure 2.2.

Table 2.1. Occurrence of some pharmaceutical compounds in waters

| Drug class | Drug | C _{max} / µgL ⁻¹ | Variability / µgL ⁻¹ |
|-------------|---------------|--------------------------------------|---------------------------------|
| NSAIDs | Ibuprofen | 373 | 0.0016-373 |
| | Acetaminophen | 246 | |
| | Tramadol | 86 | |
| | Naproxen | 53 | |
| Antibiotics | Ofloxacin | 32 | 0.001-32 |
| | Roxithromycin | 17 | |
| | Ciprofloxacin | 14 | |
| | Sulfapyridene | 12.4 | |

Table 2.2. Applied methods in pharmaceuticals detection

| Anal. meth. | Analyte | Matrix | Ref. |
|----------------------|---|--|------|
| SPE –GC –MS | Naproxen; Ibuprofen; Bisphenol A | Surface and treated waters | 17 |
| SPE –LC –MS/MS | NSAIDs; Antibiotics; | Sewage waters | 9 |
| | Fluoxetine; Citalopram; Paroxetine | Raw waters | 18 |
| ESI –LC –MS/MS | Diclofenac; Ibuprofen; Naproxen; Fluoxetine | Rivers | 10 |
| | Ibuprofen; Naproxen; Fluoxetine | Surface waters | 19 |
| LC –QTRAP –MS | Erythromycin; Sulfamethaxazole | Rivers and tap water | 6 |
| SPE –HPLC | Diclofenac; Ibuprofen; Naproxen; Carbamazepine | Wastewater | 8 |
| ESI –HPLC – MS/MS | Penicillins; Tetracycline | Sewage wastewater | 5 |
| | Ibuprofen; Mefenamic acid; Propranolol | Surface water and wastewater effluent | 20 |

*SPE–solid phase extraction; QTRAP–quadrupole–ion trap; EIS–electrospray ionization.

The environmental *fate* of these compounds is quite debated and further studies are required for elucidate all the mechanisms. The persistence, rate of spread, and bioaccumulation of pharmaceuticals is influenced by their chemistry and environmental conditions [8]. Depending on their molecular formula *e.g.*, fluorine incorporated into pharmaceutical composition, these compounds may be resistant to wastewater treatment, being discharged into natural receptors and as a consequence the biota could be affected [21]. One of the most known cases reported in many countries is the feminization of male fish due to ethinyl estradiol (EE2). Under laboratory controlled conditions some effects of feminization were observed for concentrations above 1 ngL⁻¹, but it is not yet clear whether EE2 causes or not effects on the aquatic environment.

Another example of a great impact on wildlife was the acute poisoning of oriental vultures with diclofenac. After ingestion of carcasses of livestock treated with diclofenac, the number of vultures has been dramatically reduced. Diclofenac caused acute failure of kidneys and after a few days the vultures died due to large urate deposits on internal organs. The diclofenac concentration on livestock carcasses has been higher than the lethal dose (0.1-0.2 mgKg⁻¹), the effects being imminent.

In relation with this topic, the effects of antibiotics on aquatic media should be mentioned. The antibiotic residues are suspected to induce resistances in bacteria, causing serious effects on public health. An example in this sense is tetracycline, widely used in aquaculture. This drug may not be always detected in waters due to its susceptibility to hydrolysis or disguise through binding ions or sediments [5]. Thus, by increasing the resistance of bacteria, the use of commonly antibiotics would be useless, and therefore it will be necessary to develop new antibiotics with a wider and stronger spectrum. These well-known cases are highlighting the major deficiencies in knowledge concerning the effects of pharmaceuticals on biota.

The occurrence of pharmaceuticals in sewage effluent waters has raised questions related to the efficiency of wastewater treatment plants (WWTPs). Conventional wastewater treatment plants have a step of biological degradation based on the activated sludge. The advanced WWTPs have a tertiary treatment process such as ozonisation or advanced oxidation technologies. The efficiency of the process depends on many variables, but the most important are the type and the characteristics of the WWTP. Since the majority of pharmaceuticals are hydrophobic, high removal rates will be obtained by applying advanced oxidation techniques, able to degrade the target compound [13, 22].

Although the occurrence of pharmaceuticals and the associated effects have been highlighted in several studies, at global level no clear law is regulating these aspects. In the USA, Food and Drug Administration (FDA) requests an environmental assessment of a new pharmaceutical compound. If the expected introductory concentration (EIC) of a pharmaceutical at entering into environment is higher than $1 \mu\text{gL}^{-1}$ then the product is classified as "acceptable" and no further environmental testing is required. With all this, several agencies/organizations as National Institute for Occupational Safety and Health-NIOSH, Occupational Safety and Health Administration-OSHA evaluated the pharmaceuticals and their waste and requested new pharmaceuticals testing and nevertheless new regulations for these compounds. Both organizations classified as hazardous substances more than 60 compounds, still until now no pharmaceuticals have been included into Drinking Water Contamination List. In Europe, the European Agency of Medicinal Products elaborated in accordance to European Directive 2001/83/EC a guideline for environmental risk assessment for all new and existing medicinal products [8]. Therefore, it is necessary to develop a methodology that will clarify the legislative aspect of pharmaceuticals in environment.

In order to reduce the human exposure to pharmaceuticals several recommendations such as improved disposal management, prudent use of pharmaceuticals, implement of best practices at WWTP, improved crop and agricultural practices, and reduced direct release of manufacturing facilities but also development of "greener" pharmaceuticals [19, 23] were proposed.

2.2. Anions and water quality

Surface waters and groundwater naturally contain a wide spectrum of cations and anions, *e.g.*, Na^+ , Ca^{2+} , Mg^{2+} , Cl^- , S^{2-} , etc., which occur due to geographic and climatic conditions. The assessment performed by the World Health Organization for improving water quality led to general regulations and proposed threshold values for each type of considered anions/contaminant. These regulations

were transposed then into adopted laws by each state and they may be more restrictive than WHO proposal.

Two major ions from water will be further discussed: nitrite, a member of nitrogen compounds family, and sulfide, due to its natural presence in the environment.

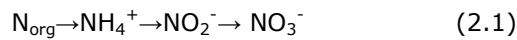
2.2.1. Nitrite and nitrate for water quality

Nitrite and nitrate are two of the most reactive members of nitrogen family [24]. Under chemical or biological processes nitrite may be oxidized to nitrate, a more stable and toxic member of this family. In Table 2.3 are gathered selected properties of these inorganic compounds.

Table 2.3. Characteristics of nitrate and nitrite

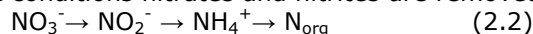
| Property | Nitrate | Nitrite |
|------------|--------------|---|
| Solubility | very soluble | very soluble |
| Reactivity | unreactive | very reactive |
| Stability | stable | unstable |
| Uses | fertilizer | food preservations (E249, E250, E251, E252) |

Nitrate occurrence in water resources is due to the intensive use of fertilizers containing nitrogen. The nitrification process that will take place is represented below,



During their growth the plants will use the necessary amount of nitrate for synthesis, the surplus will infiltrate into groundwater causing water contamination. Among water contamination, the intensive use of fertilizers will affect the used area by converting it to a vulnerable nitrate area. In the last years in North-Western Europe the spread of nitrate vulnerable areas has increased due to agricultural practices and due to increased vulnerability, high levels of nitrates were found in drinking waters. It is estimated that in Europe around 22% of the groundwater is contaminated with nitrates [25]. In Figure 2.3 the situation of nitrate vulnerability in Danube river basin is presented [26].

Under anaerobic conditions nitrates and nitrites are removed from water:



This process, known as denitrification is applied in wastewater treatment. Since it is a biological process, there is no complete its control (the quantity of oxygen will influence the final products, *e.g.*, N_{org} or NO), and as a result, effluent waters may contain sulfide and nitrite. Nitrification and denitrification of surface waters may occur depending on the temperature and the pH.

Nitrite concentrations in waters are usually lower than nitrate concentration, the main sources of nitrites being the nitrification/denitrification processes and the ammonification process resulting NH_4^+ . Usually nitrite levels in drinking-water are below 0.1 mgL^{-1} . By increasing the use of artificial fertilizers, the disposal of wastes and by changing the land use a progressive increase of nitrate levels in groundwater supplies was observed.



Figure 2.3. Nitrate vulnerable areas in the Danube river basin.

WHO recommended threshold values for both anions due to their toxic effects observed on human health, e.g., methemoglobinaemia, migraines, chronic obstructive pulmonary diseases. In Table 2.4 the threshold values adopted on Romanian legislation based on these recommendations are presented.

Table 2.4. Nitrite and nitrate threshold values proposed by WHO and transposed under Romanian legislation

| Type of water | Anion | C _{WHO} / mgL ⁻¹ | C _{RO} / mgL ⁻¹ | Law |
|----------------|------------------------------|--------------------------------------|-------------------------------------|-------------|
| Drinking water | NO ₂ ⁻ | 3 | 0.5 | 311/2004 |
| | NO ₃ ⁻ | 50 | 50 | |
| Waste water | NO ₂ ⁻ | n.a.* | 1 | GD 352/2005 |
| | NO ₃ ⁻ | n.a. | 25 | |

*n.a. – not available;

2.2.2. Sulfide for water quality

Sulfide exists in nature in three forms: hydrogen sulfide (H₂S); hydrosulfide or bisulfide ion (HS⁻), and sulfide ion (S²⁻). The equilibrium between these species is governed by the pH, at low pH the predominant specie is hydrogen sulfide, at high pH the predominant specie is sulfide ion, and around pH=7 there is a weak equilibrium. For pH higher than 13, a very complex chemistry of sulphur is noticed.

Hydrogen sulfide is produced naturally under anaerobic bacterial reduction of sulphates and sulfur-containing organic compounds and then is released as gas. It may also be released as a result of industrial activities, *e.g.*, as a recovery by-product of natural and refined gas purification. Therefore, the atmosphere contains almost 90% of the total hydrogen sulfide. Its toxicity studied for short term and medium term exposures of humans showed olfactory, respiratory and neurological effects. After inhalation, this inorganic compound is metabolized in the liver through oxidation, methylation, and reactions with metalloproteins or disulfide-containing proteins. Table 2.5 summarizes some effects observed for different concentration levels of human exposure.

Table 2.5. Human health effects of hydrogen sulfide exposure

| Exposure (mg m^{-3}) | Effect |
|---------------------------------|---|
| 0.011 | Odour threshold |
| 2.8 | Bronchial constriction of asthmatic individuals |
| 5.0 | Increased eye complaints |
| 5-29 | Eye irritation |
| >140 | Olfactory paralysis |
| >560 | Respiratory distress |
| >700 | Death |

Sulfide presence was also recorded in groundwater as a compound of geothermal waters and seawater as a compound of anoxic layer of seawater highlighted by several studies [27].

In surface waters, sulfide presence is associated generally with wastewater treatment processes or complex industrial processes. Usually, the specific rotten-egg smell of sulfide suggests the occurrence of sewage or industrial waters. Sulfide's presence in wastewater may be used for removing trace metals due to its affinity to form metallic precipitates. During water treatment sulfide can be removed by following one of the methods: aeration, oxidation, and microbiological filtration, oxidation followed by filtration, or by anion exchange.

Table 2.6. Measured levels of hydrogen sulfide in the environment

| Matrix | Sample | Concentration |
|--------|----------------------|-------------------------------|
| Air | Ambient air | 0.14 -0.4 μgm^{-3} |
| | Unpolluted air | 0.03 -0.1 μgm^{-3} |
| | Near sulphurous lake | 175 -5500 μgm^{-3} |
| Water | Well water | 1.6 -1.9 mgL^{-1} |
| | Mississippi river | 0.92 mgL^{-1} |
| | Wastewater | 3.1 -5.1 mgL^{-1} |

Due to its high reactivity, it is recommended that sulfide samples be kept under dark conditions because high temperature and low pH help H_2S to evaporate very easy. Table 2.6 presents some environmental levels of hydrogen sulfide.

Due to its high toxicity, the World Health Organization recommends for the taste and odour threshold of hydrogen sulfide in water values ranging between 0.05 and 0.1 mgL^{-1} [28]. In Romania these proposed regulations have been included into specific laws (see Table 2.7).

Table 2.7. Threshold values of sulfide under Romanian legislation

| Type of water | Limit conc. / mgL ⁻¹ | Law |
|-----------------------|---------------------------------|-------------|
| <i>Drinking water</i> | 0.1 | 311/2004 |
| <i>Waste water</i> | 0.5 | GD 188/2002 |

Taking into consideration the high impact of these anions, *e.g.*, nitrite, nitrate, and sulfide, on environment and on human health they can be considered as a water quality index.

2.3. References

- [1] A. Pal, Y. He, M. Jekel, M. Reinhard, K. Yew-Hoong Gin, Emerging contaminants of public health significance as water quality indicator compounds in the urban cycle, *Environ. Int.*, (2014) 71, 46-62.
- [2] D.J. Lapworth, N. Baran, M.E. Stuart, R.S. Wang, Emerging organic contaminants in groundwater: a review of the sources, fate and occurrence, *Environ. Pollut.*, (2012) 163, 287-303.
- [3] A. Jurado, E. Vasques-Sune, J. Carrera, M. Lopez de Alda, E. Pujades, D. Barcelo, Emerging contaminants in groundwater in Spain: a review of sources, recent occurrence and fate in European context, *Sci. Total Environ.*, (2012) 440, 82-94.
- [4] P. Verlicchi, M.A. Aukidy, E. Zambello, Occurrence of pharmaceutical compounds in urban wastewater: removal mass load and environmental risk after a secondary treatment-a review, *Sci. Total Environ.*, (2012) 429, 123-155.
- [5] R. Hirsch, T. Terner, K.Haberer, K.L. Kratzs, Occurrence of antibiotics in the aquatic environment, *Sci. Total Environ.*, (1999) 225, 109-118.
- [6] Y. Vacarcel, S. Gonzalez-Alonso, J.L. Rodriguez-Gil, A. Gill, M. Catala, Detection of pharmaceutically active compounds in the rivers and tap water of the Madrid Region (Spain) and potential ecotoxicological risk, *Chemosphere*, (2011) 84, 1336-1348.
- [7] M.S. Fram, K. Belitz, Occurrence and concentrations of pharmaceutical compounds in groundwater used for public drinking water supply in Canada, *Sci. Total Environ.*, (2011) 409, 3409-3417.
- [8] K.P. Singh, P. Rai, A.K. Singh, P. Verma, S. Gupta, Occurrence of pharmaceuticals in urban wastewater of north Indian cities and risk assessment, *Environ. Monit. Assess.*, (2014) 186, 6663-6682.
- [9] R.H. Lindberd, M. Ostman, U. Olofsson, R. Grabic, J. Fick, Occurrence and behaviour of 105 pharmaceutical ingredients in sewage waters of municipal sewer collection data, *Water Res.*, (2014) 58, 221-229.
- [10] Y. Vystavna, F. Huneau, V. Grynenko, Y. Vergels, H. Celle-Jeanetot, Pharmaceuticals in rivers of two regions with contrasted socio-economic conditions: occurrence, accumulation and comparison for Ukraine and France, *Water Air Soil Pollut.*, (2012) 223, 2111-2124.
- [11] T. Heberer, Occurrence, fate, and removal of pharmaceutical residues in the aquatic environment: a review of recent research data, *Toxicol. Lett.*, (2002) 131, 5-17.
- [12] L.H. Santos, A.N. Araujo, A. Fachini, A. Pena, C. Deleure-Matos, M.C.B.S.M. Montenegro, Ecotoxicological aspects related to the presence of

- pharmaceuticals in the aquatic environment, *J. Hazard. Materials.*, (2010) 175, 45-95.
- [13] International Federation of Pharmaceutical Manufacturers & Associations, *The pharmaceutical industry and global health. Facts and figures*, 2012.
- [14] World Health Organization, *Pharmaceuticals in drinking water*, WHO Press, Geneva, 2011
- [15] T.A. Ternes, Analytical methods for the determination of pharmaceuticals in aqueous environmental samples, *Trends Anal. Chem.*, (2001) 20(8), 419-434.
- [16] A. Kot-Wasik, J. Debska, J. Namiesnik, Analytical techniques in studies of the environmental fate of pharmaceuticals and personal-care products, *Trends Anal. Chem.*, (2007) 26(6), 557-568.
- [17] G.R. Boyd, H. Reemtsma, D.A. Grimm, S. Mitra, Pharmaceuticals and personal care products (PPCPs) in the surface and treated waters of Louisiana, USA and Ontario, Canada, *Sci. Total Environ.*, (2003) 311(1-3), 135-149.
- [18] A. Lajeunesse, C. Gagnon, S. Sauve, Determination of basic antidepressants and their n-desmethyl metabolites in raw sewage and wastewater using solid-phase extraction and liquid chromatography –tandem mass spectrometry, *Anal. Chem.*, (2008) 80, 5325-5333.
- [19] C.D. Metcalfe, X.S. Miao, B.G. Koenig, J. Struger, Distribution of acidic and neutral drugs in surface waters near sewage treatment plants in the lower Great Lakes, Canada, *Environ. Toxicol. Chem.*, (2003) 22 (12), 2881-2889.
- [20] P.H. Roberts, K.V. Thomas, The occurrence of selected pharmaceuticals in wastewater effluent and surface waters of the lower Tyne catchment, *Sci. Total Environ.*, (2006) 356, 143-153.
- [21] K. Kummerer, M. Hempel, *Green and sustainable pharmacy*, Ch. 2, Springer-Verlag Berlin, Heidelberg, 2010.
- [22] J. Rivera-Utrilla, M. Sanchez-Polo, M.A. Ferro-Garcia, G. Prados-Joyam R. Ocampo-Perez, Pharmaceuticals as emerging contaminants and their removal from water. A review, *Chemosphere*, (2013) 93, 1268-1287.
- [23] R. Halden, *Contaminants of emerging concern in the environment: ecological and human health considerations*, Ch. 17, American Chemical Society, Washington DC, 2010.
- [24] World Health Organization, *Guideline for drinking-water quality*, WHO Press, Geneva, 2003.
- [25] M. Gheju, *Chimia apelor naturale*, Editura de Vest, Timișoara, 2013.
- [26] International Commission for the Protection of the Danube River website, <http://www.icpdr.org/main/>
- [27] S.J. Duranceau, V.M. Trupiano, M. Lowenstine, S. Whidden, J. Hopp, Innovative hydrogen sulfide treatment methods: moving beyond packed tower aeration, *FWJR*, (2010) July, 4-14.
- [28] *Hydrogen sulfide: human health impact*, WHO Press, Geneva, 2003.

3. CARBON-BASED ELECTRODES

Electroanalysis, defined as „the application of electrochemistry to solve real life problems“, is used to detect species that react directly or indirectly at, or are adsorbed onto the electrode surface. Thus, the electrode material plays an important role exhibiting all the requirements for a good material, like long-term stability, low background current, and wide potential window [1].

3.1. Carbon electrodes

Nowadays, carbon electrodes are the most widely used in electroanalytical applications due to their characteristics, such as broad potential window, low background current, rich surface chemistry, chemical inertness, and low cost. However, in comparison with metal electrodes, at carbon electrodes the electron-transfer rate is strongly affected by the origin of the carbon surface. It is necessary to point out that among the type of hybridization (sp^2 or sp^3) the density of the edge and the basal planes of the surface play an important role in electron transfer. In order to improve electron-transfer rate, two aspects must be considered. The first is referred to the pretreatment procedure, especially electrochemical pretreatment before the electroanalytical application. Secondly, the carbon-based electrode type and structure represent a great importance for the electroanalytical performance.

In comparison with conventional electrodes, several types of advanced carbon-based electrodes have been reported in electroanalysis, *e.g.*, boron-doped diamond electrode, carbon nanotubes and carbon nanofibers [2].

3.1.1. Boron-doped diamond material (BDD)

Natural diamond is an allotrope form of sp^3 hybridized carbon. Some properties of diamond are gathered in Table 3.1. Due to high inherent electrical resistivity diamond cannot be used as an electrode material. Pleskov and co-workers obtained a new material—boron-doped diamond (BDD) with unique properties which have led to several applications [3-5].

Generally, doped diamond materials are obtained by chemical vapor deposition as thin doped diamond films. Using boron as dopant a *p-type semiconductor*, known as boron-doped diamond (BDD), will be obtained. It acts as an extrinsic semiconductor at low doping levels, and as a semi-metal at high doping level. So, it can be concluded that the conductivity of this material depends on the doping level. By using other species as dopant, *e.g.*, nitrogen, phosphorus or sulphur, an *n-type semiconductor* will be obtained. Also, co-doped diamond thin film material, *e.g.*, nitrogen- boron were produced and shown to be feasible.

Table 3.1. Basic properties of undoped diamond [6]

| | |
|----------------------|---|
| Thermal conductivity | 20W(cmK) ⁻¹ at 300K |
| Electronic band gap | E _{gap} =5.6 eV |
| Refractive index | 2.42 at 546nm |
| Dielectric constant | 5.45 eV |
| Dielectric strength | Ca. 10 ⁸ to 10 ⁹ Vm ⁻¹ |
| Resistivity | 10 ²⁰ Ωcm |
| Melting point | 4027 K |
| Density | 3.25 gcm ⁻³ |

For practical applications, the most used doped material is *boron-doped diamond* material because it has a wide potential window for aqueous and non-aqueous media, a low background current, a stable long-term response, low sensitivity to dissolved oxygen and inertness to adsorption (given by scan rate studies). High overpotentials for hydrogen and oxygen are reached due to the hydrogen-terminated surface characteristics of the electrode. As a consequence, a very wide potential window is reached in aqueous media. In non-aqueous media, the potential window is 1.5 larger than in aqueous media. During the assessment of chemical and electrochemical stability, low and stable background currents were recorded, suggesting a high resistance on morphological changes. In order to study the anodic corrosion, several studies were performed in acidic media and showed a decrease in surface roughness, but no loss of diamond material. However, it was observed that some electrolyte compositions could increase the corrosion rates [7].

Doped-diamond electrodes can be modified for obtaining the best performances for different uses. An important aspect is the modification by anodic/cathodic treatment in aqueous media. The freshly prepared doped-diamond materials have a hydrogen-terminated surface, which impose a hydrophobic nature, stable for several months. During anodic oxidation, the surface can be transformed from hydrogen-terminated into oxygen-terminated surface having hydrophilic behavior. The reverse process is possible by cathodic treatment in acidic media. In addition, it is possible that on the electrode surface non-diamond sp²-carbon impurities appear, but can be removed in aqueous media. By plasma treatment and chemical reactions on the surface, or by structuring the diamond films into arrays, deposition or ion implantation valuable results were obtained [4].

Boron-doped diamond electrodes are widely used in electroanalytical application, water treatment (removal of organic and inorganic pollutants, water disinfection), electrochemical energy technology [3-6, 8-11]. In electroanalytical applications, BDD was applied for individual or simultaneous detection of several compounds such as pharmaceuticals, *e.g.*, fluoxetine [12], ascorbic acid and caffeine [13], but also other organic pollutants such as synthetic colorants in food [14], pesticides [15] etc.

3.1.2. Carbon nanotubes (CNTs)

The fullerene C₆₀ discovery in 1985 enlarged the carbon allotrope family with a new nanometer-sized member, and somehow anticipated the future discovery of a new type of material, *e.g.*, carbon nanotubes. In 1991, Iijima reported in Nature for the first time "helical microtubules of graphitic carbon" obtained by synthesizing molecular carbon structures into C₆₀ by using arc-discharge evaporation methods [16]. This was the beginning of the new carbon nanotubes "era".

Conceptually, CNT can be seen as a hollow tube formed by the rolling up of a layer consisting of carbon atoms sp^2 bonded, similar to a graphene configuration. The hollow tubes can be bounded by fullerene hemisphere at the ends, and their length can vary from tens of nanometers to several microns. In 1993 single walled nanotubes were discovered, and hence, the two types of structural families of carbon nanotubes were distinguished single-walled carbon nanotubes (SWCNTs) and multi-walled carbon nanotubes (MWCNTs). These structures are presented in Figure 3.1. In Table 3.2 some characteristics of SWCNTs and MWCNTs are gathered.

Table 3.2. Characteristics of SWCNTs and MWCNTs [20]

| | SWCNTs | MWCNTs |
|------------------|--|--------------------------------|
| Obtaining method | Chemical vapour deposition-CVD | Chemical vapour deposition-CVD |
| Catalyst | Required | Not required |
| Purity | Low | High |
| Conductivity | Metallic or semiconductor depending on the band gap, which is determined by chirality and diameter | Metallic conductor |
| Young modulus | 1 TPa | 1.28 TPa |
| Price | \$500 / purified g | \$ 150 /g |

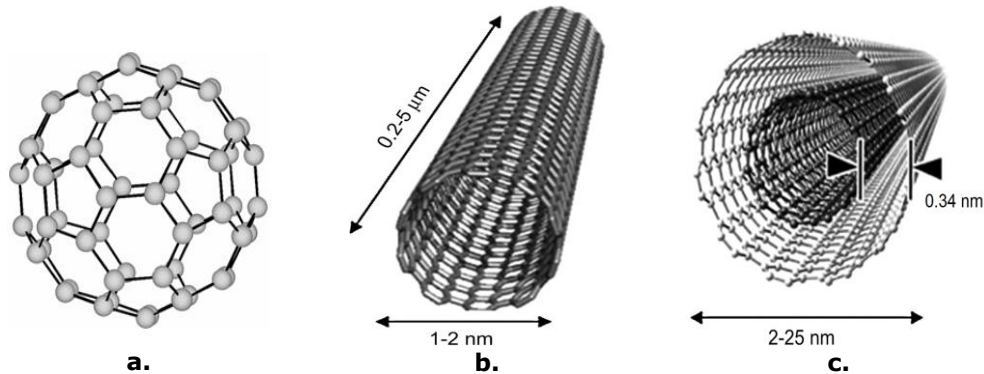


Figure 3.1. Structure of **a.** fullerene; **b.** SWCNT and **c.** MWCNT.

The electrical conductivity and the capability to form charge transfer complexes are associated with the CNTs quasi-one dimensional sp^2 hybridization and π -bonding between the carbon atoms. The π -electrons of the graphene layer are free to move above and below these layers. Therefore, they will form a band gap which assures a semi-conductive CNT behavior.

The preparation method of carbon nanotubes will influence their properties. Taking into consideration that the strength of van der Waals forces is responsible for a low dispersion and solubility of carbon nanoparticles different pre-treatment methods have been developed to overcome this aspect [17-23]. Attempts of controlling the distribution and amount of nanotubes deposited for obtaining the desired properties of material may consist in self-assembling aligned nanotubes [24], or direct growth of aligned nanotubes on the electrode's surface. Prolongo proposed an innovative dispersion, stretching, and alignment of CNTs into epoxy matrix based on chronoamperometry, by applying an electrical field to a non-cured

CNT/epoxy matrix resin using a large surface electrode [25]. Chemical functionalization of CNT surface is also applied for removing the impurities in order to achieve a good dispersion [26-29]. It was observed that under severe conditions of high temperature and long oxidation time, a good purification of MWCNTs is reached, but the crystalline structure of the material was partially damaged. Also, mechanical defects occurred during growth, purification, or alignment processes are affecting the properties of the material, but they can be introduced only with the purpose of modifying the properties of carbon nanotubes [30].

Carbon nanotubes are characterized by unique thermal, electrical, mechanical, and biological properties, which make them suitable for a wide range of applications, like chemical sensors [16, 17, 21, 31-33], catalyst support [17], intelligent material for electronic devices [22, 26], and energy storage [19]. From a sustainable energy point of view it is important to point out some remarkable applications like photo-electrochemical solar cells, and water photoelectrolysis for a hydrogen economy, photoelectrocatalytic devices for CO₂ conversion into fuels, advanced Li-batteries, supercapacitors, and fuel cells.

Currently, the use of CNTs in medical applications *e.g.*, biosensors increased due to their chemical and physical properties. As a consequence, by improving the water solubility and biocompatibility of the material during chemical functionalization a good biocompatibility without any toxic side effects with the body fluids was achieved. Thus, carbon nanotubes have been used in artificial implants, tissue engineering, drug delivery, and in cancer cell identification as cancer biomarkers [17, 21, 33].

CNTs have gained attention due to their wide use in sensing applications. By employing CNTs with modified or unmodified surfaces various compounds such as resistant organic pollutants, *e.g.*, pentachlorophenol [34], pharmaceuticals, *e.g.*, acetaminophen and ascorbic acid [35], or uric acid in the presence of ascorbic acid [36] were detected.

3.1.3. Carbon nanofibers (CNFs)

The wide use of carbon nanofibers started after 1950, even if their discovery has been recognized since 1889. Carbon nanofibers adapt cylindrical or conical structures- sp^2 hybridized that possess larger diameters in comparison with CNTs. The internal structure of carbon nanofibers varies and contains different arrangements of modified graphene sheets. As a consequence, less crystalline structures as cups-tackles/stacked coins are noticed (Figure 3.2).

In Table 3.3 some chemical and physical properties of CNFs are summeried.

Table 3.3. Chemical and physical properties of CNFs [38]

| | |
|-------------------------|---------------------------|
| Young modulus | 500 GPa |
| Tensile strenght | 3 GPa |
| Electrical conductivity | 10^3 Scm^{-1} |
| Thermal conductivity | 1900 W(mK)^{-1} |

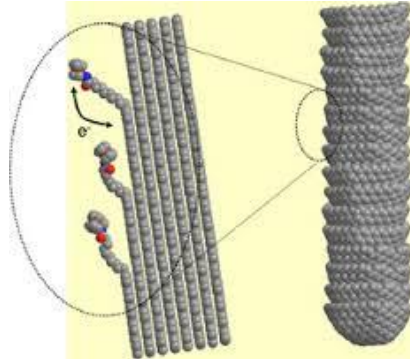


Figure 3.2. Structures of carbon nanofibers

Based on the stacked orientation of graphene layers and their fiber axis, CNFs are classified into:

- ◆ platelet graphite nanofiber, where the graphene layer is perpendicular on fiber axis;
- ◆ herrin-bone / fishbone, where between the graphene layer and the fiber axis is an angle;
- ◆ tubular graphite nanofibers, where the graphene layer and the fiber axis are parallel;

Carbon nanofibers are obtained by two methods: catalytic thermal chemical vapour deposition growth and electrospinning followed by thermal treatment. In general the first method is preferred due to the possibility of controlling the synthesis parameters as temperature, carbon source, or catalyst. For example, the temperature is affecting the morphology of the resulted nanofiber, but also, the rate of decomposition of carbon species used to obtain different nanofibers. The structure of CNF depends also on the type of catalyst and precursor used during synthesis. As a consequence, the ratio of the edge atoms vs. basal atoms is controllable, but also tunable, having as effect the improving of electroanalytical performances [37-44]. Qin and co-workers observed that for platelet graphite nanofiber the best catalytic effect was obtained due to the highest ratio of edge atoms vs. basal atoms, which enhanced the kinetics of the electrode [45]. Also, the dispersion of CNFs into a polymer matrix governs the properties of CNFs. By using ultrasonication the conductivity is improved up to $1.2 \cdot 10^{-2} \text{ Scm}^{-1}$ for 10% loading in comparison with mechanical mixing. In general, the electrical properties of the material are influenced by dispersion and percolation threshold.

Similar to CNTs, CNFs have a wide spectrum of applications in various fields *e.g.*, microfabricated field emission electron sources, microfabricated X-ray sources [37], energy storage [46, 47], nanoporous membranes-wastewater remediation [37], regenerative medicine-intracellular gene delivery devices, drug delivery [33], electrochemical sensors [39] applied in the detection of various organic pollutants, *e.g.*, pentachlorophenol [48]. For some detection applications it is possible that CNTs do not exhibit the useful signal for the studied pollutants, but good properties were achieved using CNF, an example being the detection of sulfide [49].

3.2. Chemically-modified electrodes

A new research direction has been undertaken in electrochemistry with the introduction of chemically-modified electrodes (CME) by Murray and focussed on improving sensitivity and selectivity. Until 1970 the used electrode material were C, Au, Hg, and Pt [50]. This new class of electrodes has attracted considerable interest due to their wide applications.

A chemically-modified electrode was defined as "electrode made of a conducting or semiconducting material that is coated with a selected monomolecular, multimolecular, ionic, or polymeric film of a chemical modifier and that by means of faradaic (charge-transfer) reactions or interfacial potential differences (no net charge transfer) exhibits chemical, electrochemical, and/or optical properties" [51].

In order to obtain chemically-modified electrodes four main pathways consisting in sorption, covalently modified carbon, redox polymer coating, and heterogeneous multilayers were suggested [52].

As was mentioned, for obtaining improved performances of studied materials, their properties have been modified through various procedures. As a consequence, various sensing applications based on chemically modified electrodes were developed, *e.g.*, detection of hydrogen sulfide [53], simultaneous detection of dopamine and ascorbic acid [54] etc.

3.2.1. Zeolite-modified electrodes

Since its discovery in a volcanogenic sedimentary rock, natural zeolite became a very popular material in research and as a consequence a wide variety of applications has been reported in electroanalysis, (electro)catalysis, in agriculture, soil remediation, and energy storage [55].

The structure of zeolite comprises tetrahedrally-coordinated silicon or aluminium atoms with oxygen atoms. This type of lattice leads to a microporous material (pore diameters from 0.3 to 1 nm). Such an aluminosilicate crystalline lattice exhibits molecular sieve selectivity, ion-exchange capacity and inherent catalytic properties [56]. Probably, one of the most important characteristics of zeolites is the exchange of ions with the external medium. The rate of ion-exchange is depending on the framework structure and its charge density, the size and shape of ion but also, the valence and the concentration in the electrolyte.

Among the multitude of natural zeolites, *e.g.*, clinoptilolite, mordenite, stilbite or paulingite, the most used in applications is clinoptilolite, both natural or synthetic. For some applications it is necessary to modify the natural zeolite and for that acidic/basic treatments will be applied. For obtaining zeolite modified electrodes a crucial step will be the preparation protocol. In the literature several methods are reported, which can be summarized in four main groups, *e.g.*, the dispersion of zeolite particles within binder matrix, the introduction of zeolite particles in conductive substrates, the coating on solid electrode of zeolite embedded into polymer films, and the covalent binding to an electrode surface [57]. Considering the variety of preparation methods, it is an understatement that the uses of these electrodes can only be classified into molecular recognition, charge and mass transport characterization, electroanalysis, (electro)catalysis, and energy storage [58].

Zeolite-modified electrodes have received great interest regarding their wide electroanalytical applications. Here, Walcarius classified the analytical applications as follows: direct amperometric detection [59], voltammetric detection after a pre-concentration step, indirect amperometric detection of non-electroactive species or potentiometric determinations by using zeolite membranes [60]. Even if the size and the shape of zeolites are showing promising selectivity, under amperometric studies, the results can be affected by the low specificity of adsorbants, so the working conditions should be chosen with great attention. By using zeolite-modified electrodes organic and inorganic compounds have been detected *e.g.*, glucose [61], urea [62], ascorbic acid and dopamine [63], ibuprofen [64] but also nitrite and nitrate [65].

3.2.2. Electrochemically-decorated electrodes

Electrochemically-decorated electrodes were developed as an answer to a high demand of new types of electrode materials able to improve the electroanalytical performances. Thus, nanoparticles (NPs) have attracted much attention due to their unique size-dependent properties, low cost, but also, will bring some advantages as effective catalysis and fast mass transport. From the large variety of NP materials, the most relevant for sensor application are metals, *e.g.*, Au, Ag, Pd, and metal-oxides, *e.g.*, ZnO, TiO₂.

Generally, the method of obtaining electrochemically-decorated electrodes consists in the direct electrodeposition of NPs from an appropriate salt solution on to the surface of the electrode by applying a reducing potential. During the electrodeposition, the NPs are attached to the edges or on substrate's defects, thus usually obtaining a non-uniform distribution. It was observed that the deposition time, the deposition potential, and electrolyte concentration will influence the size of the electrodeposited particles [66, 67]. Yamada and co-workers showed that the average diameter of electrodeposited particles will increase in time (in a period from 10 to 60s), but for higher values, *e.g.*, 10 minutes, the entire surface of the electrode will be covered with multilayer clusters [68].

These types of sensors has shown interesting results, but one big disadvantage is given by their stability over time. Due to working conditions *e.g.*, pH, saturation level, the surface of the electrode can be fouled, making in-situ applications impossibles. However, sensing applications of hydrogen peroxide [69], respective, nifedipine [70] on Ag NPs electrodeposited on glassy carbon substrate, but also of pharmaceuticals, *e.g.*, fluoxetine on Ag NPs electrodeposited on a carbon nanofiber substrate [71] were developed.

3.3. References

- [1] C.M.A. Brett, A. Oliveira Brett, Electrochemical sensing in solution –origins, applications and future perspectives, *J. Solid State Electrochem.*, (2011) 15, 1487-1494.
- [2] J. Wang, *Analytical electrochemistry*, 2nd Edition, John Wiley & Sons. Inc., New York, 2001.
- [3] A. Fujishima, Y. Einaga, *Diamond electrochemistry*, 1st Edition, Elsevier, 2005.
- [4] A. Kraft, Doped diamond: a compact review on a new, versatile electrode material, *Int. J. Electrochem. Sci.*, (2007) 2, 355-385.

- [5] J.H.T. Luong, K.B. Male, J.D. Glennon, Boron-doped diamond electrode: synthesis, characterization, functionalization and analytical applications, *Analyst*, (2009) 134, 1965-1979.
- [6] R.G. Compton, J.S. Foord, F. Marken, Electroanalysis at diamond-like and doped-diamond electrodes, *Electroanal.*, (2003) 15(17), 1349-1363.
- [7] C. Comninellis, Electrochemical stability of BDD electrode in acid medium, Proc. 7th Workshop Diamond Electrodes, Interlaken 19.10.2004.
- [8] T.N. Rao, A. Fujishima, Recent advances in electrochemistry of diamond, *Diam. Relat. Mater.*, (2000) 9, 384-389.
- [9] M. Panizza, E. Brillas, C. Comninellis, Application of boron-doped diamond electrodes for wastewater treatment, *J. Environ. Eng. Manag.*, (2008) 18(3), 139-153.
- [10] S. Ammar, R. Abdelhedi, C. Fox, C. Arias, E. Brillas, Electrodegradation of the dye indigo carmine at boron-doped diamond anode for wastewater remediation, *Environ. Chem. Lett.*, (2006) 4, 229-233.
- [11] F. Manea, A. Jakab, **M. Ardelean**, A. Pop, I Vlaicu, Boron-doped diamond electrode-based advanced treatment methods for drinking water, *Environ. Eng. Manag. J.*, (2014) 13 (9), 2167-2172.
- [12] **M. Ardelean**, F. Manea, R. Pode, Electrochemical detection of fluoxetine on boron-doped diamond electrode, *Int. J. Pharm. Pharm. Sci.*, (2013) 5(3), 318-322.
- [13] B.C. Lourencao, R.A. Medeiros, R.C. Rocha-Filho, O. Fatibello-Filho, Simultaneous differential pulse voltammetric determination of ascorbic acid and caffeine in pharmaceutical formulations using boron-doped diamond electrode, *Electroanal.*, (2010) 22(15), 1717-1723.
- [14] R.A. Madeiros, B.C. Lourencao, R.C. Rocha-Filho, O. Fatibello-Filho, Simultaneous voltammetric determination of synthetic colorants in food using cathodically pretreated boron-doped diamond electrode, *Talanta*, (2012) 97, 291-297.
- [15] L. Bandzuchova, L.Svorc, J. Sochr, J. Svitkova, J. Chylkova, Voltammetric method for sensitive determination of herbicide picloram in environmental and biological samples using boron-doped diamond electrode, *Electrochim. Acta*, (2013) 111, 242-249.
- [16] S. Iijima, Helical microtubules of graphitic carbon, *Nature*, (1991) 354, 56-59.
- [17] A. Quereschi, W.P.Kang, J.L. Davidson, Y. Gurbuz, Review on carbon-derived, solid-state, micro and nano sensors for electrochemical sensing applications, *Diam. Relat. Mater.*, (2009) 18, 1401-1420.
- [18] K.Scida, P.W. Stege, G. Haby, G.A. Messina, C.D. Garcia, Recent applications of carbon-based nanomaterials in analytical chemistry: critical review, *Anal. Chim. Acta*, (2011) 691(1-2), 6-17.
- [19] G. Centi, S. Perathoner, Problems and perspectives in nanostructured carbon-based electrodes for clean and sustainable energy, *Catal. Today*, (2010) 150, 151-162.
- [20] J.J. Gooding, Nanostructured electrodes with carbon nanotubes: a review on electrochemistry and applications for sensing, *Electrochim. Acta*, (2005) 50, 3049-3060.
- [21] A. Eatemadi, H. Daraee, H. Harimkhanloo, M. Kouhi, N. Zarghami, A. Akbarzadeh, M. Abasi, Y. Hanifehpour, S.W. Joo, Carbon nanotubes: properties, synthesis, purification, and medical applications, *Nanoscale Res. Lett.*, (2014) 9(1), 393-406.

- [22] I. Kang, Y.H. Hueng, J.H. Kim, J.W. Lee, R. Gollapudi, S. Subramanian, S. Narasimhadevara, D. Hurd, G.R. Kirikera, V. Shanov, M.J. Schultz, D. Shi, J. Boerio, S. Mall, M. Ruggles-Wren, Introduction to carbon nanotube and carbon nanofiber smart materials, *Composites: Part B*, (2006) 37, 382-394.
- [23] P.M. Ajayan, Nanotubes from carbon, *Chem. Rev.*, (1999) 99, 1787-1799.
- [24] Z. Liu, Z. Shen, T. Zhu, S. Hou, L. Ying, Z. Shi, Z. Gu, Organizing single-walled carbon nanotubes on gold using wet chemical self-assembling technique, *Langmuir*, (2000) 16(8), 3569-3573.
- [25] S.G. Prolongo, B.G. Meliton, G. Del Rosario, A. Urena, Simultaneous dispersion and alignment of carbon nanotubes in epoxy resin through chronoamperometry, *Carbon*, (2012) 50, 5489-5497.
- [26] X.L. Xie, Y.W. Miu, X.P. Zhou, Dispersion and alignment of carbon nanotubes in polymer matrix: a review, *Mater. Sci. Eng. R.*, (2005) 49, 89-112.
- [27] Y.J. Kim, T.S. Shin, H.D. Choi, J.H. Kwon, Y.C. Chung, H.G. Yoon, Electrical conductivity of chemically modified multiwalled carbon nanotubes/epoxy composites, *Carbon*, (2005) 43, 23-30.
- [28] F.H. Gojny, M.H.G. Wichmann, B. Fiedler, K. Schulte, Influence of different carbon nanotubes on the mechanical properties of epoxy composites-a comparative study, *Compos. Sci. Technol.*, (2005) 65, 2300-2313.
- [29] Y.S. Song, J.R. Youn, Influence of dispersion states of carbon nanotubes on physical properties of epoxy nanocomposites, *Carbon*, (2005) 43, 1378-1385.
- [30] J.M. Marulanda, Carbon nanotubes, In-Teh, Vukovar, 2010.
- [31] L. Agui, P. Yanez-Sedano, J.M. Pingarron, Role of carbon nanotubes in electroanalytical chemistry. A review, *Anal. Chim. Acta*, (2008) 622, 11-47.
- [32] B. Uslu, S.A. Ozkan, Electroanalytical application of carbon based electrodes to the pharmaceuticals, *Anal. Lett.*, (2007) 40, 817-853.
- [33] P.A. Tran, L. Zhang, T.J. Webster, Carbon nanofibers and carbon nanotubes in regenerative medicine, *Adv. Drug Deliver. Rev.*, (2009) 61, 1079-1114.
- [34] A. Remes, A. Pop, F. Manea, A. Baci, S.J. Picken, J. Schoonman, Electrochemical determination of pentachlorophenol in water on a multi-walled carbon nanotube-epoxy composite electrode, *Sensors*, (2012) 12, 7033-7046.
- [35] B. Habibi, M. Jahanbakhshi, M.S. Pournaghi-Azar, Differential pulse voltammetric simultaneous determinations of acetaminophen and ascorbic acid using single-walled carbon-nanotube modified carbon ceramic electrode, *Anal. Biochem.*, (2011) 411, 167-175.
- [36] J.S. Ye, Y. Wen, W. De Zhang, L.M. Gan, G.Q. Xu, F.S. Sheu, Selective voltammetric detection of uric acid in the presence of ascorbic acid at well-aligned carbon nanotube electrode, *Electroanal.*, (2003) 15(21), 1693-1693.
- [37] A.V. Melenchko, V.I. Merlukov, T.E. McKnight, M.A. Guillorn, K.L. Klein, D.H. Lowndes, M.L. Simpson, Vertically aligned carbon nanofibers and related structures: controlled synthesis and directed assembly, *J. Appl. Phys.*, (2005) 97, 041301-041301-39.
- [38] A. Allaoui, S.H. Hoa, M.D. Pugh, The electronic transport properties and microstructure of carbon nanofiber/epoxy composites, *Compos. Sci. Technol.*, (2008) 68, 410-416.
- [39] L. Feng, N. Xie, J. Zhong, Carbon nanofibers and their composites: a review of synthesizing, properties and applications, *Mater.*, (2014) 7, 3919-3945.
- [40] C.W. Huang, G.C. Wu, W.H. Lin, Y.Y. Li, Temperature effect on the formation of catalyst for growth of carbon nanofibers, *Carbon*, (2009) 47, 795-903.
- [41] K.P. de Jong, J.W. Geus, Carbon nanofibers: catalytic synthesis and applications, *Cat. Rev. -Sci. Eng.*, (2000) 42(4), 481-510.

- [42] S.S. Tzeng, K.H. Hung, T.H. Ko, Growth of carbon nanofibers on activated carbon fibers fabrics, *Carbon*, (2006) 44, 859-865.
- [43] D.H. Wang, S. Sihn, A.K. Roy, J.B. Baek, L.S. Tan, Nanocomposites based on vapour-grown carbon nanofibers and an epoxy: functionalization, preparation and characterization, *Eur. Polym. J.*, (2000) 46, 1404-1416.
- [44] G.G. Tibbets, M.L. Lake, K.L. Strong, B.P. Rice, A review of the fabrication and properties of vapour-grown carbon nanofiber/polymer matrix, *Compos. Sci. Technol.*, (2007), 62, 1709-1718.
- [45] Y.H. Qin, H.H. Yang, X.S. Zhang, P. Li, C.A. Ma, Effect of carbon nanofibers microstructures on electrocatalytic activities of Pd electrocatalysts for ethanol oxidation in alkaline medium, *Int. J. Hydrogen Energy*, (2010) 35, 7667-7674.
- [46] Y.J. Yang, G.J. Zhao, S. Hu, Direct current electrodeposition of carbon nanofibers in DMF, *Electrochem. Commun.*, (2007) 7, 2681-2685.
- [47] G. Zou, D. Zhang, C. Dong, H. Li, K. Xiong, L. Fei, Y. Qian, Carbon nanofibers: synthesis, characterization and electrochemical properties, *Carbon*, (2006) 44, 828-832.
- [48] A. Baciú, F. Manea, A. Remes, S. Motoc, G. Burtica, R. Pode, Anodic determination of pentachlorophenol from water using carbon nanofiber-based composite electrode, *Environ. Eng. Manag. J.*, (2010) 9(11), 1555-1562.
- [49] **M. Ardelean**, F. Manea, N. Vazsilcsin, R. Pode, Electrochemical detection of sulphide in water/seawater using nanostructured carbon-based electrodes, *Anal. Methods*, (2014) 6, 4775-4782.
- [50] Z.M. Zen, A.S. Kumar, D.M. Tsai, Recent updates of chemically modified electrodes in analytical chemistry, *Electroanal.*, (2002) 15(13), 1073-1087.
- [51] R. A. Durst, A. J. Baumner, R. W. Murray, R. P. Buck, C. P. Andrieux, Chemically modified electrodes: recommended terminology and definitions, *Pure Appl. Chem.*, (1997) 69(6), 1317-1323.
- [52] G.G. Wildegoose, C.E. Banks, H.C. Leventis, R.G. Compton, Chemically modified carbon nanotubes for use in electroanalysis, *Microchim. Acta*, (2006) 152, 187-214.
- [53] N.S. Lawrence, R.P. Deo, J. Wang, Electrochemical determination of hydrogen sulfide at carbon nanotube modified electrodes, *Anal. Chim. Acta*, (2004) 517(1-2), 131-137.
- [54] Z. Wang, J. Liu, Q. Liang, Y. Wang, G. Luo, Carbon nanotube-modified electrodes for the simultaneous determination of dopamine and ascorbic acid, *Analyst*, (2002), 127, 653-658.
- [55] S. Wang, Y. Peng, Natural zeolites as effective adsorbents in water and wastewater treatment, *Chem. Eng. J.*, (2010) 156, 11-24.
- [56] D.A. Rolison, R.J. Nowak, T.A. Welsh, C.G. Murray, Analytical implications of zeolites in overlayers at electrodes, *Talanta*, (1991) 38(1), 27-35.
- [57] A. Walcarius, Zeolite-modified electrodes in electroanalytical chemistry, *Anal. Chim. Acta*, (1999) 384, 1-16.
- [58] A. Walcarius, Zeolite-modified electrodes: analytical applications and prospects, *Electroanal.*, (1996) 8(11), 971-986.
- [59] J. Wang, A. Walcarius, Zeolite-modified carbon paste electrode for selective monitoring of dopamine, *J. Electroanal. Chem.*, (1996) 407, 183-187.
- [60] A. Walcarius, Factors affecting the analytical applications of zeolite modified electrodes: indirect detection of nonelectroactive cations, *Anal. Chim. Acta*, (1999) 388, 79-91.

- [61] A. Baciú, A. Pop, A. Remes, F. Manea, G. Burtica, Non-enzymatic electrochemical determination of glucose on silver-doped zeolite CNT composite electrode, *Adv. Sci. Eng. Med.*, (2011) 3, 13-19.
- [62] F. Manea, A. Pop, C. Radovan, P. Malchev, A. Bebeselea, G. Burtica, S. Picken, J. Schoonman, Voltammetric detection of urea on an Ag-modified zeolite-expanded graphite-epoxy composite electrode, *Sensors*, (2008) 8, 5806-5819.
- [63] A. Baciú, A. Remes, E. Ilinoiu, F. Manea, S.J. Picken, J. Schoonman, Carbon nanotubes composite for environmentally friendly sensing, *Environ. Eng. Manag. J.*, (2012) 11(2), 239-247.
- [64] F. Manea, S. Motoc, A. Pop, A. Remes, J. Schoonman, Silver-functionalized carbon nanofiber composite electrodes for ibuprofen detection, *Nanoscale Res. Lett.*, (2012) 7, 331-335.
- [65] F. Manea, A. Remes, C. Radovan, R. Pode, S. Picken, J. Schoonman, Simultaneous electrochemical determination of nitrate and nitrite in aqueous solution using Ag-doped zeolite-expanded graphite-epoxy electrode, *Talanta*, (2010) 83, 66-71.
- [66] L. Rassaei, M. Amiri, C.C. Cirtiu, M. Sillanpää, F. Marken, M. Sillanpää, Nanoparticles in electrochemical sensors for environmental monitoring, *Tr. Anal. Chem.*, (2011) 30(11), 1704-1715.
- [67] C.M. Welch, R.G. Compton, The use of nanoparticles in electroanalysis: a review, *Anal. Bioanal. Chem.*, (2006) 384, 601-619.
- [68] D. Yamada, T.A. Ivandini, M. Komatsu, A. Fujishima, Y. Einaga, Anodic stripping voltammetry of inorganic species of As^{3+} and As^{5+} at gold-modified boron doped diamond electrodes, *J. Electroanal. Chem.*, (2008) 615, 145-153.
- [69] C.M. Welch, C.E. Banks, A.O. Simm, R.G. Compton, Silver nanoparticles assemblies supported on glassy-carbon electrodes for the electro-analytical detection of hydrogen peroxide, (2005) 382, 12-21.
- [70] M. Baghayeri, M. Namadchian, H. Karimi-Maleh, H. Beitollahi, Determination of nifedipine using nanostructured electrochemical sensor based on simple synthesis of Ag nanoparticles at the surface of glassy carbon electrode: application to the analysis of some real samples, *J. Electroanal. Chem.*, (2013) 697, 53-59.
- [71] **M. Ardelean**, F. Manea, R. Pode, Silver-electrodeposited carbon nanofiber-epoxy electrode for fluoxetine detection, *APCBEE Procedia*, In press.

4. ELECTROCHEMICAL TECHNIQUES USED IN ANALYTICAL APPLICATIONS

In the recent years, the attention of scientific research groups was focused on water quality, mainly regarding the sensitive detection of organic pollutants in small volume samples assuring low limits of detection. In this sense, electrochemical techniques have become indispensable tools due to their characteristics, such as: high sensitivity, accuracy, precision, selectivity (of both target compound, but also choosing the electrode material), wide linear dynamic range and low-cost of instrumentation (important aspect from economical point of view). The recent advances in instrumentation, computerized processing of analytical signal and the innovative ideas of electrochemists had led to various approaches on applicative analysis, exploited in a large amount of scientific papers, which have imposed new trends in research fields [1-3].

The most used voltammetric methods, *e.g.*, cyclic voltammetry (CV), differential-pulsed voltammetry (DPV) and square wave voltammetry (SWV), are based on the continuously change of applied potential on electrode-surface interface, followed by the measurement of response current.

4.1. Cyclic voltammetry

Cyclic voltammetry (CV), the first experiment performed in electroanalysis studies, is one of the most versatile and used techniques due to provided information on thermodynamics of redox processes, kinetics of heterogeneous electron-transfer reactions and on coupled chemical or adsorption processes [1-4]. CV history had begun in 1938 with experimental studies. Then, in 1948 Randles and Sevcik described it was theoretically [5]. Since then, several scientific papers revealed the applicability of cyclic voltammetry on various fields: characterization of several types of materials [6, 7], determination of electrochemical behaviour of widely used organic compounds [8, 9] etc.

The experimental set-up used for obtaining cyclic voltammograms is presented in Figure 4.1 and includes a three electrodes cell. The potential relative to reference electrode (RE) is scanned at the working electrode (WE), and the resulting current monitored into the solution is flowing through the counter electrode (CE). Even if the device used for measuring the potential difference RE-WE has high impedance input, a negligible current is drawn through the reference electrode, and its potential will have a constant value equal to the value of the open circuit.

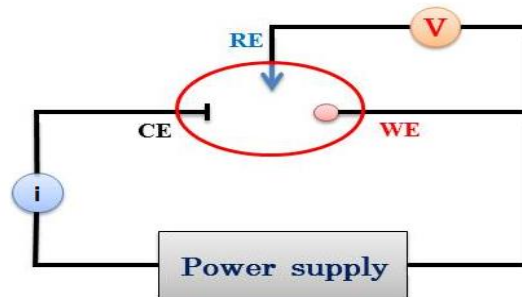


Figure 4.1. Experimental set-up used to record cyclic voltammograms

Under experimental conditions, the potential is linearly scanned forward and reverse between two extreme values by using a triangular potential waveform as it can be seen in Figure 4.2. In Figure 4.3 is presented the expected response of a reversible redox couple during a single potential cycle. The anodic current is obtained for a more positive potential of the working electrode than that of a redox couple presented in the solution (forward scan). In this case, the occurred process on electrode surface is oxidation, *e.g.*, electrons going from the solution to the electrode. Similar, the cathodic current is obtained for a more negative potential value of working electrode than the reduction potential of a redox couple (reverse scan); the corresponding process is reduction, *e.g.*, electrons flowing away from the electrode.

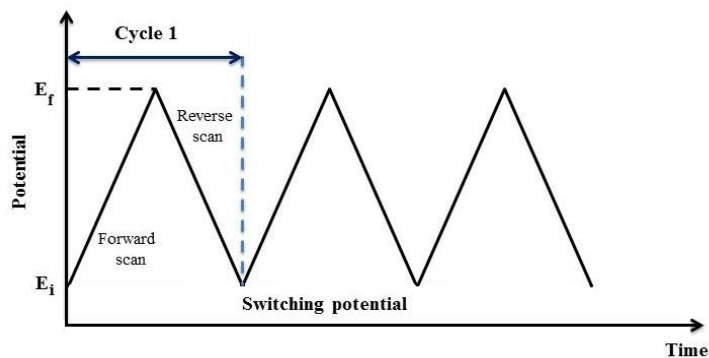


Figure 4.2. Potential-time excitation signal in a cyclic voltammetry experiment.

The recorded electrochemical signal reflects the type of occurred at the surface of the working electrode. These can present complicated pathways which involve several steps, such as: charge transfer reaction, transfer of reactant from the solution to the electrode surface, forward the product from the electrode surface into the solution, but also, possible chemical reactions preceding or following the oxidation-reduction process [10]. The simplest reaction is controlled by mass transport of electroactive species on the electrode surface, the electron transfer across the interface and the transport of products back to the solution. Mass transport may occur in three different ways:

- diffusion (spontaneous movement under the influence of concentration gradient);

- convection (induced transport to the electrode by a physical movement);
- migration (movement of charged particles along an electrical field).

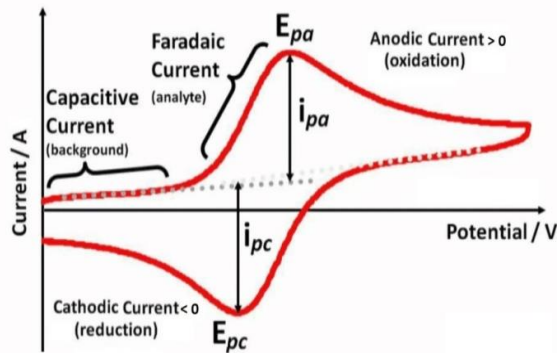


Figure 4.3. Typical cyclic voltammogram of a reversible redox couple during a single potential scan

Different concentrations of electroactive species which depend on the distance to the surface of the electrode will impose a chemical gradient. In order to balance the concentration gradient, the system response with a corresponding flux of material by diffusion. The diffusion process is described by Fick's laws [11].

In consequence, the observed faradaic current (Figure 4.3) depends on the kinetics and transport by diffusion of electroactive species. In the case of an oxidation reaction involving n electrons, at equilibrium (298 K) the Nernst equation describes the dependence potential vs. concentration of oxidized and reduced species of the redox couple:



$$E = E^{\circ'} + \frac{0.059}{n} \lg \frac{[O]}{[R]} \quad (4.2)$$

where E is the applied potential, $E^{\circ'}$ is the formal potential, $[O]$ and $[R]$ are the concentrations of oxidized and reduced species at the electrode – electrolyte interface. Still, depending on the studied system, this equation may or may not obey. As a consequence, there have been distinguished three types of systems: reversibles, irreversibles and quasi-reversibles. [2-4, 12]

Reversible systems

A reversible system is defined by a stable concentration of both oxidized and reduced species, with a rapid electron exchange on the working electrode. Considering a linear diffusion, the Fick's laws were solved by Randles-Sevcik equation, which describes the linearity peak current vs. analyte concentration:

$$I_p = 2.69 \cdot 10^5 \cdot n^{3/2} \cdot AD^{1/2} \cdot Cv^{1/2} \quad (4.3)$$

where I_p is the peak current (A), n is the number of transferred electrons (equivalent/mol), A is the electrode surface area (cm^2), D is the diffusion coefficient (cm^2s^{-1}), C is the analyte concentration (molL^{-1}) and v is the scan rate (Vs^{-1}).

The position of the peaks on potential axis is related to the formal potential of redox couple, defined by:

$$E^{o'} = \frac{E_{pa} + E_{pc}}{2} \quad (4.4)$$

where E_{pa} and E_{pc} are the anodic and cathodic potential peaks.

The peak potential is given by the following relationship:

$$E_p = E_{1/2} - 1.109 \frac{RT}{nF} \quad (4.5)$$

where $E_{1/2}$ is the half-wave potential (V), R is the universal gas constant ($8.314 \text{ JK}^{-1}\text{mol}^{-1}$), T is the temperature (K), n is the number of transferred electrons in the reaction and F is the Faraday constant ($F=96487 \text{ C}$).

The half-wave potential is defined as:

$$E_{1/2} = E^{o'} + \frac{RT}{nF} \ln \left(\frac{D_R}{D_O} \right)^{1/2} \quad (4.6)$$

where D_O and D_R are the coefficients of diffusion for oxidized and reduced species.

In practice, the peak potential is quite broad, and usually the half peak potential, defined as in equation 4.7 is used:

$$E_{p/2} = E_{1/2} + 1.09 \frac{RT}{nF} \quad (4.7)$$

As it can be observed, the peak potential is independent of peak current (I_p) and scan rate, but it is proportional with the square root of the scan rate [4, 13].

Irreversible systems

For an irreversible process, the rate of mass transport is higher than the rate of charge transfer. In this case, the Nernst equilibrium is not accomplished and an important change in the shape of voltammogram is noticed. By increasing the scan rate, a more pronounced anodic-cathodic peak separation is observed, which in time will be minimized until the complete disappearance of cathodic peak (Figure 4.4).

In this case, for a slow (irreversible) reaction, the peak current is defined by:

$$I_p = 2.99 \cdot 10^5 \cdot n \cdot a^{1/2} \cdot n_a^{1/2} \cdot AD^{1/2} \cdot Cv^{1/2} \quad (4.8)$$

where I_p is the peak current (A), n is the number of transferred electrons (equivalent/mol), a is the transfer coefficient and n_a is the number of the electrons involved in charge-transfer step, A is the electrode surface area (cm^2), D is the diffusion coefficient (cm^2s^{-1}), C is the analyte concentration (molL^{-1}) and v is the potential scan rate (Vs^{-1}).

For peak potential, a shift to the scan rate is reported and is defined as:

$$E = E^{o'} - \frac{RT}{an_a F} \left[0.78 - \ln \frac{k^o}{D^{1/2}} + \ln \left(\frac{an_a F v}{RT} \right)^{1/2} \right] \quad (4.9)$$

where k^o is the heterogeneous rate constant and a is the transfer coefficient.

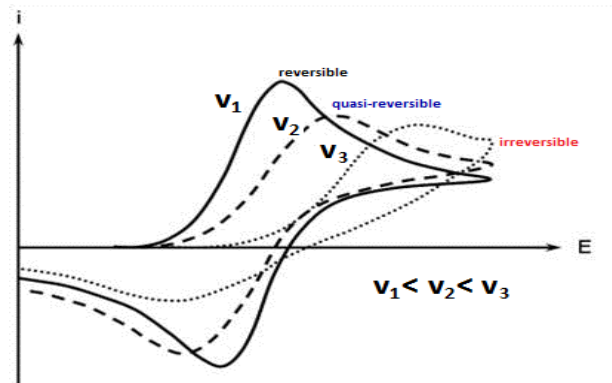


Figure 4.4. Scan rate vs. irreversibility dependence.

In comparison with previously presented systems, here the peak potential value is higher than $E^{o'}$, with the over potential related to the heterogeneous rate constant (k^o) and transfer coefficient. By increasing the scan rate of 10 times, a shifting of $1.15RT/aF$ ($30/an$ mV at 25°C) is noticed. Therefore, by decreasing an , a more drawn-out voltammogram is obtained. As regarding the peak current, its values is proportional with the bulk concentration, but its height will be lower. The absence of cathodic peak current is not always specific to an irreversible process, similar behavior being observed for the systems where the charge transfer is followed by a fast and irreversible chemical reaction.

Quasi-reversible systems

These types of systems introduced by Matsuda and Ayabe [14] are intermediate between reversible and irreversible systems and present some electron-transfer kinetics limitations. The extend of irreversibility increases with the increment of the scan rate, but in the same time a decrease in the peak current related to reversible case is noticed. Also, the separation between anodic and cathodic peaks increases. In general, for limited values of heterogeneous rate constant on the range $0.3v^{1/2} \geq k^o \geq 2 \cdot 10^{-5} v^{1/2} \text{ cm s}^{-1}$, the system is considered quasi-reversible.

The peak current of a quasi-reversible system is given by:

$$I_p = I_p(\text{rev}) * K(\Lambda, a) \quad (4.10)$$

$$\Lambda = \frac{k^o}{(D_O^{1-a} D_R^a)^{1/2}} \quad (4.11)$$

where $I_p(\text{rev})$ is the reversible value of I_p , and $K(\Lambda, a)$ is a function of quasi-reversible system which depends on Λ , a specific parameter of this type of system. This function is solved by numerical methods.

The peak potential is given by:

$$E_p = E_{1/2} - Y(\Lambda, a) \left(\frac{RT}{F} \right) \quad (4.12)$$

where $Y(\Lambda, a)$ is a function of quasi-reversible system.

The parameters $K(\Lambda, a)$ and $Y(\Lambda, a)$ attain limiting values characteristic of reversible or totally irreversible processes as Λ varies.

In Table 4.1 are gathered the reversibility conditions for each type of system.

Table 4.1. Reversibility conditions used applied in cyclic voltammetry

| Reversible | Irreversible | Quasi-reversible |
|---|---|--|
| $\Delta E_p = E_{pa} - E_{pc} = 0.059/n$ (V) | lack of cathodic peak current | I_{pa} increase with v , but not proportionally |
| $ E_p - E_{p/2} = 0.059/n$ (V) | $i_{pa} \approx v^{1/2}$ | $ I_{pa}/I_{pc} = 1$ if $\alpha_c = \alpha_a = 0.5$ |
| $ I_{pa}/I_{pc} = 1$ | $E_p - E_{p/2} = 0.048/an$ (V) | $\Delta E_p > 0.059/n$, increase with v |
| $i_p \approx v^{1/2}$ | Shifting with $0.048/an$ of E_{pa} for an increment of $10 \cdot v$ | Shifting of E_{pa} to more positive values if v increase |
| E_p independent of v | | |

It is possible that a reversible process at low values of scan rates to become irreversible at high values of scan rates by passing through an intermediate condition.

This technique used for acquiring qualitative information on electrochemical reactions presents a low limit of detection, caused not by the poor sensitivity of the methods, but rather by the high capacitive current which results when the potential is swept.

Cyclic voltammetry is not sensitive enough for trace determinations of studied analytes, but provides useful information on analyte reaction mechanism, further applied on optimization procedures of analytical conditions.

4.2. Differential-pulsed voltammetry

This technique is a very useful and powerful tool for direct trace level determinations of organic compounds due to its large applicability and high sensitivity. It belongs to pulsed techniques, based on the application of potential pulse changes. Differential-pulsed voltammetry (DPV) was proposed by Baker and Gardner in 1960 as an improvement to polarographic techniques. The main purpose of it is the enhancement of the faradic current by minimizing the interfering capacitive currents, or simple the investigation of the decay rate of faradic current by taking into consideration the decay of capacitive current (the decay of charging current is considerably faster than the decay of faradic current) [10, 15].

Beside high sensitivity, this technique provides information regarding the oxidation states, the kinetics of studied reaction [16], the recognition of complexation effects [17] and the characterization of electrode material [18-20].

Under DPV conditions, during a pulse period the current is periodically sampled twice, first before the pulse application (I_1) and then at the end of the

pulse (I_2). The contribution of non-Faradaic processes (principally capacitive currents) to the recorded signal is greatly reduced by subtracting I_1 from I_2 . In Figure 4.5 are presented the pulse excitation signal and the corresponding voltammogram recorded (the plot represents $\Delta I = I_1 - I_2$ vs. potential progression).

The most important parameters of this technique are:

- pulse amplitude (a) defined as the height of applied pulse;
- pulse width (δ) defined as the time period for which the pulse is maintained;
- pulse period (t) defined as the time of one cycle of potential variation;
- sample width (τ) defined as time period at which after the potential pulse application the current is measured.

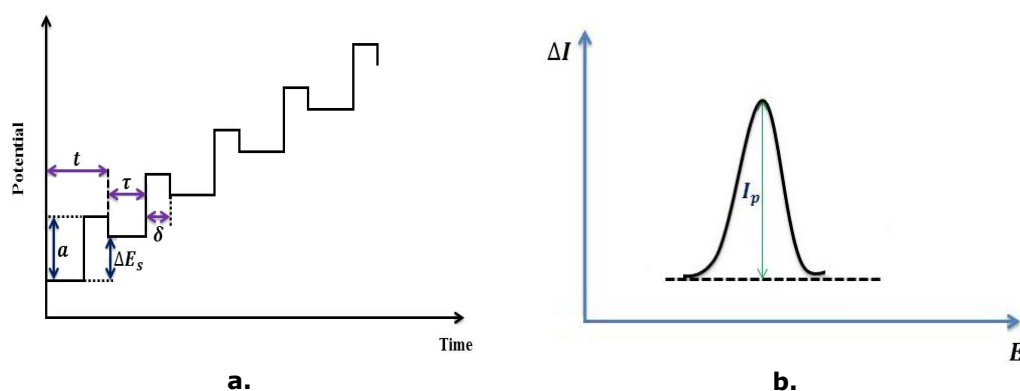


Figure 4.5. a. Pulse excitation signal and **b.** corresponding differential-pulsed voltammogram

Aoki and co-workers had established the peak current values for reversible, irreversible and quasi-reversible reactions at planar stationary electrodes [22], but also at microcylinder electrodes [23]. The peak current of a reversible system recorded on a stationary planar electrode is given by the relationship:

$$I_p = \frac{n F A D^{1/2} C}{\sqrt{n t_m}} \left(\frac{1-\sigma}{1+\sigma} \right) \quad (4.13)$$

$$\sigma = \frac{\exp\left(\frac{nF}{RT}\right)}{\left(\frac{\Delta E}{2}\right)} \quad (4.14)$$

Still, the results obtained by Aoki [22] were not in good agreement with those obtained by Legeai and co-workers for microdisk electrodes [24]. By reducing the intervals of between the pulses and reducing the radius of microelectrode, an increasing contribution of spherical diffusion was observed. Among these theoretical aspects, various studies are discussing the effects of electroanalytical parameters, e.g., sweep rate [25], or the new advances in electrode kinetics [26].

In practice, the most commonly used parameters are amplitude (a), step potential (ΔE_s) and scan rate (v). The selection of these parameters is requiring a trade-off among sensitivity, resolution and speed since for larger pulse amplitude broader and larger peaks were noticed. For pulse amplitude are recommended values between 10 to 100 mV as a good compromise between large values of peak

current and resolution. For pulse amplitude values higher than 100 mV, the signal may be distorted even if the peak will be stronger. Following the same principle, for scan rate are recommended values below 20 mVs^{-1} . Therefore, pulse amplitude of 25-50 mV and scan rate of 5 mVs^{-1} are usually preferred.

In order to obtain the best performances in relation with the electroanalytical parameters, optimization procedures were proposed. Most of them begin with a detailed study of working conditions, *e.g.*, supporting electrolyte, the pH of the solutions, and then step by step the operating parameters (a , v , t , ΔE_s) are optimized. There have been noticed few directions:

- influence of amplitude and scan rate vs. peak current
- influence of amplitude, scan rate and modulation time vs. peak current.

Some results obtained under optimized DPV conditions are presented in Table 4.2.

Table 4.2. Optimization criteria and the results obtained under optimization procedures

| Criteria | Analyte | Electrode | Supporting electrolyte | Optimized parameters | LOD | Ref. |
|------------------------------|--|-------------|---------------------------------------|------------------------------|---|------|
| a; v vs. I_p | Phenolic acids in cotton | GCE | 0.2M phosphate buffer, pH=3 | a=50mV v=50mV/s | 0.033 μM 0.055 μM | 27 |
| | Silymarin (SMR) Vitamin E acetate (VEA) | GCE | 0.08M Britton Robinson buffer, pH=2.8 | a=90mV v=120mV/s | 0.03mg/L SMR; 0.01mg/L VEA | 28 |
| a; v; τ vs. I_p | Ascorbic Acid (AA) Caffeine (CAF) | BDD treated | 0.1M H_2SO_4 | a=100mV v=60mV/s t=15s | 19 μM AA 7 μM CAF | 29 |
| | Albendazole | BDD treated | 0.05M H_2SO_4 | a=75mV v=20mV/s t=7s | 0.0625 μM | 30 |
| | Paracetamol (PAR) Caffeine (CAF) | BDD | 0.2M acetate buffer, pH=4.5 | a=100mV v=70mV/s t=7s | 0.49 μM PAR 0.035 μM CAF | 31 |

Beside these, a new type of optimization based on factorial design was proposed for glyphosate determination in water, soil and vegetable samples by Teofilo and co-workers [32].

By increasing the ratio between faradic and non-faradic current, under DPV conditions the limit of quantification reach about 10^{-8} M of the concentration level. Thus, the sensitivity is highly increased and the characteristics of analytical application are improved. In consequence, this technique is very suitable for trace analysis of organic compounds, species with great environmental interest, or forensics.

4.3. Square wave voltammetry

Originated from Kalousek commutator and Baker's square wave polarography, the format proposed by Osteryoung [33] became the most popular approach of square wave voltammetry (SWV) due to measurement of the current at the end of each half cycle [34].

SWV, a powerful tool widely used in electroanalysis, is a large amplitude technique where a waveform composed of a symmetrical square wave, superimposed on a staircase, is applied to the working electrode. During a square wave cycle the current is sampled twice: first at the end of the forward pulse (I_1), and then, secondly at the end of the reverse pulse (I_2), the resulting voltammogram displaying the difference $\Delta I = I_1 - I_2$ vs. the staircase potential. A typical pulse excitation signal and the corresponding voltammogram are presented in Figure 4.6.

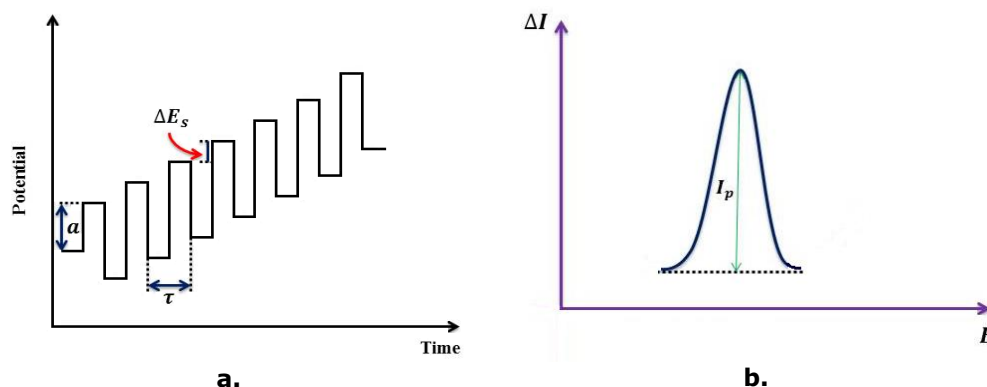


Figure 4.6. **a.** Pulse excitation signal and **b.** corresponding square wave voltammogram.

The most important parameters of SWV are listed below:

- frequency (f)
- pulse amplitude (a)
- step potential (ΔE_s)
- scan rate (v)

defined by the following relationships [35]:

$$f = \frac{1}{\tau} \quad (4.15)$$

$$v = \frac{\Delta E_s}{\tau} = f * \Delta E_s \quad (4.16)$$

where τ is defined as the time period at which, after the potential pulse application, the current is measured.

In practice, the use of frequency values below 250 Hz ($250 \geq f \geq 8$) and the use of potential amplitude values below 25 mV ($25 \geq a \geq 5$) are recommended.

There are several advantages of employing SWV: high speed in analysis by reducing the scan time due to a high effective scan rate, accuracy, lower consumption of electroactive compounds in comparison with DPV and reduced problems with blocking of the electrode surface. The SWV sensitivities are higher than the ones obtained under DPV conditions due to the larger net current obtained (the

responses SWV vs. DPV are 4 times higher for reversible system and 3 times higher for irreversible system) [36].

SWV technique can be used in both electrokinetic and analytical studies [37]. The theoretical aspects regarding the kinetics on electrode surface have been developed by groups of Osteryoung [33, 38] and Lovric [39, 40]. Approaches related to the use of constant scan rate or a potential -corrected SW voltammograms have also been studied [41, 42].

For a reversible system the peak current is given by the relationship:

$$\Delta I_p = -nFAD^{1/2}\Delta\Psi_p f^{1/2}C_0 \quad (4.17)$$

$$\Delta\Psi_p = -\Delta I/nFAc_0(Df)^{1/2} \quad (4.18)$$

The discrimination criteria regarding the type of the process occurred at electrode surface is presented below [43]:

- totally irreversible reaction

$$\frac{\Delta E_p}{\Delta \log(f)} = -\frac{2.3RT}{nF} \quad (4.19)$$

- reversible reaction with only the reactant or the product adsorbed

$$\frac{\Delta E_p}{\Delta \log(f)} = -\frac{2.3RT}{2nF} \quad (4.20)$$

- reversible reaction with reactant or product adsorbed

$$\frac{\Delta E_p}{\Delta \log(f)} = 0 \quad (4.21)$$

The optimization of operating parameters will lead to improvements in relation with the sensitivity. In this context an optimization method has been proposed by a research group from Chemical Institute of São Carlos, Brazil. Prior to the optimization procedure, the influence of pH vs. the peak current and peak potential is studied.

Then, step by step the operating parameters (f , a , ΔE_s) are optimized:

- i. influence of frequency vs. peak current

The optimum value of frequency is given by the frequency value after which the effects of peak current are almost negligible. In addition, this step provides information in relation with some oxidation mechanism aspects (Table 4.3).

Table 4.3. Dependence frequency vs. peak current in relation with the type of reaction

| Type of reaction | f vs. I |
|------------------|-----------------------|
| Reversible | $I = k \cdot f^{1/2}$ |
| Quasi-reversible | non linear |
| Irreversible | $I = k \cdot f$ |

ii. *influence of amplitude vs. peak current*

The optimum value of amplitude is considered the highest value for which a linear dependence a vs. I is obtained, before the saturation plateau is reached [44].

i. *influence of step potential vs. peak current*

Larger values of ΔE_s will affect the resolution of the achieved voltammogram, and in consequence smaller values are recommended.

Table 4.4. Research studies that applied the optimization methodology

| Analyte | Electrode | Supporting electrolyte | Optimized parameters | LOD | Ref. |
|----------------------|-----------|--------------------------------------|------------------------------|----------------------|------|
| acetylsalicylic acid | BDD-H | 0.01M H ₂ SO ₄ | f=50 Hz a=40mV ΔE=2mV | 2μM | 45 |
| benzophenone-3 | BDD | 0.1M Britton Robinson buffer, pH=6 | f=90 Hz a=20mV ΔE=2mV | 0.137μM | 46 |
| carbaryl | BDD | 0.1M Britton Robinson buffer, pH=5.5 | f=100Hz a=50mV ΔE=2mV | 5.5μgL ⁻¹ | 47 |
| 4-nitrophenol | BDD | 0.1M Britton Robinson buffer, pH=6 | f=100 Hz a=50mV ΔE=2mV | 8.4μgL ⁻¹ | 48 |

The limit of detection and the limit of quantification are extremely low under SWV. For a pre-concentration step, these limits can reach 10⁻¹² -10⁻¹⁰ M.

4.4. Chronoamperometry

One of the simplest techniques, chronoamperometry is used when cyclic voltammetry does not offer sufficient information regarding the electrode mechanism. The potential of the working electrode is stepped from a value where no faradic reaction occurs until a value for which the concentration of electroactive species is almost zero. The dependence time vs. current is plotted. In Figure 4.7 are presented the excitation signals for a single and a double chronoamperometry step. Since the mass transport is controlled only by diffusion, the changes in concentration gradient in the vicinity of electrode surface are reflected on current – time curve. Under these conditions, the current decay is given by Cottrell equation [2]:

$$I_p = \frac{n F A D^{1/2} C}{(\pi^* t)^{1/2}} = k t^{-1/2} \quad (4. 21)$$

Also, as a consequence of these theoretical aspects, chronoamperometry is used often for determining the coefficient of diffusion of electroactive species or for determining the electroactive surface area of the working electrode.

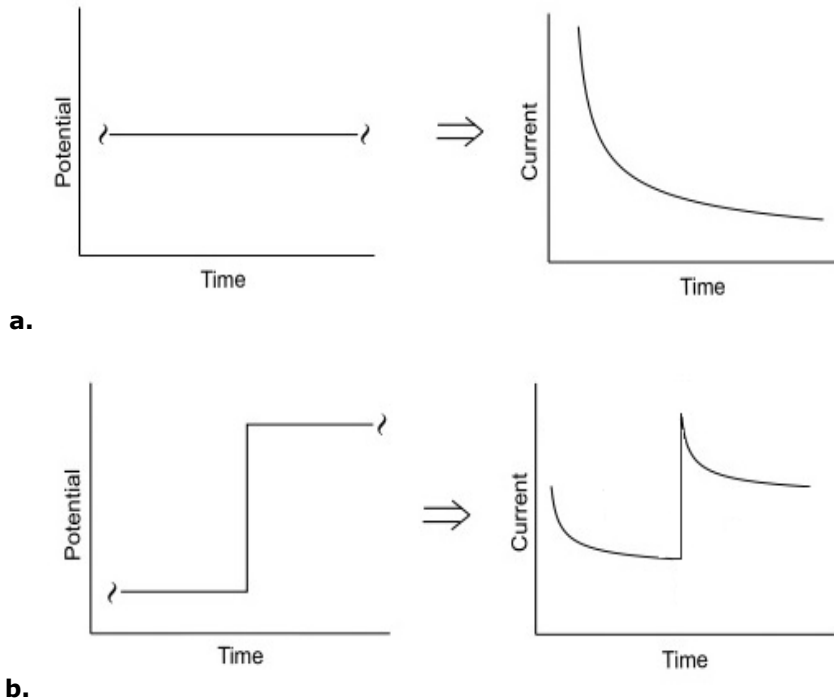


Figure 4. 7. Potential –time waveform (left) and current-time response (right) in **a.** single step, **b.** double step of chronoamperometry

Based on the results obtained on cyclic voltammetry, which represent a key-reference in choosing the detection potential, chronoamperometry is used with success to study electrode reactions that occur in several steps (see Figure 4.7.b).

Chronoamperometry is widely used in electroanalytical applications, due to its easy operation in stirred or un-stirred solution. It also can be automated for in-field monitoring of different pollutants.

4.5. References

- [1] P. Kissinger, W.P. Heineman, Laboratory techniques in electroanalytical chemistry, 2nd Edition, Marcel Dekker, Inc., New York, 1996.
- [2] J. Wang, Analytical electrochemistry, 2nd Edition, John Wiley & Sons. Inc., New York, 2001.
- [3] A.J. Bard, L.R. Faulkner, Electrochemical methods. Fundamentals and applications, 2nd Edition, John Wiley & Sons. Inc., New York, 2001.
- [4] C.M.A. Brett, A. M. Oliveira Brett, Electrochemistry. Principles, methods and applications, Oxford University Press Inc., New York, 1993.
- [5] J.E.B. Randles, A ray cathode ray polarograph. Part II.—The current-voltage curves, *Trans. Faraday Soc.*, (1948) 44, 327-338.
- [6] J.F. Rusling, S.L. Suib, Characterizing materials with cyclic voltammetry, *Adv. Mater.*, (1996) 6(12), 922-930.

- [7] M. Panizza, G. Cerisola, Influence of anode material on the electrochemical oxidation of 2-naphthol. Part 1. Cyclic voltammetry and potential step experiments, *Electrochim. Acta*, (2003) 48, 3491-3497.
- [8] S. Chevion, M.A. Roberts, M. Chevion, The use of cyclic voltammetry for the evaluation of antioxidant capacity, *Free Radical Bio. Med.*, (2000) 28(6), 860-870.
- [9] **M. Ardelean**, F. Manea, R. Pode, Silver-electrodeposited carbon nanofiber-epoxy electrode for fluoxetine detection, *APCBEE Procedia*, In press.
- [10] B. Uslu, S.A. Ozkan, Electroanalytical methods for the determination of pharmaceuticals: a review of recent trends and developments, *Anal. Lett.*, (2011) 44, 2644-2702.
- [11] R.G. Compton, E. Laborda, K. R. Ward, *Understanding voltammetry: simulation of electrode processes*, Imperial College Press, London, 2014.
- [12] A. Kellenberger, N. Vaszilcsin, *Electrochimia stării solide*, Ed. Politehnica, Timișoara, 2013.
- [13] D.H. Evans, K.M. O'Connell, R.A. Peterson, M. J. Kelly, Cyclic voltammetry, *J. Chem. Educ.*, (1983) 60(4), 290-293.
- [14] H. Matsuda, Y. Ayabe, Theoretical analysis of polarographic waves. I. Reduction of simple metals, *B Chem. Soc. Japan*, (1955) 28(6), 422-428.
- [15] P. Zanello, *Inorganic electrochemistry: theory, practice and applications*, The Royal Society of Chemistry, Cambridge, 2003.
- [16] M. Zelic, M. Lovric, Components of the net current in differential pulse voltammetry. Part 2. Kinetics and adsorption, *Electroanal.*, (2011) 23(3), 642-650.
- [17] R.A. Osteryoung, J. Osteryoung, *Pulse voltammetric methods of analysis*, *Phil. Trans. R. Lond. A*, (1981) 302, 315-326.
- [18] J. Wang, B. Greene, C. Morgan, Carbon paste electrodes modified with cation-exchange resin in differential pulse voltammetry, *Anal. Chim. Acta*, (1984) 158, 15-22.
- [19] J. Wang, B.A. Freiha, Preconcentration and differential pulse voltammetry of butylated hydroxyanisole at a carbon paste electrode, *Anal. Chim. Acta*, (1983) 154, 87-94.
- [20] P. Sobrova, M. Pyvolova, J. Hubalek, V. Adam, R. Kizek, Voltammetry as a tool for characterization of CdTe quantum dots, *Int. J. Mol. Sci.*, (2013) 14, 13497-13510.
- [21] D. Harvey, *Modern Analytical Chemistry*, The McGraw-Hill Companies, Inc., Boston, 2000
- [22] K. Aoki, K. Tokuda, H. Matsuda, Theory of differential pulse voltammetry at stationary planar electrodes, *J. Electroanal. Chem.*, (1984) 175, 1-13.
- [23] S. Sujaritvanichpong, K.Aoki, K. Tokuda, H. Matsuda, Voltammetry at microcylinder electrodes. Part IV. Normal and differential pulse voltammetry, *J. Electroanal. Chem.*, (1986) 199, 271-283.
- [24] S. Legeai, M. Chatelut, O. Vittori, Differential pulse voltammetry at microdisk electrodes, *Electrochim. Acta*, (2005) 50, 4089-4096.
- [25] A. Molina, F. Martinez-Ortiz, E. Laborda, R.G. Compton, Characterization of slow charge transfer processes in differential pulse voltammetry at spherical electrodes and microelectrodes, *Electrochim. Acta*, (2010) 55, 5163-5177.
- [26] A. Molina, E. Laborda, E.I. Rogers, F. Martinez-Ortiz, C. Serna, J.G. Limon-Petersen, N.V. Rees, R.G. Compton, Theoretical and experimental study of differential pulse voltammetry at spherical electrodes: measuring diffusion coefficient and formal potential, *J. Electroanal. Chem.*, (2009) 634, 73-81.

- [27] G. Magarelli, J. Gomes da Silva, I.A. de Souza Filho, I.S. Dourado Lopes, J. Rodrigues de Souza, L. Vieira Hoffmann, C.S. Pires de Castro, Development and validation of a voltammetric method for determination of total phenolic acids in cotton cultivars, *Microchem. J.*, (2013) 109, 23-28.
- [28] E.M. Hassan, E.F. Khamis, E.I. El-Kimary, M.A. Barary, Development of a differential pulse voltammetric method for the determination of sylimarin/vitamin E acetate mixture in pharmaceuticals, *Talanta*, (2008) 74(4), 773-778.
- [28] G. Magarelli, J. Gomes da Silva, I.A. de Souza Filho, I.S. Dourado Lopes, J. Rodrigues de Souza, L. Vieira Hoffmann, C. Silva Pires de Castro, Development and validation of a voltammetric method for determination of total phenolic acids in cotton cultivars, *Microchem. J.*, (2013) 109, 23-28.
- [29] B.C. Lourencao, R.A. Medeiros, R.C. Rocha-Filho, O. Fatibello-Filho, Simultaneous differential pulse voltammetric determination of ascorbic acid and caffeine in pharmaceutical formulations using boron-doped diamond electrode, *Electroanal.*, (2010) 22(15), 1717-1723.
- [30] B.C. Lourencao, M. Baccarin, R.A. Medeiros, R.C. Rocha-Filho, O. Fatibello-Filho, Differential pulse voltammetric determination of albendazole in pharmaceutical tablets using a cathodically pretreated boron-doped diamond electrode, *J. Electroanal. Chem.*, (2013) 707, 15-19.
- [31] B.C. Lourencao, R.A. Medeiros, R.C. Rocha-Filho, L.H. Mazo, O. Fatibello-Filho, Simultaneous voltammetric determination of paracetamol and caffeine in pharmaceutical formulations using a boron-doped diamond electrode, *Talanta*, (2009) 78(3), 748-752.
- [32] R.T. Teofilo, E.L. Reis, C. Reis, G.A. da Silva, J.F. Paiva, L.T. Kubota, Glyphosate determination in soil, water and vegetables using DPV optimized by response surface methodology, *Port. Electrochem. Acta*, (2008) 26(4), 325-337.
- [33] J.G. Osteryoung, R.A. Osteryoung, Square wave voltammetry, *Anal. Chem.*, (1985) 57(1), 101A-110A.
- [34] B. Dogan-Topal, S.A. Ozkan, B. Uslu, The analytical applications of square wave voltammetry on pharmaceutical analysis, *Open Chem. Biomed. Methods J.*, (2010) 3, 56-73.
- [35] NOVA - Voltammetric analysis tutorial, <http://www.metrohm-autolab.com/index.html>
- [36] E. Laborda, F. Martinez-Ortiz, A. Molina, Study of electrochemical processes with coupled homogeneous chemical reaction in differential pulse voltammetry at spherical electrodes and microhemispheres, *Electroanal.*, (2010) 22(16), 1857-1866.
- [37] V. Mirceski, S. Komorosky-Lovric, M. Lovric, Square wave voltammetry. Theory and applications, Springer, Berlin, 2007.
- [38] J.J. O'Dea, A. Ribes, J.G. Osteryoung, Square-wave voltammetry applied to the totally irreversible reduction of an adsorbate, *J. Electroanal. Chem.*, (1993) 345, 287-301.
- [39] M. Lovric, Square-wave voltammetry of an adsorbed reactant, *J. Electroanal. Chem.*, (1988) 248, 239-253.
- [40] S. Komorosky-Lovric, M. Lovric, Square-wave voltammetry of quasi-reversible surface redox reactions, *J. Electroanal. Chem.*, (1995) 384, 115-122.
- [41] V. Mirceski, D. Guziejewski, K. Lusichkov, Electrode kinetic measurements with square-wave voltammetry at a constant scan rate, *Electrochim. Acta.*, (2013) 114, 667-673.

- [42] V. Mirceski, R. Gulaboski, M. Lovric, I. Bogeski, R. Kappl, M. Hoth, Square-wave voltammetry: a review of the recent progress, *Electroanal.*, (2013) 25(11), 2411-2422.
- [43] D. de Souza, S.A.S. Machado, L.A. Avaca, Voltametria de onda quadrada. Primeira parte: aspectos teoreticos, *Quim. Nova*, (2003) 26(1), 81-89.
- [44] L. Codognoto, S.A.S. Machado, L.A. Avaca, Square wave voltammetry on boron doped diamond electrodes for analytical determinations, *Diam. Relat. Mater.*, (2002) 11(9), 1670-1675.
- [45] E.R. Sartori, R.A. Madeiros, R.C. Rocha-Filho, O. Fatibello-Filho, Square-wave voltammetric determination of acetylsalicylic acid in pharmaceutical formulations using a boron-doped diamond electrode without the need of previous alkaline hydrolysis step, *J. Braz. Chem. Soc.*, (2009) 20(2), 360-366.
- [46] M.T. Laranjeira, F. de Lima, S.C. de Oliveira, V. Souza Ferreira, R.T. Soares de Oliveira, Analytical determination of benzophenone-3 in sunscreen preparations using boron-doped diamond electrodes, *Am. J. Anal. Chem.*, (2011) 2, 383-391.
- [47] L. Codognoto, S.T. Tanimoto, E.A. Pedrosa, H.B. Suffredini, S.A.S. Machado, L.A. Avaca, Electroanalytical determination of carbaryl in natural waters on boron-doped diamond electrode, *Electroanal.*, (2006) 18(3), 253-258.
- [48] V.A. Pedrosa, L. Codognoto, L.A. Avaca, Electroanalytical determination of 4-nitrophenol by square wave voltammetry on diamond electrodes, *J. Braz. Chem. Soc.*, (2003) 14(4), 530-535.

5. MOTIVATION, SCOPE AND THESIS OBJECTIVES

The occurrence of newly identified contaminants or emerging pollutants in water sources is of continued concern for the health and safety of public consuming.

Surface waters contaminated by point and diffuse pollution sources continue to enlarge pollution ranges and levels in the environment.

In the past, research priorities have been focused on priority pollutants as POPs, pesticides, toxic metals, radionuclides. Recently, the attention of the research community shifted to emerging pollutants. However, these pollutants are currently undergoing a regularization process, although the directives and legal framework are not yet set-up. As a consequence, very few precautions and monitoring were taken to control their presence in water.

Pharmaceuticals represent an important class that belongs to emerging pollutants and their presence in water is attributed to personal hygiene products, pharmaceuticals industry waste, hospital waste, and therapeutic drugs. Pharmaceuticals have a broad range of physico-chemical characteristics and there is no standardized or common method for their analysis.

Based on these considerations, this study focused on the development of a rapid and low-cost procedure for pharmaceuticals detection in aqueous solutions using electrochemical techniques and carbon-based electrode materials. In addition, the same carbon-based electrode materials were used for the detection of specific anions in water, which also contribute to the water quality.

The aim of this study is to develop a simple method for the simultaneous electrochemical determination/monitoring of pharmaceuticals in water providing a real challenge taking into account specific characteristics of the analytical/electroanalytical method, *e.g.*, accuracy, reproducibility, selectivity, interference.

Carbon-based electrode materials are widely used in electroanalysis. Conventional carbon electrode material exhibits the disadvantage of a low rate of electron transfer during an oxidation process on the electrode surface that limits their practical applications in electroanalysis. To overcome this problem, new forms of nanostructured carbon, *e.g.*, carbon nanotubes and carbon nanofibers will be used to develop composite electrode materials. For comparison, an advanced commercial boron-doped diamond electrode will be tested. In addition, the integration of silver as electrocatalyst will be studied for enhancement of electroanalytical performance. Also, specific features of the advanced electrochemical techniques are exploited to improve the electroanalytical parameters.

To achieve the aim of this study, the following specific objectives were proposed:

- Voltammetric/amperometric detection of pharmaceuticals. Two approaches are considered for this objective, one refers to pharmaceuticals as emerging pollutants in water and the other to the pharmaceutical dosage for clinical use.

- Development of nanostructured carbon-based composite electrode suitable for electroanalysis;
- Elaboration of silver-modified nanostructured carbon-based composite electrodes to enhance the electroanalytical performance;
- Morphological, electrical, and electrochemical characterization of nanostructured carbon-based composite electrodes in relation with the electroanalysis applications;
- Elaboration of detection schemes/protocols for the individual/simultaneous analysis of pharmaceuticals in aqueous solution;
- Elaboration of detection schemes/protocols for the individual/simultaneous analysis of anions in water.

Selection of pharmaceuticals as therapeutic group for the investigation of their electrochemical detection using nanostructured carbon-based composite electrode based on most recurrent drugs detected in water:

- i) antidepressants (fluoxetine)
- ii) non-steroidal anti-inflammatories (naproxen)
- iii) antibiotics (tetracycline)

For each pharmaceutical, an individual detection scheme is elaborated and also simultaneous pharmaceutical detection is taken into account.

Carbon nanotubes-epoxy and carbon nanofibers-epoxy composite electrodes were obtained and tested for electroanalysis of pharmaceuticals in this study. For comparison, a boron-doped diamond electrode was used to develop protocols for the detection of pharmaceuticals.

A second approach of this study is related to the detection of certain anions in water. Sulfide was selected for the electroanalysis due to its presence in seawater and its limitation regulations imposed for surface/groundwater. Also, taking into account the effect of nitrite to human health, its presence is important to be detected in water, especially in the identification of nitrate vulnerable areas.

This study represents the first and prerequisite stage for the practical application of the detection strategies for in-field water quality monitoring in relation with pharmaceuticals as pollutants and anions as pollution index.

6. PREPARATION OF CARBON-BASED COMPOSITE ELECTRODES

6.1. Materials

During experimental studies, two types of electrodes were used, *e.g.*, commercial and laboratory-made electrodes characterized by disc geometry. A boron-doped diamond electrode (BDD) was purchased from Windsor Scientific Ltd, United Kingdom, and commercial silver electrode (Ag) from Metrohm, Switzerland. Several types of nanostructured carbon based composite electrodes, mainly consisting of carbon nanofibers or carbon nanotubes, were prepared in our laboratory.

Carbon nanofibers (CNF) were purchased from Applied Sciences Inc., Cerdaville, Ohio (Pyrograf III- PR24 AGLD) and were characterized having an average diameter of 60-150 nm and an average length of 30-100 nm.

Carbon nanotubes (CNTs) synthesized by catalytic carbon vapor deposition were produced by Nanocyl™, Belgium. These are characterized having a 90% content of CNT, with a carbon purity of 90 %, average diameter of 9.5 nm, average length of 1.5 μm , and surface area of 250-300 m^2g^{-1} .

Silver-modified zeolite was prepared by ion-exchange using clinoptilolite natural zeolite purchased from Mirsid, Romania, which contains 68% wt. clinoptilolite [1].

The binding material used in electrode preparation was epoxy resin - Araldite®LY5052 purchased from Huntsman Advanced Materials, Switzerland.

Various nanostructured carbon based composite electrode compositions were prepared and are summarized in Table 6.1.

Table 6.1. Carbon-based composite electrodes prepared in the laboratory

| Electrode abbrev. | Composition of prepared electrode |
|-------------------|---|
| CNF | carbon nanofiber (20%)–epoxy resin (80%) |
| AgZ-CNF | silver-modified zeolite (20%) carbon nanofiber (20%)–epoxy resin (60%) |
| Ag-CNF | carbon nanofiber (20%)–epoxy resin (80%), electrochemically decorated with silver |
| CNT | carbon nanotubes (20%)–epoxy resin (80%) |
| AgZ-CNT | silver-modified zeolite (20%)carbon nanotubes (20%)–epoxy resin (60%) |

6.2. Preparation methodology of carbon-based composite electrodes

6.2.1. Preparation of CNF/CNT composite electrodes

Carbon nanofibers and carbon nanotubes were dispersed in tetrahydrofuran, 99.9% (THF, Sigma Aldrich) by ultrasonication using a Cole-Parmer® 750-Watt Ultrasonic Processor. After 10 minutes epoxy resin was added into the solution of CNF/THF (CNT/THF) in a ratio that leads to a composition of 20% wt. CNF/CNT and 80% wt. epoxy resin of the composite. Then, the sonication process was continued for obtaining a homogeneous mixture. The resulted mixture was dried for about 12 hours in a vacuum oven at 60 °C to remove the solvent.

For achieving high levels of dispersion and distribution of the nanostructured carbon filler within the insulating matrix, an effective two-roll mill procedure (TRM) was applied to prepare the electrode composition. During this procedure, the temperature was maintained at 70 °C, at a mixing speed of 10, respectively 20 rpm. The curing agent with a weight ratio epoxy resin-curing agent of 100:38 was added to the CNF/CNT-epoxy resin mixture. The mixing process was continued for another 20 minutes to ensure the uniform distribution within of composite mixture. The resulting mixture was then poured into PVC tubes and cured for 24 h in a vacuum oven at 80°C. After cooling down at room temperature, CNF/CNT composite electrodes with a disc surface area of 19.63 mm² were obtained. The electrical contact was made with a copper wire [2].

The schematical procedure for CNF/CNT electrode preparation is presented in the Figure 6.1.

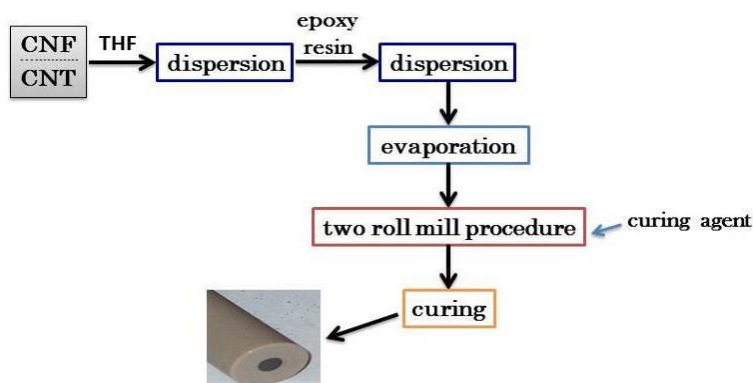


Figure 6.1. Schematically protocol of CNF/CNT composite electrode preparation

6.2.2. Preparation of AgZ-CNF/AgZ-CNT composite electrode

The preparation of AgZ-CNF/AgZ-CNT composite electrode is similar to the preparation of CNF/CNT composite electrodes. Carbon nanofibers respectively carbon nanotubes were dispersed together with natural zeolite, doped with silver, into tetrahydrofuran (THF) by ultrasonication. The procedure described in Section 6.2.1 was then followed step by step, and AgZ-CNF and AgZ-CNT composite electrodes are obtained [3]. The ratio between the components was chosen to reach

20% wt. CNF/CNT, 20% wt. silver-doped natural zeolite, and 60% wt. epoxy resin. A schematically preparation protocol of these composite electrodes is presented in Figure 6.2.

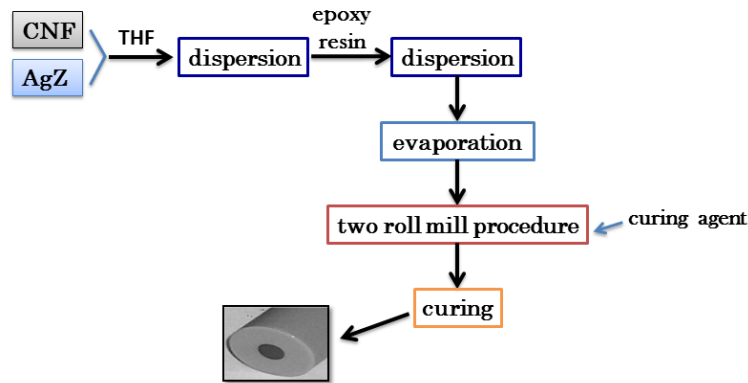


Figure 6.2. Schematically protocol of AgZ-CNF composite electrode preparation

6.2.3. Preparation of Ag-CNF composite electrodes

The surface area of a simple CNF composite electrode previously described was electrochemically decorated with silver nanoparticles. The electrochemical decoration consisted in maintaining the composite electrode at a potential value of -0.4 V/SCE for 120 s in 0.1M AgNO_3 solution. After electrodeposition, the surface of the electrode was rinsed in distilled water. Then, the new developed electrode was ready to be used.

6.3. Techniques and methods for electrode characterization

6.3.1. Morphology characterization

Scanning electron microscopy (SEM) is a qualitative technique which provides information on the morphology and particle agglomeration, their size, shape and distribution by recording and analysing micrograph images.

The morphology characterization of carbon-based composite materials was realized using an XL20, Philips Scanning Electron Microscope, with an acceleration voltage of 15 kV, an Inspect S PANalytical model coupled with energy dispersive X-rays analysis detector (EDX) with an acceleration voltage of 30kV and a Quanta 400 FEG, FEI.

6.3.2. Electrical characterization

The samples of composite materials used for measuring electrical conductivity were pressed into a rectangular shape with electrical contacts provided by a silver paste. The electrical conductivity was determined by a four-point probe (FPP) method [4] based on DC conductivity measurements by using a digital

multimeter DMM 2000 and a current source Keithley 6221 DC. In a current range $-10 \text{ mA} \div 10 \text{ mA}$ the potential of each sample was recorded. The results were then plotted and based on the slope the composite material resistance was determined.

6.3.3. Electrochemical characterization

All the electrochemical studies were performed using an Autolab potentiostat-galvanostat PGSTAT 302 (Eco Chemie, The Netherlands) controlled by a PC using the GPES 4.9 software and a three-electrode cell (Figure 6.3). The electrochemical cell consists of a working electrode (composite electrode or commercial electrode), a platinum counter electrode, and a saturated calomel reference electrode (SCE). The measurements were carried out at room temperature without further temperature control. Prior to use, the working electrode was mechanically cleaned by polishing with $0.2 \mu\text{m}$ Al_2O_3 powder, and then washed in distilled water. Before the detection measurements, an electrochemical pre-treatment by ten repeated cycles was performed.

The supporting electrolyte, $0.1 \text{ M Na}_2\text{SO}_4$ solution, was prepared using Na_2SO_4 of analytical purity (Merck, Germany) with distilled water.

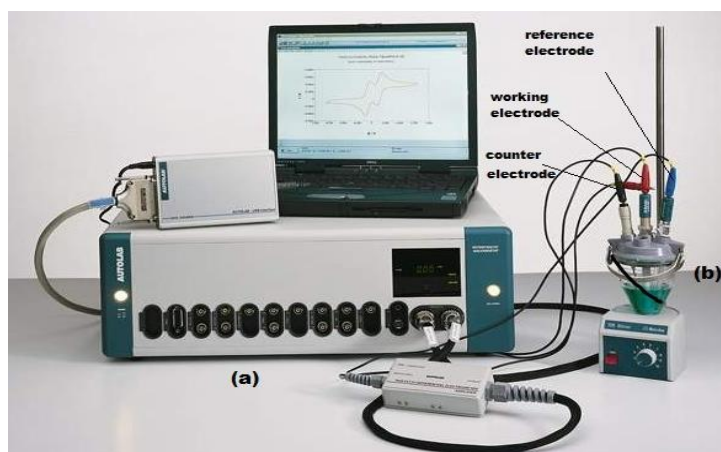


Figure 6.3. a) Image of a potentiostat / galvanostat type PGSTAT 302 (EcoChemie); b) three-electrode cell.

6.4. References

- [1] C. Orha, A. Pop, C. Lazau, I. Grozescu, V. Tiponut, F. Manea, Structural characterization and the sorption properties of the natural and synthetic zeolite, *J. Optoelectron. Adv. Mater.*, (2011) 13(5-6), 544-549.
- [2] **M. Ardelean**, F. Manea, N. Vasilcsin, R. Pode, Electrochemical detection of sulphide in water/seawater using nanostructured carbon-epoxy composite electrodes, *Anal. Methods*, (2014) 6, 4775-4782.

- [3] F. Manea, S. Motoc, A. Pop, A. Remes, J. Schoonman, Silver-functionalized carbon nanofiber composite electrodes for ibuprofen detection, *Nanoscale Res. Lett.*, (2012) 7, 331-335.
- [4] V.S. Mironov, J.K. Kim, M. Park, S. Lim, W.K. Cho, Comparison of electrical conductivity data obtained by four-electrode and four-point probe methods for graphite-based polymer composites, *Polym. Test.*, (2007) 26(4), 547-555.

7. CHARACTERIZATION OF CARBON-BASED COMPOSITE ELECTRODES

7.1. Morphology of carbon-based composite electrodes

SEM images of fractured surfaces of composite electrodes were recorded to study the bulk distribution and the structure of conductive carbon filler within the epoxy matrix. In Figure 7.1 the SEM images of CNF and AgZ-CNF composite electrodes are presented.

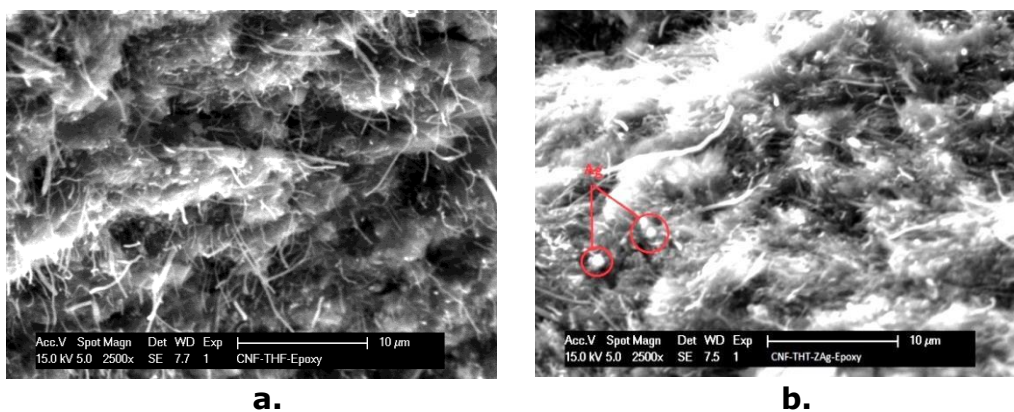


Figure 7.1. SEM image of: **a.** CNF, **b.** AgZ-CNF composite electrode.

For both composite electrodes a homogeneous distribution is observed. Even if there is a tendency in CNF to form agglomerates due to the nanoscale diameters, but by using a suitable solvent and combined steps in the mixing process, agglomeration phenomena were avoided. In the case of silver-doped natural zeolite-modified carbon nanofiber composite material a well-integrated and smooth morphology of carbon nanofibers and Ag-modified zeolite particles are observed within the epoxy matrix.

For a silver electrochemically decorated carbon nanofiber composite electrode, silver particles were distributed randomly on the electrode surface, mostly deposited in aggregated form and characterized having various sizes (Figure 7.2). The presence of silver on the surface of the composite electrode was also confirmed by the EDX spectrum of the electrode surface (Figure 7.3).

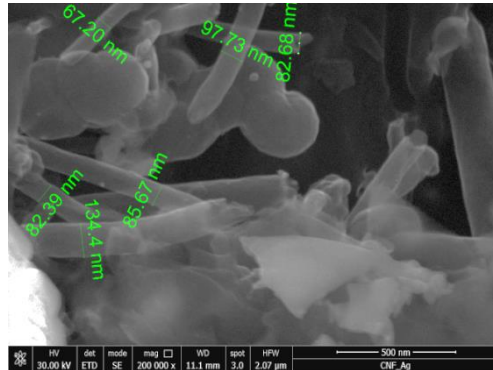


Figure 7. 2. SEM image of Ag-CNF composite electrode.

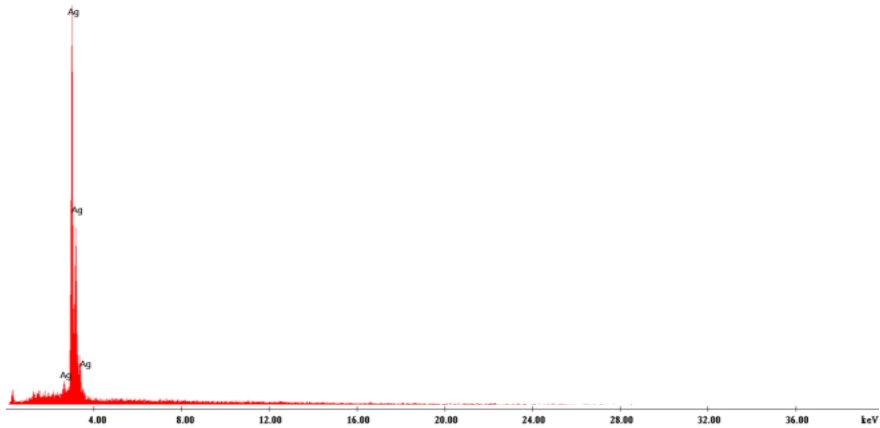


Figure 7.3. EDX spectrum of Ag-CNF composite electrode.

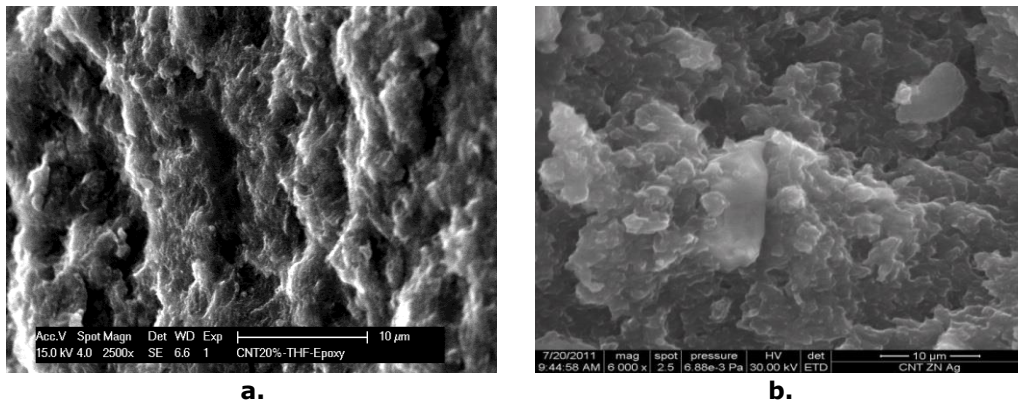


Figure 7.4. SEM image of: **a.** CNT and **b.** AgZ-CNT composite electrode.

For CNT composite electrode a more homogenous dispersion of carbon nanotubes into the epoxy matrix without agglomeration aspects is observed (Figure

7.4.a). As expected for the AgZ-CNT composite electrode, a more porous surface is noticed, due to the presence of zeolite particles within the epoxy matrix (Figure 7.4.b).

7.2. Electrical conductivity of carbon-based composite electrodes

The carbon fillers play an important role in electrical conductivity of a composite, the percolation threshold concentration being the discrimination factor. Since the fillers are dispersed individually, or agglomerated in small clusters into the matrix, at low concentrations of the fillers, the electrical conductivity is determined by the conductivity of a pure, electrically insulating polymer matrix. If the percolation threshold is exceeded, then an important increase in composite material conductivity is due to the linked fillers. For enhancing the electrical conductivity of a composite, it is necessary to evaluate the parameters which could affect the percolation threshold, *e.g.*, filler ration in the matrix, filler/filler interactions, orientation angle of the fillers [1-3], and eliminate any stress induced in the preparation process of the composite. Based on the previous studies in our laboratory 20% carbon filler was found to be the optimum composition of the composite electrode.

The ohmic behavior of the composite material was studied by plotting the recorded potential values for each sample in the current range -10 mA ÷ +10 mA. The value of electrical conductivity (σ) was then determined by the following equation:

$$\sigma = G \frac{l}{S} \quad (7.1)$$

where G is the conductance (S), l is the shiftiness of the sample (m), and S is the surface area (m²).

The results obtained for electrical conductivity of the composite electrodes are gathered in Table 7.1.

Table 7.1. Electrical conductivity of composite electrodes

| Electrode type | Electrical conductivity, σ (Sm ⁻¹) |
|----------------|---|
| CNF | 24.9 |
| AgZ-CNF | 40.9 |
| CNT | 59.6 |
| AgZ-CNT | 91.0 |

The AgZ presence affects the electrical conductivity of the composite. Even if the zeolite is an insulator material, the electrical conductivity of AgZ-CNT composite electrode is higher than the electrical conductivity of CNT composite electrode (91.0 Sm⁻¹ vs. 59.6 Sm⁻¹), the enhancement being attributed to the silver contained in the silver-modified zeolite.

It may be concluded that the electrical conductivity of the composite electrodes depends on the type of conductive filler, *e.g.*, CNF vs. CNT, the loading of the filler, and the distribution of the filler within the epoxy matrix. The conductivity values for all tested electrodes showed that they are suitable for the electrochemical applications, envisaging electrochemical detection.

7.3. Electrochemical characterization of carbon-based composite electrodes

Cyclic voltammetry, one of the most frequently applied electrochemical techniques, represents an important and useful tool for obtaining kinetic information regarding the redox system, and it is widely used in order to determine the electroactive surface of the electrode, the diffusion coefficient, and redox potentials for the analytical systems.

The electroactive surfaces of the composite electrodes were determined by recording the cyclic voltammograms at several scan rate values in the presence of 4mM $K_3Fe(CN)_6$. In Table 7.2 a simple assessment of the system reversibility is presented.

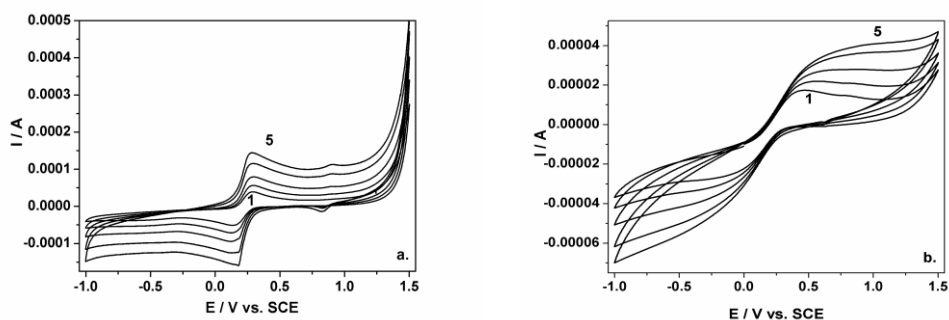
Table 7.2. Assessment criteria of the reversible system

| Criteria / Type of system | Reversible system |
|---|--|
| <ul style="list-style-type: none"> ■ peak separation $\Delta E_p = E_{pa} - E_{pc}$ | $\Delta E_p = 0.059/n$ (V) n -number of electrons exchanged |
| <ul style="list-style-type: none"> ■ peak current $\Delta I = I_{pa}/I_{pc}$ | $\Delta I = 1$ |

In Figure 7.5 the cyclic voltammograms of all carbon based composite electrodes used in this study are presented recorded at different scan rates (0.025, 0.05, 0.1, 0.2 and 0.3 Vs^{-1}) in 1M KNO_3 supporting electrolyte and in the presence of 4 mM $K_3Fe(CN)_6$. For all tested electrodes, clear and well defined current peaks on both anodic and cathodic branches were observed, these being attributed to the redox couple.

In Figures 7.6 and 7.7 the evolution of the peak potential in relation with the logarithm of the scan rate are presented, and the dependence of anodic and cathodic peak current in relation with the square root of the scan rate which gives information about the overall mechanistic aspects of the redox couple process that occur on the electrodes.

The characteristics of the well-known standard ferri/ferrocyanide oxidation process studies on the carbon-based composite electrodes taking into consideration the reversibility of the redox system are gathered in Tables 7.3 – 7.5.



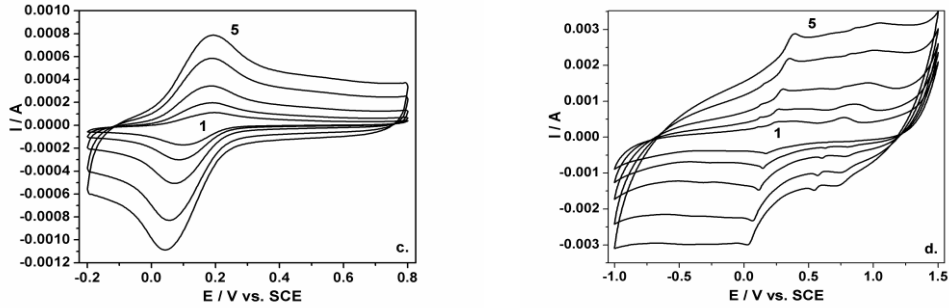


Figure 7.5. Cyclic voltammograms recorded on carbon-based composite electrode in 1M KNO_3 supporting electrolyte and in the presence of 4mM $\text{K}_3\text{Fe}(\text{CN})_6$ at different potential scan rates 1- 0.025, 2- 0.05, 3- 0.1, 4- 0.2, 5- 0.3 Vs^{-1} in the potential range from -1 to +1.5 V/SCE at: **a.** CNF electrode; **b.** AgZ-CNF electrode; **c.** CNT electrode; **d.** AgZ-CNT electrode.

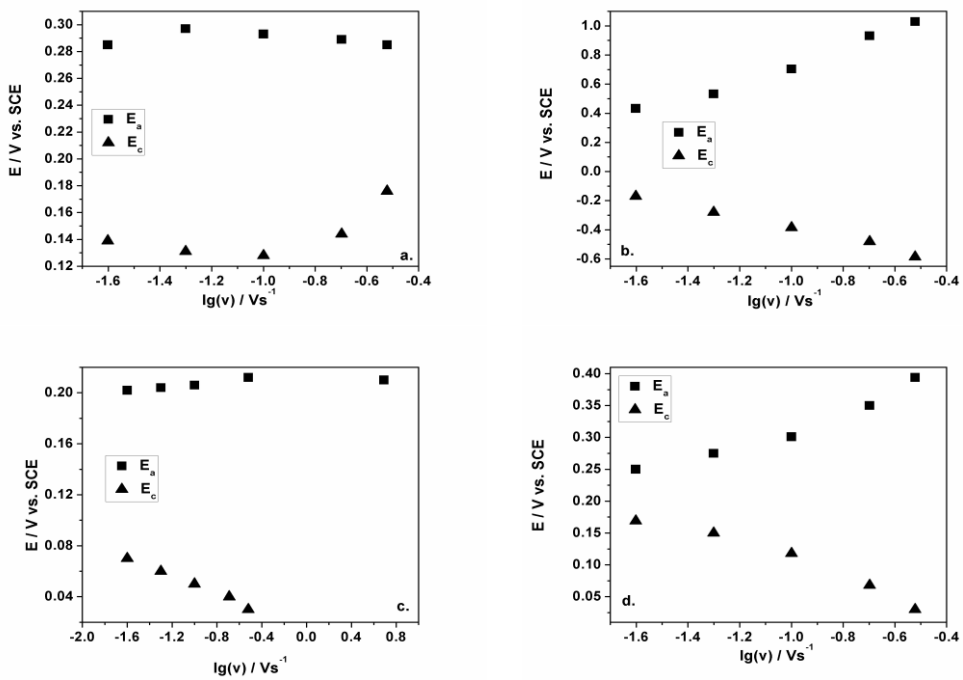


Figure 7.6. Plots of the anodic and cathodic peaks vs. the logarithm of the scan rate: 0.025, 0.05, 0.1, 0.2, 0.3, Vs^{-1} , of CV recorded on: **a.** CNF electrode; **b.** AgZ-CNF electrode; **c.** CNT electrode; **d.** AgZ-CNT electrode.

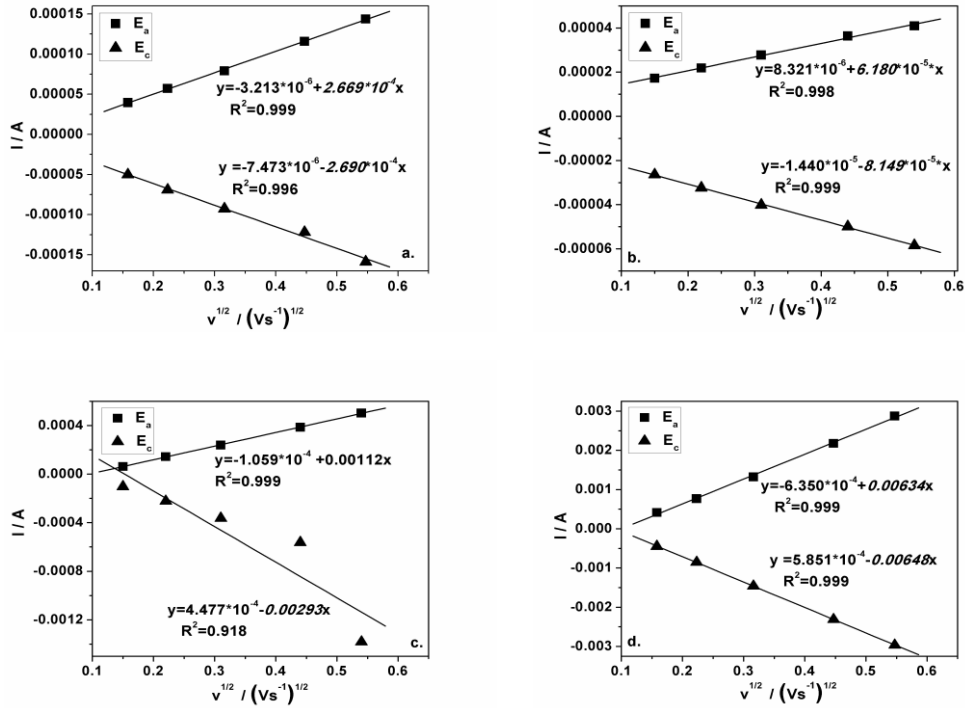


Figure 7.7. Calibration plots of the anodic and cathodic peak current vs. the square root of the scan rate: 0.025, 0.05, 0.1, 0.2, 0.3, Vs⁻¹ of CV recorded on: **a.** CNF electrode; **b.** AgZ-CNF electrode; **c.** CNT electrode; **d.** AgZ-CNT electrode.

Table 7.3. The electrochemical parameters of the redox system (ferri/ferrocyanide) determined from the anodic and cathodic branches of CVs on carbon nanofibers-based composite electrodes

| | | CNF | | | AgZ-CNF | | | |
|----------|-------|-----------------------|------------------------|-------------------------|---------|------------------------|------------------------|--------|
| | | v (Vs ⁻¹) | E (V) | I (A) | ΔI (A) | E (V) | I (A) | ΔI (A) |
| Anodic | 0.025 | 0.285 | 4.95*10 ⁻⁵ | 3.60*10 ⁻⁵ | 0.433 | 1.72*10 ⁻⁵ | 1.37*10 ⁻⁵ | |
| | 0.05 | 0.297 | 5.71*10 ⁻⁵ | 5.04*10 ⁻⁵ | 0.533 | 2.18*10 ⁻⁵ | 1.61*10 ⁻⁵ | |
| | 0.1 | 0.293 | 7.91*10 ⁻⁵ | 6.78*10 ⁻⁵ | 0.704 | 2.77*10 ⁻⁵ | 1.78*10 ⁻⁵ | |
| | 0.2 | 0.289 | 1.15*10 ⁻⁴ | 9.56*10 ⁻⁵ | 0.932 | 3.63*10 ⁻⁵ | 1.90*10 ⁻⁵ | |
| | 0.3 | 0.285 | 1.43*10 ⁻⁴ | 11.53*10 ⁻⁵ | 1.029 | 4.09*10 ⁻⁵ | 1.85*10 ⁻⁵ | |
| Cathodic | 0.025 | -0.030 | -5.01*10 ⁻⁵ | -4.77*10 ⁻⁴ | -0.170 | -2.64*10 ⁻⁵ | -2.33*10 ⁻⁵ | |
| | 0.05 | -0.118 | -6.90*10 ⁻⁵ | -6.46*10 ⁻⁴ | -0.280 | -3.23*10 ⁻⁵ | -2.65*10 ⁻⁵ | |
| | 0.1 | -0.136 | -9.25*10 ⁻⁵ | -8.41*10 ⁻⁴ | -0.385 | -4.01*10 ⁻⁵ | -2.96*10 ⁻⁵ | |
| | 0.2 | -0.223 | -1.21*10 ⁻⁴ | -10.78*10 ⁻⁴ | -0.481 | -4.99*10 ⁻⁵ | -3.26*10 ⁻⁵ | |
| | 0.3 | -0.182 | -1.58*10 ⁻⁴ | -13.97*10 ⁻⁴ | -0.182 | -0.00296 | -8.72*10 ⁻⁴ | |

Table 7.4. The electrochemical parameters of the redox system (ferri/ferrocyanide) determined from the anodic and cathodic branches of CVs on carbon nanotubes-based composite electrodes

| | v (Vs ⁻¹) | CNT | | | AgZ-CNT | | |
|----------|---------------------------------|-----------------|------------------------|-------------------------|-----------------|------------------------|------------------------|
| | | E (V) | I (A) | ΔI (A) | E (V) | I (A) | ΔI (A) |
| Anodic | 0.025 | 0.202 | 1.08*10 ⁻⁴ | 0.62*10 ⁻⁴ | 0.250 | 4.13*10 ⁻⁴ | 1.16*10 ⁻⁴ |
| | 0.05 | 0.204 | 1.93*10 ⁻⁴ | 1.43*10 ⁻⁴ | 0.275 | 7.66*10 ⁻⁴ | 2.08*10 ⁻⁴ |
| | 0.1 | 0.206 | 3.36*10 ⁻⁴ | 2.38*10 ⁻⁴ | 0.301 | 0.00132 | 4.06*10 ⁻⁴ |
| | 0.2 | 0.210 | 5.75*10 ⁻⁴ | 3.86*10 ⁻⁴ | 0.350 | 0.00217 | 6.03*10 ⁻⁴ |
| | 0.3 | 0.212 | 7.72*10 ⁻⁴ | 5.02*10 ⁻⁴ | 0.394 | 0.00287 | 8.08*10 ⁻⁴ |
| Cathodic | 0.025 | 0.07 | -1.66*10 ⁻⁴ | -1.02*10 ⁻⁴ | -0.037 | -4.47*10 ⁻⁴ | -1.94*10 ⁻⁴ |
| | 0.05 | 0.06 | -2.92*10 ⁻⁴ | -2.22*10 ⁻⁴ | -0.118 | -8.53*10 ⁻⁴ | -3.49*10 ⁻⁴ |
| | 0.1 | 0.05 | -5.00*10 ⁻⁴ | -3.62*10 ⁻⁴ | -0.136 | -0.00146 | -5.38*10 ⁻⁴ |
| | 0.2 | 0.04 | -8.22*10 ⁻⁴ | -5.62*10 ⁻⁴ | -0.223 | -0.00231 | -7.39*10 ⁻⁴ |
| | 0.3 | 0.03 | 1.00*10 ⁻⁴ | -13.81*10 ⁻⁴ | -0.182 | -0.00296 | -8.72*10 ⁻⁴ |

Table 7.5. The reversibility parameters of the ferri/ferrocyanide redox system on tested carbon-based electrodes

| Electrode | ΔE | I_{pa}/ I_{pc} |
|------------------|-----------|---------------------------------------|
| CNF | 0.146 | 0.850 |
| AgZ-CNF | 1.106 | 0.695 |
| CNT | 0.156 | 1.050 |
| AgZ-CNT | 0.207 | 0.790 |

When the rate of the electron transfer is higher than the rate of the mass transport, then the electrode process is defined as electrochemically reversible. In this case, the values of the i_{pa}/i_{pc} are close to the theoretical value for a reversible process taking into account the limits of the experimental conditions (Table 7.5). Still, the non-compensated resistance given by the supporting electrolyte could impose values that are not in the limits of the diagnostics criteria for an electrochemically reversible one-electron process, but can suggest the electrochemical reversibility of the electron transfer on the cyclic voltammetric time scale. No zero intercept was noticed for the linear dependences of peak current vs. square root of the scan rate in KNO₃ solutions for all tested electrodes. The explanation is given in principal by the nature and the concentration of the supporting electrolyte, but also by the electrode. The ion pairs of the ferricyanide and the cation of the supporting electrolyte influence the shapes of peak current vs. square root of the scan rate dependences and, therefore the rate of the electrode processes is controlled both by the diffusion and adsorption of these components at the electrode surface.

Information about the electroactive surface area is based on the diffusion coefficient determined using the Randles-Sevcik equation [4]:

$$I_p = 2.69 \times 10^5 A D^{1/2} n^{3/2} \nu^{1/2} C \quad (7.2)$$

where A represents the area of the electrode (cm²), n the number of electrons participating in the reaction and is here equal to 1, D the apparent diffusion coefficient of the molecule in solution, C the concentration of the probe molecule in the solution (4 mM), and ν the scan rate (V s⁻¹).

The apparent diffusion coefficient and the electroactive surface area of the nanostructured carbon-based composite electrodes used in this study were

determined and are gathered in Table 7.6. For all composite electrodes the electroactive surface area is higher than the geometrical area.

Table 7.6. The apparent diffusion coefficient and the electroactive surface area of the carbon nanostructured based composite electrodes

| Electrode | D_a ($\text{cm}^2 \text{s}^{-1}$) | Electroactive surface area (cm^2) | A (cm^2) | Electroactive surface area/ Geometrical area |
|-----------|--|--|------------------------|--|
| CNF | 1.349×10^{-6} | 0.352 | 0.1963 | 1.80 |
| AgZ-CNF | 0.153×10^{-5} | 0.313 | 0.1963 | 1.60 |
| CNT | 2.668×10^{-5} | 0.473 | 0.1963 | 2.41 |
| AgZ-CNT | 4.300×10^{-5} | 0.411 | 0.1963 | 2.10 |

As it was expected for all tested carbon-based composite electrodes the electroactive surface area is higher than the geometrical one, a common peculiarity of the composite electrodes surface. In addition, nanostructured carbon increased the electroactive surface, which is in direct relation with morphological aspects (carbon size, geometry and distribution). The presence of zeolite slightly influenced negatively the electroactive surface area due to its insulating character and morphological properties.

The results of morphological, electrical, and electrochemical characterization revealed a great potential of the prepared nanostructured carbon-based composite electrodes for various electrochemical applications, this study being focused on amperometric/ voltammetric detection of certain pollutants in aqueous solutions.

7.4. References

- [1] J.Y. Li, G.M. Choi, Percolation behaviour of conductor-insulator composite with varying aspect ratio on conductive fiber, *J. Electroceram.*, (1999) 3, 361-369.
- [2] F. Du, J.E. Fischer, K.I. Winey, Effects of nanotubes alignment on percolation conductivity in carbon nanotubes/polymer composites, *Phys. Rev. B.*, (2005) 72, 121404(R) -121404-4.
- [3] E. Asedegbega-Nieto, B. Bachiller-Baeza, D.G. Kuvshinov, F.R. Garcia-Garcia, E. Chukanov, G.G. Kuvshinov, A.Guerrero-Ruiz, I. Rodrigues-Ramos, Effect of carbon support nano-structures on the performance of Ru catalyst in the hydrogenation of paracetamol, *Carbon*, (2008) 46, 1046-1052.
- [4] A. Baciú, A. Remes, E. Ilinoiu, F. Manea, S.J. Picken, J. Schoonman, Carbon nanotubes composite for environmentally friendly sensing, *Environ. Eng. Manage. J.*, (2012) 11(2), 239-246.

8. ELECTROCHEMICAL DETECTION OF PHARMACEUTICALS

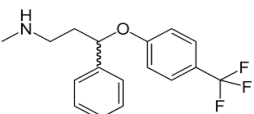
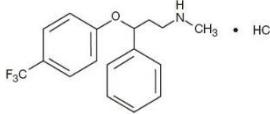
8.1. Electrochemical detection of fluoxetine in water

8.1.1. Introduction

Fluoxetine (FXT), N-Methyl-gamma-(4-(trifluoromethyl) phenoxy) benzene-propanamine, is a selective serotonin reuptake inhibitor (SSRI) antidepressant. Its hydrochloride derivative is commonly known as Prozac [1]. This pharmaceutical compound is used in the treatment of major depressive disorder, obsessive-compulsive disorder, bulimia nervosa, and also, premenstrual dysphoric disorder. Some properties of fluoxetine and fluoxetine hydrochloride are gathered in Table 8.1.

After oral administration, fluoxetine is extensively metabolized in the liver by N-demethylation into norfluoxetine, its active metabolite. It blocks the re-uptake of serotonin at the neuronal membrane, enhancing the action of serotonin on 5HT_{1A} autoreceptors. After 6-8 hours peak plasma revealed the presence of fluoxetine. The half-life for acute administration is ranging between 1 to 3 days and for chronic administration between 6 to 8 days. About 80% of drug dose is eliminated through kidneys with less than 10% of the parent drug [2-4]. Blood concentrations of 1.3 mgL⁻¹ for fluoxetine and of 0.9 mgL⁻¹ for norfluoxetine have been associated with fatalities. Serum levels of 0.96 mgL⁻¹ for fluoxetine and 0.42 mgL⁻¹ for norfluoxetine have been associated with seizure.

Table 8.1. Information on fluoxetine and fluoxetine hydrochloride

| | Fluoxetine | Fluoxetine hydrochloride |
|---------------------------|--|---|
| <i>Molecular formula</i> | C ₁₇ H ₁₈ F ₃ NO  | C ₁₇ H ₁₉ ClF ₃ NO  |
| <i>Molecular weight</i> | 309.32613 g mol ⁻¹ | 345.78707 g mol ⁻¹ |
| <i>pKa</i> | 10.01 | 8.7 |
| <i>Log K_{oc}</i> | 4.65 | - |
| <i>Melting point</i> | 179-182°C | 158-163 °C |
| <i>Solubility</i> | 14mg ml ⁻¹ (20 °C) in water | 12.5mg ml ⁻¹ in ethanol |

The wide use of this drug made it to be detected in surface water [5], sewage treatment plants [6], downstream sewage treatment plants [7,8], wastewater treatment plant effluent [9-11] in US, Canada, and Northern and Western Europe. The higher concentrations detected in wastewater treatment plant influent were ranging from 91 ngL⁻¹ up to 175.5 ngL⁻¹ [12,13].

Because this drug does not biodegrade rapidly in wastewater treatment plants, it being resistant to hydrolysis, photolysis, and microbial degradation, and it can also be adsorbed by sediments (this aspect could explain the level of surface concentration). Under dark conditions fluoxetine is quite stable, the degradation process occurring at pH lower than 1 [14].

The fate and the effects of fluoxetine in the environment have been studied intensively and this compound is considered one of the most acute toxic pharmaceuticals [15]. Brooks and co-workers reported higher concentrations of fluoxetine and its metabolite in the brain and liver of exposed fish than in muscles [16]. Due to its basicity ($pK_a=10.01$), fluoxetine is presented in water in neutral form at high pH values and a bioaccumulation in fish induced by pH was reported [11, 17]. Among those effects, it was reported also that fluoxetine is influencing the growth, fecundity, and reproduction depending on species, *e.g.*, inhibit growth in *H. azteca* [18, 19].

Several methods have been developed in order to detect fluoxetine, mostly based on high performance liquid chromatography (HPLC) coupled with mass spectroscopy (MS) [7, 11, 13]. Among those, electroanalytical techniques have also been employed in fluoxetine quantification from pharmaceutical formulations, the obtained results being in good agreement with the regulation from the official pharmacopeias. Various electroanalytical procedures have been developed and good results ($LOD > 5 \mu M$) were obtained for electrochemical sensors [20-22]. Dropping mercury electrodes ($LOD=0.099 \mu M$) [3] and glassy carbon electrodes ($LOD=1 \mu M$) [23-25] were used to evaluate quantitatively fluoxetine based on its reduction and oxidation process. However, taking into account that the potential toxicity of mercury limits its use as electroanalytical tool and not a very good sensitivity reached on a GC electrode, a fast electroanalytical method involving a stable, environmental and health friendly electrode material that allows to detect FXT in the aqueous media is desired.

Reagents

Fluoxetine was provided by Lilly (Pantheon, France). The stock solution was prepared using ethanol (PAM Corporation, Romania) and 0.1 M NaOH solution (Merck, Germany) in a volume ratio of 1:1 in order to obtain 1 mM FXT solution.

The supporting electrolyte was 0.1 M Na_2SO_4 solution, prepared using Na_2SO_4 of analytical purity (Merck, Germany) with distilled water.

CNF, AgZ-CNF, and CNT composite electrodes were tested for fluoxetine detection in comparison with a commercial boron-doped diamond (BDD) electrode.

8.1.2. Electrochemical characterization of carbon-based materials in the presence of fluoxetine

Prior to select the electrodes to perform the detection experiments, the electrochemical behavior of tested electrodes in the presence of fluoxetine was studied by cyclic voltammetry.

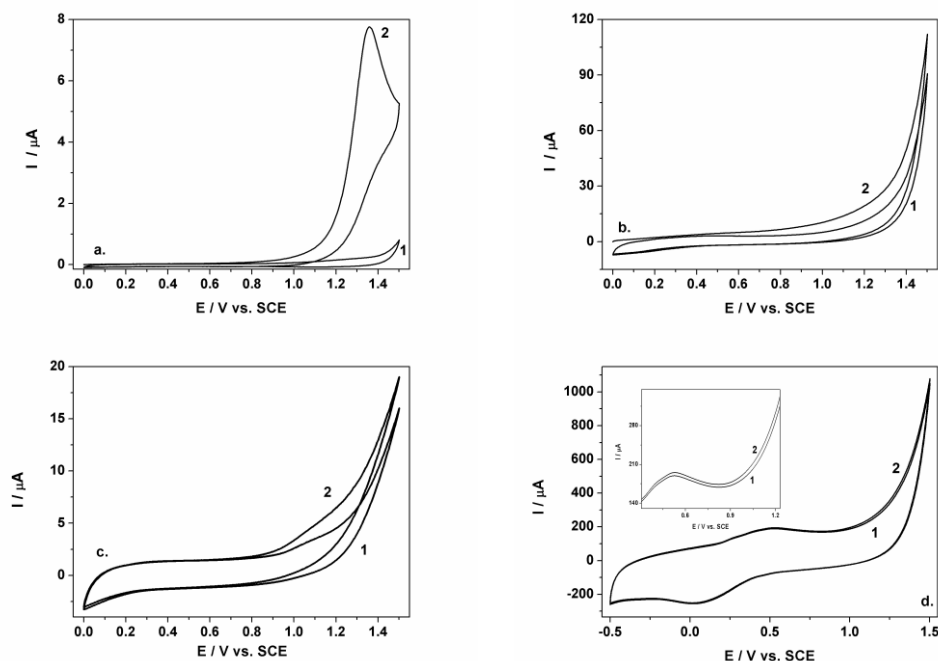


Figure 8.1. Cyclic voltammograms recorded in 0.1 M Na₂SO₄ supporting electrolyte (curve 1) on **a.** BDD electrode in the of 0.5 μM FXT (curves 2), **b.** CNF, **c.** AgZ-CNF, **d.** CNT electrode in the presence of 1 μM FXT (curves 2) at a potential scan rate of 0.05 Vs⁻¹.

In Figure 8.1 are presented the cyclic voltammograms recorded in 0.1 M Na₂SO₄ supporting electrolyte on the three types of carbon-based composite electrodes: CNF, AgZ-CNF and CNT in the presence of 1 μM FXT, and also recorded on the BDD electrode in the presence of 0.5 μM FXT.

For all tested composite electrode materials, except carbon nanotubes, for which the CVs almost overlapped, good properties in relation with clear oxidation peaks were obtained.

Table 8.2 summaries the useful signals of fluoxetine oxidation as obtained for the tested electrodes.

Table 8.2. Useful signals of FXT on tested electrodes

| Type of electrode | Potential range (V/SCE) | E _{ox} (V/SCE) | ΔI (μA) |
|-------------------|-------------------------|-------------------------|--------------|
| BDD | 0 → +1.5 | 1.350 | 7.500 |
| CNF | | 1.075 | 6.594 |
| AgZ-CNF | | 1.060 | 1.070 |
| CNT | -0.5 → +1.5 | 0.515 | 5.490* |

*This signal is not a real one due to the observation that the oxidation peak potential appeared on CNT in the presence of FXT and is attributed to carbon oxidation that is favoured in the presence of FXT. For this reason, CNT was not selected for further electrochemical detection of FXT.

For further electrochemical studies, two types of composite materials were selected, *e.g.*, carbon nanofiber and carbon nanofiber modified with silver-doped natural zeolite. Also, the BDD electrode was selected due to its potential value and for comparison with the composite electrodes.

8.1.2.1. Electrochemical detection of fluoxetine on BDD electrode

A systematic study regarding the electrochemical behaviour of fluoxetine on a BDD electrode was investigated using cyclic voltammetry (CV), envisaging detection application. Figure 8.2 shows the cyclic voltammograms recorded at this electrode using 0.1 M Na_2SO_4 supporting electrolyte within the potential range from 0 to +1.5 V/SCE with the concentration range 0.05 - 0.5 μM FXT. The corresponding oxidation peak of fluoxetine was observed at the potential value of +1.35 V/SCE. Also, the anodic current increased directly proportionally with the FXT concentration (see Figure 8.2.b). It should be mentioned that the same experiments were carried out for a glassy carbon electrode (GCE) because it can be regarded as a conventional carbon electrode versus BDD as advanced carbon electrode.

In comparison with the GCE, where the FXT oxidation process occurred at a less positive potential value of +1.13 V/SCE (the results are not presented here), the sensitivity achieved on the BDD electrode was higher than the one achieved for the GCE, *e.g.*, $15.87 \mu\text{A}\mu\text{M}^{-1}$ vs. $4.36 \mu\text{A}\mu\text{M}^{-1}$.

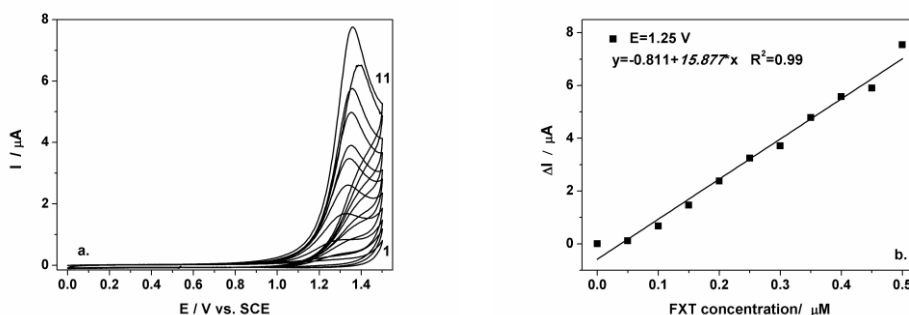


Figure 8.2. a. Cyclic voltammograms recorded at BDD electrode in 0.1 M Na_2SO_4 supporting electrolyte (curve 1) in the presence of 0.05-0.5 μM FXT (curves 2-11), at a potential scan rate of 0.05 Vs^{-1} in a potential range from 0 to +1.5 V/SCE; b. The calibration plot of the currents recorded at $E=+1.35 \text{ V/SCE}$ vs. FXT concentrations.

The effect of the scan rate on the electrooxidation of 0.5 μM FXT on the BDD electrode was studied to elucidate some mechanistic aspects. In Figure 8.3 CVs recorded for 0.5 μM FXT using the BDD electrode in 0.1M Na_2SO_4 supporting electrolyte at various scan rates (0.01; 0.02; 0.03; 0.04; 0.05; 0.075; 0.1; 0.2 Vs^{-1}) are presented. Figure 8.3.b shows the dependence of the anodic peak currents versus the square root of the scan rates.

The anodic current corresponding to FXT oxidation increased linearly with the square root of the scan rate ($v^{1/2}$), indicating that the oxidation reaction of FXT is a diffusion-controlled process at the BDD electrode. The FXT oxidation potential shifted towards positive potential when increasing the scan rate indicating that the electrooxidation process is irreversible (Figure 8.3.c), which is supported also by the lack of a cathodic peak corresponding to the anodic one.

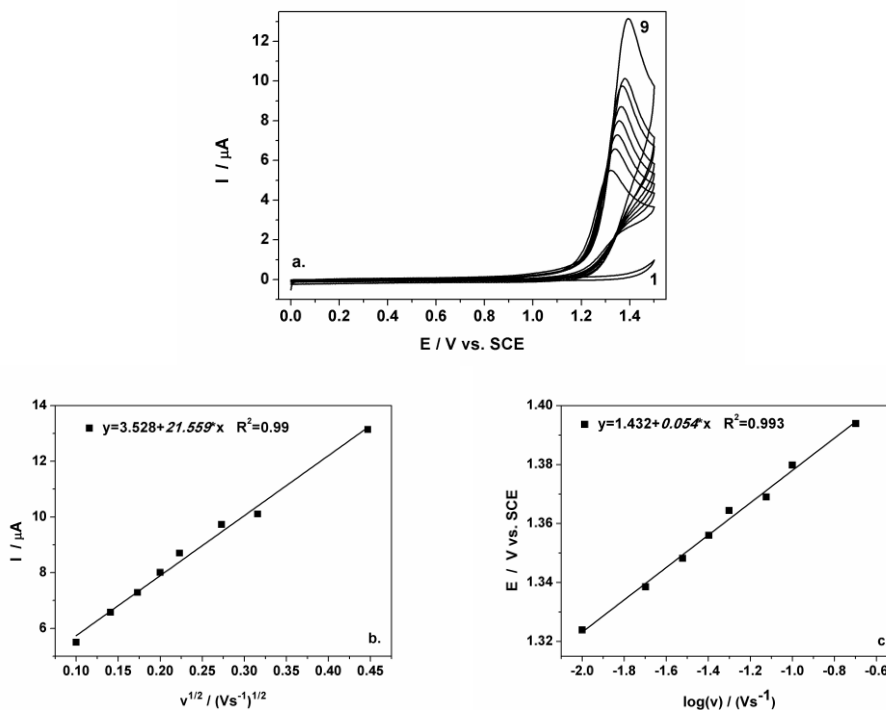


Figure 8.3. **a.** Cyclic voltammograms on BDD electrode in 0.1 M Na₂SO₄ (curve 1) supporting electrolyte in the presence of 0.5 μM FXT at different scan rates 0.01 - 0.2 Vs⁻¹ (curves 2-9); **b.** The calibration of the anodic peak current vs. the square root of the scan rate; **c.** The calibration plot of the peak potential E vs. log (v).

Taking into account the literature data regarding the mechanistic aspects of fluoxetine oxidation on a GCE, it can be assumed also that on the BDD electrode, FXT oxidation occurred based on the reaction (8.1) [20]:



where R is presented in Figure 8.4.

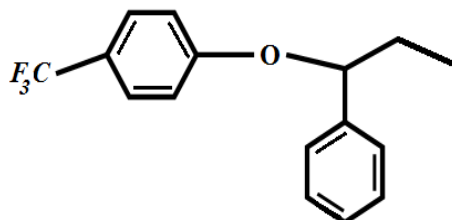


Figure 8.4. Molecular structure of radical R.

The fluoxetine oxidation process involved mainly its secondary amine group oxidation from the molecular structure. Also, it must be considered that it is very

well-known that the presence of the aromatic ring-based organics represents a very complex oxidation process on the carbon-based electrodes involving both the adsorption of the reactant/intermediate or oxidation products and the formation of passive, non-conductive layers of oligomer products of the oxidation process on their surface by electro-polymerization [26].

This aspect was noticed only for glassy carbon electrode, when starting with the second scan, the oxidation peak decreased and the background current as capacitive component increased (an undesired aspect) due to the formation of the non-conductive layer on the electrode surface. No similar behaviour was found for the BDD electrode, for which no significant decrease of the oxidation peak height was noticed after the first scan and also no significant modification of background current occurred.

It is well-known that voltammetric detection results can be improved using other advanced voltammetric techniques, *e.g.*, differential-pulsed voltammetry (DPV), square wave voltammetry (SWV). In the first step, to improve the electroanalytical parameters, differential-pulsed voltammetry (DPV) has been employed as technique for the assessment of FXT detection on the BDD electrode. For achieving the best performance with this technique, the operating parameters, *e.g.*, modulation amplitude (a), step potential (ΔE_s) and scan rate (ν) were optimized step by step based on a useful signal reached for oxidation of 0.2 μM FXT. The useful signal was determined as the difference between the anodic peak current and the background current. The results of optimization process are presented in Table 8.3 and it can be noticed that the optimized operating parameters were $a=0.2$ V, $\Delta E_s=0.05$ V and $\nu=0.025$ Vs^{-1} .

Table 8.3. The useful signal recorded for 0.2 μM FXT detection at various operating DPV parameters

| a (V) | ΔE_s (V) | ν (Vs^{-1}) | ΔI_p (μA) |
|--------------|------------------------------------|---|---|
| 0.025 | 0.05 | 0.05 | 0.390 |
| 0.05 | | | 1.050 |
| 0.2 | | | 22.938 |
| 0.2 | 0.01 | 0.05 | 4.334 |
| | 0.025 | | 5.619 |
| | 0.05 | | 22.938 |
| 0.2 | 0.05 | 0.025 | 27.182 |
| | | 0.05 | 22.938 |
| | | 0.1 | 26.576 |

Figure 8.5 presents as example the optimization of the step potential by maintaining a constant modulation amplitude of 0.2 V and a scan rate of 0.05 Vs^{-1} . For step potential values of 0.01V, respectively 0.025 V, the detection peak is shifting to more positive values. For a step potential value of 0.05 V a small shifting to the less positive potential value is observed, but a disadvantage in this case is represented by the sharpened voltammogram, which does not assure reproducibility.

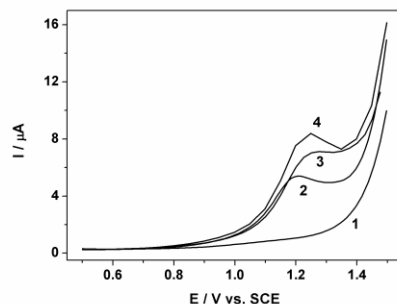


Figure 8.5. Differential-pulsed voltammograms recorded on BDD electrode in 0.1 M Na_2SO_4 supporting electrolyte (curve 1) in the presence of 0.2 μM FXT in a potential range from +0.5 to +1.5V/SCE at modulation amplitude of 0.2V, potential scan rate of 0.05 Vs^{-1} and step potential of 0.01V (curve 2), 0.025V (curve 3), 0.05V (curve 4).

Figure 8.6 depicts the DPVs recorded with the BDD electrode under optimized conditions, and as it is expected for pulsed voltammetry technique, the oxidation peak appeared at less positive potential value vs. CV (+1.25 V/SCE vs. +1.35 V/SCE). Also, a higher sensitivity was achieved ($81.21 \mu\text{A}\mu\text{M}^{-1}$ vs. $15.87 \mu\text{A}\mu\text{M}^{-1}$).

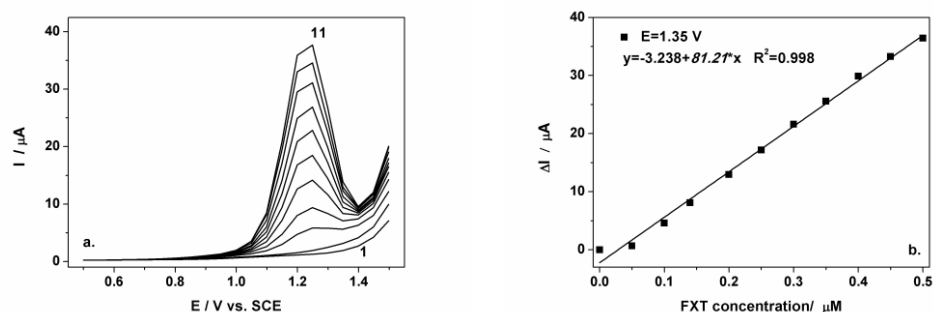


Figure 8.6. a. Differential-pulsed voltammograms recorded on BDD electrode under optimized conditions: modulation amplitude of 0.2V, step potential of 0.05V and potential scan rate of 0.025 Vs^{-1} in a potential range from +0.5 to +1.5V vs. SCE in 0.1 M Na_2SO_4 supporting electrolyte (curve 1) in the presence of different FXT concentrations: 0.05- 0.5 μM (curves 2-11); **b.** The calibration plots of the currents recorded at $E = +1.25 \text{ V/SCE}$ vs. FXT concentration.

The optimal operating parameters determined for DPV, *e.g.*, the modulation amplitude of 0.2 V and step potential of 0.05 V were also used for square wave voltammetry (SWV). An important operating parameter of this techniques which is directly related to the intensity of the analytical signal and the sensitivity is the frequency. Thus, an easy optimization was performed for this parameter. By varying the frequency in a range from 10 to 100 Hz, a substantial improvement in relation with the sensitivity was achieved (Table 8.4).

Table 8.4. The electroanalytical parameters of FXT detection at BDD electrode using SWV at different frequencies

| f (Hz) | E _{ox} (V/SCE) | Sens. (μAμM ⁻¹) | R ² | LOD (μgL ⁻¹) | LOQ (μgL ⁻¹) |
|--------|-------------------------|-----------------------------|----------------|--------------------------|--------------------------|
| 10 | 1.200 | 83.435 | 0.999 | 0.710 | 2.370 |
| 50 | 1.247 | 170.787 | 0.999 | 0.124 | 0.416 |
| 75 | 1.270 | 203.732 | 0.998 | 0.163 | 0.540 |
| 100 | 1.250 | 244.106 | 0.996 | 0.530 | 1.780 |

For all the studied frequencies (10, 50, 75, and 100 Hz) a good linearity of the anodic peak current vs. FXT concentration was observed. This aspect also supports the diffusion-controlled process for FXT electrooxidation. Still, the best sensitivity was achieved for the frequency of 100 Hz and no reproducible signal was obtained for the frequency higher than this value.

Figure 8.7 presents the square-wave voltammograms recorded with the BDD electrode in 0.1 M Na₂SO₄ supporting electrolyte recorded under a modulation amplitude of 0.2 V, step potential of 0.05 V and a frequency of 50 Hz. The voltammograms reveal a shaped and well-defined peak.

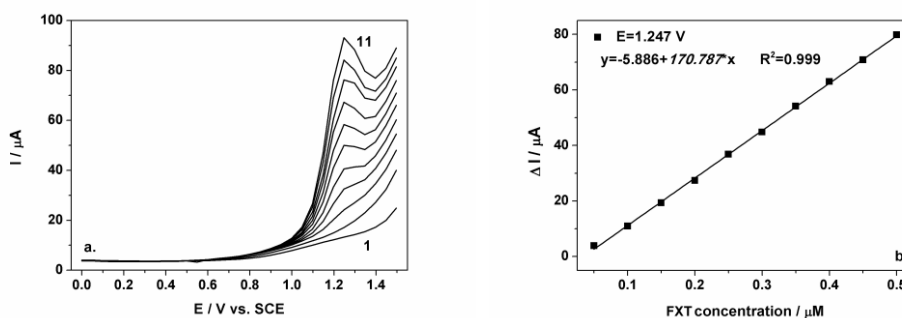


Figure 8.7. **a.** Square-wave voltammograms recorded on BDD electrode under 0.2 V modulation amplitude, 0.05 V step potential, 50 Hz frequency in a potential range from 0 to +1.5V/SCE in 0.1 M Na₂SO₄ supporting electrolyte (curve 1) in the presence of 0.05- 0.5 μM FXT (curves 2-11); **b.** The calibration plot of the currents recorded at E = +1.247 V/SCE vs. FXT concentration.

Figure 8.8 shows the square-wave voltammograms recorded with the BDD electrode in 0.1 M Na₂SO₄ supporting electrolyte under the optimised working conditions, a good linear dependence of peak current vs. FXT concentrations has been obtained. In comparison, with Figure 8.7, at frequency of 100 Hz (Figure 8.8), the signal become more fragmented due to high scan rate potential, which imposes a decrease in resolution.

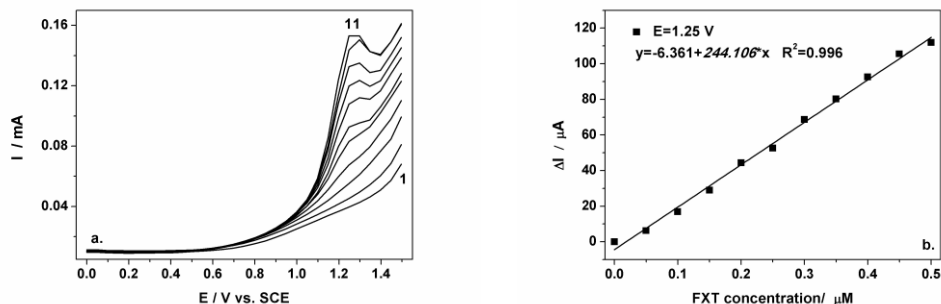


Figure 8.8. **a.** Square-wave voltammograms recorded on BDD electrode under optimized conditions: 0.2 V modulation amplitude, 0.05 V step potential, 100 Hz frequency in a potential range from 0 to +1.5 V/SCE in 0.1 M Na₂SO₄ supporting electrolyte (curve 1) in the presence of 0.05- 0.5 μM FXT (curves 2-11); **b.** The calibration plot of the currents recorded at E = +1.25 V/SCE vs. FXT concentration.

In comparison with CV and DPV, under SWV operating parameters for all tested frequencies good performances were obtained in relation with the sensitivity, the best value being obtained as expected for the highest value of frequency (Tables 8.4 and 8.5).

However, for practical working applications the optimum analytical procedure should involve the use of chronoamperometry (CA), which represents the easiest electroanalytical technique. The operating conditions for chronoamperometry recording are based on the existing well-established essential points of reference provided by the voltammograms. Thus, a serie of chronoamperograms was recorded at the potential value of + 1.4 V/SCE within a FXT concentrations ranging between 0.05 and 0.4 μM.

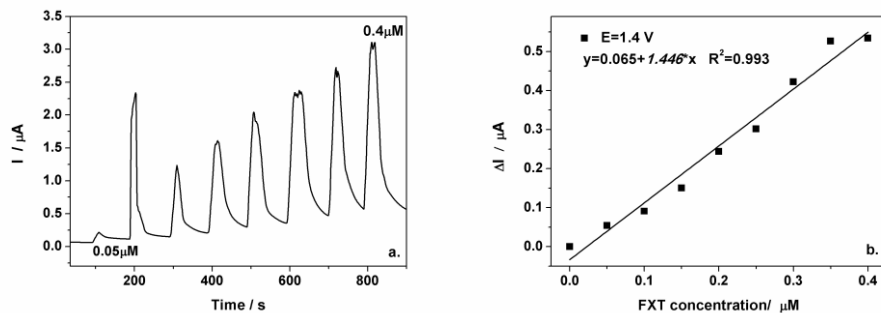


Figure 8.9. **a.** Chronoamperogram recorded at E = +1.4V/SCE on BDD electrode in 0.1 M Na₂SO₄ supporting electrolyte and in the presence of 0.05-0.4 μM FXT; **b.** The calibration plots of the currents vs. FXT concentrations.

The current response of FXT oxidation increased linearly with FXT concentration (Figure 8.9.b), but a lower sensitivity was achieved, probably due to electrode fouling. This behavior suggested that the chronoamperometry technique is not suitable for FXT detection with enhanced electroanalytical parameters.

The electroanalytical parameters for concentration ranges where a linear dependence was obtained at the various potential values in relation with the applied electrochemical techniques are gathered in Table 8.5. The limit of detection (LOD)

and the limit of quantification (LOQ) were evaluated based on $3S_B/b$ and respectively, $10S_B/b$ [27], where S_B is the standard deviation of the mean value of three voltammograms/amperegrams of the blank and b is the slope of the straight line in the analytical curve by using each electrochemical technique.

Table 8.5. The analytical parameters obtained at a BDD electrode using electrochemical techniques

| Tech. | E_{ox} (V/SCE) | Sens. ($\mu A \mu M^{-1}$) | R^2 | RSD (%) | LOD ($\mu g L^{-1}$) | LOQ ($\mu g L^{-1}$) |
|-------|---------------------|---------------------------------|-------|------------|---------------------------|---------------------------|
| CV | 1.35 | 15.870 | 0.990 | 6.54 | 0.982 | 3.270 |
| DPV | 1.25 | 81.210 | 0.998 | 0.25 | 0.037 | 0.123 |
| SWV | 1.25 | 244.106 | 0.996 | 0.34 | 0.530 | 1.780 |
| CA | 1.40 | 1.446 | 0.993 | 5.10 | 4.680 | 15.610 |

The reproducibility of the electrode using the above-mentioned techniques was evaluated for three replicate measurements of FXT detection as relative standard deviation (RSD). The maximum value of RSD is 6.54 %, hence a good reproducibility.

A recovery test was performed by analyzing three parallel tap water samples, which contained $5 \mu g L^{-1}$ FXT. This test was run using 0.1 M Na_2SO_4 as supporting electrolyte and a recovery of 96 % with a RSD of 2.8 % was found for FXT determination using SWV operated with the above-presented optimum operating parameters. Finally, the results obtained with this method were compared with those obtained by means of a conventional UV-VIS spectrophotometrical method recorded at the wavelength of 263 nm. Based on the results obtained, it can be concluded that the two methods lead to very close results and that the accuracy of the proposed SWV method is good.

Based on these presented results, it can be concluded that:

- The BDD electrode exhibited the useful properties for the anodic oxidation and the voltammetric/ampereometric detection of fluoxetine in aqueous solutions, the anodic oxidation process being diffusion-controlled.
- The best performance in relation to the sensitivity was obtained using square-wave voltammograms operated at 0.2 V modulation amplitude, 0.05 V step potential, and 100 Hz frequency, and the lowest limit of detection was obtained under differential-pulsed voltammetry operating parameters, *e.g.*, 0.2V modulation amplitude, 0.05 V step potential and 0.025 Vs^{-1} scan rate.
- The accuracy of the applied methods was excellent as compared to the detection results obtained using the conventional UV-VIS spectrophotometric method.
- The BDD electrode represents a suitable alternative for fluoxetine determination in real water sample and also, in pharmaceutical formulations, and the proposed pulsed voltammetric-based methodologies can be a valuable tool for the fluoxetine analysis. The selection of technique is based on concrete aim in relation to either sensitivity or detection limit.

8.1.2.2. Electrochemical detection of fluoxetine on CNF electrode

In electroanalysis, a lower value of oxidation potential is very desirable. The previously presented results obtained with the BDD electrode are very promising, still the detection potential values are quite high and another type of material that would allow the FXT detection on a lower potential value and also would show a good sensitivity represents an improved alternative, very desired in electroanalysis.

Therefore, a new composite electrode based on carbon nanofibers was developed and preliminary above-presented results related to the peak value corresponding to fluoxetine oxidation are very promising.

The electrochemical behaviour of FXT on a CNF electrode was studied, the results being presented in Figure 8.10. For the CNF electrode, the FXT oxidation process started at +0.3 V/SCE and increased until +0.6 V/SCE, after which a wide plateau is achieved. Starting from +1.2 V/SCE the presence of sodium hydroxide used to prepare the stock solution is detected and the oxygen depletion overlapped it.

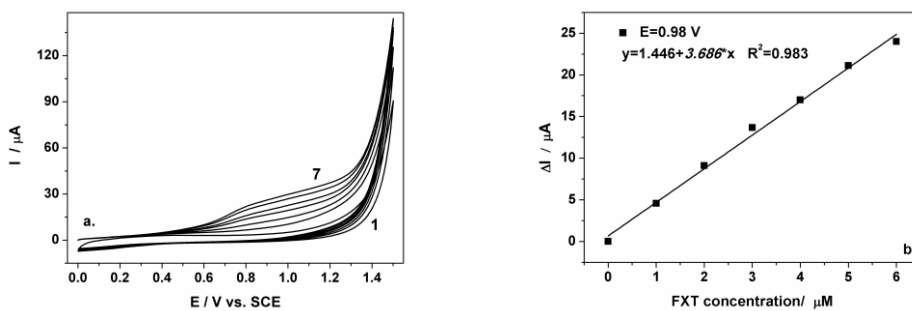


Figure 8.10. a. Cyclic voltammograms recorded at CNF electrode in 0.1 M Na₂SO₄ supporting electrolyte (curve 1) and in the presence of 1-6 μM FXT (curves 2-7), at a potential scan rate of 0.05 Vs⁻¹ in a potential range from 0 to +1.5 V/SCE; **b.** The calibration plot of the currents recorded at E = +0.98 V/SCE vs. FXT concentrations.

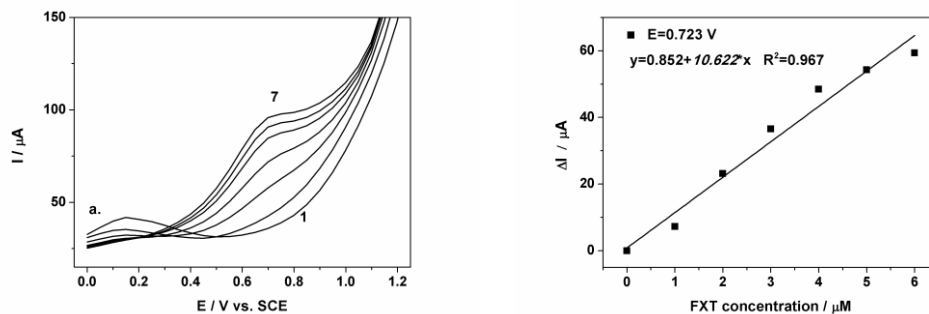


Figure 8.11. a. Differential-pulsed voltammograms recorded on CNF electrode under modulation amplitude of 0.2V, step potential of 0.05V and potential scan rate of 0.025 Vs⁻¹ in a potential range from 0 to +1.25 V/SCE in 0.1 M Na₂SO₄ supporting electrolyte (curve 1) and in the presence of 0-6 μM FXT (curves 2-7); **b.** The calibration plot of the currents recorded at E = +0.723 V/SCE vs. FXT concentrations.

In comparison with the BDD electrode the value of the FXT detection potential is shifted to less positive values and the sensitivity obtained is lower than the previous one (3.686 μAμM⁻¹ vs. 15.87 μAμM⁻¹). As in the case of the BDD electrode, the lack of cathodic peak suggests an irreversible oxidation process and it can be assumed that on the CNF electrode the oxidation process is controlled by diffusion indicated by the linear dependence of the anodic peak currents vs. FXT concentrations. Based on the detection results achieved using the BDD electrode,

DPV operated under optimized conditions was applied also for the CNF electrode and the results are presented in Figure 8.11.

In comparison with cyclic voltammetry, the oxidation peak potential is shifting to less positive values of oxidation potential (+0.723 V/SCE vs. +0.92 V/SCE), and a better sensitivity was obtained. In comparison with the BDD electrode, using CNF the voltammograms present a better resolution and the peak potential shifted to less positive values. This suggests that the carbon nanofiber electrode represents a good option for fluoxetine detection.

The effect of the scan rate was studied by applying DPV. In Figure 8.12 the DPVs recorded on the CNF electrode are presented under new operating parameters, *e.g.*, a modulation amplitude of 0.05V, a step potential of 0.01V, and a scan rate of 0.001 Vs⁻¹.

As expected, a smaller value for sensitivity was reached (0.734 vs. 10.622 $\mu\text{A}\mu\text{M}^{-1}$). However, the oxidation process started at +0.45 V/SCE and a well-defined peak is reached at +0.721 V/SCE. A different behavior was observed due to the appearance of a new oxidation peak at +1.1 V/SCE. Its presence could be explained by oxygen evolution. At concentrations higher than 5 μM FXT this peak tends to flatten by reaching the saturation level.

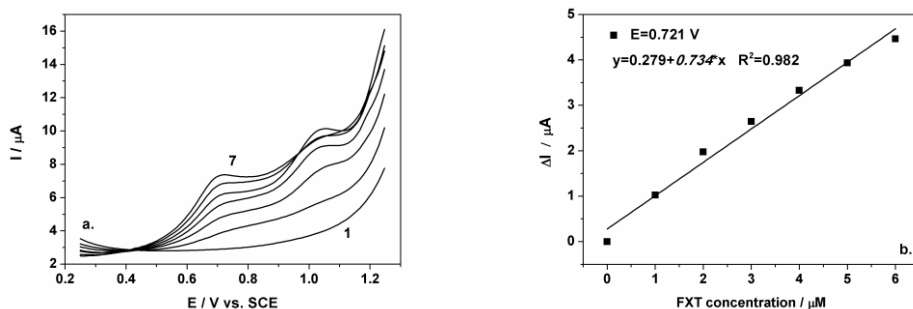


Figure 8.12. a. Differential-pulsed voltammograms recorded on CNF electrode under optimized conditions: modulation amplitude of 0.05V, step potential of 0.01V and potential scan rate of 0.001 Vs⁻¹ in a potential from +0.25 to +1.25 V/SCE in 0.1 M Na₂SO₄ supporting electrolyte (curve 1) in the presence of 0-6 μM FXT (curves 2-7); b. The calibration plot of the currents recorded at E = +0.721 V/SCE vs. FXT concentration.

In Table 8.6 the electroanalytical parameters obtained for fluoxetine detection with the CNF electrode are gathered.

Table 8.6. The electroanalytical parameters obtained on CNF electrode

| Tech. | E _{ox} (V/SCE) | Sens. ($\mu\text{A}\mu\text{M}^{-1}$) | R ² | RSD (%) | LOD (μM) | LOQ (μM) |
|------------|----------------------------|--|----------------|------------|--------------------------|--------------------------|
| CV | 0.980 | 3.686 | 0.983 | 3.52 | 0.133 | 0.446 |
| DPV | 0.723 | 10.622 | 0.967 | 3.62 | 0.385 | 1.285 |

Based on the presented results, it can be concluded that:

- Good properties regarding fluoxetine detection with CNF electrode were obtained.
- The best performances in relation with the sensitivity was obtained for DPV under the same optimized conditions as obtained for the BDD electrode.

■ Good values for limit of detection, respectively, limit of quantification were obtained for both cyclic voltammetry and differential-pulsed voltammetry experiments.

8.1.2.3. Electrochemical detection of fluoxetine on AgZ-CNF electrode

The use of a catalyst in the electroanalytical applications has generated another class of electrodes referred to as chemically-modified electrodes (CMEs), which possess electrocatalytic activity reflected in improved electroanalytical performance [28-30].

As discussed previously, the value of +0.92 V/SCE achieved for fluoxetine detection with the CNF electrode is too high and other pharmaceuticals or organic pollutants from water could interfere with it.

Zeolites, used as modifying agents represent a useful and promising approach due to their characteristics, *e.g.*, shape, size and charge selectivity, physical and chemical stability and catalyst support. Improved electroanalytical parameters by using zeolite-modified electrodes have been previously reported [31-33]. Moreover, metal ion-doped zeolites allow exploitation of ion-exchange capacity of zeolite for the development of electrochemical sensors for the sensing of non-electroactive inorganic or organic species [34, 35]. Also, the zeolites-supported electrocatalyst can be exploited to improve the performance of the analytical sensing devices.

Therefore, a new composite electrode based on silver natural zeolite and carbon nanofiber was developed. In order to underline the effect of silver within the CNF matrix comparative detection studies were carried out in the preliminary stage on a commercial silver electrode. In Figure 8.13 the cyclic voltammograms recorded on a commercial silver electrode in a narrow potential window from -0.35 V/SCE to +0.35 V/SCE are presented. A value of +0.312 V/SCE for the detection potential was found for the fluoxetine oxidation process. These results (+0.312 V/SCE for Ag electrode vs. +0.92 V/SCE for CNF electrode) are very promising for the electroanalytical applications.

It must be mentioned that the voltammetric detection experiments performed on the commercial Ag electrode within a larger potential window (the results are not presented here) led to the absence of a fluoxetine detection signal because another oxidation process of silver species and oxygen evolution interfered.

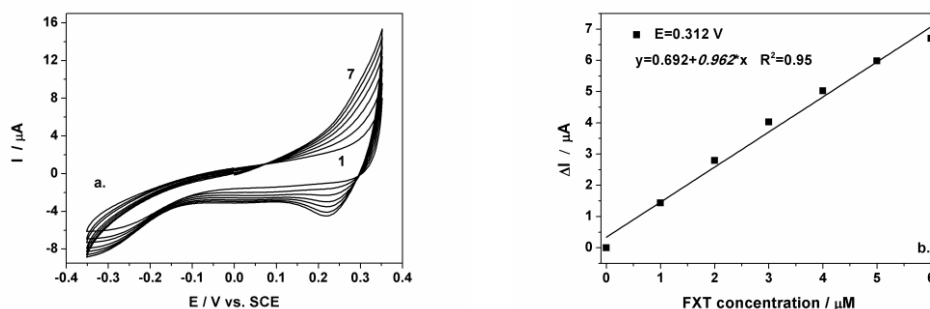


Figure 8.13.a. Cyclic voltammograms recorded at Ag electrode in 0.1 M Na₂SO₄ supporting electrolyte (curve 1) in the presence of 1-6 μM FXT (curves 2-7) at a potential scan rate of 0.05 Vs⁻¹ in a potential range from -0.35 to +0.35 V/SCE; **b.** The calibration plot of the currents recorded at E=+0.312 V/SCE vs. FXT concentration.

The electrochemical behavior of the new composite electrode was studied using cyclic voltammetry in two potential windows, *e.g.*, a narrow one specific for silver from -0.35 V/SCE to +0.35 V/SCE and an extended one specific for carbon nanofiber from 0 to +1.5 V/SCE. The results are presented in Figures 8.14 and 8.15.

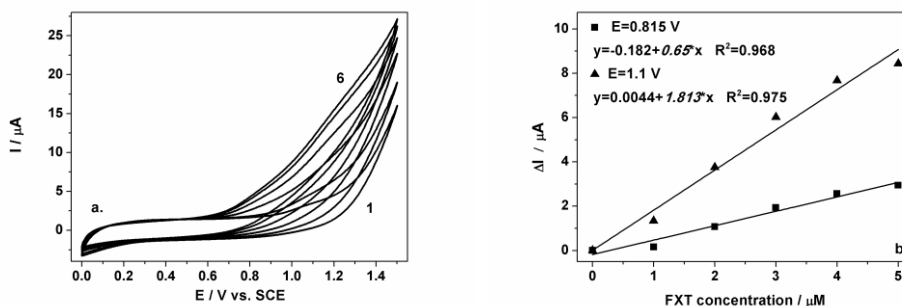


Figure 8.14. **a.** Cyclic voltammograms recorded at AgZ-CNF electrode in 0.1 M Na₂SO₄ supporting electrolyte (curve 1) in the presence of 1-5 μM FXT (curves 2-6) at potential scan rate of 0.05 Vs⁻¹ in a potential range from 0 to +1.5 V/SCE; **b.** Calibration plots of the currents vs. FXT concentration.

Within the extended potential window specific for carbon nanofibers, the irreversible oxidation process of fluoxetine occurred in two stages and a higher anodic peak current was recorded at +1.1 V/SCE, characteristic for CNF behavior in the presence of FXT. For the narrow potential window the oxidation process presented a large cathodic plateau that suggests the reversibility of the process that involves a silver redox process. It must be mentioned that the sensitivities reached at low potential values are similar for both conditions (0.623 vs. 0.65 μAμM⁻¹), which supports a good reproducibility of the silver-based detection results. At higher potential values, a better sensitivity was achieved. However, this sensitivity is slightly lower in comparison with the CNF electrode. For further studies the narrow potential window was preferred.

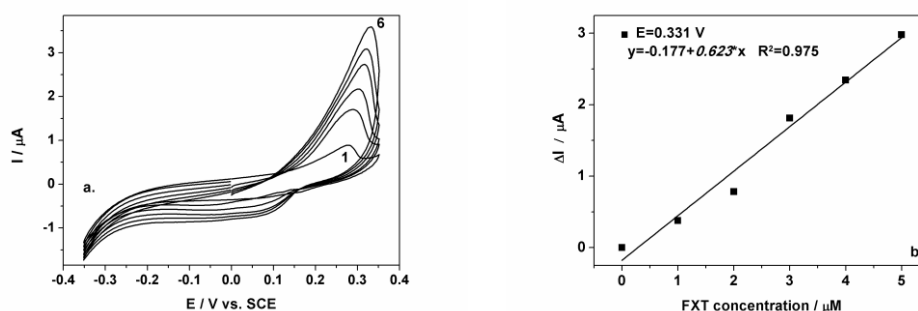


Figure 8.15. **a.** Cyclic voltammograms recorded at AgZ-CNF electrode in 0.1 M Na₂SO₄ supporting electrolyte (curve 1) in the presence of 1-5 μM FXT (curves 2-6) at potential scan rate of 0.05 Vs⁻¹ in a potential range from -0.35 to +0.35 V/SCE; **b.** Calibration plot of the currents recorded at E = +0.331 V/CSE vs. FXT concentration.

These results are promising, but an improvement in sensitivity in the narrow potential window was taken into account. Even if the adsorption of FXT on the composite electrode not being desired, due to electrode fouling, this aspect could be exploited in a positive way to detect FXT at the trace level [36], and a preconcentration step was proposed. After adding the analyte and stirring, the mixed solution remained at open circuit potential for 30 minutes, after which the voltammograms were recorded. The results are presented in Figure 8.16.

An improvement in sensitivity was observed ($2.007 \mu\text{A}\mu\text{M}^{-1}$ vs. $0.623 \mu\text{A}\mu\text{M}^{-1}$) and also the limit of detection was improved. The cathodic peak becomes more pronounced, and it is shifting to more negative potential values, an aspect that could be exploited for other reduction studies envisaging detection results on the cathodic branch. However, this aspect is beyond the aim of our study. It must be noticed that for a commercial silver electrode the application of the preconcentration step did not lead to an enhancement of the sensitivity indicating that fluoxetine sorption occurred on the CNF and not on the Ag surface.

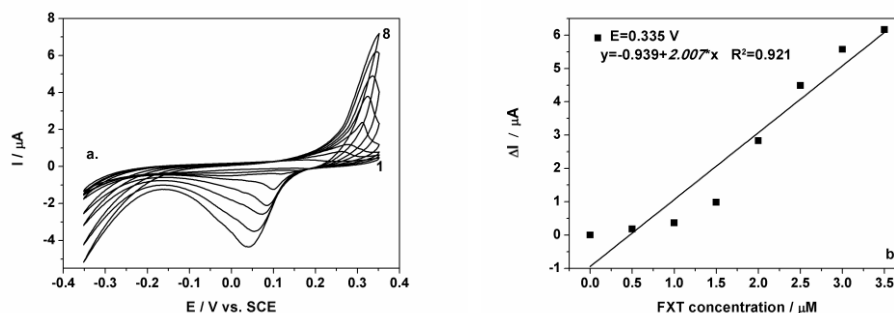


Figure 8.16. **a.** Cyclic voltammograms recorded at AgZ-CNF electrode in 0.1 M Na_2SO_4 supporting electrolyte (curve 1) in the presence of 0.5-3.5 μM FXT (curves 2-8) at potential scan rate of 0.05 V s^{-1} in the potential range from -0.35 to +0.35 V/SCE; **b.** Calibration plot of the currents recorded at $E = +0.335 \text{ V/SCE}$ vs. FXT concentration.

Chronoamperometry, one of the simplest techniques was applied for fluoxetine detection and the results are presented in Figure 8.17.a.

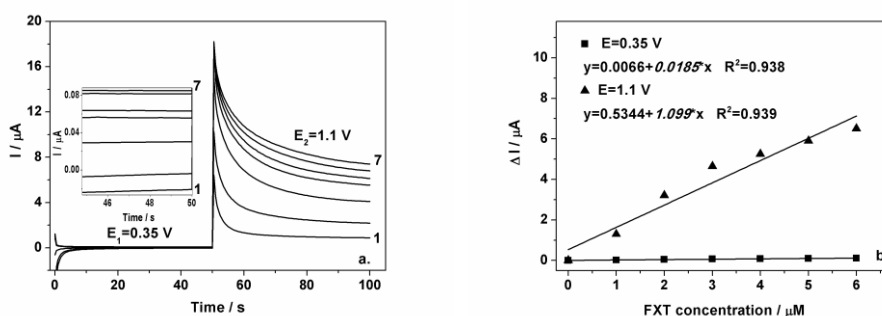


Figure 8.17. **a.** Chronoamperograms recorded at AgZ-CNF electrode in 0.1 M Na_2SO_4 supporting electrolyte (curve 1) at the potential values of $E_1 = +0.35 \text{ V/SCE}$ and $E_2 = +1.1 \text{ V/SCE}$ in the presence of 1-6 μM FXT (curves 2-7); Inset: Detail of chronoamperograms recorded at potential value of $E_1 = +0.35 \text{ V/SCE}$; **b.** Calibration plots of the currents recorded at $E_1 = +0.35 \text{ V/SCE}$ and $E_2 = +1.1 \text{ V/SCE}$ vs. FXT concentration.

The specific induced properties of Ag and carbon nanofiber on this electrode were previously discussed, two values of detection potential were used, *e.g.*, $E=+0.35$ V/SCE specific for Ag and $E=+1.1$ V/SCE specific for carbon nanofiber. The sensitivities obtained in this case are $0.0185 \mu\text{A}\mu\text{M}^{-1}$ for $E=+0.35$ V/SCE, respectively, $1.099 \mu\text{A}\mu\text{M}^{-1}$ for $E=+1.1$ V/SCE (Figure 8.17.b).

Therefore, to simulate practical applications, chronoamperometry-BIA (BIA-batch injection analysis) was applied for fluoxetine detection by using a continuous adding method.

In Figure 8.18.a and Figure 8.19.a the chronoamperograms recorded for each detection potential individually are presented.

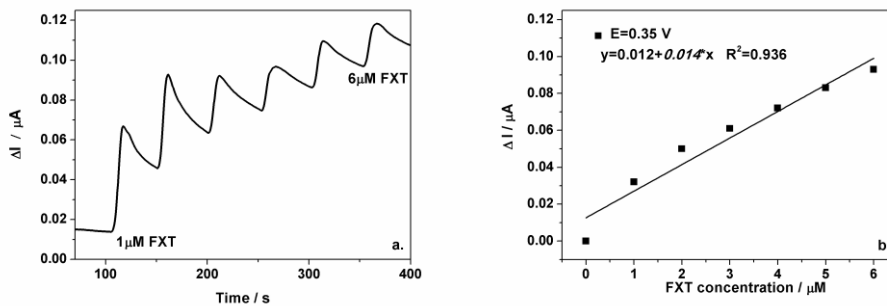


Figure 8.18. a. Chronoamperograms recorded at AgZ-CNF electrode in $0.1 \text{ M Na}_2\text{SO}_4$ supporting electrolyte at the potential values of $+0.35$ V/SCE in the presence of $1\text{--}6 \mu\text{M}$ FXT; **b.** Calibration plot of the currents vs. FXT concentrations recorded at $E=+0.35$ V/SCE.

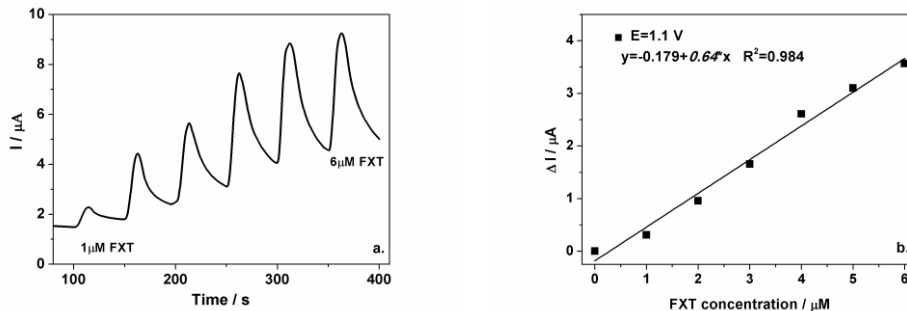


Figure 8.19. a. Chronoamperograms recorded at AgZ-CNF electrode in $0.1 \text{ M Na}_2\text{SO}_4$ supporting electrolyte at the potential values of $+1.1$ V/SCE in the presence of $1\text{--}6 \mu\text{M}$ FXT; **b.** Calibration plot of the currents vs. FXT concentrations recorded at $E=+1.1$ V/SCE.

For both potential values good linearity peak currents vs. FXT concentration were obtained, still the values were lower than the ones obtained for the previously case: 0.014 vs. $0.018 \mu\text{A}\mu\text{M}^{-1}$ for $E_1=+0.35$ V/SCE, and 0.64 vs. $1.099 \mu\text{A}\mu\text{M}^{-1}$ for $E_2=+1.1$ V/SCE (see Figure 8.18.b and Figure 8.19.b). Generally, a difference between CA and CV sensitivities is obtained. For both detection potential values, the sensitivities obtained under CA operating conditions were lower than the ones

obtained under CV operating conditions, e.g., 0.014 vs. 0.623 $\mu\text{A}\mu\text{M}^{-1}$ for $E_1=+0.35$ V/SCE, and 0.64 vs. 1.813 $\mu\text{A}\mu\text{M}^{-1}$ for $E_2=+1.1$ V/SCE.

Based on the results presented in Table 8.7, it can be concluded that:

- The AgZ-CNF electrode exhibited properties for fluoxetine detection in aqueous solution. Silver presence led to improved electroanalytical performance related to the detection potential.
- The proposed preconcentration step improved the sensitivity and also indicating that this electrode could be suitable for fluoxetine detection at trace concentration levels.
- This type of electrode could represent a good and eco-friendly alternative in fluoxetine detection.

Table 8.7. Electroanalytical parameters obtained at AgZ-CNF electrode for fluoxetine detection

| Tech. | E_{ox} (V/SCE) | Sens. ($\mu\text{A}\mu\text{M}^{-1}$) | R^2 | RSD (%) | LOD (μM) | LOQ (μM) |
|--------|----------------------------|--|-------|------------|--------------------------|--------------------------|
| CV | 0.331 | 0.623 | 0.975 | 6.08 | 0.187 | 0.626 |
| | 0.815 | 0.650 | 0.968 | 12.98 | 1.099 | 3.664 |
| | 1.100 | 1.813 | 0.975 | 8.46 | 0.520 | 1.733 |
| CV_ads | 0.335 | 2.007 | 0.921 | 3.05 | 0.019 | 0.064 |
| CA | 0.350 | 0.018 | 0.938 | 8.16 | 0.254 | 0.849 |
| | 1.100 | 1.009 | 0.939 | 4.50 | 0.113 | 0.379 |
| CA-BIA | 0.350 | 0.014 | 0.936 | 7.05 | 0.292 | 0.974 |
| | 1.100 | 0.640 | 0.984 | 6.95 | 0.549 | 1.831 |

8.1.2.4. Electrochemical detection of fluoxetine on Ag-CNF electrode

As previously discussed, silver inclusion in the electrode composition represents a useful and promising approach due to its high catalytic activity [28, 29]. The preliminary studies performed on a commercial silver electrode showed interesting features regarding fluoxetine detection at lower values of oxidation potential. Within this context, a new type of electrode based on silver electrodeposition on carbon nanofibers for Ag-CNF was developed to analyse the presence of fluoxetine in water.

The electrochemical behavior of Ag-CNF electrode in the presence of various concentrations of FXT was studied as in the case of AgZ-CNF electrode by cyclic voltammetry in two potential windows, e.g., first for an extended potential window from 0 to +1.5 V/SCE corresponding to CNF behavior, and secondly for a narrow potential window specific for silver from 0 to +0.45 V/SCE. The results are presented in Figures 8.20 and 8.21.

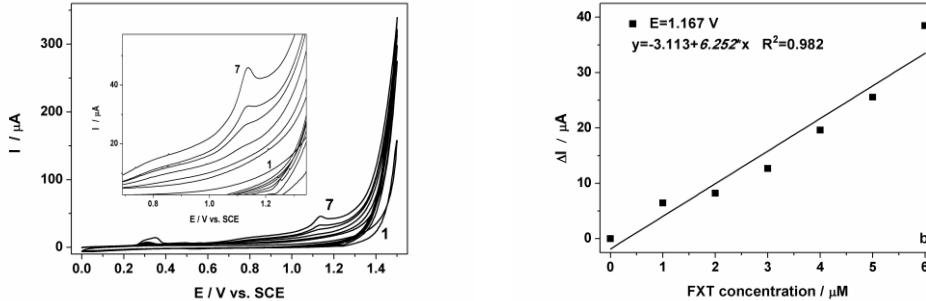


Figure 8.20. **a.** Cyclic voltammograms recorded at Ag-CNF electrode in 0.1 M Na₂SO₄ supporting electrolyte (curve 1) in the presence of 1-6 μM FXT (curves 2-7) at potential scan rate of 0.05 Vs⁻¹ in a potential range from 0 to +1.5 V/SCE; **b.** The calibration plot of the currents recorded at E=+1.167 V/SCE vs. FXT concentration.

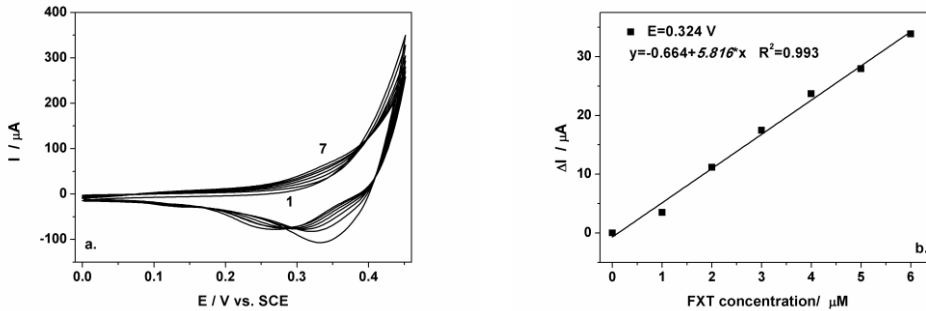


Figure 8.21. **a.** Cyclic voltammograms recorded at Ag-CNF electrode in 0.1 M Na₂SO₄ supporting electrolyte (curve 1) in the presence of 1-6 μM FXT (curves 2-7) at potential scan rate of 0.05 Vs⁻¹ in a potential range from 0 to +0.45 V/SCE; **b.** The calibration plot of the currents recorded at E=+0.324 V/SCE vs. FXT concentration.

It can be noticed that the CV shape reveals characteristics of the presence of both silver and CNF by the anodic current peaks corresponding to FXT oxidation involving silver recorded at the potential value of +0.3 V/SCE and further oxidation of FXT directly on CNF that started at the potential value of about +0.6 V/SCE. A good linearity of the peak current vs. FXT concentration was found in both potential windows (Figures 8.20.b and 8.21.b). The results show a synergetic effect for the sensitivities in relation with each single commercial Ag and CNF composite electrode. Thus, the sensitivity of 5.816 μAμM⁻¹ was achieved at the potential value of +0.324 V/SCE for the Ag-CNF electrode in comparison with 0.962 μAμM⁻¹ for the commercial Ag electrode, and 6.252 μAμM⁻¹ was achieved at the potential value of +1.167 V/SCE vs. 3.868 μAμM⁻¹ for the CNF electrode.

Based on the voltammetric results, chronoamperometry was applied for two potentials of +0.35 V/SCE and +1.1 V/SCE in the presence of various FXT concentrations. The results are presented in Figure 8.22. Because the current response was lower at the potential value of +0.35 V/SCE, a detail of the chronoamperograms is presented in the inset of Figure 8.22.a. A good linearity of current vs. FXT concentration was observed for both potential values with good correlation coefficients.

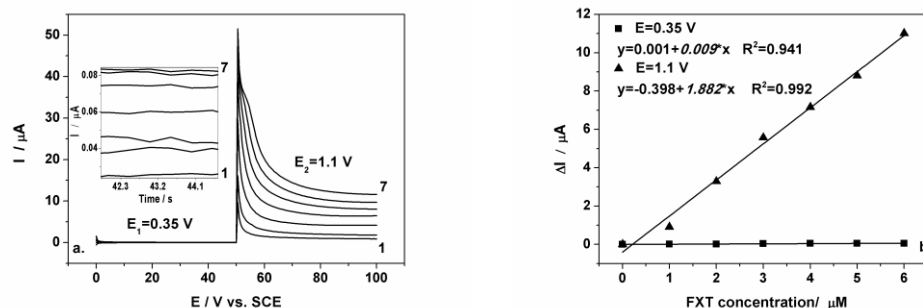


Figure 8.22. a. Chronoamperograms recorded on Ag-CNF electrode at the potential values of $E_1 = +0.35\text{V/SCE}$ and $E_2 = +1.1\text{V/SCE}$ in $0.1\text{M Na}_2\text{SO}_4$ supporting electrolyte (curve 1) in the presence of $1\text{-}6\ \mu\text{M}$ FXT (curves 2-7); Inset: Detail of chronoamperograms recorded at $+0.35\text{V/SCE}$ potential value; b. Calibration plots of the currents vs. FXT concentrations.

Table 8.8. The electroanalytical parameters obtained for Ag-CNF electrode

| Tech. | E_{ox} (V/SCE) | Sens. ($\mu\text{A}\mu\text{M}^{-1}$) | R^2 | RSD (%) | LOD (μM) | LOQ (μM) |
|-------|----------------------------|--|-------|------------|--------------------------|--------------------------|
| CV | 0.324 | 5.816 | 0.993 | 0.73 | 0.081 | 0.270 |
| | 1.167 | 6.262 | 0.982 | 4.82 | 0.189 | 0.631 |
| CA | 0.350 | 0.009 | 0.992 | 24.75 | 2.380 | 7.934 |
| | 1.100 | 1.882 | 0.992 | 5.39 | 0.079 | 0.266 |

Based on the results obtained for fluoxetine detection on Ag-CNF electrode as gathered in Table 8.8, it can be concluded that:

- The Ag-CNF composite electrode exhibited the synergetic effect in relation to the sensitivity for fluoxetine detection in aqueous solution in comparison with commercial silver electrode (Ag) and carbon nanofiber (CNF) composite electrode using CV technique.
- The best performances in relation with the limit of detection, and limit of quantification are obtained by employing chronoamperometry at a detection potential of $+1.1\text{V/SCE}$.
- Also, the results of this study are very promising for the practical application for fluoxetine detection in aqueous solution avoiding the potential interference.

8.1.3. Conclusions

In Table 8.9 all the electroanalytical parameters obtained on selected electrodes on optimized operation condition for fluoxetine detection are gathered.

Based on these results, it can be concluded that:

- For all tested electrodes, e.g., BDD, CNF, AgZ-CNF, Ag-CNF good properties were revealed regarding fluoxetine detection.
- The best results regarding sensitivity and lowest limit of detection, and lowest limit of quantification were obtained on BDD electrode. Yet, the high values obtained for detection potential could represent an impediment for electroanalytical applications, due to a possible cumulative effect caused by other organic pollutants detected at similar potential values.
- The use of composite materials based on carbon nanofibers and silver catalyst on CNF resulted an important enhanced results regarding the detection potential of

fluoxetine.

■ Selection of the electrode and electrochemical techniques should be based on the specific conditions for the detection applications.

Table 8.9. The electroanalytical parameters obtained for fluoxetine detection on tested electrodes

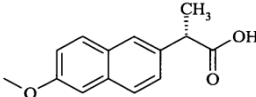
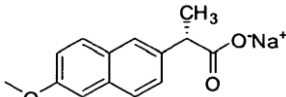
| Electr. | Tech. | E _{ox} (V/SCE) | Sens. ($\mu\text{A } \mu\text{M}^{-1}$) | R ² | RSD (%) | LOD (μM) | LOQ (μM) |
|----------------|-------------------|----------------------------|--|----------------|------------|-----------------------|-----------------------|
| BDD | CV | 1.350 | 15.870 | 0.990 | 6.54 | $3.17 \cdot 10^{-3}$ | $10.57 \cdot 10^{-3}$ |
| | DPV | 1.250 | 81.210 | 0.998 | 0.25 | $0.11 \cdot 10^{-3}$ | $0.39 \cdot 10^{-3}$ |
| | SWV | 1.250 | 244.110 | 0.996 | 0.34 | $1.71 \cdot 10^{-3}$ | $5.75 \cdot 10^{-3}$ |
| | CA | 1.400 | 1.446 | 0.993 | 5.10 | 0.015 | 0.050 |
| CNF | CV | 0.980 | 3.686 | 0.983 | 3.52 | 0.133 | 0.446 |
| | DPV | 0.723 | 10.622 | 0.967 | 3.62 | 0.385 | 1.285 |
| AgZ-CNF | CV _{ads} | 0.335 | 2.007 | 0.921 | 3.05 | 0.019 | 0.064 |
| Ag-CNF | CV | 0.324 | 5.816 | 0.993 | 0.73 | 0.081 | 0.270 |
| | | 1.167 | 6.252 | 0.982 | 4.82 | 0.189 | 0.631 |

8.2. Electrochemical detection of naproxen in water

8.2.1. Introduction

Naproxen (NPX) - (2S)-2-(6-methylnaphthalen-2-yl) propionic acid is a non-steroidal anti-inflammatory drug from the phenylpropanoic acid class, used in the treatment of osteoarthritis, rheumatoid arthritis, degenerative joint disease, ankylosing spondylitis, acute gout, and primary dysmenorrhea [37-40]. As other NSAIDs, the activity of naproxen inhibits the cyclooxygenase enzymes and the biosynthesis of certain prostaglandins is prevented [41]. Naproxen is rapidly absorbed (sodium salts are more easily absorbed) in the plasma, and then, it is extensively metabolized in the liver to 6-desmethylnaproxen. After approximately 13 hours (half-life in plasma) it is eliminated. Approximately 95% of the drug is excreted in urine as unchanged naproxen (< 1%) and 6-desmethylnaproxen (< 1%) and their glucuronide or other conjugates (66-92%). At patients with renal impairments, these metabolites could accumulate and cause other problems.

Table 8.10. Information on naproxen and naproxen sodium

| | Naproxen (NPX) | Naproxen Sodium (NPX-Na) |
|---------------------|---|--|
| Molecular formula | $\text{C}_{14}\text{H}_{14}\text{O}_3$  | $\text{C}_{14}\text{H}_{13}\text{NaO}_3$  |
| Molecular weight | 230.25916 g mol^{-1} | 252.240989 g mol^{-1} |
| pKa | 4.15 | |
| Log K _{oc} | 3.2 | |
| Melting point | 153°C | |
| Water solubility | 15.9 mg L^{-1} (25°C)* | 250 g L^{-1} ** |

*Sources PubChem website; **Roche, technical information on Naproxen Sodium [42];

It is an odourless, white to creamy-white crystalline substance, freely soluble in methanol, ethanol, and water at high pH values. In Table 8.10 some properties of naproxen in comparison with naproxen sodium are gathered.

With annual consumption of over 35 t (35.07 t in 2000) in England [15], naproxen traces were found in rivers, drinking waters, influent and effluent sewage treatment plant in several countries (Canada, Sweden, Belgium, Germany, Slovenia, USA, China, Japan, South Korea) with concentration ranging between 31 ngL⁻¹ and 12.5 µgL⁻¹ [6, 8, 13, 15]. Since, the environmental long-term effects of continuous low-level exposure to naproxen, as well as other drugs, are not well studied even for levels of the ngL⁻¹ to µgL⁻¹ of these compounds were detected in sewage, river, and stream waters.

Ecotoxicology studies revealed that naproxen and its photoproducts are causing several acute and chronic effects in the environment. Acute toxicity tests on naproxen established that LC₅₀ and EC₅₀ values are ranging in the 1-100 mgL⁻¹. Chronic exposure to naproxen caused inhibition on *C. dubia* growth population at low concentrations levels (µgL⁻¹). Photoproducts of naproxen were found to be more toxic than the parent compound, therefore, degradation of this pharmaceutical compound in wastewater treatment plants is being desired. Studies performed in sewage treatment plants (equipped with mechanical treatment, biological treatment, and chemical treatment) yielded a high decrease in naproxen concentration during the biological treatment, the removal of acidic NSAID compounds being achieved by biodegradation and not by adsorption to particles. In general the rates of naproxen removal are ranging between 50% and 98%. Therefore, new improvements in sewage treatment plants for total removal of pharmaceuticals are desired [43, 44].

Reagents

Naproxen (NPX) was provided by AC Helcor SRL, Romania. A stock solution of 1mM was prepared by using 0.1 M NaOH solution (Merck, Germany).

8.2.2. Electrochemical detection of naproxen

Several research studies that discuss the electrochemical behaviour of naproxen are set up for non-aqueous media. In Table 8.11 the results obtained in these studies are summarized.

Table 8.11. Electrochemical studies performed in naproxen detection

| Elect. | Meth. | Supp. electrol. | E _{ox} (V/SCE) | Sens. (µAµM ⁻¹) | LOD | Linear range | Ref. |
|-----------------|----------|---------------------------------------|-------------------------|-----------------------------|---------|--------------|------|
| GCE | BIA, PAD | 0.05M PBS, pH=7 | 0.95 | 0.036 | 0.3µM | 10-100 µM | 45 |
| DyNW /CPE | CV, SWV | 0.05M PBS, pH=7 | 0.88 | 0.387 | 0.5nM | 1-500nM | 39 |
| ZnO/M WCNT/ CPE | CV, SWV | 0.1M PBS, pH=7 | 0.90 | 0.356 | 0.23 µM | 1-200 µM | 46 |
| BDD | CV, DPV | 0.1MLiClO ₄ + acetonitrile | 1.41 | 0.4049 | 30nM | 0.5-50mM | 47 |
| Pt | LSV, DPV | 0.1MLiClO ₄ + acetonitrile | 1.44 | 0.114 | 1µM | 1-25 µM | 40 |

In our study, two types of carbon-based materials were tested for naproxen detection, the CNF-based composite electrode and the BDD electrode. It should be mentioned that the supporting electrolyte is different compared to the supporting electrolyte reported in the literature, taking into account the final application in water source.

In this study, BDD and CNF-composite electrodes were tested for naproxen detection. The results are presented in Figure 8.23, and Figure 8.24. With the BDD electrode, a similar oxidation potential as the one found by Suryanarayanan and co-workers [47] was obtained (1.425 V/SCE vs. 1.44 V/Ag/AgCl). In this case, the oxidation process started at about +0.95 V/SCE, and at +1.425 V/SCE a well-defined oxidation peak was measured. The lack of a cathodic peak suggests an irreversible process. Based on these observations and taking into account the previous results of Suryanarayanan [47] it can be concluded, that even in aqueous media the oxidation process is controlled by diffusion. A good linearity of the anodic currents vs. NPX concentration was obtained with a sensitivity of $5.364 \mu\text{A}\mu\text{M}^{-1}$.

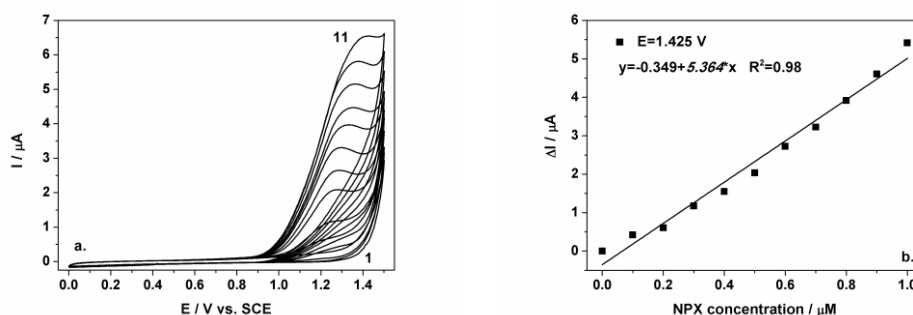


Figure 8.23. a. Cyclic voltammograms recorded on BDD electrode in 0.1 M Na_2SO_4 supporting electrolyte (curve 1) in the presence of 50 μL 0.1M NaOH (curve 2) and 0.1-1 μM NPX (curves 3-12), at a potential scan rate of 0.05 Vs^{-1} in a potential range from 0 to +1.5 V/SCE; **b.** Calibration plot of the currents recorded at $E = +1.425 \text{ V/SCE}$ vs. NPX concentration.

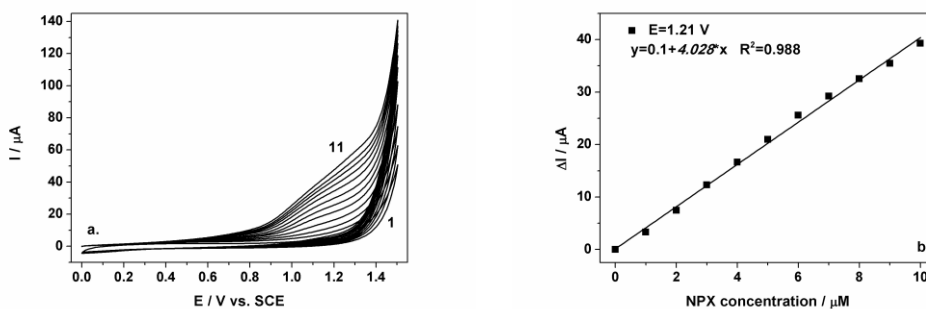


Figure 8.24. a. Cyclic voltammograms recorded on CNF electrode in 0.1 M Na_2SO_4 supporting electrolyte (curve 1) in the presence of 50 μL 0.1M NaOH (curve 2) and 1-10 μM NPX (curves 3-12), at a potential scan rate of 0.05 Vs^{-1} in a potential range from 0 to +1.5 V/SCE; **b.** Calibration plot of the currents recorded at $E = +1.21 \text{ V/SCE}$ vs. NPX concentration.

For electroanalytical applications, the value of +1.425 V/SCE obtained for the oxidation potential is quite high. The tests performed with the CNF composite

electrode allowed a small decrease of the oxidation potential. In Figure 8.24 the results obtained by employing cyclic voltammetry are presented.

With the CNF electrode the oxidation process started at +0.4 V/SCE and the peak current slightly increased until +0.9 V/SCE after which a more pronounced width peak was noticed. Since the stock solution was prepared by using sodium hydroxide, the influence of the hydroxide was studied and no relevant peaks were recorded. As a precaution, before adding the analyte, a 50 μL volume of sodium hydroxide was added to the supporting electrolyte. Also, the lack of a cathodic peak was noticed, suggesting the irreversibility of the oxidation process. A good linearity anodic current vs. naproxen concentration was observed. For an oxidation potential of +1.21 V/SCE a sensitivity of $4.028 \mu\text{A}\mu\text{M}^{-1}$ was achieved.

For both electrodes good properties in relation with the naproxen oxidation peak were determined, Table 8.12 summaries the results obtained with these electrodes. The useful signal obtained with the BDD electrode is almost the same as the value for the CNF electrode (5.393 μA vs. 5.313 μA). The CNF composite electrode revealed a shifting of the oxidation potential to less positive values (+1.425 V/SCE for the BDD electrode vs. +1.14 V/SCE for the CNF electrode), and it had been selected for further studies.

Table 8.12. Useful signal of naproxen oxidation on tested electrodes

| Electrode | Analyte | E_{ox} (V/SCE) | I (μA) | I_0 (μA) | ΔI (μA) |
|-----------|-----------------|-------------------------|---------------------|-------------------------|------------------------------|
| BDD | 1 μM | 1.425 | 6.539 | 1.146 | 5.393 |
| CNF | 1 μM | 1.140 | 10.483 | 4.684 | 5.318 |

For an improvement in relation with the sensitivity and oxidation potential, differential pulse voltammetry was employed. Under the optimized conditions for fluoxetine detection with the BDD (modulation amplitude of 0.2V, step potential of 0.05V, and scan rate of 0.025Vs^{-1}), a good linearity and better sensitivity were obtained. In Figure 8.25 are presented the voltammograms obtained under these conditions for NPX detection with the BDD electrode.

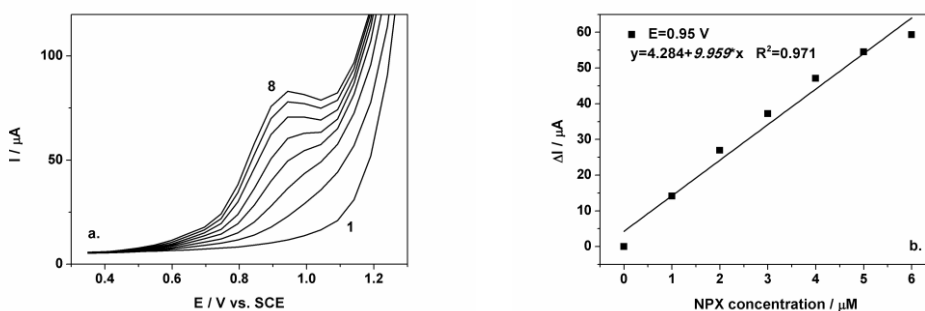


Figure 8.25. a. Differential-pulsed voltammograms recorded on CNF electrode under modulation amplitude of 0.2V, step potential of 0.05V and potential scan rate of 0.025Vs^{-1} in a potential range from +0.35 to +1.35 V/SCE in 0.1 M Na_2SO_4 supporting electrolyte (curve 1) in the presence of 50 μL 0.1M NaOH (curve 2) and 1-6 μM NPX (curves 3-8); b. Calibration plot of the currents recorded at $E = +0.95\text{V/SCE}$ vs. NPX concentration.

In this case, the oxidation process started at about +0.45 V/SCE and a well-defined peak was observed at +0.95 V/SCE. In comparison with cyclic voltammetry, the oxidation potential shifted to more negative values for DPV (+0.95 V/SCE vs.

+1.21 V/SCE) and an improved sensitivity was obtained ($9.959 \mu\text{A}\mu\text{M}^{-1}$ vs. $4.028 \mu\text{A}\mu\text{M}^{-1}$).

Square wave voltammetry was employed for obtaining comparable electroanalytical parameters as obtained with differential-pulsed voltammetry. By using a modulation amplitude of 0.05V, a step potential of 0.005V and a frequency of 10 Hz, a sensitivity of $4.366 \mu\text{A}\mu\text{M}^{-1}$ was obtained (Figure 8.26.b).

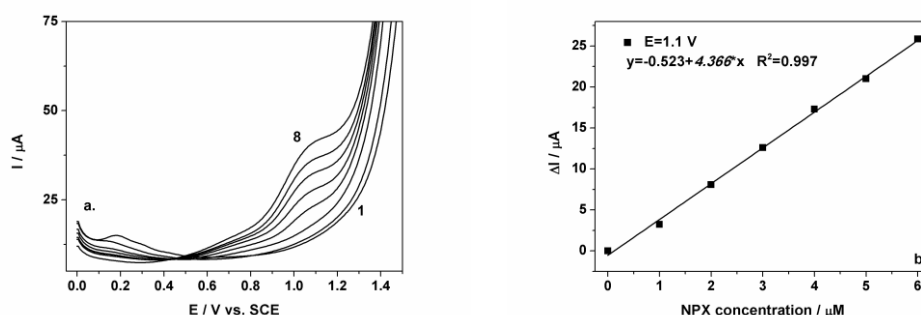


Figure 8.26. a. Square-wave voltammograms recorded on CNF electrode under modulation amplitude of 0.05V, step potential of 0.005V and a frequency of 10 Hz in a potential range from 0 to +1.45 V/SCE in 0.1 M Na_2SO_4 supporting electrolyte (curve 1) in the presence of 50 μL 0.1M NaOH (curve 2) and 1-6 μM NPX (curves 3-8); b. Calibration plot of the currents recorded at $E = +1.1\text{V/SCE}$. vs. NPX concentration.

In comparison with DPV under similar conditions, a slightly shifting to more positive values of oxidation potential was observed (+1.1 V/SCE vs. +0.95 V/SCE). Also a small decrease of sensitivity was noticed ($4.366 \mu\text{A}\mu\text{M}^{-1}$ vs. $9.959 \mu\text{A}\mu\text{M}^{-1}$). This decrease of sensitivity value is explained by the use of small values for operating parameters, e.g., modulation amplitude 0.05V for SWV vs. 0.2V for DPV. The sensitivity obtained for SWV is similar with the one obtained for CV.

8.2.3. Conclusions

In Table 8.13 all the electroanalytical parameters obtained for naproxen detection in aqueous media on CNF electrode are gathered.

Table 8.13. Electroanalytical parameters obtained on studied electrodes for naproxen detection

| Electrode | Tech. | E_{ox} (V/SCE) | Sens. ($\mu\text{A}\mu\text{M}^{-1}$) | R^2 | RSD (%) | LOD (μM) | LOQ (μM) |
|-----------|-------|----------------------------|--|-------|------------|--------------------------|--------------------------|
| BDD | CV | 1.425 | 5.364 | 0.980 | 4.42 | 0.027 | 0.090 |
| CNF | CV | 1.210 | 4.028 | 0.988 | 5.20 | 0.133 | 0.444 |
| | DPV | 0.950 | 9.959 | 0.971 | 4.24 | 0.146 | 0.450 |
| | SWV | 1.100 | 4.366 | 0.997 | 19.01 | 0.124 | 0.415 |

Based on those results, it can be concluded that:

- Both BDD and CNF electrodes exhibit the properties for naproxen detection in aqueous media, its oxidation process being controlled by diffusion.

- The best performance in relation with the sensitivity was obtained by employing DPV under optimized conditions, *e.g.*, modulation amplitude of 0.2V, step potential of 0.05V, and a scan rate of 0.025 Vs⁻¹.
- The best performances in relation with the limit of detection and the limit of quantification were obtained by employing cyclic voltammetry with BDD electrode.
- The CNF electrode exhibited better performance with regard to the detection potential due to a higher electrocatalytic activity towards NPX oxidation.

8.3. Electrochemical detection of tetracycline in water

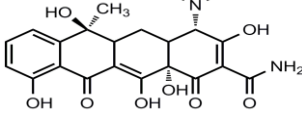
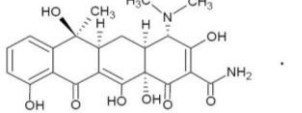
8.3.1. Introduction

Tetracycline (TC) is a widely used broad spectrum antibiotic with an antibacterial activity against almost all gram positive and gram negative bacteria. Discovered in the late 1940s as natural products of *Streptomyces* bacteria, tetracyclines are a large family of antibiotics [48,49].

The tetracyclines act by blocking the binding of aminoacyl tRNA to the A site on the ribosome. Tetracyclines inhibit protein synthesis on isolated 70S or 80S (eucaryotic) ribosomes and in both cases their effect is on the small ribosomal subunit.

It is an odourless, yellow crystalline powder, soluble in methanol, ethanol, and water at high pH values. In Table 8.13 some properties of tetracycline in comparison with tetracycline hydrochloride are gathered.

Table 8.14. Information on tetracycline and tetracycline hydrochloride

| | Tetracycline | Tetracycline hydrochloride |
|---------------------------|---|--|
| <i>Molecular formula</i> | $C_{22}H_{24}N_2O_8$  | $C_{22}H_{25}ClN_2O_8$  · HCl |
| <i>Molecular weight</i> | 444.43456 gmol ⁻¹ | 480.8955 gmol ⁻¹ |
| <i>pKa</i> | 3.3; 7.7; 9.7 | |
| <i>Log K_{oc}</i> | -1.37 | |
| <i>Melting point</i> | 172.5°C | 214°C |
| <i>Water solubility</i> | 231 mgL ⁻¹ (25°C) | 50mg mL ⁻¹ |

The rate of tetracycline removal by adsorption onto struvite was affected by the pH of the solution, contact time, and struvite concentration, the lowest rate of 8.4% being obtained for a pH=7.7. As no mechanism of decomposition other than photo-degradation is known for tetracycline, it remains in the sediment for a long period. In intensive fish farming, infections are treated by feeding antimicrobial agents directly into the water, the used substances entering into sediments directly from the water [50].

Reagents

Tetracycline was provided by Antibiotice, Iasi, Romania. A stock solution of 1 mM was prepared by using 0.1 M NaOH solution (Merck, Germany).

8.3.2. Electrochemical detection of tetracycline

Electrochemical studies on tetracycline detection were set up mainly for acidic media, and in general used glassy carbon electrodes modified with ionic liquid-carbon nanotubes paste, an iron/zinc cations-exchanged montmorillonite catalyst, or nickel-implanted boron doped diamond thin film electrode, and even gold microelectrode [51-57]. All these approaches were applied for tetracycline detection in food products, pharmaceutical formulations, and in water. The detection potentials of tetracycline are above +1.4 V/SCE and a less positive potential value is desired for electroanalysis applications. To accomplish this, a composite electrode based on carbon nanofiber was tested and the electrochemical behavior of tetracycline using this composite electrode is presented in Figure 8.27.

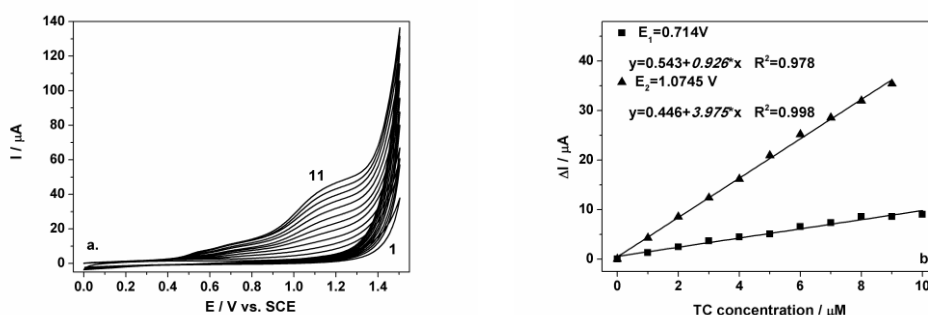


Figure 8.27. a. Cyclic voltammograms recorded on CNF electrode in 0.1 M Na₂SO₄ supporting electrolyte (curve 1) in the presence of 50 μ L 0.1M NaOH (curve 2) and 1-10 μ M TC (curves 3-12), at a potential scan rate of 0.05 Vs⁻¹ in a potential range from 0 to +1.5 V/SCE; b. Calibration plots of the currents recorded at E₁=+0.714 V/SCE and E₂=+1.0745 V/SCE vs. TC concentrations.

It is seen that the oxidation process started at about +0.4 V/SCE and that two oxidation steps were identified, the second starting at +0.95 V/SCE. Also, as reported by Gan [51] and Treepevijit [54], the lack of a cathodic peak is noticed, suggesting an irreversible oxidation process. A good linearity of anodic current vs. tetracycline concentration was obtained for both regions with correlation coefficients higher than 0.975 (the obtained sensitivities were 0.926 and 3.975 μ A μ M⁻¹), which suggests an oxidation process controlled by diffusion.

For improving the electroanalytical performances regarding tetracycline detection with the CNF electrode, pulsed techniques were employed. By applying the same optimized conditions as in the case of the BDD electrode used in fluoxetine detection, *e.g.*, modulation amplitude of 0.2V, step potential of 0.05V, and scan rate of 0.025 Vs⁻¹ a slightly increased sensitivity was obtained (0.926 vs. 1.376 μ A μ M⁻¹, respectively, 3.975 vs. 5.215 μ A μ M⁻¹). Also, in the case of detection potential a shift to more negative values is observed (+0.48 V/SCE vs. +0.714 V/SCE for peak 1, and +0.925V/SCE vs. +1.075V/SCE for peak 2). The results are presented in Figure 8.28.

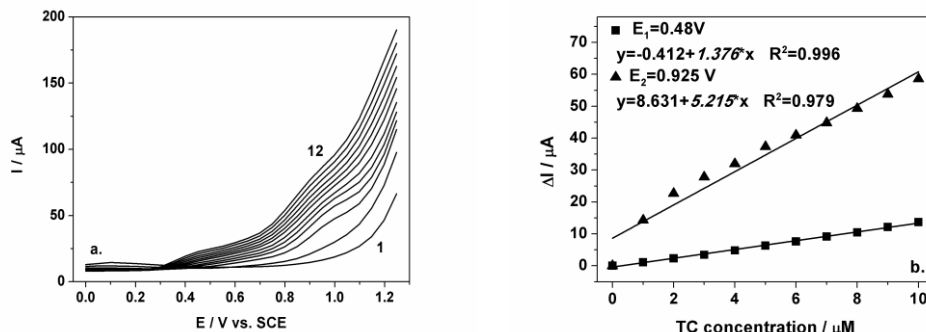


Figure 8.28. **a.** Differential-pulsed voltammograms recorded on CNF electrode under modulation amplitude of 0.2V, step potential of 0.05V and potential scan rate of 0.025 Vs^{-1} in a potential range from 0 to +1.25 V/SCE in 0.1 M Na_2SO_4 supporting electrolyte (curve 1) in the presence of 50 μL 0.1M NaOH (curve 2) and 1-10 μM TC (curves 3-12); **b.** Calibration plot of the currents recorded at $E_1 = +0.48 \text{ V/SCE}$ and $E_2 = +0.925 \text{ V/SCE}$ vs. TC concentrations.

For obtaining comparable electroanalytical parameters with differential-pulsed voltammetry, square-wave voltammetry was employed. The square wave voltammograms recorded with a modulation amplitude of 0.2V, a step potential of 0.05V, and a frequency of 100Hz are presented in Figure 8.29. As in the case of cyclic voltammetry, square wave voltammetry confirms that the oxidation process occurred in two steps. In comparison with previously DPV results, for the first peak a small increase for sensitivity is noticed: 1.376 vs. $1.753 \mu\text{A}\mu\text{M}^{-1}$ and for the oxidation potential: $+0.48 \text{ V/SCE}$ vs. $+0.645 \text{ V/SCE}$. As for the second peak, which is slightly shifting to more positive values ($+1.02 \text{ V/SCE}$ vs. $+0.925 \text{ V/SCE}$), the achieved sensitivity is lower than in the case of DPV (4.252 vs. $5.215 \mu\text{A}\mu\text{M}^{-1}$). More investigations using the pulsed-voltammetric techniques in relation with the optimization process are required.

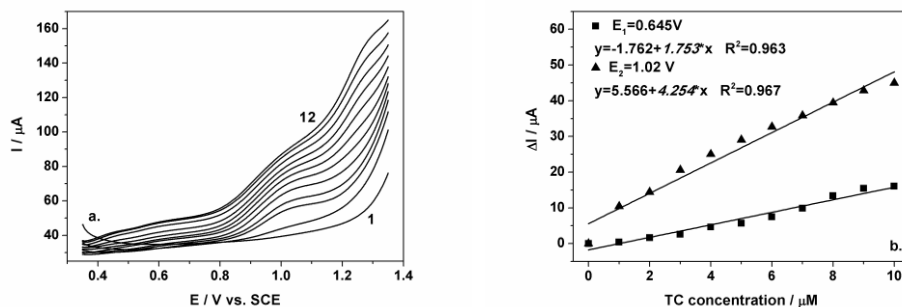


Figure 8.29. **a.** Square wave voltammograms recorded on CNF electrode under optimized conditions: modulation amplitude of 0.2V, step potential of 0.05V and a frequency of 100 Hz in a potential range from +0.35 to +1.35 V/SCE in 0.1 M Na_2SO_4 supporting electrolyte (curve 1) in the presence of 50 μL 0.1M NaOH (curve 2) and 1-10 μM TC (curves 3-12); **b.** Calibration plots of the currents recorded at $E_1 = +0.645 \text{ V/SCE}$ and $E_2 = +1.02 \text{ V/SCE}$ vs. TC concentrations.

Based on voltammetric results, chronoamperometry was employed for tetracycline detection. Since the oxidation process occurred in two steps, a two

levels chronoamperometry was applied for $E_1=+0.75$ V/SCE and $E_2=+1.2$ V/SCE, the results being presented in Figure 8.30. A good linearity peak current vs. TC concentration was obtained, but the values of sensitivities were smaller than the ones obtained by CV.

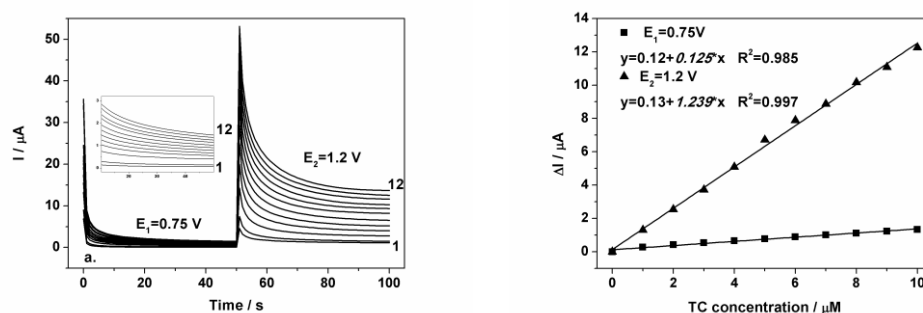


Figure 8.30. a. Chronoamperograms recorded on CNF electrode at the potential values of $E_1=+0.75$ V/SCE and $E_2=+1.2$ V/SCE in 0.1 M Na₂SO₄ supporting electrolyte (curve 1) in the presence of 50 μ L 0.1 M NaOH (curve 2) and 1-10 μ M TC (curves 3-12); Inset: Detail of chronoamperograms recorded at +0.75 V/SCE potential value; b. Calibration plots of the currents vs. TC concentrations.

8.3.3. Conclusions

In Table 8.14 the electroanalytical parameters obtained for tetracycline detection in aqueous media on CNF electrode are gathered.

Table 8.14. Electroanalytical parameters obtained on studied electrodes for tetracycline detection

| Tech. | E_{ox} (V/SCE) | Sens. ($\mu A/\mu M^{-1}$) | R^2 | RSD (%) | LOD (μM) | LOQ (μM) |
|-------|---------------------|---------------------------------|-------|------------|--------------------|--------------------|
| CV | 0.714 | 0.926 | 0.978 | 7.74 | 0.248 | 0.828 |
| | 1.0745 | 3.975 | 0.998 | 3.07 | 0.055 | 0.184 |
| DPV | 0.480 | 1.376 | 0.996 | nd* | nd | nd |
| | 0.925 | 5.215 | 0.976 | 3.88 | 0.165 | 0.551 |
| SWV | 0.645 | 1.753 | 0.963 | nd | nd | nd |
| | 1.020 | 4.254 | 0.967 | 8.50 | 0.441 | 1.470 |
| CA | 0.750 | 0.125 | 0.985 | 9.50 | 0.527 | 1.759 |
| | 1.200 | 1.239 | 0.997 | 9.75 | 0.088 | 0.293 |

*nd - not determined

Based on these results, it can be concluded that:

- The CNF electrode exhibited the properties for tetracycline detection in aqueous media, the oxidation process being controlled by diffusion.
- The best performance in relation with the sensitivity was obtained by employing DPV under optimized conditions, *e.g.*, modulation amplitude of 0.2V, step potential of 0.05V, and a scan rate of 0.025V.
- The best performances in relation with the lowest limit of detection and limit of quantification were obtained by employing cyclic voltammetry with the CNF electrode.

8.4. Simultaneous electrochemical detection of pharmaceuticals in water

As discussed previously, the pharmaceutical effects on the environment are wide and very dangerous for fauna and biota. This is the reason for which detection methods that would detect simultaneously pharmaceutical compounds without any interference are desired.

Electrochemical methods are powerful and versatile tools that offer high sensitivity, accuracy, precision, and a linear dynamic range with low cost of instrumentation [58, 59]. Therefore, based on the results obtained for the individual detection of fluoxetine, naproxen and tetracycline with the carbon nanofiber composite electrode, an approach regarding simultaneous detection of these three pharmaceutical compounds is proposed.

8.4.1. Simultaneous electrochemical detection of naproxen and fluoxetine

The simultaneous detection of naproxen and fluoxetine was studied under similar conditions as the individual detection having as reference points the detection characteristics of each pharmaceutical compound. The cyclic voltammograms recorded with the CNF electrode in the potential range from 0 to +1.5 V/SCE are presented in Figure 8.31.

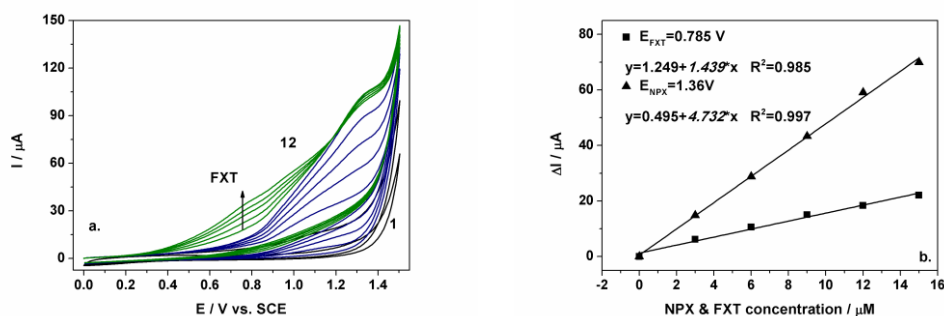


Figure 8.31. a. Cyclic voltammograms recorded on CNF electrode in 0.1 M Na_2SO_4 supporting electrolyte (curve 1) in the presence of 50 μL 0.1M NaOH (curve 2) and 3-15 μM NPX (curves 3-7), and 3-15 μM FXT (curves 8-12) at a potential scan rate of 0.05 Vs^{-1} in a potential range from 0 to +1.5 V/SCE; b. Calibration plots of the currents recorded at $E_{\text{NPX}} = +1.36 \text{ V/SCE}$ and $E_{\text{FXT}} = +0.785 \text{ V/SCE}$ vs. NPX and FXT concentrations.

Based on the results achieved for each individual fluoxetine and naproxen, the question arises as to whether fluoxetine could be detected in the presence of naproxen with the CNF electrode, because the sensitivity for naproxen was better than that for fluoxetine.

The working procedure for detection consisted of two steps, e.g., first the naproxen was added to the solution until a concentration of 15 μM NPX, and subsequently FXT was added until a concentration of 15 μM FXT was obtained. As can be noticed from Figure 8.31 well-defined and good separated peaks were obtained for both analytes. The results related to the sensitivities are gathered in Table 8.16.

Table 8.16 Electroanalytical parameters obtained for individual and simultaneous detection of fluoxetine and naproxen on CNF electrode

| Type | Analyte | E_{ox} (V/SCE) | Sens. ($\mu A\mu M^{-1}$) | Conc. range (μM) |
|--------|---------|------------------|-----------------------------|-------------------------|
| Indiv. | FXT | 0.980 | 3.686 | 0→10 |
| | NPX | 1.210 | 4.028 | 0→10 |
| Sim. | FXT | 0.785 | 1.439 | 0→15 |
| | NPX | 1.360 | 4.732 | 0→15 |

The differences between the values of fluoxetine sensitivities could be explained by a possible fouling effect due to its previous applications for naproxen detection without any cleaning step between the measurements.

Differential-pulsed voltammetry was also employed under the condition of 0.2 V modulation amplitude, 0.1 V step potential, and 0.05 Vs^{-1} scan rate. The results obtained under these conditions are presented in Figure 8.32.

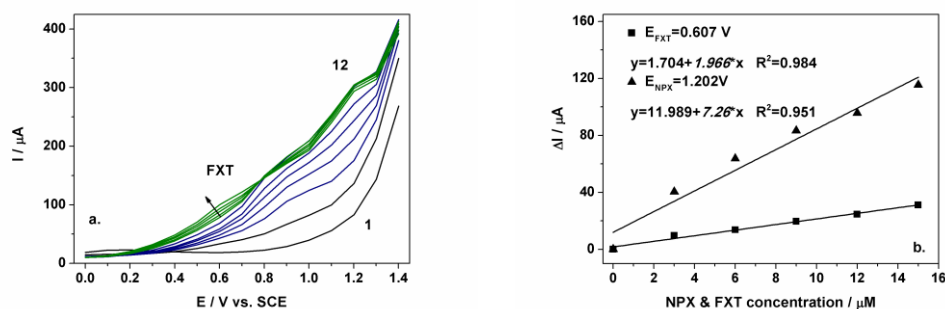


Figure 8.32. a. Differential pulsed voltammograms recorded on CNF electrode under conditions: of 0.2V modulation amplitude, 0.1V step potential and 0.05 Vs^{-1} potential scan rate for a potential range from 0 to +1.4 V/SCE in 0.1 M Na_2SO_4 supporting electrolyte (curve 1) in the presence of 50 μL 0.1M NaOH (curve 2) and 3 -15 μM TC (curves 3-7), and 3 -15 μM FXT (curves 8-12); b. Calibration plot of the currents $E_{NPX}=+1.202V/SCE$ and $E_{FXT}=+0.607V/SCE$ vs. NPX and FXT concentrations.

As expected, besides the improved sensitivities (1.966 vs. 1.439 $\mu A\mu M^{-1}$ for fluoxetine and 7.26 vs. 4.732 $\mu A\mu M^{-1}$ for naproxen) the oxidation potential is shifted to less positive values (+0.604 V/SCE vs. +0.785 V/SCE for fluoxetine and +1.202 V/SCE vs. 1.36 V/SCE for naproxen). This aspect could be exploited to electroanalysis applications and the problems related to analytes interferences are minimized.

In comparison with the simultaneous detection using cyclic voltammetry, an increase in both sensitivity and oxidation potential was observed. The results are presented in Table 8.17.

Table 8.17. Electroanalytical parameters obtained for simultaneous detection of fluoxetine and naproxen on CNF electrode

| Tech. | Analyte | E_{ox} (V/SCE) | Sens. ($\mu A\mu M^{-1}$) | Conc. range (μM) |
|-------|---------|------------------|-----------------------------|-------------------------|
| CV | FXT | 0.785 | 1.439 | 0→15 |
| | NPX | 1.360 | 4.732 | 0→15 |
| DPV | FXT | 0.604 | 1.966 | 0→15 |
| | NPX | 1.202 | 7.26 | 0→15 |

Based on these results it can be concluded that:

- Both analytes, naproxen and fluoxetine, were detected with the CNF composite electrode, well defined and separated peaks being obtained for each analyte.
- The performances in relation with sensitivity and oxidation potential for both analytes were obtained under DPV operating conditions, *e.g.*, 0.2V modulation amplitude, 0.1V step potential, and 0.05Vs⁻¹ scan rate.

8.4.2. Simultaneous electrochemical detection of tetracycline and fluoxetine

In this case the situation is different, because the oxidation of tetracycline on the CNF electrode occurs in two steps, the first one at a potential value at which fluoxetine is oxidized, and a cumulative effect between fluoxetine and tetracycline at the potential value of about +0.8 V/SCE is expected. Following the previously described working protocol, the detection of tetracycline and fluoxetine was studied in the potential range from 0 to +1.35 V/SCE and the results are presented in Figure 8.33.

In Table 8.18 are gathered all the electroanalytical parameters obtained in fluoxetine, respectively, tetracycline individually and simultaneous detection with the CNF electrode by employing cyclic voltammetry.

Table 8.18. Electroanalytical parameters obtained for individual and simultaneous detection of fluoxetine and tetracycline on CNF electrode

| Type | Analyte | E _{ox} (V/SCE) | Sens. (μAμM ⁻¹) | Conc. range (μM) |
|--------|---------|-------------------------|-----------------------------|------------------|
| Indiv. | FXT | 0.980 | 3.686 | 0→10 |
| | TC | 0.714 | 0.926 | 0→10 |
| | | 1.0745 | 3.975 | |
| Sim. | FXT | 0.815 | 0.323 | 0→10 |
| | TC | 0.815 | 0.960 | 0→2.5 |
| | | 1.140 | 3.695 | |

In the case of fluoxetine, a smaller value for the sensitivity was obtained. As it was mentioned, a possible cause could be the fouling of the electrode. Still, the peak potential shifted to less negative values. In the case of tetracycline, no significant difference was noticed, as it was expected.

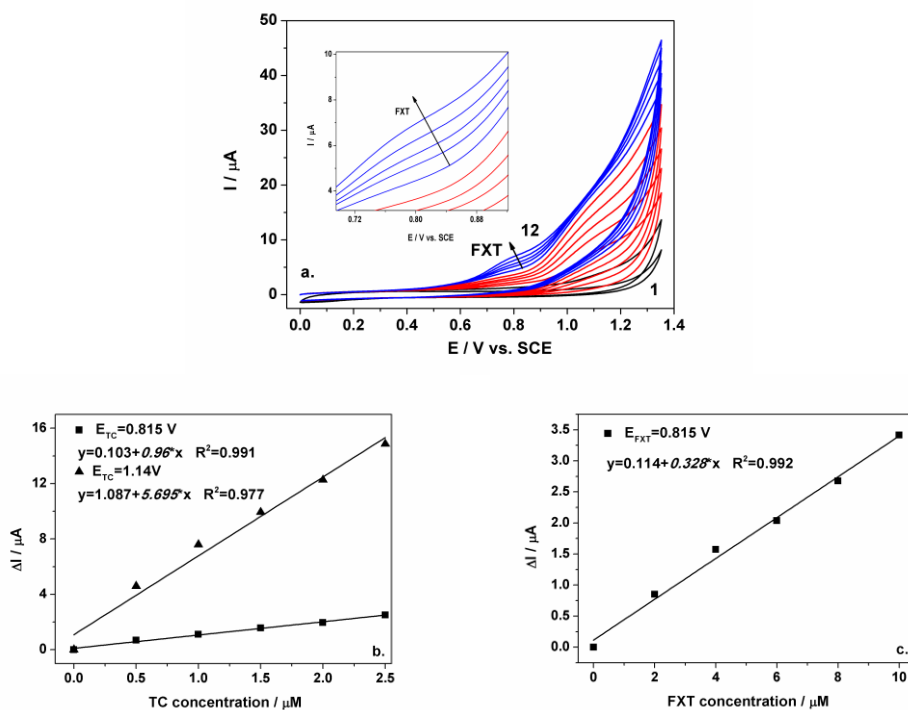


Figure 8.33. a. Cyclic voltammograms recorded on CNF electrode in 0.1 M Na_2SO_4 supporting electrolyte (curve 1) in the presence of 50 μL 0.1M NaOH (curve 2) and 0.5-2.5 μM TC (curves 3-7), and 2-10 μM FXT (curves 8-14) at a potential scan rate of 0.05 Vs^{-1} in a potential range from 0 to +1.35 V/SCE; b. Calibration plots of the currents recorded at $E_1 = +0.815 \text{ V/SCE}$ and $E_2 = +1.14 \text{ V/SCE}$ vs. TC concentrations; c. Calibration plot of the currents recorded at $E = +0.815 \text{ V/SCE}$ vs. FXT concentrations.

Pulsed techniques, *e.g.*, differential-pulsed voltammetry and square-wave voltammetry were applied for the simultaneous detection of fluoxetine and tetracycline for improving the electroanalytical parameters.

The operating parameters used were modulation amplitude 0.2V, step potential 0.05V, and scan rate 0.025 Vs^{-1} for DPV and the corresponding voltammograms are presented in Figure 8.34.

As for SWV, also a modulation amplitude of 0.2V and step potential of 0.05V was used along with a frequency of 100 Hz. The square wave voltammograms obtained are presented in Figure 8.35.

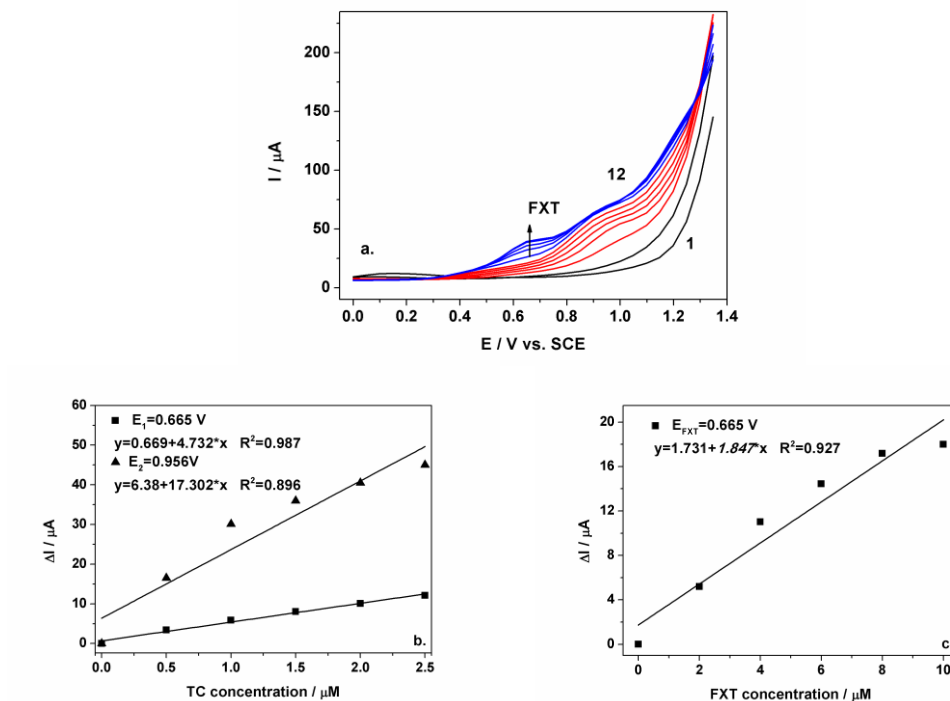
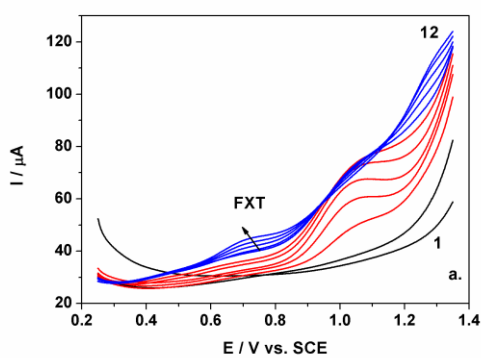


Figure 8.34. a. Differential-pulsed voltammograms recorded on CNF electrode under optimized conditions: modulation amplitude of 0.2V, step potential of 0.05V and potential scan rate of 0.025 Vs^{-1} in a potential range from 0 to +1.35 V/SCE in 0.1 M Na_2SO_4 supporting electrolyte (curve 1 in the presence of $50 \mu\text{L}$ 0.1 NaOH (curve 2) and 0.5 - $2.5 \mu\text{M}$ TC (curves 3-7), and 2 - $10 \mu\text{M}$ FXT (curves 8-12); b. Calibration plots of the currents at $E_1 = +0.665 \text{ V/SCE}$ and $E_2 = +0.956 \text{ V/SCE}$ vs. TC concentrations; c. Calibration plot of the currents vs. FXT concentration recorded at $E_{\text{FXT}} = +0.665 \text{ V/SCE}$.



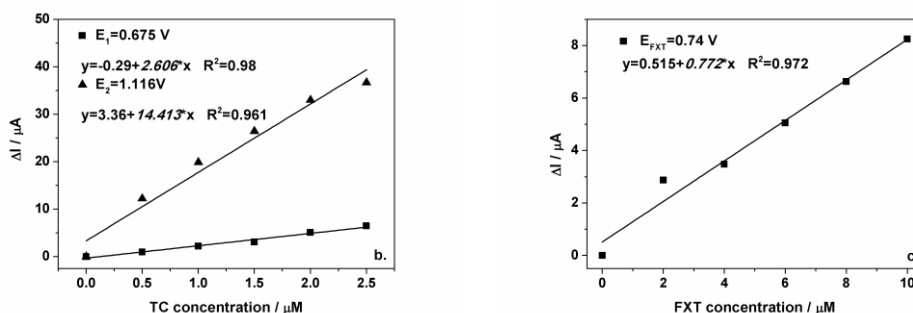


Figure 8.35. a. Square-wave voltammograms recorded on CNF electrode under optimized conditions: modulation amplitude of 0.2V, step potential of 0.05V and a frequency of 100 Hz in a potential range from 0 to +1.35V/SCE in 0.1 M Na_2SO_4 supporting electrolyte (curve 1) in the presence of 50 μL 0.1M NaOH (curve 2) and 0.5-2.5 μM TC (curves 3-7), and 2-10 μM FXT (curves 8-12); b. Calibration plots of the currents recorded at $E_1 = +0.675\text{V/SCE}$ and $E_2 = +1.116 \text{ V/SCE}$ vs. TC concentrations; c. Calibration plot of the currents recorded at $E = +0.74\text{V/SCE}$ vs. FXT concentrations.

The results obtained on CNF composite electrode for simultaneous detection of fluoxetine and tetracycline, are gathered in Table 8.19. The best performances in relation with the sensitivity and peak potential for simultaneous detection of those compounds were obtained under differential pulsed voltammetry operating conditions, e.g., 0.2V modulation amplitude, 0.05 V step potential, and 0.025Vs^{-1} scan rate.

Table 8.19. Electroanalytical parameters obtained for simultaneous detection of fluoxetine and tetracycline on CNF electrode

| Tech. | Analyte | E_{ox} (V/SCE) | Sens. ($\mu\text{A}\mu\text{M}^{-1}$) | Conc. range (μM) |
|-------|---------|-------------------------|---|-------------------------------|
| CV | FXT | 0.815 | 0.323 | 0→10 |
| | TC | 0.815 | 0.960 | 0→2.5 |
| 1.140 | | 3.695 | | |
| DPV | FXT | 0.665 | 1.847 | 0→10 |
| | TC | 0.665 | 4.732 | 0→2.5 |
| 0.956 | | 17.302 | | |
| SWV | FXT | 0.740 | 0.772 | 0→10 |
| | TC | 0.675 | 2.606 | 0→2.5 |
| 1.116 | | 14.413 | | |

8.4.3. Conclusions

Based on the previously results, it may be concluded that fluoxetine was detected in the presence of either naproxen or tetracycline because the signal for fluoxetine detection is the lowest.

The best performances were obtained under DPV conditions for both detection schemes naproxen-fluoxetine and tetracycline-fluoxetine by employing the same modulation amplitude of 0.2 V and specific values for step potential and scan rate for each pharmaceutical combination, e.g., 0.1V step potential and 0.05Vs^{-1} scan rate for naproxen-fluoxetine combination and 0.05 V step potential and 0.025Vs^{-1} scan rate for tetracycline-fluoxetine combination.

Also, CNF composite electrode is very promising for the detection of the pharmaceuticals in water. Further studies will be conducted to detect selectively a certain pharmaceutical avoiding any interference.

8.5. Bibliography

- [1] PubChem website
<https://pubchem.ncbi.nlm.nih.gov/compound/fluoxetine#section=Top>
- [2] DrugBank website, <http://www.drugbank.ca/drugs/DB00472>
- [3] H.P.A. Nouws, C. Delerue-Matos, A.A. Barros, J.A. Rodrigues, A. Santos-Silva, F. Borges, Square-wave adsorptive-stripping voltammetric detection in the quality control of fluoxetine, *Anal. Lett.*, (2007) 42, 1131-1146.
- [4] US Food and Drug Administration website, <http://www.fda.gov/>
- [5] D. Kolpin, E. Furlong, M. Meyer, E. M. Thurman, S.D. Zaugg, L.B. Barber, H.T. Buxton, Pharmaceuticals, hormones, and other organic wastewater contaminants in U.S. streams, 1999-2000: a national reconnaissance, *J. Environ. Sci. Technol.*, (2002) 36, 1202-1211.
- [6] S. Zorita, L. Martensson, L. Mathiasson, Occurrence and removal of pharmaceuticals in a municipal sewage treatment system in the south of Sweden, *Sci. Total Environ.*, (2009) 407, 2760-2770.
- [7] S. Gonzalez Alonso, M. Catala, R. Romo Maroto, J.L. Rodriguez Gil, A. Gil de Miguel, Y. Valcarcel, Pollution by psychoactive pharmaceuticals in the Rivers of Madrid metropolitan area (Spain), *Envir. Intern.*, (2010) 36, 195-201.
- [8] L.H. Santos, A.N. Araujo, A. Fachini, A. Pena, C. Deleure-Matos, M.C.B.S.M. Montenegro, Ecotoxicological aspects related to the presence of pharmaceuticals in the aquatic environment, *J. Hazard. Materials.*, (2010) 175, 45-95.
- [9] A. Batt, M. S. Kostich, M. J. Lazorchak, Analysis of ecologically relevant pharmaceuticals in wastewater and surface water using selective solid-phase extraction and UPLC-MS/MS, *Anal. Chem.*, (2008) 80 (13), 5021-5030.
- [10] S. Esteban, Y. Valcarcel, M. Catala, M. Gonzalez Castromil, Psychoactive pharmaceuticals residues in the watersheds of Galicia (Spain), *Gac. Sanit.*, (2012) 26 (5), 457-459.
- [11] C.D. Metcalfe, S. Chu, C. Judt, H. Li, K.D. Oakes, M.R. Servos, D.M. Andrews, Antidepressants and their metabolites in municipal wastewater, and downstream exposure in an urban watershed, *Environ. Toxicol. Chem.*, (2010) 29 (1), 79-89.
- [12] D. Baker, B. Kasprzyk-Hordern, Multi-residue analysis of drugs of abuse in wastewater and surface water by solid-phase extraction and liquid chromatography-positive electrospray ionisation tandem mass spectrometry, *J. Chromatogr. A.*, (2011) 1218, 1620-1631.
- [13] C.D. Metcalfe, X.S. Miao, B.G. Koenig, J. Struger, Distribution of acidic and neutral drugs in surface waters near sewage treatment plants in the lower Great Lakes, Canada, *Environ. Toxicol. Chem.*, (2003) 22 (12), 2881-2889.
- [14] J.W. Kwon, K.L. Armruster, Laboratory persistence and fate of fluoxetine in aquatic environments, *Environ. Toxicol. Chem.*, (2006) 25 (10), 2561-2568.
- [15] K. Fent, A.A. Weston, D. Caminada, Ecotoxicology of human pharmaceuticals, *Aquat. Toxicol.*, (2006) 76, 122-129.

- [16] B.W. Brooks, C.M. Foran, S.M. Richards, J. Weston, P.K. Turner, J.K., Stanley, K.R. Solomon, M. Slattery, T.W. La Point, Aquatic ecotoxicology of fluoxetine, *Toxicol. Letters.*, (2003) 142, 169-183.
- [17] Y. Nakamura, H. Yamamoto, J. Sekizawa, T. Kondo, N. Hirai, N. Tatarazako, The effects of pH on fluoxetine in Japanese medaka (*Oryzias latipes*): acute toxicity in fish larvae and bioaccumulation in juvenile fish, *Chemosphere*, (2008) 70, 865-873.
- [18] A.R.R. Pery, M. Gust, B. Vollant, M. Ramil, G. Fink, T. Ternes, J. Garric, Fluoxetine effects assesment on the life cycle of aquatic invertebrates, *Chemosphere*, (2008) 73, 300-304.
- [19] K. Kummerer, *Pharmaceuticals in the environment. Source, fate, effects, risks*, Springer, Berlin, 2008.
- [20] M.R. Ganjali, F. Faridbod, H. Rashedi, M. Hosseini, M. Hosseini, P. Norouzi, Fluoxetine determination by PVC membrane and nano-composite carbon paste electrodes, *Int. J. Electrochem. Sci.*, (2011) 6, 2299-2311.
- [21] E.M. Hussein, F.M. Abdel-Gawad, Y.M. Issa, Ion-selective electrodes for determination of fluoxetine in capsules and in biological fluids, *Biochem. Eng. J.*(2011) 53, 210-215.
- [22] E.S. Papas, C.N. Chaldezios, J. Atta-Politou, M.A. Koupparis, Construction of a fluoxetine ion chemical sensor and its application for the determination of pKa value of fluoxetine conjugated acid, complexation study with β -cyclodextrin and formulations assay, *Anal. Lett.*, (2010) 43, 2171-2183.
- [23] E.M. Garrido, J. Garrido, R. Calheiros, M.P.M. Marques, F. Borges, Fluoxetine and norfluoxetine revisited: new insights into the electrochemical and spectroscopic properties, *J. Phys. Chem. A.*, (2009) 113(36), 9934-9944.
- [24] R.P. Lencastre, C. Delerue-Matos, J. Garrido, F. Borges, E.M. Garrido, Voltammetric quantification of fluoxetine: application to quality control and quality assurance processes, *J. Food and Drug Anal.*, (2006) 14 (3), 242-246.
- [25] A. Mohammadi, A.B. Moghaddam, E. Alikhani, K. Eilkhani, S. Mozaffari, Electrochemical quantification of fluoxetine in pharmaceutical formulation using carbon nanoparticles, *Micro & Nano Letters, IET*, (2013) 8(12), 853 - 857.
- [26] A. Remes, A. Pop, F. Manea, A. Baci, S.J. Picken, J. Schoonman, Electrochemical determination of pentachlorophenol in water on a multi-wall carbon nanotubes-epoxy composite electrode, *Sensors*, (2012) 12(6), 7033-7046.
- [27] A. Bebeselea, F. Manea, G. Burtica, L. Nagy, G. Nagy, The electrochemical determination of phenolic derivates using multiple pulsed amperometry with graphite based electrodes, *Talanta*, (2010) 80, 1068-1072.
- [28] B. Habibi, M. Jahanbakhshi, Silver nanoparticles/multi walled carbon nanotubes nanocomposite modified electrodes: voltammetric determination of clonazepam, *Electrochim. Acta*, (2014) 118, 10-17.
- [29] F. Manea, S. Motoc, A. Pop, A. Remes, J. Schoonman, Silver-functionalized carbon nanofiber composite electrodes for ibuprofen detection, *Nanoscale Res. Lett.*, (2012) 7, 331-335.
- [30] Y. Liu, D. Wang, Y. Xu, H. Hou, T. You, A novel and simple route to prepare Pt nanoparticle-loaded carbon nanofiber electrode for hydrogen peroxide sensing, *Biosens. Bioelectron.*, (2011) 26(11) 4585-4890.
- [31] F. Manea, M. Ihos, A. Remes, G. Burtica, J. Schoonman, Electrochemical determination of diclofenac sodium in aqueous solution on Cu-doped zeolite-expanded graphite-epoxy electrode, *Electroanal.*, (2010) 22(17-18), 2058-2063.

- [32] C. Ratiu, C. Lazau, C. Orha, I. Grozescu, A. Pop, D. Sonea, F. Manea, G. Burtica, J. Schoonman, Using zeolite-modified electrode for the electrochemical determination of 4-aminophenol from water, *Environ. Eng. Manag. J.*, (2009) 8(4), 825-830.
- [33] A. Pop, F. Manea, C. Radovan, P. Malchev, A. Bebeselea, C. Proca, G. Burtica, S. Picken, J. Schoonman, Amperometric detection of 4-chlorophenol on two types of expanded graphite based composite electrodes, *Electroanal.*, (2008) 20(22), 2460-2466.
- [34] A. Walcarius, S. Rozanska, J. Bessière, J. Wang Screen-printed zeolite-modified carbon electrodes, *Analyst*, (1999) 124, 1185-1190.
- [35] A. Walcarius, Zeolite-modified electrodes in electroanalytical chemistry, *Anal. Chim. Acta*, (1999) 384, 1-16.
- [36] A. P. Brown, F.C. Anson, Cyclic and differential pulse voltammetric behavior of reactants confined to the electrode surface, *Anal. Chem.*, (1977) 49(11), 1589-1595.
- [37] PubChem website, <https://pubchem.ncbi.nlm.nih.gov/compound/156391>
- [38] DrugBank website, <http://www.drugbank.ca/drugs/DB00788>
- [39] P. Norouzi, F. Dousty, M.R. Ganjali, R. Daneshgar, Dysprosium nanowire modified carbon paste electrode for the simultaneous detection of naproxen and paracetamol: applications in pharmaceuticals formulations and biological fluids, *Int. J. Electrochem. Sci.*, (2009) 4, 1371-1386.
- [40] N. Adhoum, L. Monser, M. Toumi, K. Boujlél, Determination of naproxen in pharmaceuticals by differential pulse voltammetry at a platinum electrode, *Anal. Chim. Acta*, (2003) 495, 69-75.
- [41] J.J. Li, M.B. Norton, E.J. Reinhard, G.D. Anderson, S.A. Gregory, P.C. Isakson, C.M. Koboldt, J.L. Masferrer, W.E. Perkins, K. Seibert, Y. Zhang, B.S. Zweifel, D.B. Reitz, Novel terphenyls as selective cyclooxygenase-2 inhibitors and orally active anti-inflammatory agents, *J. Med. Chem.*, (1996) 39(9) 1846-1856.
- [42] Roche, Naproxen sodium, safety data sheet, <http://www.roche.com>
- [43] M. Isidori, M. Lavorgna, A. Nardelli, A. Parrella, L. Previtiera, M. Rubino, Ecotoxicity of naproxen and its phototransformation products, *Sci. Total Environ.*, (2005) 348, 93-101.
- [44] O.A.H. Jones, N. Voulvoulis, J.N. Lester, The occurrence and removal of selected pharmaceutical compounds in a sewage treatment works utilizing activated sludge treatment, *Environ. Pollut.*, (2007) 145, 738-744.
- [45] J.S. Stefano, A.P de Lima, R.H.O. Montes, E.M. Richter, R.A.A. Muñoz, Fast determination of naproxen in pharmaceutical formulations by batch injection analysis with pulsed amperometric detection, *J. Braz. Chem. Soc.*, (2012) 23(10), 1834-1838.
- [46] J. Tashkhourian, B. Hemmateenejad, H. Beigizadeh, M. Hoseini-Sarvari, Z. Razmi, ZnO nanoparticles and multiwalled carbon nanotubes modified carbon paste electrode for determination of naproxen using electrochemical techniques, *J. Electroanal. Chem.*, (2014) 714-715, 103-108.
- [47] V. Suryanarayanan, Y. Zhang, S. Yolshihara, T. Shirakashi, Voltammetric assay of naproxen in pharmaceutical formulations using boron doped diamond electrode, *Electroanal.*, (2005) 17(11), 925-932.
- [48] PubChem website, <https://pubchem.ncbi.nlm.nih.gov/compound/54675776>
- [49] DrugBank, <http://www.drugbank.ca/drugs/DB00759>
- [50] K. Kummerrer, Antibiotics in the aquatic environment-A review -Part I, *Chemosphere*, (2009) 75, 417-434.

- [51] T. Gan, Z. Shi, J. Sun, Y. Liu, Simple and novel electrochemical sensor for the determination of tetracycline based on iron/zinc cations-exchanged montmorillonite catalyst, *Talanta*, (2014) 121, 187-193.
- [52] G. Guo, F. Zhao, F. Xiao, B. Zeng, Voltammetric determination of tetracycline by using multi-wall carbon nanotube-ionic liquid film coated glassy carbon electrode, *Int. J. Electrochem. Sci.*, (2009) 4, 1365-1372.
- [53] Y. J. Kim, Y.S. Kim, J.H. Niazi, M.B. Gu, Electrochemical aptasensor for tetracycline detection, *Bioprocess. Biosyst. Eng.*, (2010) 33, 31-37.
- [54] S. Treetepvijit, S. Chuanuwatanakul, Y. Einaga, R. Satc, O. Chailapakul, Electroanalysis of tetracycline using nickel-implanted boron-doped diamond electrodes thin film electrode applied in flow injection system, *Analyt. Sci.*, (2005) 21, 531-535.
- [55] D. Vega, L. Agui, A. Gonzales-Cortes, P. Yanez-Sedeno, J.M. Pingrarron, Voltammetry and amperometric detection of tetracyclines at multi-walled carbon nanotube modified electrodes, *Anal. Bioanal. Chem.*, (2007) 389, 951-958.
- [56] H. Wang, H. Zhao, X. Quan, Gold modified microelectrode for tetracycline direct detection, *Front. Environ. Sci. Eng.*, (2012) 6(3), 313-319.
- [57] L. Zhou, D.J. Li, L. Gai, J.P. Wang, Y.B. Li, Electrochemical aptasensor for detection of tetracycline with multiwalled carbon nanotubes amplification, *Sensor Actuat. B*, (2012) 162, 201-208.
- [58] S.A. Ozkan, B. Uslu, H.Y. Abdoul-Enein, Analysis of pharmaceuticals and biological fluids using modern electroanalytical techniques, *Anal. Chem.*, (2000) 33(3), 155-181.
- [59] A. Doménech-Carbó, L. M. de Carvalho, M. Martini, G. Cebrián-Torrejón, Voltammetric /amperometric screening of compounds of pharmacological interest, *Anal. Chem.*, (2014) 33(3), 173-199.

9. ELECTROCHEMICAL DETECTION OF ANIONS IN WATER

9.1. Electrochemical detection of sulfide anion in water

9.1.1. Introduction

Free sulfide (H_2S , HS^- , S^{2-}) is an important component of the aquatic environment. Widely found in natural water samples and wastewater, it serves as a very important pollution index for water, especially due to its potential to poison many aquatic organisms, even at micromolar concentrations [1-3].

Sulfide can be released into aquatic environments through the anaerobic degradation of sulfur-containing proteins, amino acids, or other types of organic components. Sulfide salts are frequently used in industrial waste streams to minimize the transport of several toxic metals, *e.g.*, mercury and lead into the environment through precipitation reactions [4]. The total level of sulfide in waste discharges has been limited because of its toxicity, oxygen depletion, and production of H_2S . Clinical cases of sulfide poisoning typically present at levels from 30 to 3000 $\mu\text{g L}^{-1}$ and its lethal doses upon exposure to H_2S can vary in the range 300–1000 $\mu\text{g L}^{-1}$ [5].

In aqueous media sulfide can be found as a function of pH in different forms, *e.g.*, dissolved H_2S , bisulfide ion (HS^- , $\text{pK}_{\text{a}1}=6.88$), and sulfide ion (S^{2-} , $\text{pK}_{\text{a}2}=14.15$). Sulfur cycling and speciation have been studied in various seawaters, *e.g.*, Black Sea [6, 7] and Adriatic Sea [8]. The sulfide maximum concentration of 423 μM was determined and three distinct zones of water were found in the central basin of the Black Sea, *e.g.*, the oxic (0-65 m), the anoxic/nonsulfidic (65-100 m) and the sulfidic zone (>100m) [6].

For the electrochemical detection of free sulfide three main electrochemical methods are reported, *e.g.*, the potentiometry using a $\text{Ag}/\text{Ag}_2\text{S}$ ion-selective electrode [9], the voltammetry [10, 11], and the amperometry [12]. For sulfide determination below 1 μM , a preconcentration step (stripping technique) is required. As example, anodic stripping voltammetry (ASV) associated with a mercury film electrode has been reported [13], but the toxicity of mercury limits its application. A stripping chronopotentiometry procedure has been developed using a vibrating gold micro-wire electrode for sulfide determination in hydrothermal seawater samples as reported by Aumond et al. [2].

Lawrence and co-workers studied the electrochemical behavior of sulfide on various carbon substrates [14, 15]. For an edge plane-pyrolytic graphite (EPPG) electrode, the sulfide oxidation had started at 0 V/SCE until +0.3V/SCE, after which a steady response is obtained. By applying the cyclic voltammetry technique with this electrode were obtained good results in relation with the sensitivity and limit of detection for sulfide. Table 9.1 summaries some results obtained on sulfide detection.

Table 9.1. Analytical parameters obtained on various carbon substrates on sulfide detection

| Type of electrode | Sensitivity ($\mu\text{A}\mu\text{M}^{-1}$) | Linear range (μA) | LOD (μM) | Ref. |
|-------------------|---|--------------------------------|-----------------------|------|
| EPPG | 0.0112 | 5-60 | 4.9 | 14 |
| CVD-CNT-GC | 0.1150 | 1.25-112.5 | 0.3 | 15 |
| ARC-CNT-GC | 0.0020 | 12.5-87.5 | 12.5 | |
| Bare GC | 0.0050 | 12.5-50 | 12.5 | |

* **CVD-CNT-GC** –glassy-carbon (GC) modified electrode with carbon nanotubes (CNT) obtained by chemical vapor deposition (CVD); **ARC-CNT-GC** –glassy-carbon (GC) modified electrode with carbon nanotubes (CNT) obtained by ARC method;

Reagents

Sodium sulfide was obtained from Merck (Germany) and a 1 mM stock solution was prepared using distilled water. The supporting electrolyte was 0.1 M Na_2SO_4 solution, prepared using Na_2SO_4 of analytical purity (Merck, Germany) and distilled water.

9.1.2. Carbon-based materials tested for sulfide detection

In order to detect sulfide anions in aqueous media and to obtain very good performances three types of carbon-based composite electrodes (carbon nanofiber – CNF, carbon nanotubes–CNT and silver-modified zeolite carbon nanotube–AgZ-CNT) and a commercial boron-doped diamond electrode (BDD) were tested, the results being presented in Figure 9.1.

The useful signal (ΔI) which was used to select the most suitable composite electrodes for the detection was determined as the difference between the peak current for 0.5mM sulfide concentration and the background current (see Table 9.2).

Table 9.2. Useful signal of composite and commercial tested electrodes

| Electrode | Potential range (V) | E_{ox} (V/SCE) | ΔI (μA) |
|-----------|---------------------|------------------|------------------------------|
| BDD | 0 → +1 | 0.415 | 0.998 |
| | | 0.920 | 22.927 |
| CNF | -0.5 → +1.1 | 0.715 | 69.400 |
| CNT | | 0.415 | 19.819 |
| AgZ-CNF | | 0.795 | 37.524 |

Based on the results presented in Table 9.2 and in Figure 9.1 the best useful signal was obtained for the CNF electrode. Therefore, this type of electrode was selected for further studies and for comparison the BDD commercial electrode was also selected. The BDD commercial electrode was also selected due its characteristics - a wide potential window in aqueous solutions, low background currents, chemical and mechanical stability, and resistance to fouling [16].

The electrochemical behavior of sulfide using the selected electrodes (BDD and CNF) was studied by cyclic voltammetry using 0.1M sodium sulfate as supporting electrolyte, the results being presented in Figures 9.2 and 9.3.

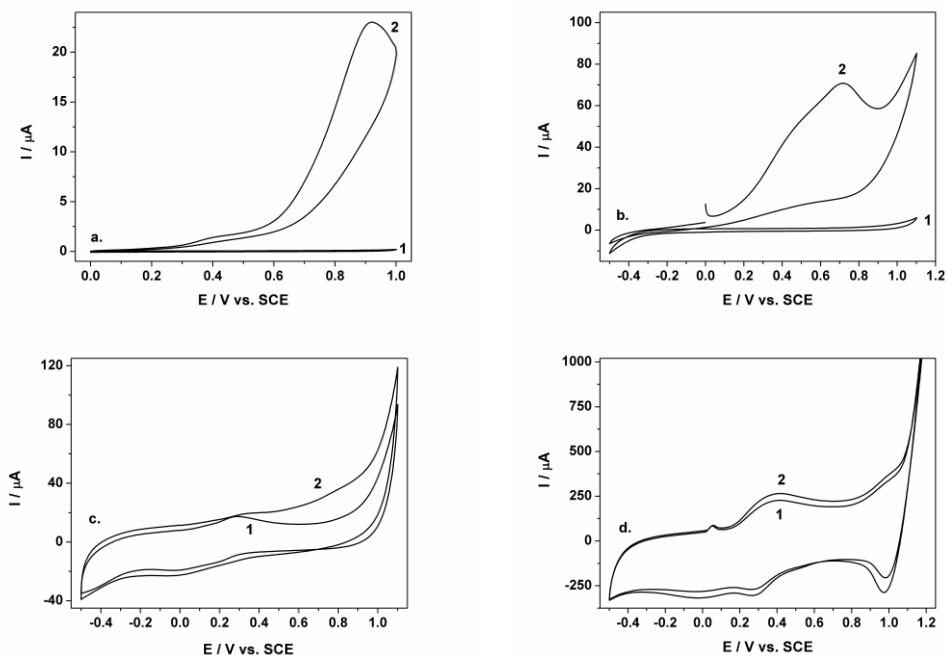


Figure 9.1. Cyclic voltammograms recorded on: **a.** BDD, **b.** CNF, **c.** CNT, **d.** AgZ-CNT electrode in 0.1 M Na_2SO_4 supporting electrolyte (curve 1) in the presence of 0.5 mM (curves 2) sulfide, at a potential scan rate of 0.05 Vs^{-1} in a potential range from 0 to +1 V/SCE for BDD electrode and from -0.5 to +1.1V/SCE for composite electrodes.

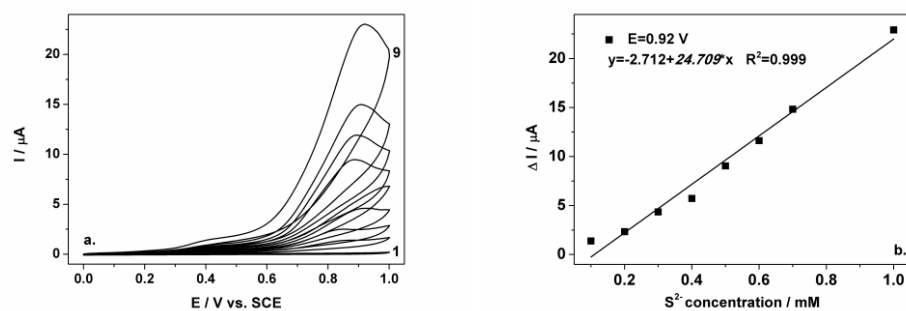


Figure 9.2. a. Cyclic voltammograms recorded on BDD electrode in 0.1 M Na_2SO_4 supporting electrolyte (curve 1) in the presence of 0.1-0.7; 1 mM sulfide (curves 2-9), at a potential scan rate of 0.05 Vs^{-1} in a potential range from 0 to +1 V/SCE; **b.** The calibration plot of the currents recorded at $E=+0.92 \text{ V/SCE}$ vs. sulfide concentrations.

For the BDD electrode the oxidation process of sulfide started at about +0.2 V/SCE, a clear oxidation peak was noticed around +0.9 V/SCE (Figure 9.2.a), and a smaller oxidation peak is observed at about +0.4 V/SCE, suggesting that sulfide oxidation to elemental sulfur occurred in two steps. The calibration plot obtained for the peak corresponding to +0.92 V/SCE revealed a good linearity between anodic current and sulfide concentration, with a correlation coefficient value of 0.999.

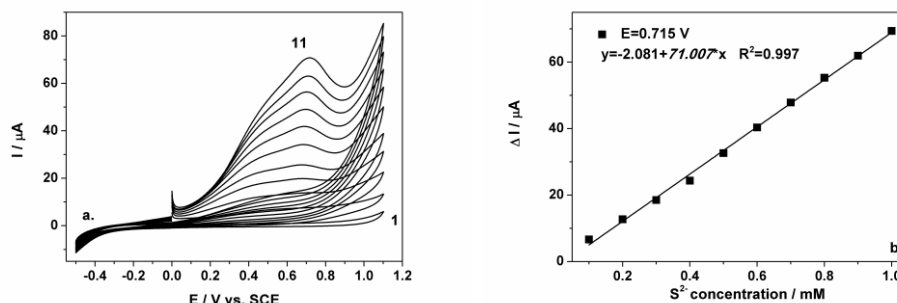


Figure 9.3. **a.** Cyclic voltammograms recorded on CNF electrode in 0.1 M Na₂SO₄ supporting electrolyte (curve 1) in the presence of 0.1-1 mM sulfide (curves 2-11) at a potential scan rate of 0.05 Vs⁻¹ in a potential range from -0.5 to +1.1 V/SCE; **b.** The calibration plot of the currents recorded at E= +0.715 V/SCE vs. sulfide concentrations.

Under similar conditions the CNF composite electrode was tested (Figure 9.3). In comparison with the BDD electrode, at this electrode the oxidation process begins at -0.3 V/SCE and a well-defined peak occurs at +0.715 V/SCE, a lower value of potential than for the BDD electrode (+0.92 V/SCE). Based on the voltammogram shape, especially for low concentrations, it can be proposed that a two-step oxidation process occurred. Increasing sulfide concentration, causes the first peak to be shifted to more positive potential values and "forms" a well-defined peak at +0.92 V/SCE. The sensitivity on CNF electrode is almost three times higher than the one obtained for BDD electrode (71.007 vs. 24.708 μAmM⁻¹). This promising behavior makes CNF electrode suitable for testing in seawater for direct anodic detection of sulfide.

Since sulfide is an almost „natural“ component in several seas (the anoxic and sulfidic layer), a method for sulfide detection in seawater is proposed. In natural environment the presence of free sulfide occurs at depths over 200 meters, and sampling could be difficult. Therefore, a new supporting electrolyte composition generically named *simulated seawater* and consisting of a 0.1M Na₂SO₄+1M NaCl solution was used for ensuring the natural salinity of the aquatic media. The question that arises is whether the high concentration of chloride affects or not the sulfide detection by a possible generation of chlorine. In Figure 9.4 the comparative electrochemical behaviors of the BDD and the CNF composite electrodes in 0.1M Na₂SO₄ and simulated seawater are presented.

For the CNF electrode, at a potential value higher than +1 V/SCE the chlorine evolution process was noticed. To avoid chlorine evolution, the potential window was narrowed at +1.1 V/SCE. The large potential window and implicitly, the high overpotential for chlorine and oxygen evolution are found and desired for direct anodic detection of sulfide on carbon-based electrodes without chlorine interference.

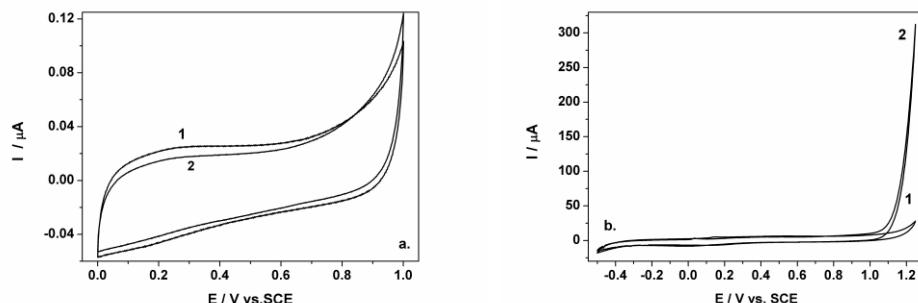


Figure 9.4. Cyclic voltammograms recorded at **a.** BDD and **b.** CNF electrode in 0.1 M Na_2SO_4 supporting electrolyte (curve 1) and simulated seawater (curve 2) at a potential scan rate of 0.05 V s^{-1} .

As a consequence, the simulated seawater was tested for sulfide detection using both electrodes. The results are presented in Figures 9.5 and 9.6. With the BDD electrode the sulfide oxidation process exhibits a similar behaviour as in the case of sodium sulfate. It started at 0 V/SCE, and at around +0.4 V/SCE the first oxidation peak is observed. The second and well-defined peak is observed at +0.915 V/SCE. The use of this new supporting electrolyte induces a small decrease of the signal and the oxidation peaks is slightly shifted to more negative values (+0.915 V/SCE vs. +0.92 V/SCE). For the CNF electrode, the oxidation started at -0.3 V/SCE and the current increased rapidly until +0.4 V/SCE, after which a large plateau suggesting a slow process is observed. In comparison with sodium sulfate, in the presence of chlorine, the oxidation peaks are slightly shifted to more positive values (+0.8 V/SCE vs. +0.715 V/SCE), and a decrease in sensitivity is noticed (59.983 vs. $71.007 \mu\text{A m}^{-1}$).

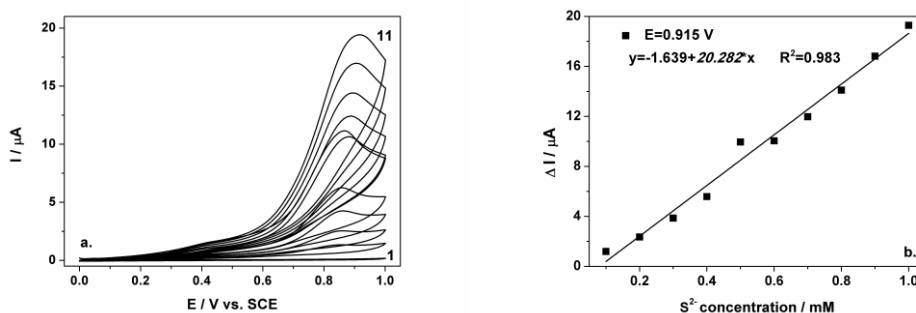


Figure 9.5. a. Cyclic voltammograms recorded on BDD electrode in simulated seawater (curve 1) supporting electrolyte in the presence of 0.1-1 mM sulfide (curves 2-11), at a potential scan rate of 0.05 V s^{-1} in a potential range from 0 to +1 V/SCE; **b.** The calibration plot of the currents recorded at $E = +0.915 \text{ V/SCE}$ vs. sulfide concentrations.

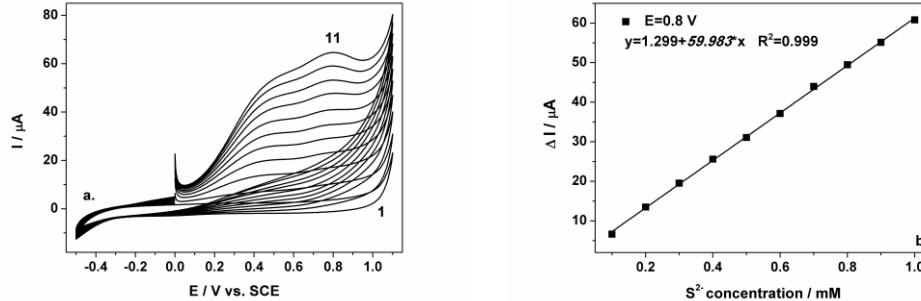
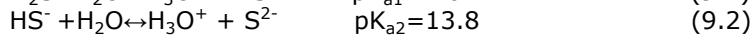
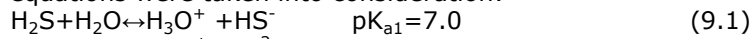


Figure 9.6. **a.** Cyclic voltammograms recorded on CNF electrode in simulated seawater (curve 1) supporting electrolyte in the presence of 0.1-1 mM sulfide (curves 2-11) at a potential scan rate of 0.05 Vs^{-1} in a potential range from -0.5 to +1.1 V/SCE; **b.** The calibration plot of the currents recorded at $E=+0.8 \text{ V/SCE}$ vs. sulfide concentrations.

To study the effect of pH on the oxidation process of sulfide, the following equilibrium equations were taken into consideration:



In accordance with the distribution diagram of sulfide species [17] presented in Figure 9.7 a CV test was conducted in the presence of 0.05 mM sulfide and simulated seawater at pH values of 4, 7 and 11, the results being presented in Figure 9.8.

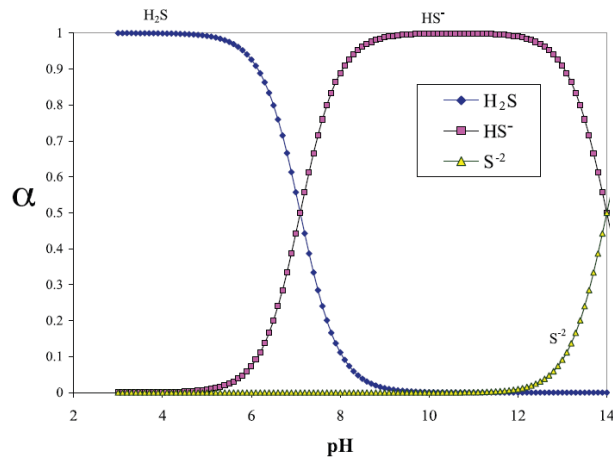


Figure 9.7. The distribution diagram of sulfide species. *Source: Duranceau et al. (2010)

The useful signal was determined as the difference between the peak current corresponding to the oxidation of 0.05 mM sulfide and the background current (see Table 9.3). The oxidation potential value shifted slightly towards negative direction with the increase of pH value. Based on these results and taking into account the pH value of real seawater (between 7.2 and 8.4), the pH value of 7 was chosen as optimum.

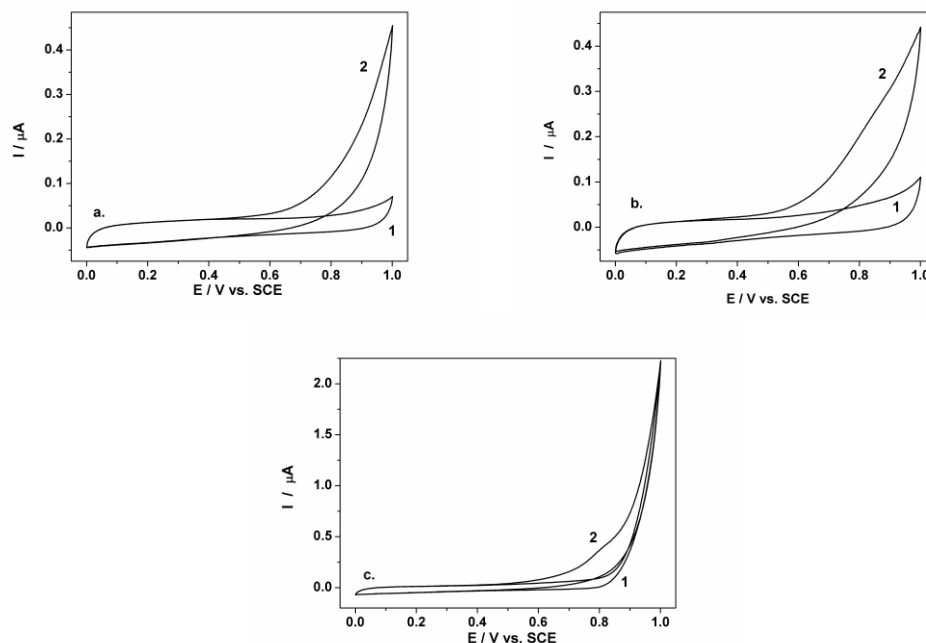


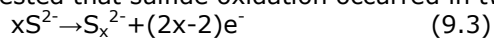
Figure 9.8. Cyclic voltammograms recorded on BDD electrode in simulated seawater (curve 1) supporting electrolyte in the presence of 0.05 mM sulfide (curve 2) at a potential scan rate of 0.05 Vs^{-1} in a potential range from -0.5 to $+1.1 \text{ V/SCE}$ at a pH value of **a.** 4; **b.** 7; **c.** 11.

Table 9.3. Useful signals obtained for different pH values on BDD electrode

| pH value | $E_{\text{ox}} \text{ (V/SCE)}$ | $\Delta I \text{ (}\mu\text{A)}$ |
|----------|---------------------------------|----------------------------------|
| 4 | 0.825 | 0.110 |
| 7 | 0.840 | 0.190 |
| 11 | 0.810 | 0.291 |

The effect of the scan rate was studied for elucidating aspects regarding the mechanism of sulfide oxidation, the results being presented in Figures 9.9 and 9.10.

A good linearity was obtained for anodic peak current vs. square root of scan rates, this indicating that a diffused-controlled oxidation process occurred on both electrodes. In both cases, the lack of the cathodic peak corresponding to the anodic one is observed, so the oxidation process is an irreversible one. Based on these results, it can be suggested that sulfide oxidation occurred in two steps:



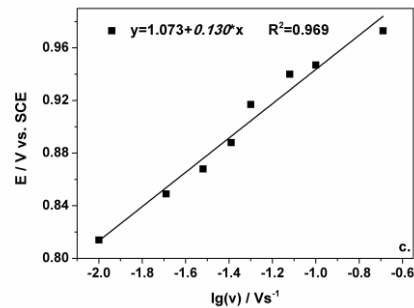
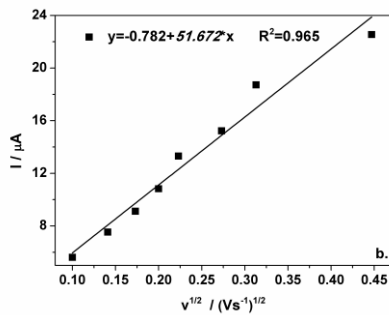
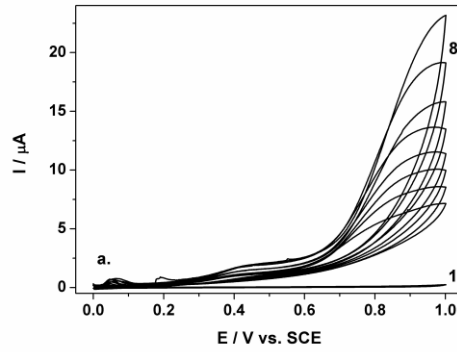
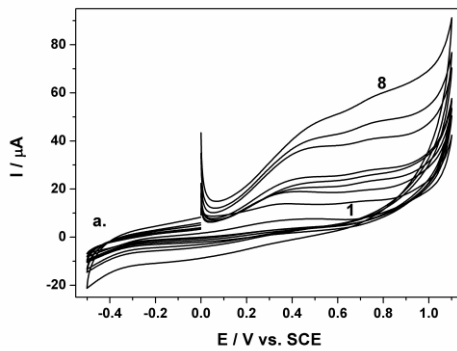


Figure 9.9. **a.** Cyclic voltammograms recorded on BDD electrode in simulated seawater (curve 1) supporting electrolyte in the presence of 0.5 mM sulfide in a potential range from 0 to +1 V/SCE, at different scan rates: 0.01, 0.02, 0.03, 0.04, 0.05, 0.075, 0.1, 0.2 Vs^{-1} (curves 2-8); **b.** The calibration plots of the anodic peak current vs. square root of the scan rate; **c.** The calibration plots of the peak potential E vs. $\lg(v)$.



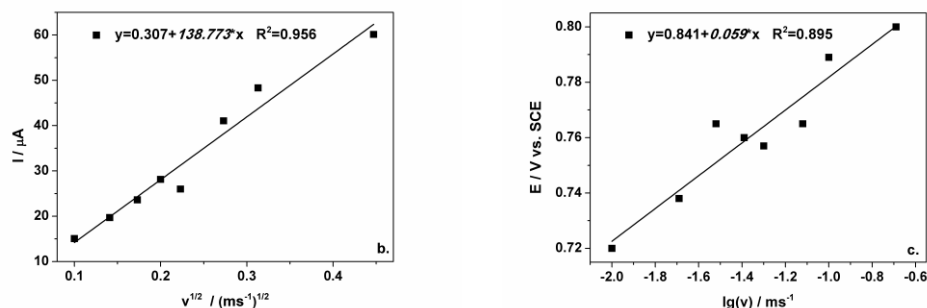


Figure 9.10. **a.** Cyclic voltammograms recorded on CNF electrode in simulated seawater supporting electrolyte (curve 1) in the presence of 0.5 mM sulfide in a potential range from 0 to +1.1 V/SCE, at different scan rates: 0.01, 0.02, 0.03, 0.04, 0.05, 0.075, 0.1, 0.2 Vs^{-1} (curves 1-8); **b.** The calibration plots of the anodic peak current vs. square root of the scan rate; **c.** The calibration plots of the peak potential E vs. $\log(v)$.

In conclusion, even if the anodic peaks are more pronounced with the BDD, the sensitivity is low in comparison with the one obtained with the CNF electrode due to the catalytic effect of CNFs towards sulfide oxidation. These promising results made the CNF electrode suitable for the direct anodic detection of sulfide in seawater.

In comparison with cyclic voltammetry, pulsed techniques are more sensitive and promising in detection studies.

In differential-pulsed voltammetry (DPV) the operating parameters play an important role on electroanalytical performance. Thus, pulse amplitude (a), step potential (ΔE_s), and scan rate (v) were optimized in direct relation to the sensitivity and the results are presented in Table 9.4.

The best sensitivity for sulfide detection was achieved for pulse amplitude of 0.2 V, a step potential of 0.05 V and a scan rate of 0.05 Vs^{-1} , these conditions being considered more suitable for further studies. The DP voltammograms recorded under these parameters in a potential range from -0.2V to +1V are presented in Figure 9.11. Also, during the optimization process it was observed the evolution of the oxidation peak, which shifted to more negative values, a desirable condition in electroanalysis.

Table 9.4. The dependence of the sensitivity on the operating DPV parameters: modulation amplitude (a), step potential (ΔE_s) and scan rate (v)

| a (V) | ΔE_s (V) | v (Vs^{-1}) | Sens. (μAmM^{-1}) | Figure |
|---------|------------------|--------------------------|--------------------------------|--------|
| 0.05 | 0.01 | 0.05 | 15.658 | 9.12. |
| 0.1 | 0.01 | 0.05 | 32.496 | 9.13. |
| | 0.02 | | 35.838 | |
| | 0.05 | | 58.570 | |
| 0.2 | 0.01 | 0.05 | 61.124 | 9.14. |
| | 0.02 | 0.05 | 71.782 | |
| 0.2 | 0.02 | 0.1 | 75.858 | |
| 0.2 | 0.05 | 0.05 | 86.350 | 9.11. |
| | | 0.1 | 75.555 | |
| 0.2 | 0.1 | 0.1 | 68.750 | 9.15. |

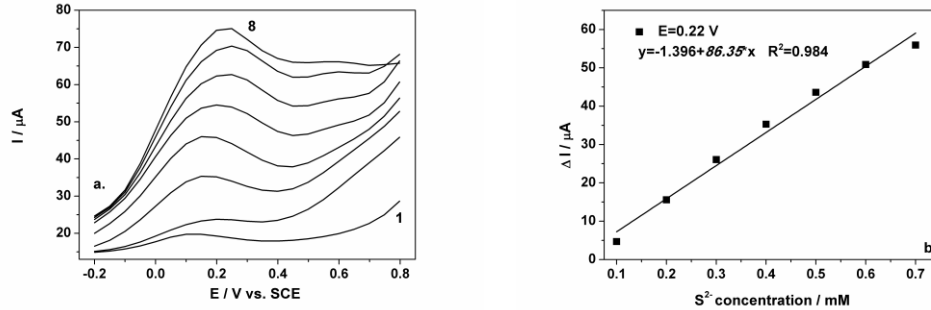


Figure 9.11. a. Differential-pulsed voltammograms recorded on CNF electrode in simulated seawater supporting electrolyte (curve 1) under optimized conditions: $a=0.2\text{V}$; $\Delta E_s=0.05\text{V}$; $v=0.05\text{Vs}^{-1}$, in a potential range from -0.2 to $+1$ V/SCE in the presence of 0.1 - 0.7 mM sulfide (curves 2-8); **b.** The calibration plot of the currents recorded at $E=+0.22$ V/SCE vs. sulfide concentration.

For example, at a pulse amplitude of 0.05 V, a step potential of 0.01 V and a scan rate of 0.05 Vs^{-1} , the oxidation peak occurred at about $+0.7$ V/SCE in comparison with $+0.22$ V/SCE under the above-specified optimized conditions. As in cyclic voltammetry, two oxidation peaks were observed, suggesting the two step oxidation process (Figure 9.12). By maintaining the scan rate at 0.05 Vs^{-1} , and modifying the values of pulse amplitude and step potential to 0.1 V, respectively 0.02 V (Figure 9.13), the sensitivity doubles (35.838 vs. 15.658 μAmM^{-1}). The oxidation peak potential values differ not much ($+0.696$ V/SCE vs. $+0.66$ V/SCE).

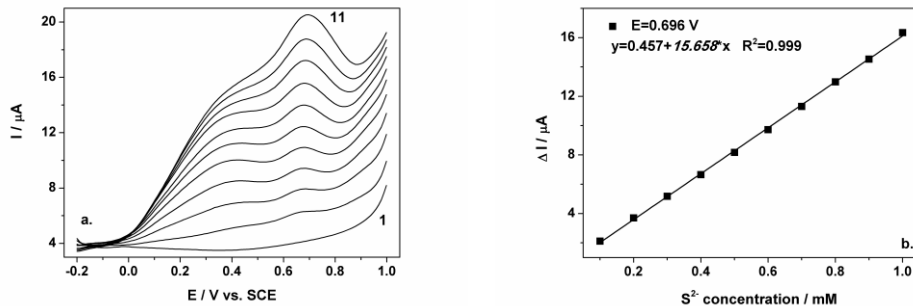


Figure 9.12. a. Differential-pulsed voltammograms recorded on CNF electrode in simulated seawater supporting electrolyte (curve 1) under: $a=0.05\text{V}$; $\Delta E_s=0.01\text{V}$; $v=0.05\text{Vs}^{-1}$, in a potential range from -0.2 to $+1$ V/SCE in the presence of 0.1 - 1 mM sulfide (curves 2-11); **b.** The calibration plot of the currents recorded at $E=+0.696$ V/SCE vs. sulfide concentration.

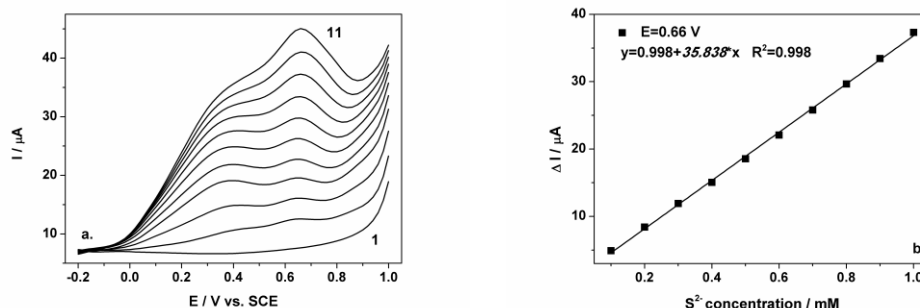


Figure 9.13. a. Differential-pulsed voltammograms recorded on CNF electrode in simulated seawater supporting electrolyte (curve 1) under: $a=0.1\text{V}$; $\Delta E_s=0.02\text{V}$; $v=0.05\text{Vs}^{-1}$, in a potential range from -0.2 to $+1$ V/SCE in the presence of 0.1 - 1 mM sulfide (curves 2-11); **b.** The calibration plot of the currents recorded at $E = +0.66$ V/SCE vs. sulfide concentration.

For a higher amplitude of about 0.2 V, the second oxidation peak has a small tendency of flattening, while the first peak is shifted to more negative values and is well defined (Figure 9.14). If the scan rate and step potentials are increased (Figure 9.15), a sharpening tendency is noticed. The oxidation process begins at -0.1 V/SCE and due to the high scan rate the two steps of this process are not very well defined. The second oxidation peak occurred at about $+0.6$ V/SCE and it is visible in the concentration range 0 - 0.5 mM. After 0.6 mM the peak is shifted to more negative values until $+0.3$ V/SCE. Based on these results it was concluded to maintain a reasonable value for the scan rate, and as a consequence, for the step potential in order to avoid the sharpening of the voltammograms.

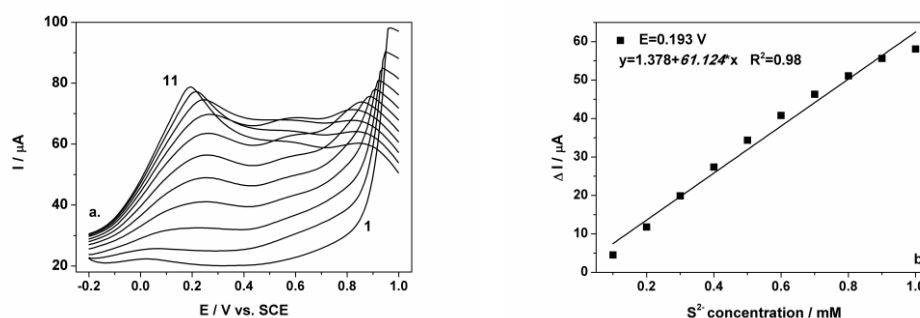


Figure 9.14. a. Differential-pulsed voltammograms recorded on CNF electrode in simulated seawater supporting electrolyte (curve 1) under: $a=0.2\text{V}$; $\Delta E_s=0.01\text{V}$; $v=0.05\text{Vs}^{-1}$, in a potential range from -0.2 to $+1$ V/SCE in the presence of 0.1 - 1 mM sulfide (curves 2-11); **b.** The calibration plot of the currents recorded at $E = +0.193$ V/SCE vs. sulfide concentration.

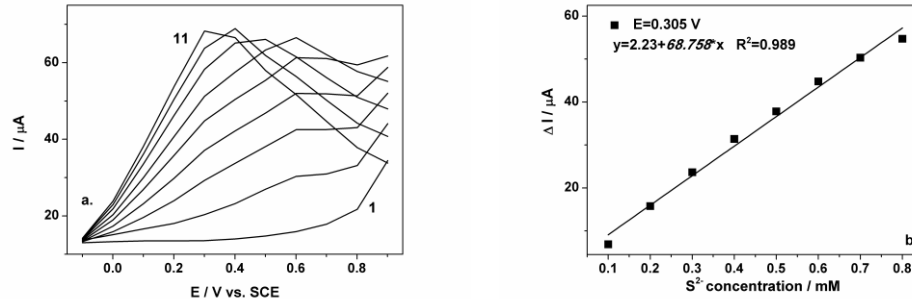


Figure 9.15. a. Differential-pulsed voltammograms recorded on CNF electrode in simulated seawater supporting electrolyte (curve 1) under: $a=0.2\text{V}$; $\Delta E_s=0.1\text{V}$; $v=0.1\text{Vs}^{-1}$, in a potential range from -0.1 to $+0.9$ V/SCE in the presence of 0.1 - 0.8 mM sulfide (curves 2-9); **b.** The calibration plot of the currents recorded at $E=+0.305$ V/SCE vs. sulfide concentration.

Another pulsed technique, square wave voltammetry (SWV), was employed for sulfide detection. Applying the optimized operating conditions established for DPV, *e.g.*, pulse amplitude, step potential, the frequency as the most important parameter of this technique was optimized in order to improve the electroanalytical performance. The results obtained after this step are presented in Table 9.5.

For all the studied frequencies, *e.g.*, 10, 25 and 50 Hz (Figures 9.16-9.18), a good linearity between the anodic peak current and sulfide concentration was observed, which also supported the diffusion-controlled process for sulfide electrooxidation. However, the best sensitivity was achieved for SWV at a frequency of 50 Hz and this value was selected as optimum.

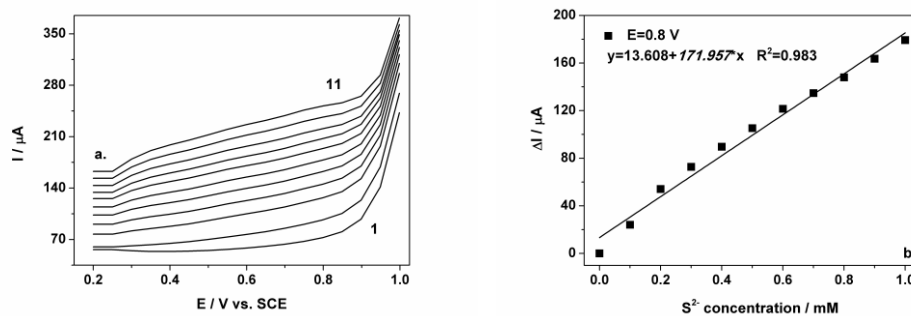


Figure 9.16. a. Square-wave voltammograms recorded on CNF electrode in simulated seawater supporting electrolyte (curve 1) under: $a=0.2\text{V}$; $\Delta E_s=0.05\text{V}$; $f=10$ Hz in a potential range from $+0.2$ to $+1$ V/SCE in the presence of 0.1 - 1 mM sulfide (curves 2-11); **b.** The calibration plot of the currents recorded at $E=+0.8$ V/SCE vs. sulfide concentration.

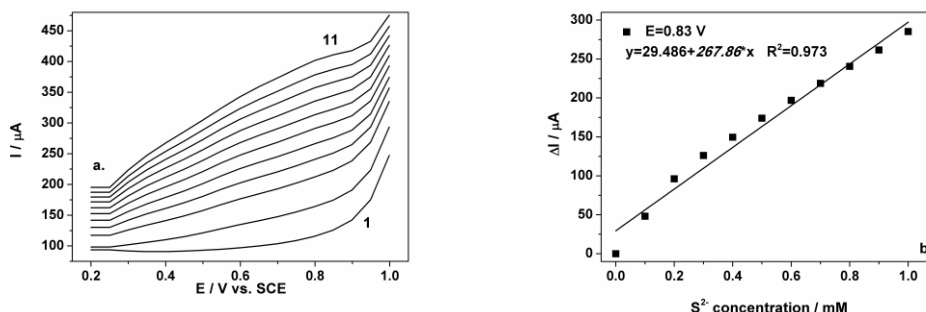


Figure 9.17. a. Square-wave voltammograms recorded on CNF electrode in simulated seawater supporting electrolyte (curve 1) under: $a=0.2\text{V}$; $\Delta E_s=0.05\text{V}$; $f=25\text{ Hz}$ in the potential range from $+0.2$ to $+1\text{ V/SCE}$ in the presence of 0.1 - 1 mM sulfide (curves 2-11); **b.** The calibration plot of the currents recorded at $E=+0.83\text{ V/SCE}$ vs. sulfide concentration.

The high values of step potential are imposing scan rates higher than 0.05Vs^{-1} and as a consequence, the square-wave voltammograms have a linear shape without any well defined oxidation peak.

Figure 9.18 presents the square-wave voltammograms recorded under the optimized conditions: 0.2 V pulse amplitude, 0.05 V step potential, and 50 Hz frequency in simulated seawater for a potential range from $+0.2$ to $+1\text{ V/SCE}$. In comparison with CV and DPV, the SWV technique operated under optimized conditions allowed to achieve the best electroanalytical performance regarding the sensitivity (Table 9.6).

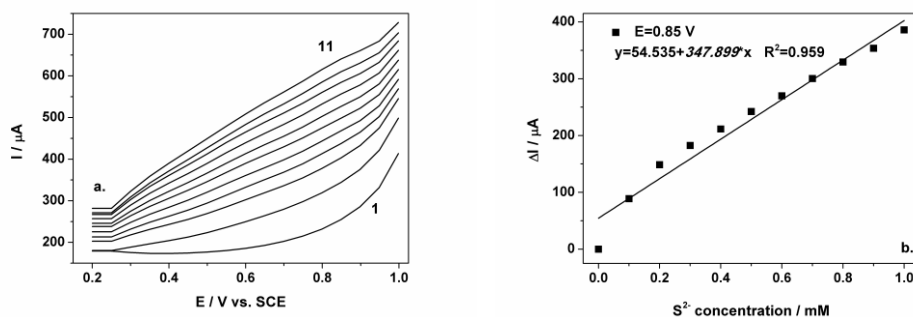


Figure 9.18. a. Square-wave voltammograms recorded on CNF electrode in simulated seawater supporting electrolyte (curve 1) under optimized conditions: $a=0.2\text{V}$; $\Delta E_s=0.05\text{V}$; $f=50\text{ Hz}$ in a potential range from $+0.2$ to $+1\text{ V/SCE}$ in the presence of 0.1 - 1 mM sulfide (curves 2-11); **b.** The calibration plot of the currents recorded at $E=+0.85\text{ V/SCE}$ vs. sulfide concentration.

Table 9.5. The dependence of sensitivity and correlation coefficient on square-wave voltammetry frequency applied under the optimized operating conditions: modulation amplitude of 0.2 V and step potential of 0.05 V

| f (Hz) | E_{ox} (V/SCE) | Sens. (μAmM^{-1}) | R^2 |
|-----------|-------------------------|--------------------------------|--------------|
| 10 | 0.80 | 171.957 | 0.983 |
| 25 | 0.83 | 267.860 | 0.973 |
| 50 | 0.85 | 347.899 | 0.958 |

Considered being one of the easiest electrochemical techniques, chronoamperometry (CA) was employed based on the existing well-established essential point of reference provided by the voltammograms. Figure 9.19 presents the current-time profiles recorded after 100 seconds, obtained by setting the working electrode at +0.9 V/SCE for the established concentration range. The linear dependence between current and concentration is also valid, although the sensitivity is lower than that obtained for cyclic voltammetric technique (17.027 vs. 59.983 μAmM^{-1}).

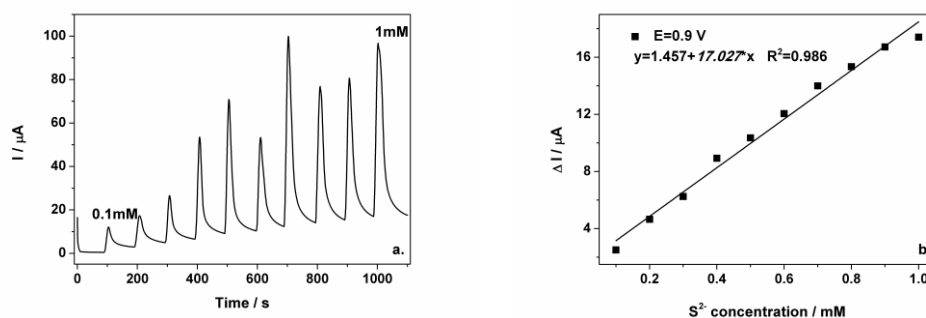


Figure 9.19. a. Chronoamperogram recorded on CNF electrode in simulated seawater supporting electrolyte at $E = +0.9$ V/SCE in the presence of 0.1-1 mM sulfide concentrations. b. The calibration plot of the currents vs. sulfide concentration.

In Table 9.6 all the electroanalytical parameters obtained in the sulfide detection by applying electrochemical techniques are gathered. The best performances for pulsed techniques regarding the sensitivity were obtained by employing square wave voltammetry under optimized conditions, and in relation with the lowest limit of detection by employing differential pulse voltammetry under optimized conditions.

Table 9.6. Electroanalytical parameters obtained for the detection of sulfide in sodium sulphate and simulated seawater on studied electrode by applying electrochemical techniques

| | Tech. | SE | E_{ox} (V/SCE) | Sens. (μAmM^{-1}) | R^2 | RSD (%) | LOD (mgL^{-1}) | LOQ (mgL^{-1}) |
|------------|-------|-----|----------------------------|-----------------------------------|-------|------------|------------------------------|------------------------------|
| BDD | CV | ss | 0.920 | 24.709 | 0.999 | 2.40 | 0.011 | 0.039 |
| | | ssw | 0.915 | 20.282 | 0.983 | 3.46 | 0.020 | 0.069 |
| CNF | CV | ss | 0.715 | 71.007 | 0.997 | 3.84 | 0.060 | 0.202 |
| | | ssw | 0.800 | 59.983 | 0.997 | 2.32 | 0.141 | 0.470 |
| | DPV | | 0.220 | 86.350 | 0.984 | 0.22 | 0.048 | 0.161 |
| | SWV | ssw | 0.855 | 347.899 | 0.958 | 3.40 | 0.941 | 3.139 |
| | CA | | 0.900 | 17.027 | 0.986 | 12.90 | 0.401 | 1.337 |

*SE-supporting electrolyte; ss-0.1M Na_2SO_4 ; ssw- simulated seawater

9.1.3. Application on surface water sample

Several scientific studies underline that carbon-based composite electrodes can be seen as either ordered (array) or randomized micro/nanoelectrode ensembles [18]. Since a microarray/nanoarray peculiarity is given by the ability to deliver the

current response in the absence of any supporting electrolyte, this aspect was tested with a CNF electrode under CV, SWV and CA conditions for a surface water sample taken from the Bega river (N: 45.77288^o; E: 21.77047^o).

The current responses obtained with the CNF electrode in the presence of a real water sample are presented in Figures 9.20 – 9.22, and the electroanalytical results are gathered in Table 9.7.

Table 9.7. Electroanalytical parameters obtained for the detection of sulfide in a real sample (Bega river) at CNF electrode by applying electrochemical techniques

| Tech. | E _{ox} (V/SCE) | Sensitivity (μAmM^{-1}) | R ² | RSD (%) | LOD (mgL^{-1}) | LOQ (mgL^{-1}) |
|-------|----------------------------|---|----------------|------------|------------------------------|------------------------------|
| CV | 0.850 | 37.619 | 0.985 | 6.95 | 0.288 | 0.963 |
| SWV | 1.435 | 108.44 | 0.998 | 0.24 | 0.117 | 0.390 |
| CA | 0.900 | 15.882 | 0.996 | 4.94 | 0.056 | 0.187 |

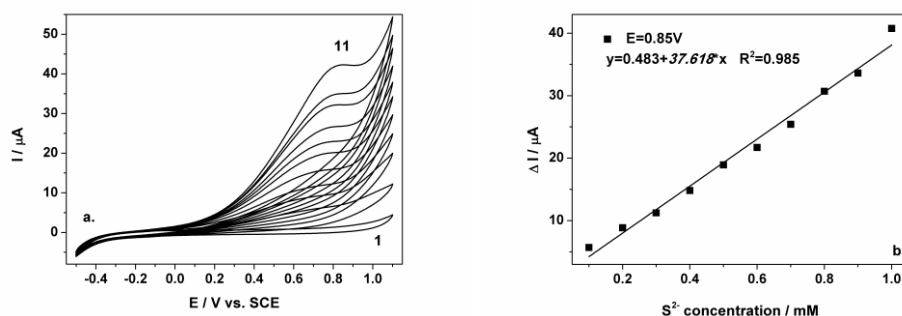


Figure 9.20. **a.** Cyclic voltammograms recorded on CNF electrode in a real water sample (curve 1) in the presence of 0.1-1 mM sulfide (curves 2-11), at a potential scan rate of 0.05 Vs^{-1} in a potential range from -0.5 to +1.1 V/SCE; **b.** The calibration plot of the currents recorded at $E = +0.85$ V/SCE vs. sulfide concentration.

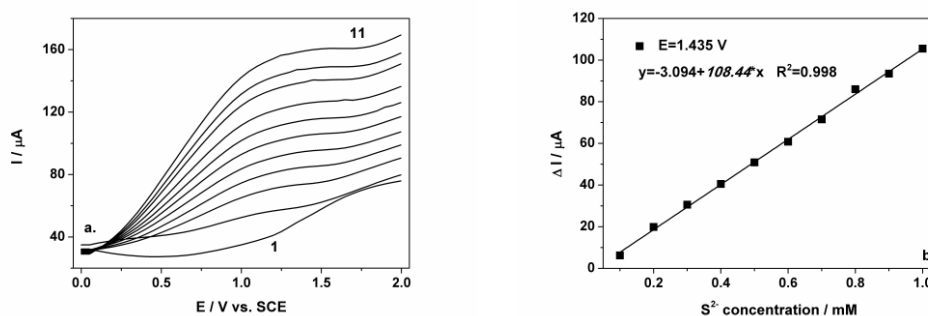


Figure 9.21. **a.** Square-wave voltammograms recorded on CNF electrode in a real water sample (curve 1) under optimized conditions: $a = 0.2\text{V}$; $\Delta E_s = 0.05\text{V}$; $f = 50$ Hz in a potential range from 0 to +2 V/SCE in the presence of 0.1-1 mM sulfide (curves 2-11); **b.** The calibration plot of the currents recorded at $E = +1.435$ V/SCE vs. sulfide concentration.

The best sensitivity was obtained, as in the case of simulated seawater, by employing the SWV technique ($108.44 \mu\text{AmM}^{-1}$), although there is a significant difference between this value and the one achieved for the simulated water

($347.899 \mu\text{A}\text{mM}^{-1}$). This could be explained by the higher value of ionic strength of the water. Perhaps surprising, the lowest limit of detection, and respectively, the lowest limit of quantification were obtained for the CA technique (statistical computation of the small values of the blank led to this result).

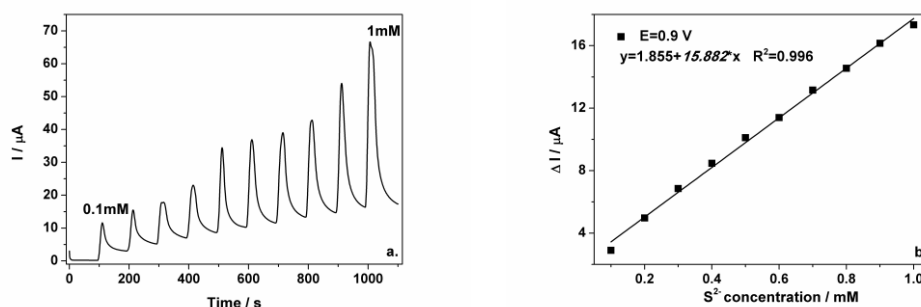


Figure 9.22. **a.** Chronoamperogram recorded on CNF electrode in a real water sample at $E = +0.9 \text{ V/SCE}$ in the presence of 0.1-1 mM sulfide concentrations. **b.** The calibration plot of the currents vs. sulfide concentrations.

9.1.4. Conclusions

Based on the presented results, it can be concluded that:

- Both boron-doped diamond (BDD) and carbon nanofiber-epoxy (CNF) electrodes exhibit the useful properties for the anodic oxidation and the voltammetric detection of sulfide from aqueous solutions. The anodic oxidation of sulfide using these electrodes is a diffusion-controlled process, which is very desired for the electroanalysis application.
- Cyclic voltammetry results obtained in the presence of various sulfide concentrations showed that the CNF electrode exhibited superiority regarding the sensitivity for sulfide detection in comparison with the BDD electrode, and due to the electrocatalytic effect on the sulfide detection.
- In comparison with CV, pulsed-voltammetric techniques allowed increasing the sulfide detection. The best sensitivity in simulated seawater was achieved under optimized square-wave voltammetry technique with modulation amplitude of 0.2 V, step potential of 0.05, and frequency of 50 Hz. The lowest limit of detection and lowest limit of quantification were achieved using the optimized differential-pulsed voltammetry technique (0.048 mgL^{-1} , respectively 0.161 mgL^{-1}).
- The application on a surface water sample reveals a promising beginning for in-field applications of the carbon nanofiber-epoxy composite electrode for voltammetric/amperometric detection of sulfide in seawater/surface water.

9.2. Simultaneous electrochemical detection of sulfide and nitrite anions in water

9.2.1. Introduction

Nitrite (NO_2^-) has been widely used in industrial and agricultural production and is a toxic inorganic contaminant, hazardous to humans and others organisms

health. The presence of nitrite in drinking water could cause serious human diseases as methemoglobinemia and stomach cancer by the production of N-nitrosamines. The maximum concentration limit in drinking water recommended by the World Health Organization is 3 mgL^{-1} as nitrite ion or 0.09 mgL^{-1} as nitrite-nitrogen. For meat products a 200 ppm maximum allowed concentration was established. The lethal dose of nitrite for humans is considered to be 33 mg per kg body weight. Several studies had revealed the bioaccumulation of nitrites at high concentration levels into aquatic organism via gill epithelia, causing serious economic losses to aquaculture production [19-21].

In seawater, the nitrite concentrations are ranging between 10 up to 20 μM . Due to its photochemical stability, nitrite is an important source of OH^- and contributes to the degradation of persistent pollutants. Still, nitrite can also induce the formation of harmful compounds via aromatic photonitration (nitration as well as nitrosation processes can generate carcinogenic and mutagenic compounds) [22]. As a consequence, it is very important to develop detection and monitoring strategies of this inorganic compound.

A variety of strategies based on spectrophotometry, ion chromatography, flow-injection analysis, and capillary electrophoresis have been proposed for detecting and monitoring nitrite. Nevertheless, these methods are laborious to perform or require chemical reagents, hence electrochemical approaches are more favourable due to rapid response and simple operation. In general, the use of silver is preferred due to a large observed enhancement in nitrite detection [20-24].

As it was previously presented, sulfide, another type of anion widely found in water, produces harmful effects on biota. Since sulfide and nitrite coexist in the aquatic ecosystem and the cumulative effects in the environment will have a great impact, a strategy for their simultaneous detection is desired.

Reagents

Sodium nitrite was provided by Merck (Germany) and a 1 mM stock solution was prepared using distilled water. The supporting electrolyte was 0.1 M Na_2SO_4 solution, prepared using Na_2SO_4 of analytical purity (Merck, Germany) and distilled water.

9.2.2. Simultaneous electrochemical detection of sulfide and nitrite at a boron-doped diamond electrode using voltammetric/ amperometric techniques

The electrochemical behavior of nitrite has been studied mainly using glassy carbon electrodes, or by using several types of chemically-modified electrodes such as Ag-doped zeolite-expanded graphite-epoxy composite electrode and electrodeposited Ag nanoparticles on a pure graphite sheet. In comparison with these electrode materials, a boron-doped diamond electrode possesses a wide potential window, low background current, promising characteristics for applying it to nitrite detection.

In Figure 9.23 the cyclic voltammograms recorded with the BDD electrode in 0.1M Na_2SO_4 supporting electrolyte for 0.2-1 mM nitrite concentration range from +0.5 to +1.5 V/SCE potential range are presented.

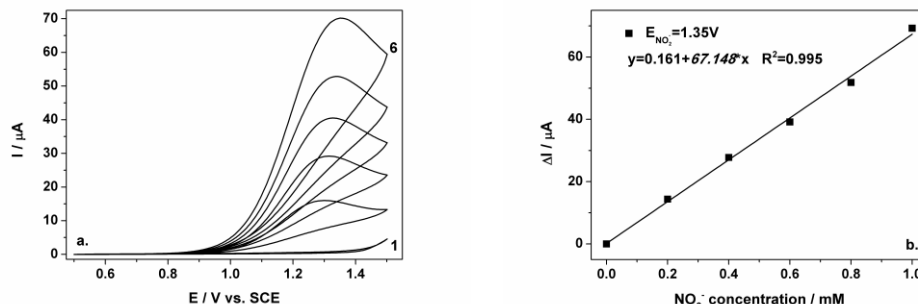


Figure 9.23. **a.** Cyclic voltammograms recorded at BDD electrode in 0.1 M Na₂SO₄ supporting electrolyte (curve 1) in the presence of 0.2-1mM nitrite (curves 2-6), at a potential scan rate of 0.05 Vs⁻¹ in a potential range from +0.5 to +1.5 V/SCE; **b.** Calibration plot of the current recorded at E = +1.35 V/SCE vs. nitrite concentrations.

As can be noticed, the oxidation process of nitrite started at +0.9 V/SCE, but a well-defined oxidation peak occurred at +1.35 V/SCE. The good linearity anodic of the peak current vs. nitrite concentration suggests a diffusion-controlled process. The lack of cathodic peak suggests an irreversible oxidation process of nitrite.

Figure 9.24 presents the voltammograms recorded with the BDD electrode in the presence of both anions. The working protocol consisted of two steps: first, the sulfide (the inset of Figure 9.24.a) was added until a concentration of 0.1 mM was reached, and then in the second step the nitrite was added until a concentration of 0.1 mM was reached. From the inset of Figure 9.24.a a wide plateau is observed, suggesting slow sulfide oxidation. After adding the nitrite, the anodic peak characteristic for nitrite oxidation appeared and increased with nitrite concentration, as in Figure 9.24.a. For both anions good sensitivity values were obtained and for the oxidation potential value no significant changes were observed.

These promising results suggest that boron-doped diamond electrode material is a promising material which can be used for the simultaneous detection of these anions.

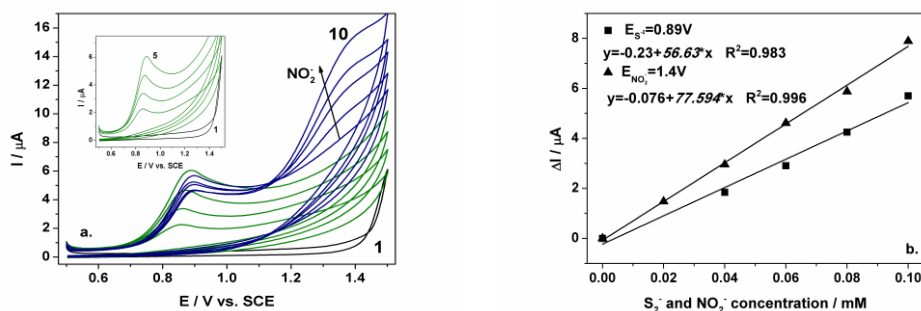


Figure 9.24. **a.** Cyclic voltammograms recorded at BDD electrode in 0.1 M Na₂SO₄ supporting electrolyte (curve 1) in the presence of 0.02-0.1mM sulfide (curves 2-5; Inset of figure), and 0.02-0.1mM nitrite (curves 6-10) at a potential scan rate of 0.05 Vs⁻¹ in a potential range from +0.5 to +1.5 V/SCE; **b.** Calibration plots of the currents recorded at E = +0.89 V/SCE for sulfide and E = +1.4 V/SCE for nitrite vs. anion concentrations.

As a control measure to verify the reproducibility, another protocol was proposed which consisted of alternative additions of specific aliquots volume of sulfide and nitrite until a concentration of 0.2 mM was reached for each anion in the mixture. The results are presented in Figure 9.25.

After the additions of sulfide and nitrite aliquots, two different shapes of voltammograms were observed (curve 2 vs. curve 3) suggesting the capability of boron-doped diamond material of detecting both anions without any interference. The values of sensitivities obtained by applying this procedure are in good agreement with the ones obtained for the previously presented working protocol, e.g., $55.644 \mu\text{AmM}^{-1}$ vs. $55.63 \mu\text{AmM}^{-1}$ for sulfide and $67.371 \mu\text{AmM}^{-1}$ vs. $77.595 \mu\text{AmM}^{-1}$ for nitrite.

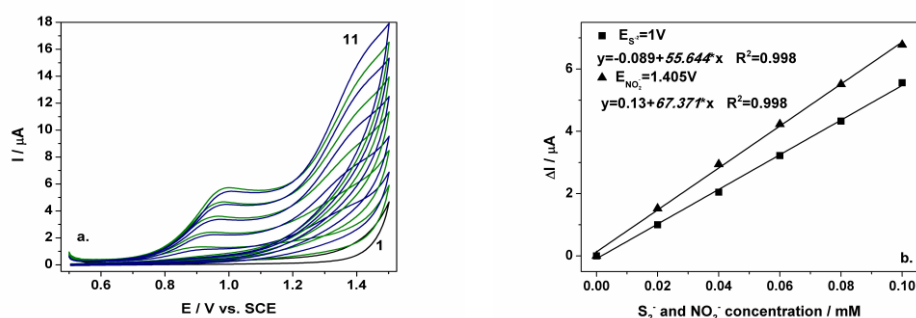


Figure 9.25. a. Cyclic voltammograms recorded at BDD electrode in 0.1 M Na_2SO_4 supporting electrolyte (curve 1) in the presence of 0.02-0.1mM sulfide (curves 2-11) at a potential scan rate of 0.05Vs^{-1} in a potential range from +0.5 to +1.5 V/SCE; b. Calibration plots of the currents recorded at $E = +1 \text{V/SCE}$ for sulfide and $E = +1.405 \text{V/SCE}$ for nitrite vs. anion concentrations.

In Table 9.8 all the results obtained for simultaneous sulfide and nitrite detection on BDD electrode by employing cyclic voltammetry are gathered. These results confirm again that by using this type of electrode material the simultaneous detection of both sulfide and nitrite anions can be achieved without any interference and that good linearity of peak current vs. anion concentration was obtained in both cases.

Table 9.8. Electroanalytical parameters obtained on BDD electrode in simultaneous detection of sulfide and nitrite

| Type | Anl. | E_{ox} (V/SCE) | Sens. (μAmM^{-1}) | R^2 | RSD (%) | LOD (mgL^{-1}) | LOQ (mgL^{-1}) |
|------|-----------------|----------------------------|-----------------------------------|-------|------------|------------------------------|------------------------------|
| Ind. | NO_2^- | 1.350 | 67.148 | 0.995 | 2.6 | 0.306 | 1.022 |
| Sim. | S^{2-} | 0.890 | 56.630 | 0.983 | 8.5 | 0.187 | 0.624 |
| | NO_2^- | 1.400 | 77.594 | 0.996 | 3.1 | 0.298 | 0.994 |
| | S^{2-} | 1.000 | 55.644 | 0.998 | 6.2 | 0.158 | 0.528 |
| | NO_2^- | 1.405 | 67.371 | 0.998 | 4.3 | 0.550 | 1.835 |

Pulsed techniques, e.g., differential-pulsed voltammetry and square-wave voltammetry were employed for obtaining improvements regarding the values of sensitivity and oxidation potential. For differential-pulsed voltammetry two different sets of operating parameters were tested (Table 9.8). The results obtained by employing 0.1V modulation amplitude, 0.025V step potential and 0.025Vs^{-1} scan

rate, are presented in Figure 9.26. The working protocol consisted of adding the sulfide in the first step, and subsequently in the second step adding nitrite until a limit concentration of 0.1 mM was reached for each anion. For both anions well-defined peaks were recorded, *e.g.*, for sulfide at about +0.8 V/SCE and for nitrite at about +1.3 V/SCE. These results confirm that both anions can be detected simultaneous without any interference.

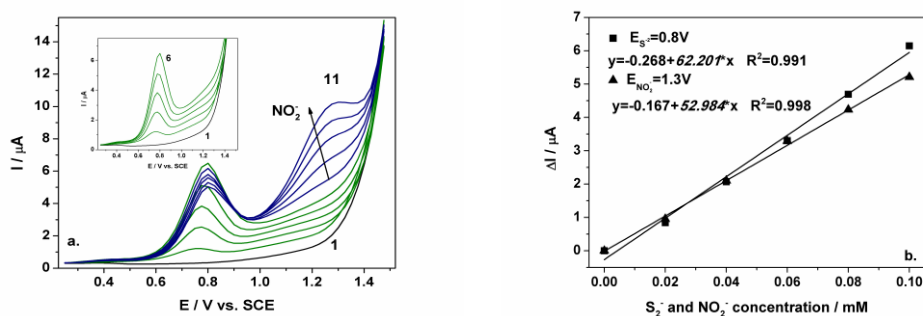


Figure 9.26. **a.** Differential-pulsed voltammograms recorded at BDD electrode in 0.1 M Na_2SO_4 supporting electrolyte (curve 1) in the presence of 0.02-0.1mM of sulfide (curves 2-6) and a mixture of 0.1mM sulfide and 0.02-0.1mM nitrite (curves 7-11), under 0.1V modulation amplitude, 0.025V step potential, and 0.025Vs^{-1} scan rate in a potential range from +0.25 to +1.5 V/SCE; **b.** Calibration plots of the currents recorded at $E = +0.8\text{V/SCE}$ for sulfide and $E = +1.3\text{V/SCE}$ for nitrite vs. anion concentrations.

Then, the simultaneous addition effect of sulfide and nitrite mixture over oxidation process was studied under the following conditions: modulation amplitude of 0.2V, step potential of 0.01V and scan rate of 0.1Vs^{-1} , the results being presented in Figure 9.27.

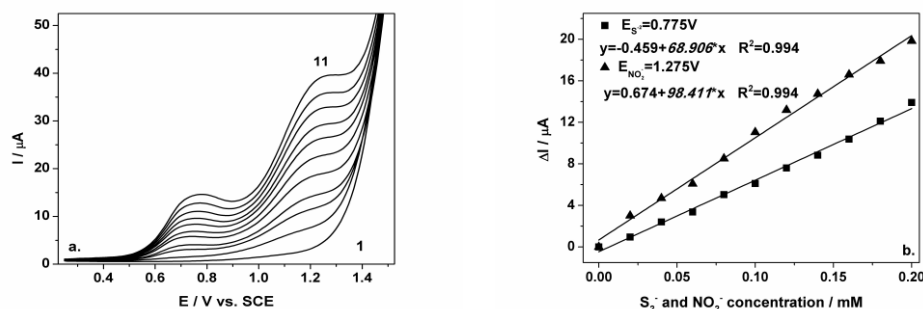


Figure 9.27. **a.** Differential-pulsed voltammograms recorded at BDD electrode in 0.1 M Na_2SO_4 supporting electrolyte (curve 1) in a mixture of 0.02-0.2 mM sulfide and 0.02-0.2 mM nitrite (curves 2-11), under 0.2V modulation amplitude, 0.01V step potential, and 0.1Vs^{-1} scan rate in a potential range from +0.25 to +1.5 V/SCE; **b.** Calibration plots of the currents recorded on $E = +0.775\text{V/SCE}$ for sulfide and $E = +1.275\text{V/SCE}$ for nitrite vs. anion concentrations.

As it was observed in previously performed studies using this electrode, a good peak separation was obtained under these conditions, also an enhancement in relation with the sensitivity was achieved (Table 9.9). Even if the scan rate has a

high value, no changes in DPV resolution were observed. Also, a slight shifting to more negative values was noticed for both oxidation potentials of these anions (+0.775 vs. +0.89 V/SCE for sulfide, and +1.275 vs. +1.35 V/SCE for nitrite).

In Table 9.9 all the electroanalytical parameters obtained with the BDD electrode for the simultaneous detection of sulfide and nitrite under DPV operating conditions are gathered.

Table 9.9. Electroanalytical parameters obtained under DPV operating conditions on BDD electrode

| a (V) | ΔE_s (V) | v (Vs^{-1}) | Anl. | E_{ox} (V/SCE) | Sens. (μAmM^{-1}) | R^2 | RSD (%) | LOD (mgL^{-1}) | LOQ (mgL^{-1}) |
|-------|------------------|-----------------|----------|------------------|--------------------------|-------|---------|--------------------|--------------------|
| 0.1 | 0.025 | 0.025 | S^{2-} | 0.8 | 62.201 | 0.991 | 3.44 | 0.018 | 0.061 |
| | | | NO_2^- | 1.35 | 52.984 | 0.998 | 3.23 | 0.244 | 0.747 |
| 0.2 | 0.01 | 0.1 | S^{2-} | 0.775 | 68.906 | 0.994 | 0.33 | 0.003 | 0.010 |
| | | | NO_2^- | 1.275 | 98.411 | 0.994 | 1.89 | 0.155 | 0.519 |

Square wave voltammetry was employed in order to obtain comparable analytical parameters as obtained differential-pulsed voltammetry. A similar working protocols as the one described previously was used for both anions. An optimization procedure was performed, and in Table 9.10 all the results are gathered.

Table 9.10. Optimization of operating parameters of SWV and electroanalytical obtained on BDD electrode for simultaneous detection of sulfide and nitrite

| a (V) | ΔE_s (V) | f (Hz) | Anl. | E_{ox} (V/SCE) | Sens. (μAmM^{-1}) | R^2 | RSD (%) | LOD (mgL^{-1}) | LOQ (mgL^{-1}) |
|-------|------------------|--------|----------|------------------|--------------------------|-------|---------|--------------------|--------------------|
| 0.01 | 0.001 | 50 | S^{2-} | 0.920 | 11.377 | 0.996 | 1.95 | 0.050 | 0.168 |
| | | | NO_2^- | 1.355 | 7.747 | 0.975 | 2.22 | 0.350 | 1.166 |
| | | 100 | S^{2-} | 0.918 | 14.615 | 0.998 | 2.68 | 0.094 | 0.315 |
| | | | NO_2^- | 1.385 | 11.000 | 0.970 | 7.35 | 1.821 | 6.070 |
| 0.1 | 0.01 | 10 | S^{2-} | 0.850 | 65.462 | 0.993 | 6.70 | 0.140 | 0.468 |
| | | | NO_2^- | 1.340 | 121.331 | 0.996 | 6.54 | 0.357 | 1.191 |
| | | | S^{2-} | 0.850 | 61.304 | 0.997 | 1.12 | 0.011 | 0.039 |
| | | | NO_2^- | 1.350 | 135.720 | 0.992 | 3.41 | 0.180 | 0.601 |
| 0.2 | 0.01 | 10 | S^{2-} | 0.800 | 95.573 | 0.998 | 0.44 | 0.006 | 0.020 |
| | | | NO_2^- | 1.300 | 177.629 | 0.993 | 1.30 | 0.087 | 0.291 |
| | 0.02 | 10 | S^{2-} | 0.805 | 71.959 | 0.99 | 1.54 | 0.029 | 0.098 |
| | | | NO_2^- | 1.300 | 183.713 | 0.966 | 5.40 | 0.822 | 2.742 |
| 0.5 | 0.02 | 10 | S^{2-} | 0.515 | 63.441 | 0.97 | 1.04 | 0.056 | 0.188 |
| | | | NO_2^- | 1.035 | 161.284 | 0.982 | 0.91 | 0.064 | 0.215 |

The effect of the scan rate was studied using a 0.01V modulation amplitude and a 0.001V step potential and employing high values of frequency, e.g., 50 Hz and 100 Hz. As expected for such small values of operating parameters, an important decrease in sensitivity values, which are lower than the ones obtained using CV, is noticed. The square-wave voltammograms recorded under these conditions are presented in Figures 9.28 and 9.29. In both cases, good linearities of peak currents vs. anions concentrations were obtained yet, no increase of the sensitivity or detection potential was noticed.

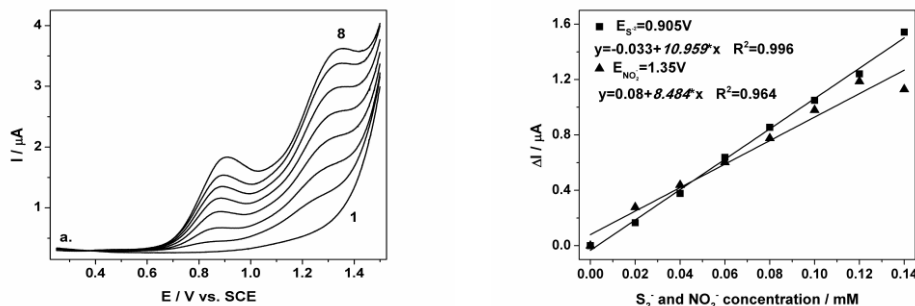


Figure 9.28. a. Square wave voltammograms recorded on a BDD electrode under 0.001 V step potential and 0.01 V modulation amplitude, 50 Hz frequency, scan rate 0.05Vs^{-1} , in a potential range from +0.25 to +1.5 V/SCE in 0.1 M Na_2SO_4 supporting electrolyte (curve 1) and in the presence of 0.02– 0.14 mM sulfide and 0.02–0.14 mM nitrite concentrations (curve 2-8); b. Calibration plots of the currents recorded on $E = +0.905\text{V/SCE}$ for sulfide and $E = +1.35\text{V/SCE}$ for nitrite vs. anion concentrations.

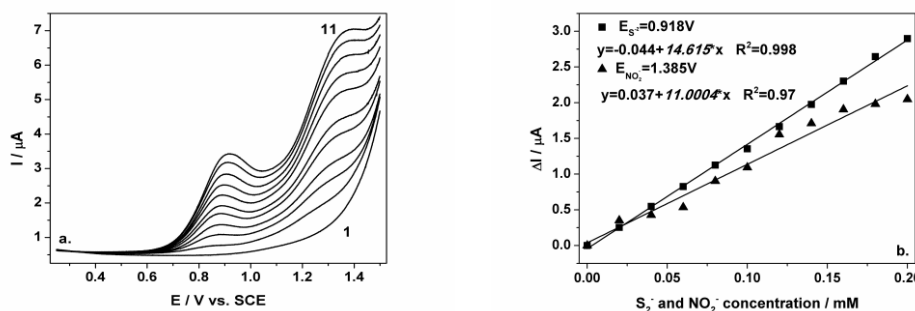


Figure 9.29. a. Square wave voltammograms recorded on a BDD electrode under 0.001 V step potential and 0.01 V modulation amplitude, 100 Hz frequency, scan rate 0.1Vs^{-1} , in a potential range from +0.25 to +1.5 V/SCE in 0.1 M Na_2SO_4 supporting electrolyte (curve 1) and in the presence of 0.02– 0.2 mM sulfide and 0.02–0.2 mM nitrite concentrations (curve 2 - 11); b. Calibration plots of the currents recorded on $E = +0.918\text{V/SCE}$ for sulfide and $E = +1.385\text{V/SCE}$ for nitrite vs. anion concentrations.

Subsequently, two different working protocols were investigated under the same operating parameters, *e.g.*, 0.1V modulation amplitude, 0.01V step potential, 10 Hz frequency, and 0.1Vs^{-1} scan rate. The results are presented in Figures 9.30 and 9.31. The results obtained for both working protocols are in good agreement regarding the sensitivity and the detection potential (Table 9.10).

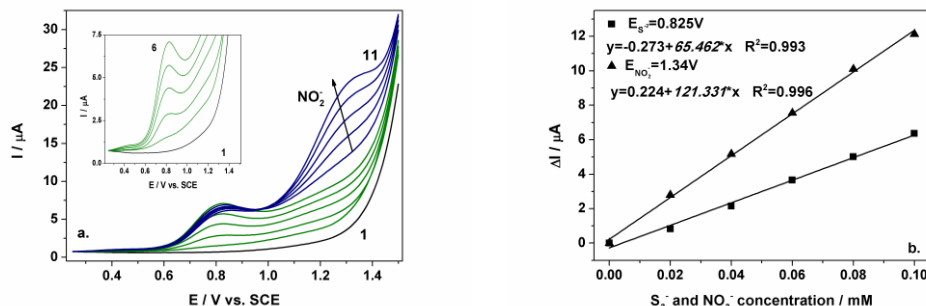


Figure 9.30. **a.** Square wave voltammograms recorded at BDD electrode in 0.1 M Na_2SO_4 supporting electrolyte (curve 1) in the presence of 0.02-0.1 mM of sulfide (curves 2-6) and a mixture of 0.1mM sulfide and 0.02-0.1mM nitrite (curves 7-11), under 0.1V modulation amplitude, 0.01V step potential, and 10 Hz frequency in a potential range from +0.25 to +1.5 V/SCE; **b.** Calibration plots of the currents recorded on $E = +0.825$ V/SCE for sulfide and $E = +1.34$ V/SCE for nitrite vs. anion concentrations.

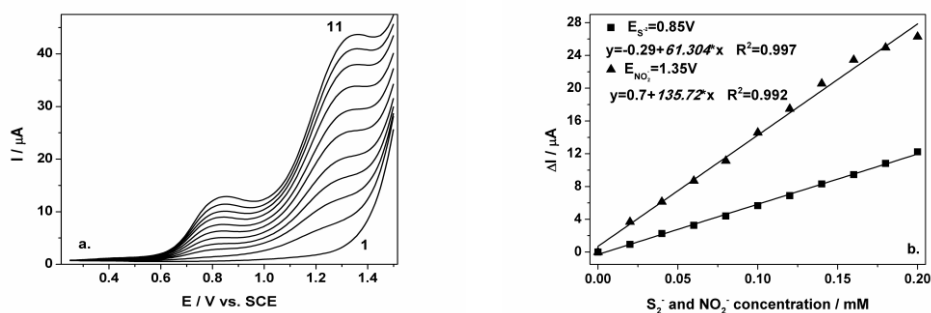


Figure 9.31. **a.** Square wave voltammograms recorded at BDD electrode in 0.1 M Na_2SO_4 supporting electrolyte (curve 1) in a mixture of 0.02-0.2 mM sulfide and nitrite (curves 2-11), under 0.1V modulation amplitude, 0.01V step potential, and 10Hz frequency in a potential range from +0.25 to +1.5 V/SCE; **b.** Calibration plots of the currents recorded on $E = +0.58$ V/SCE for sulfide and $E = +1.35$ V/SCE for nitrite vs. anions concentrations.

Since the modulation amplitude is in direct relation with the current response, the increase of the modulation amplitude value was tested by maintaining a constant value of frequency of 10 Hz for different values of the step potential. Under 0.2 V modulation amplitude and 10 Hz frequency, the influence of step potential and in consequence of scan rate was studied for 0.01V and 0.02V. The results are presented in Figures 9.32 and 9.33.

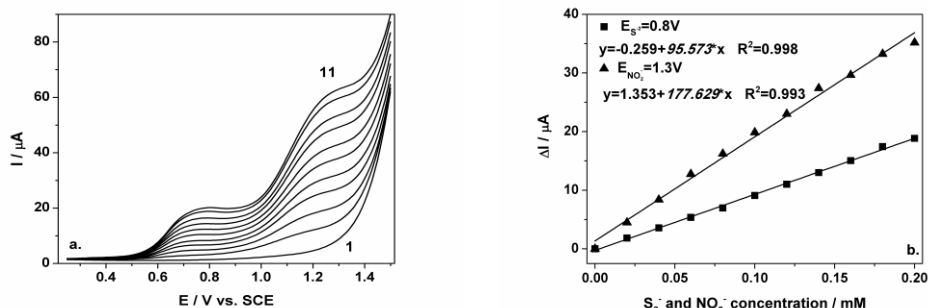


Figure 9.32. a. Square wave voltammograms recorded at BDD electrode in 0.1 M Na_2SO_4 supporting electrolyte (curve 1) in a mixture of 0.02-0.2 mM sulfide and of 0.02-0.2 mM nitrite (curves 2-11), under 0.2V modulation amplitude, 0.01V step potential and 10 Hz frequency in a potential range from +0.25 to +1.5 V/SCE; **b.** Calibration plots of the currents recorded on $E = +0.8$ V/SCE for sulfide and $E = +1.3$ V/SCE for nitrite vs. anion concentrations.

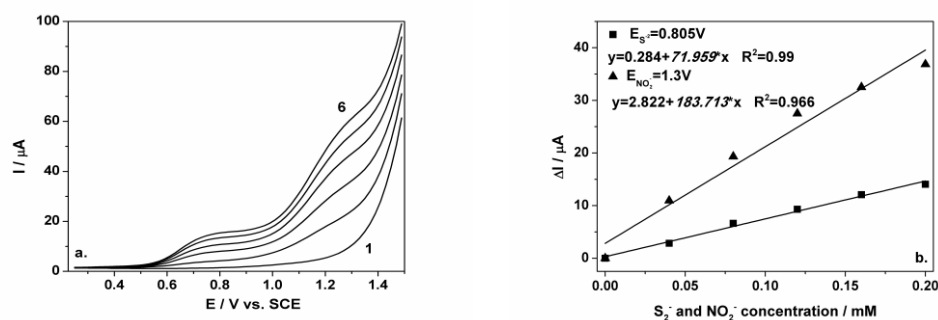


Figure 9.33. a. Square wave voltammograms recorded on a BDD electrode under 0.02 V step potential and 0.2 V modulation amplitude, 10 Hz frequency, scan rate 0.2Vs^{-1} , in a potential range from +0.25 to +1.5 V/SCE in 0.1 M Na_2SO_4 supporting electrolyte (curve 1) and in the presence of 0.02–0.2 mM sulfide and 0.02–0.2 mM nitrite concentrations (curve 2 - 6); **b.** Calibration plots of the currents recorded on $E = +0.805$ V/SCE for sulfide and $E = +1.3$ V/SCE for nitrite vs. anion concentrations.

In both cases, good linearity of peak currents vs. anion concentrations was obtained. And, by employing a higher step potential value, e.g., 0.02V, the best performance for simultaneous nitrite detection in this study was obtained (183.713 vs. $177.629 \mu\text{AmM}^{-1}$).

Further, by maintaining a constant value for the step potential (0.02V), the frequency (10Hz) and the scan rate (200mVs^{-1}), and for modulation amplitude a value of 0.5V was applied, the results are presented in Figure 9.34. In comparison with all tested operating parameters, in this case an important shift to more negative values was observed for the detection potential ($+0.515$ V/SCE vs. $+0.8$ V/SCE for sulfide and $+1.035$ V/SCE vs. $+1.3$ V/SCE for nitrite).

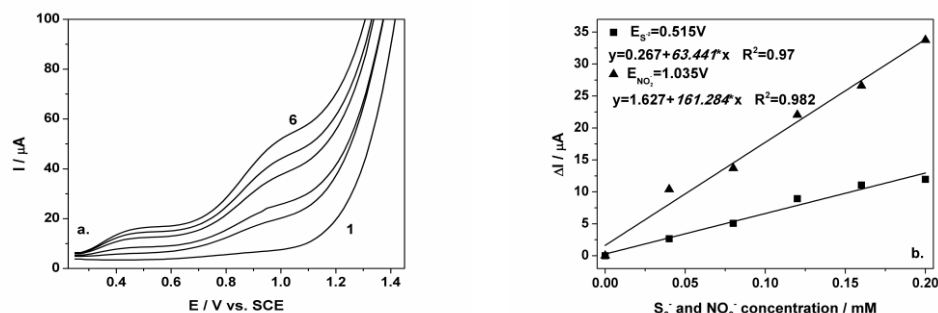


Figure 9.34. a. Square wave voltammograms recorded on a BDD electrode under 0.02 V step potential and 0.5 V modulation amplitude, 10 Hz frequency, scan rate 0.2 V s^{-1} , in a potential range from +0.25 to +1.5 V vs. SCE in 0.1 M Na_2SO_4 supporting electrolyte (curve 1) and in the presence of 0.02– 0.2 mM sulfide and 0.02– 0.2 mM nitrite concentrations (curve 2 - 6), b. Calibration plots of the currents recorded on $E = +0.515 \text{ V/SCE}$ for sulfide and $E = +1.035 \text{ V/SCE}$ for nitrite vs. anion concentrations.

Chronoamperometry, a simple electrochemical technique, was applied in simultaneous sulfide and nitrite detection. Based on voltammetric responses obtained by cyclic voltammetry two detection potentials were used: $E_1 = +0.85 \text{ V/SCE}$ specific for the sulfide anion and $E_2 = +1.25 \text{ V/SCE}$ specific for the nitrite anion, the results being presented in Figure 9.35. The working protocol included two steps, e.g., first, the nitrite was added until a concentration of 0.1 mM was reached (step 1) and then sulfide was added (step 2) for the same concentration range. During step 1, no signal for nitrite was noticed at +0.85 V/SCE (because this potential is specific to sulfide). When the potential is changed to +1.25 V/SCE, an important signal was observed. During step 2, for +0.85 V/SCE, the signal specific to sulfide is observed, influencing also the signal recorded at +1.25 V/SCE. As expected, the values of sensitivities as obtained by applying this technique are the lowest achieved for simultaneous detection.

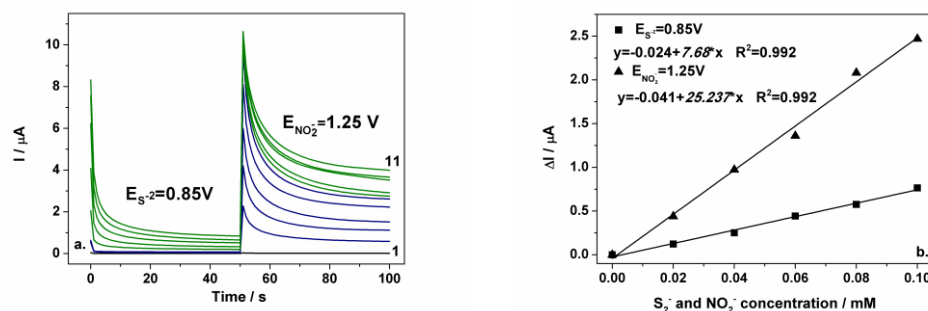


Figure 9.35. a. Chronoamperograms recorded at BDD electrode in 0.1 M Na_2SO_4 supporting electrolyte (curve 1) in a mixture of 0.02-0.1mM sulfide and 0.02-0.1mM nitrite (curves 2-6; see inset) and in the presence of 0.02-0.1mM nitrite (curves 7-11), under potentials $E_1 = +0.85 \text{ V/SCE}$ for sulfide and $E_2 = +1.25 \text{ V/SCE}$ for nitrite; b. Calibration plot of the currents recorded at $E = +0.85 \text{ V/SCE}$ for sulfide, respectively $E = +1.25 \text{ V/SCE}$ for nitrite vs. anion concentrations.

These results are valuable because they offer a distinct perspective regarding in-field applications and confirm once again the applicability of this type of material for simultaneous detection of nitrite and sulfide anions.

In Table 9.11 the analytical parameters obtained with the BDD electrode for simultaneous nitrite and sulfide anion detection are gathered.

Table 9.11. Electroanalytical parameters obtained for the simultaneous detection of nitrite and sulfide anions on BDD electrode

| Tech. | Anl. | E_{ox} (V/SCE) | Sens. (μAmM^{-1}) | R^2 | RSD (%) | LOD (mgL^{-1}) | LOQ (mgL^{-1}) |
|-------|-----------------|---------------------|-----------------------------------|-------|------------|------------------------------|------------------------------|
| CV | S^{2-} | 0.890 | 56.630 | 0.983 | 8.50 | 0.187 | 0.624 |
| | NO_2^- | 1.400 | 77.594 | 0.996 | 3.10 | 0.298 | 0.994 |
| DPV | S^{2-} | 0.775 | 68.906 | 0.994 | 0.33 | 0.003 | 0.010 |
| | NO_2^- | 1.275 | 98.411 | 0.994 | 1.89 | 0.155 | 0.519 |
| SWV | S^{2-} | 0.800 | 95.573 | 0.998 | 0.44 | 0.006 | 0.020 |
| | NO_2^- | 1.300 | 177.629 | 0.993 | 1.30 | 0.087 | 0.291 |
| CA | S^{2-} | 0.850 | 7.680 | 0.992 | 5.97 | 0.315 | 0.105 |
| | NO_2^- | 1.200 | 25.237 | 0.992 | 3.97 | 0.032 | 0.109 |

In Table 9.12 the concentration threshold values for both anions established by Romanian authorities for drinking water and discharged waste water into natural water bodies are presented.

Table 9.12. The legal threshold values of both anions according to Romanian legislation

| Type of water | Anion | C_{RO} (mgL^{-1}) | Law |
|----------------|-----------------|--------------------------------|-------------|
| Drinking water | S^{2-} | 0.1 | 311/2004 |
| | NO_2^- | 0.5 | |
| Waste water | S^{2-} | 0.5 | GD 352/2005 |
| | NO_2^- | 1.0 | |

Taking into account the legal threshold values presented in Table 9.12, the best performances in relation with the limit of detection and, respectively, limit of quantification determined for simultaneous detection of both anions were obtained under optimized SWV operating parameters of 0.2V modulation amplitude, 0.01V step potential, 0.1Vs^{-1} scan rate, and 10 Hz frequency.

9.2.3. Conclusions

Based on these results, it can be concluded that:

- Boron-doped diamond electrode exhibits properties for simultaneous sulfide and nitrite detection in aqueous media. The oxidation process for both anions is controlled by diffusion.
- The best performance in relation with the sensitivity was obtained by applying square wave voltammetry under the following operational conditions: 0.2 V modulation amplitude, 0.01V step potential, 0.1 V scan rate, and frequency 10Hz.
- The best performance in relation with the limit of detection, respectively limit of quantification for simultaneous sulfide and nitrite detection was obtained for square

wave voltammetry conditions: 0.2V modulation amplitude, 0.01V step potential, and 10 Hz frequency.

■ The chronoamperometry results confirm that boron-doped diamond material is suitable for real applications in relation with the simultaneous detection of sulfide and nitrite anions.

9.3. References

- [1] Y. Yang, M. Yang, H. Wang, J. Jiang, G. Shen, R. Yu, An amperometric horseradish peroxidase inhibition biosensor based on a cysteamine self-assembled monolayer for the determination of sulfides, *Sens. Actuators B*, (2004) 102, 162-168.
- [2] V. Aumond, M. Waeles, P. Salaun, K. Gibbon-Walsh, C.M.G. van den Berg, P.M. Sarradin, R.D. Riso, Sulfide determination in hydrothermal seawater samples using a vibrating gold micro-wire electrode in conjunction with stripping chronopotentiometry, *Anal. Chim. Acta*, (2012) 753, 42-47.
- [3] L.L. Paim, N.R. Stradiotto, Electrooxidation of sulfide by cobalt pentacyanonitrosylferrate film on glassy carbon electrode by cyclic voltammetry, *Electrochim. Acta*, (2010) 55, 4144-4147.
- [4] Y. Dilgin, S. Canarslan, O. Ayyildiz, B. Ertek, G. Nisli, Amperometric determination of sulfide based on its electrocatalytic oxidation at a pencil graphite electrode modified with quercetin, *Electrochim. Acta*, (2012) 66, 173-179.
- [5] N.S. Lawrence, J. Davis, R.G. Compton, Analytical strategies for the detection of sulfide: a review, *Talanta*, (2000) 52, 771-784.
- [6] G.W. Luther III, T.M. Church, D. Powell, Sulfur speciation and sulfide oxidation in the water column of the Black Sea, *Deep Sea Res. Part A*, (1991) 38, S1121-S1137.
- [7] M. Yucel, S.K. Konovalov, T.S. Moore, C.P. Janzen, G.W. Luther III, Sulfur speciation in the upper Black Sea sediments, *Chem. Geol.*, (2010) 269, 364-375.
- [8] I. Ciglencecki, B. Cosovic, Electrochemical study of sulfur species in seawater and marine phytoplankton cultures, *Mar. Chem.*, (1996) 52, 87-97.
- [9] S. Peiffer, T. Frevert, Potentiometric-determination of heavy metal sulphide solubilities using a pH₂S (glass/Ag⁰, Ag₂S) electrode cell, *Analyst*, (1987) 112, 951-954.
- [10] P.J. Brendel, G.W.III. Luther, Development of a gold amalgam voltammetric microelectrode for the determination of dissolved Fe, Mn, O₂, and S(-II) in porewaters of marine and freshwater sediments, *Environ. Sc. Technol.*, (1995) 29, 751-761.
- [11] T.J. Waite, C. Kraiya, R.E. Trouwborst, S. Ma, G.W. Luther III, An investigation into the suitability of bismuth as an alternative to gold-amalgam as a working electrode for the in situ determination of chemical redox species in the natural environment, *Electroanal.*, (2006) 18, 1167-1172.
- [12] P. Jeroschewski, C. Steuckart, M. Kuhl, An amperometric microsensor for the determination of H₂S in aquatic environments, *Anal. Chem.*, (1996) 68, 4351-4357.

- [13] D. Huang, B. Xu, J. Tang, J. Luo, L. Chen, L. Yang, Z. Yang, S. Bi, Indirect determination of sulfide ions in water samples at trace level by anodic stripping voltammetry using mercury film electrode, *Anal. Methods*, (2010) 2 154-158.
- [14] J. Lawrence, K.L Robinson, N.S. Lawrence, Electrochemical determinations of sulfide at various carbon substrates: a comparative study, *Anal Science*, (2007) 23, 673-676.
- [15] N.S. Lawrence, R. P.Deo, J. Wang, Electrochemical determinations of hydrogen sulfide at carbon nanotube modified electrodes, *Anal Chim. Acta*, (2004) 517, 131-137.
- [16] Y. Einaga, Diamond electrodes for electrochemical analysis. *J. Appl. Electrochem.*, (2010) 40, 1807-1816.
- [17] S.J. Duranceau, V.M. Trupiano, M. Lowenstine, S. Whidden, J. Hopp, Innovative hydrogen sulfide treatment methods: moving beyond packed tower aeration, *FWJR*, (2010) July, 4-14.
- [18] S. Ramirez-Garcia, S. Alegret, F. Cespedes, R.J. Forster, Carbon composite electrodes: surface and electrochemical properties, *Analyst*, (2002) 127, 1512-1519.
- [19] Z. Yiling, Z. Dean, L. Daoliang, Electrochemical and other methods for detection and determination of dissolved nitrite: a review, *Int. J. Electrochem. Sci.*, (2015) 10, 1144-1168.
- [20] F. Manea, A. Remes, C. Radovan, R. Pode, S. Picken, J. Schoonman, Simultaneous electrochemical determination of nitrate and nitrite in aqueous solution using Ag-doped zeolite-expanded graphite-epoxy electrode, *Talanta*, (2010) 83, 66-71.
- [21] E. Menart, V. Javonovski, S.B. Hocevar, Silver particles-decorated carbon paste electrode based on ionic liquid for improved determination of nitrite, *Electrochem. Commun.*, (2015) 52, 45-48.
- [22] P. Calza, D. Vione, A. Novelli, E. Pelizzeti, C. Minero, The role of nitrite and nitrate ions as photosensitizers in the phototransformation of phenolic compounds in seawater, *Sci. Total Environ.*, (2012) 439, 67-75.
- [23] M. Pal, V. Ganesan, Electrochemical determination of nitrite using silver nanoparticles modified electrode, *Analyst*, (2010) 135, 2711-2716.
- [24] L. Guadagnini, D. Tonelli, Carbon electrodes unmodified and decorated with silver for the determination of nitrite, nitrate and iodate, *Sensor Actuat B*, (2013) 188, 806-814.

10. GENERAL CONCLUSIONS

The topic of this PhD thesis is included under the extended framework of water quality. Over the last years many efforts have been focused on maintaining and improving the quality of water. Recently a new class of pollutants, generically called emerging pollutants were detected in various matrices, *e.g.*, surface water, groundwater etc. Their occurrence, fate, behaviour and effects over the environment are subjecting many laborious debates mainly on setting standards for their detection that should be transposed further into global regulations. Usually, the most recurrent employed analysis methods, *e.g.*, LC, HPLC are time and reagent consuming. For this reason, developing simple and low-cost methods that assure fast response, high sensitivity and selectivity by using small reagents volumes are desired. Electroanalysis is offering a good alternative to these classical methods through the selection of electrode material that will ensure high performances.

Therefore, taking into account that no standardized or common methods were set-up for their detection, the major objective of this thesis was the development of rapid and low-cost procedure for their determination in aqueous media using powerful electrochemical techniques and carbon-based material. The selection of target analytes was done based on pharmaceuticals occurrence in water. There were selected three types of pharmaceutical compounds belonging to different therapeutic drug classes: fluoxetine-antidepressants, naproxen-NSAIDs and tetracycline-antibiotics. In addition, the quality of water was studied in relation with some common anions - nitrite and sulfide, by using the same electrode materials and electrochemical techniques.

For achieving these major objectives, it was established a working protocol consisting in the following stages:

- Development of nanostructured carbon-based composite electrode suitable for electroanalysis;
- Elaboration of silver-modified nanostructured carbon-based composite electrodes to enhance the electroanalytical performance;
- Morphology, electrical and electrochemical characterization of nanostructured carbon-based composite electrodes in relation with the electroanalysis applications;
- Voltammetric/amperometric detection of pharmaceuticals by elaboration of detection schemes/protocols for the individual/simultaneous analysis of these compounds in aqueous matrix;
- Voltammetric/amperometric detection of anions by elaboration of detection schemes/protocols for the individual/simultaneous analysis of these compounds in water.

Several unmodified and silver-modified carbon based composite electrodes were successfully synthesized and obtained by using two-roll mill procedure: carbon nanofiber -epoxy resin (CNF), silver-modified zeolite carbon nanofiber-epoxy resin (AgZ-CNF), silver electrochemically decorated carbon nanofiber -epoxy resin (Ag-CNF), carbon nanotubes-epoxy resin (CNT) and silver-modified zeolite carbon nanotubes -epoxy resin (AgZ-CNT).

The morphology and electrical characterization of these electrodes concluded that by using two-roll mill procedure and tetrahydrofuran (THF) as dispersing agent, good distribution of carbon fillers, *e.g.*, CNF, CNF within the epoxy matrix was assured, as it was observed through SEM images. Also, the presence of silver-modified zeolite and silver electrochemically decorated particles within the epoxy matrix was evidenced by SEM and EDX images.

The electrical conductivity of the composite electrodes depends on the type of conductive filler, *e.g.*, CNF, CNF, the loading of the filler and the distribution of the filler within the epoxy matrix. Also, the presence of silver-modified zeolite within the epoxy enhance the electrical properties of the composite.

The electrochemical behaviour of ferri/ferrocyanide redox system allowed to determine the electroactive surface area of these composite electrodes. The electroactive areas exhibited by these electrodes were higher than the geometrical ones, nanostructured carbon enhancing the electroactive surface. Even if the zeolite influenced negatively the electroactive area due to its characteristics, all the tested electrodes showed great potential of nanostructured carbon which makes them suitable for electroanalytical applications.

For each selected pharmaceutical compound individual/simultaneous voltammetric/amperometric detection strategies were developed.

Individual detection

a. Fluoxetine

The electrochemical behaviour of fluoxetine was studied on the new developed electrodes, *e.g.*, CNF, AgZ-CNF, Ag-CNF and CNT, but also on two commercial electrodes, *e.g.*, BDD and Ag. For BDD commercial electrode optimization procedures were performed for pulsed techniques, *e.g.*, differential-pulsed voltammetry and square wave voltammetry, which allowed to achieve the best performances in relation with the sensitivity ($244.106 \mu\text{A}\mu\text{M}^{-1}$) and the lowest limit of detection ($0.037 \mu\text{gL}^{-1}$). The exploitation of carbon-based composite electrodes allowed improving the performances in relation with the detection potential (+0.98 V/SCE for CNF electrode vs. +1.35 V/SCE for BDD electrode). The inclusion of silver within the composite matrix allowed shifted the detection potential to more negative values, *e.g.*, +0.324 V/SCE for Ag-CNF and +0.335 V/SCE for AgZ-CNF. A synergic effect in relation to the sensitivity for fluoxetine detection in aqueous solution in comparison with commercial silver electrode (Ag) and carbon nanofiber (CNF) composite electrode using CV techniques was exhibited using Ag-CNF electrode. In addition, the chemical modification of CNF with silver-modified zeolite allowed to detect the target analyte at trace level.

b. Naproxen

The comparative electrochemical behavior of naproxen was studied at CNF electrode and at BDD electrode as a control measure. The composite electrode was selected for further studies due to exhibited performances in relation with the detection potential (+1.14 V/SCE for CNF electrode vs. +1.425 V/SCE for BDD electrode). The use of pulsed techniques, *e.g.*, differential-pulsed voltammetry, square-wave voltammetry shifted the detection potential to less positive values and improved the sensitivity. The best performances for these parameters were obtained under differential-pulsed voltammetry conditions.

c. Tetracycline

In this case, the electrochemical behavior of tetracycline was studied only at CNF electrode and it was noticed that tetracycline oxidation process which occurs in two steps is controlled by diffusion. By using pulsed techniques, the

electroanalytical parameters, *e.g.*, detection potential and sensitivity were enhanced under differential-pulsed voltammetric conditions.

Simultaneous detection

By using CNF composite electrode, the simultaneous detection of fluoxetine and naproxen, and also fluoxetine and tetracycline, detection strategies were developed, fluoxetine being considered as a reference compound. For both simultaneous scheme of detection, *e.g.*, naproxen-fluoxetine and tetracycline-fluoxetine, well-defined and separated oxidation peaks were obtained, and any interference was avoided. Also, by employing pulsed techniques, *e.g.*, differential-pulsed voltammetry and square wave voltammetry improved performances were obtained.

Carbon nanofiber material showed interesting peculiarities in relation with the electrochemical detection of these pharmaceutical compounds. These results constitute a good base for further electroanalytical applications in real water samples.

The presence of anions, *e.g.*, nitrite, sulfide in water proved to be harmful for aquatic environment, but also for human health. For this reason, detection methods that will provide fast response and high sensitivity of selected anions: sulfide and nitrite are desired in applications of water quality control.

Detection studies of sulfide were performed on two types of electrodes: BDD-commercial electrode and CNF-composite electrode in two matrices: 0.1M Na₂SO₄ classical supporting electrolyte and a new electrolyte generically called simulated seawater consisting in 0.1M Na₂SO₄+1M NaCl. For both types of supporting electrolytes, CNF electrode exhibited superiority, and it was selected for further studies. By employing pulsed voltammetric techniques, an enhancement regarding the sensitivity value was noticed, the best performance being obtained under square wave voltammetry conditions. Also, by optimizing the operating DPV parameters a shift to more negative values of detection potential was noticed (from +0.696 V/SCE to +0.193 V/SCE).

The microarray behaviour of CNF electrode was studied in the presence of sulfide for a surface water sample, important results being achieved. This application is a promising beginning for in-field applications of carbon nanofiber-epoxy electrode for voltammetric/ampereometric detection of sulfide in water/seawater.

Simultaneous detection of nitrite and sulfide was studied on BDD electrode, their results showing good peculiarities of BDD electrode for sensitive and simultaneous detection. The best performances in relation with the lowest limit of detection were obtained under optimized square wave voltammetry conditions. The results achieved for SWV conditions related to the limit of detection and limit of quantification showed that by this proposed methodology both anions can be detected simultaneously in good agreement with the Romanian legislation. Thus, this type of material is promising for development of in-situ applications.

The original contributions of this thesis are related to:

- adjustment of synthesis method for obtaining silver nanoparticles by electrochemical deposition on composite material substrates applied in direct detection of pharmaceuticals;
- exploitation of voltammetric techniques for optimizing the operating parameters (differential-pulsed voltammetry, square wave voltammetry)
- elaboration of detection protocols of preconcentration-voltammetric detection type for improving the electroanalytical performances for quantitative detection of pharmaceuticals;

- elaboration of simultaneous detection protocols for pharmaceuticals compounds;
- elaboration of individual/simultaneous detection protocols for sulfide and nitrite detection and their validation in surface water/seawater applications.

The results presented in this PhD thesis may constitute a basis for further research work:

- elaboration of simultaneous detection protocols for pharmaceuticals detection in real water samples by exploiting the microarray behaviour of CNF composite electrode, the interference study is imposed;
- elaboration of simultaneous detection protocols for anions detection in real water samples by exploiting the microarray behaviour of CNF composite electrode;
- elaboration of simultaneous detection protocols for pharmaceuticals and anions, *e.g.*, fluoxetine and nitrite detection in a real water samples by exploiting the microarray behaviour of CNF composite electrode;
- design of an individual/multi-selective sensor based on composite materials for in-situ applications;
- modification of composite electrode material for achieving improved selectivity and sensitivity for pharmaceuticals detection.

LIST OF PUBLICATIONS AND CONFERENCE PRESENTATIONS

List of published publications

- [1] M. Ardelean, F. Manea, R. Pode, Electrochemical detection of fluoxetine using boron-doped diamond electrode, *Int. J. Pharm. Pharm. Sci.*, 5(3), 2013, 318-322, *SJR=0.48*.
- [2] M. Ardelean, F. Manea, N. Vazsilcsin, R. Pode, Electrochemical detection of sulphide in water/seawater using nanostructured carbon-based electrodes, *Anal. Methods*, 6(13), 2014, 4775-4782, **ISI, F.I.=1.938**.
- [3] F. Manea, A. Jakab, M. Ardelean, A. Pop, I. Staicu, Boron-doped diamond electrode-based advanced treatment methods for drinking water, *Environ. Eng. Manag. J.*, 13(9), 2014, 2167-2172, **ISI, F.I.=1.258**.
- [4] M. Ardelean, F. Manea, R. Pode, Silver electrodeposited carbon nanofiber-epoxy electrode for fluoxetine detection, *APCBEE Procedia*, In Press

List of submitted publications

- [1] A. Baci, M. Ardelean, A. Pop, R. Pode, F. Manea, Simultaneous voltammetric/ amperometric determination of sulfide and nitrite in water at BDD electrode, submitted to *Sensors*
- [2] M. Ardelean, F. Manea, A. Pop, R. Pode, J. Schoonman, Voltammetric/ amperometric detection of fluoxetine in water at silver-modified zeolite carbon nanofiber electrode submitted to 8th International Conference of Environmental Engineering and Management, 9-11 September 2015, Iași, Romania

Conference presentations

- [1] Electrochem 2012: Electrochemical Horizons, 2 - 4 September 2012, Dublin, Ireland (poster presentation)
- [2] Fourth Regional Symposium on Electrochemistry South-East Europe, 26 - 30 May 2013, Ljubljana, Slovenia (poster presentation)
- [3] Summer School on Electrochemistry for Environmental and Biomedical Applications, 17-21 June 2013, Cluj Napoca, Romania (poster presentation)

150 List of publications and conference presentations

[4] 6th International Conference on Chemical, Biological and Environmental Engineering (ICBEE 2014), 15 -16 September 2014, Paris, France (oral presentation)

**Excellent paper of the session*

[5] 33^{ème} Conference Roumaine De Chemie, NOMARES, 01-03 October 2014, Căciulata, Vâlcea, Romania (poster presentation)